(2)

AFGL-TR-88-0061

Intersystem Collisional Transfer of Excitation in the Mesosphere and in the Laboratory

William Benesch
Beverly Carragher
Jeff Morrill

University of Maryland
Institute for Physical Science and Technology
College Park, MD 20742

March 1987

Final Report
November 3, 1983 - December 31, 1986

APPROVED FOR PUBLIC RELEASE; DISTRIBUTION UNLIMITED

AIR FORCE GEOPHYSICS LABORATORY
AIR FORCE SYSTEMS COMMAND
UNITED STATES AIR FORCE
HANSCOM AIR FORCE BASE, MASSACHUSETTS 01731-5000

"This technical report has been reviewed and is approved for publication"

Arthur Corman
Contract Manager

George A. Vanasse
Branch Chief

FOR THE COMMANDER

R. Earl Good
Division Director

This report has been reviewed by the ESD Public Affairs Office (PA) and is releasable to the National Technical Information Service (NTIS).

Qualified requestors may obtain additional copies from the Defense Technical Information Center. All others should apply to the National Technical Information Service.

If your address has changed, or if you wish to be removed from the mailing list, or if the addressee is no longer employed by your organization, please notify AFGL/DAA, Hanscom AFB, MA 01731. This will assist us in maintaining a current mailing list.

Do not return copies of this report unless contractual obligations or notices on a specific document requires that it be returned.

PAGES _____

ARE

MISSING

IN

ORIGINAL

DOCUMENT

Unclassified
SECURITY CLASSIFICATION OF THIS PAGE

REPORT DOCUMENTATION PAGE

Form Approved
OMB No 0704-0188

1a. REPORT SECURITY CLASSIFICATION Unclassified	1b RESTRICTIVE MARKINGS
2a. SECURITY CLASSIFICATION AUTHORITY	3. DISTRIBUTION/AVAILABILITY OF REPORT Approved for public release; Distribution unlimited
2b. DECLASSIFICATION/DOWNGRADING SCHEDULE	
4. PERFORMING ORGANIZATION REPORT NUMBER(S)	5. MONITORING ORGANIZATION REPORT NUMBER(S) AFGL-TR-88-0061
6a. NAME OF PERFORMING ORGANIZATION University of Maryland 6b. OFFICE SYMBOL (If applicable)	7a. NAME OF MONITORING ORGANIZATION Air Force Geophysics Laboratory
6c. ADDRESS (City, State, and ZIP Code) Institute for Physical Science & Technology College Park, MD 20742	7b. ADDRESS (City, State, and ZIP Code) Hanscom AFB Massachusetts 01731-5000
8a. NAME OF FUNDING/SPONSORING ORGANIZATION 8b. OFFICE SYMBOL (If applicable)	9. PROCUREMENT INSTRUMENT IDENTIFICATION NUMBER F19628-84-K-0017
8c. ADDRESS (City, State, and ZIP Code)	10 SOURCE OF FUNDING NUMBERS PROGRAM ELEMENT NO. 61102F; PROJECT NO. 2310; TASK NO. G4; WORK UNIT ACCESSION NO. BD

11. TITLE (Include Security Classification)
Intersystem Collisional Transfer of Excitation in the Mesosphere and in the Laboratory

12. PERSONAL AUTHOR(S)
William Benesch, Beverly Carragher, Jeff Morrill

13a. TYPE OF REPORT	13b. TIME COVERED	14. DATE OF REPORT (Year, Month, Day)	15. PAGE COUNT
FINAL REPORT	FROM 11-3-83 TO 12-31-86	1987 March	294

16. SUPPLEMENTARY NOTATION

17. COSATI CODES			18. SUBJECT TERMS (Continue on reverse if necessary and identify by block number)
FIELD	GROUP	SUB-GROUP	aurora, molecular nitrogen spectra, excitation of atmospheric species.

19. ABSTRACT (Continue on reverse if necessary and identify by block number)

The report describes a program of experimentation involving the emission spectra of auroral species and the processes and mechanisms leading to the production of their spectra. Emphasis is on the temporal evolution of the spectrum, particularly as brought about by the intersystem collisional transfer of excitation. This latter process becomes important in auroral spectra at or near mesospheric altitudes where the collision frequency becomes comparable with the transition probability from the excited state of the auroral emitter. The experiments have been undertaken in several modes, but in every case the observational technique is that of time-resolved spectroscopy by means of which we are able to detect changes in the emitted spectrum on a collision-by-collision basis. Previously unreported effects are described which fall in the category of molecular excitation energy storage and release. Examples are given of possible superradiance where particular vibrational levels of molecular nitrogen become temporarily overpopulated with respect to those in adjacent electronic states. Keywords:

20. DISTRIBUTION/AVAILABILITY OF ABSTRACT	21. ABSTRACT SECURITY CLASSIFICATION
☐ UNCLASSIFIED/UNLIMITED ☐ SAME AS RPT ☐ DTIC USERS	Unclassified
22a. NAME OF RESPONSIBLE INDIVIDUAL Arthur Corman	22b. TELEPHONE (Include Area Code) (617) 377-3694
	22c. OFFICE SYMBOL AFGL/LSI

DD Form 1473, JUN 86 *Previous editions are obsolete.*

SECURITY CLASSIFICATION OF THIS PAGE
Unclassified

CONTENTS

FINAL REPORT

INTRODUCTION

This program has comprised a series of investigations of excitation processes in auroral species under various conditions, notably at a variety of collision frequencies corresponding to a range of altitudes. In our laboratory experimentation, emphasis first centered on high-current pulsed discharges in nitrogen atmospheres contained within a large-volume Pyrex tube. More recently, we have developed several low-current, low-power small-volume discharges in order to obtain spectra under a broader range of conditions and environments than had proved possible within the confines of the large system.

Much of the work undertaken in the present effort has been described in the dissertation of Jeff Morrill which is presented here as Appendix A. It is our intention to publish most of this material in the near future in several papers, the first of which is now in final form and which is presented as Appendix B.

In the following sections, we will be discussing the general trend of the investigation, from the initial expectations to the final results. Particular emphasis will be placed on those findings which have not been covered in the Appendices A and B where the many of the results may be found but which do not contain references to the more recent experiments, data, and conclusions.

In applying these results to an enhanced understanding of auroral processes, we have always been cognizant of the circumstance that much auroral

activity takes place in an environment characterized by considerably lower collision frequencies than those of laboratory discharges. On the other hand, with time-resolved spectroscopy capable of time resolution extending to the sub-microsecond level, we have been able to examine the spectral evolution of auroral features on a collision-by-collision basis down to and including spectra which occur effectively prior to the first collision after excitation. This ability to probe the processes of spectral and population evolution under a variety of environmental conditions is evident in the discussions of the experiments in the appendices. We have, in fact, been able to refine those techniques considerably further in successor experiments with state-of-the-art instrumentation, and the more advanced methods will be described below.

HIGHLIGHTS OF RESEARCH FINDINGS

In the course of these investigations, we have uncovered a wealth of effects involving the evolution of nitrogen molecular level populations and the associated spectra both during and after direct electron excitation from the ground state. We will describe briefly the most interesting of these effects, and discuss our present understanding of them. As the discussion proceeds, it should be noted that all of the effects mentioned appear to be associated with hidden sources of excitaton, i.e. stored energy that is transferred into the $B\ ^3\Pi_g$ state by means other than the direct electron excitation from the quiescent ground state, $X\ ^1\Sigma_g^+$.

Three New Effects

[1] The first effect is illustrated in Figure 1 which shows excitation history of the v=1 level of the $B\ ^3\Pi_g$ state. The quantity recorded and graphed is the emitted band intensity which is proportional on a moment by moment basis to the level population. Briefly stated, the v=1 level rises monotonically throughout the current pulse (~ 4 μsec) as contrasted to all levels of other electronic states whose populations begin to fall as soon as pulse current reaches a maximum (~ 1 μsec).

The interpretation of this special behavior of the $B\ ^3\Pi_g$ is that, as opposed to the $C\ ^3\Pi_u$ and $B\ ^2\Sigma_u^+$ states, it is not entirely dependent upon electrons energetic enough to excite from the $X\ ^1\Sigma_g^+$ v=0 level, but is the recipient of excitation from metastable sources with energies well above the lowest vibrational level of the molecule.

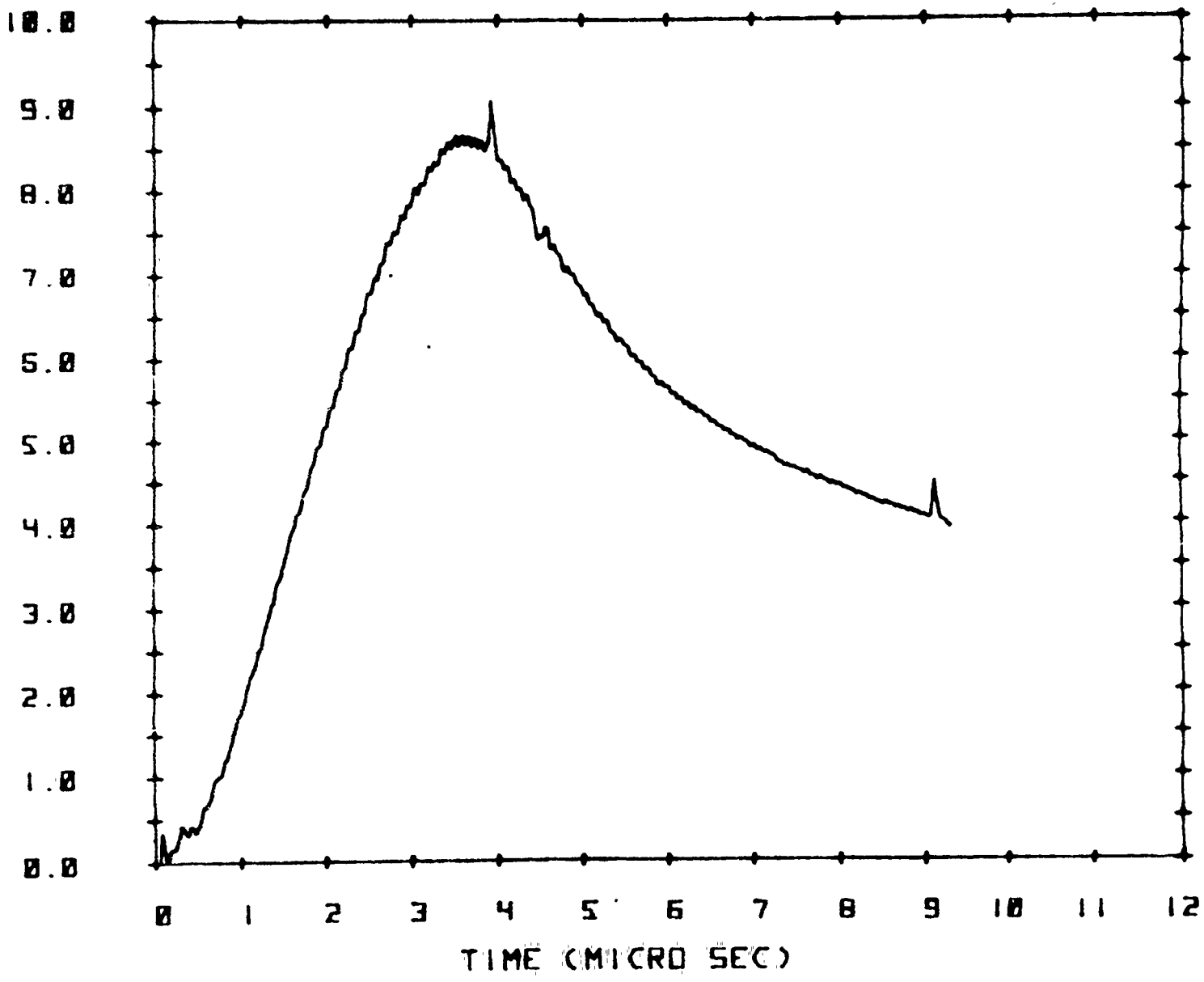
10.0
9.0
8.0
7.0
6.0
5.0
4.0
3.0
2.0
1.0
0.0
0 1 2 3 4 5 6 7 8 9 10 11 12
TIME (MICRO SEC)

[2] The second effect is illustrated in Figure 2 which shows three decay curves for the nitrogen 1PG 5-2 band taken at pressures of 30, 120 and 400mT. The top curve is for the low pressure, bottom curve for the high pressure; the vertical scale is logarithmic. The three curves rise in unison during the pulse, then drop precipitously when the current ceases, faster than the radiative depletion rate of the upper level, v=5, and finally settle into a long decay corresponding to a level depletion rate much smaller than its radiative decay. All of the decay rates are found to increase with pressure. Note particularly that in the afterglow domain, the observed lifetime here (1/e time) is some 100 microseconds as contrasted with the radiative lifetime of v=5 which is 6 microseconds.

One interpretation of the dogged persistence of the emission from the $B\ ^3\Pi_g$ state could lie in a hidden source of excitation which continues to feed into the levels long after the initial energizing pulse has ended. Alternatively, a mechanism for preventing emission from the already populated levels would provide for a similar lengthening of the emission profile of the $B\ ^3\Pi_g$ state. For the present, we favor the latter explanation as to the major cause. The argument goes as follows: The four states $B\ ^3\Pi_g$, $A\ ^3\Sigma_u^+$, $B'\ ^3\Sigma_u^-$ and $W\ ^3\Delta_u$ are all connected by intersystem collisional transfer and have been shown to equilibrate excitation among themselves very rapidly and attain a common lifetime for emission.

Accordingly, any excitation spends most of its existence in one or another of the long-lived states, but may only be emitted while residing in the $B\ ^3\Pi_g$. This, of course, considerably lengthens the time of residence within the nitrogen molecule. It does seem, however, that the very extensive observed

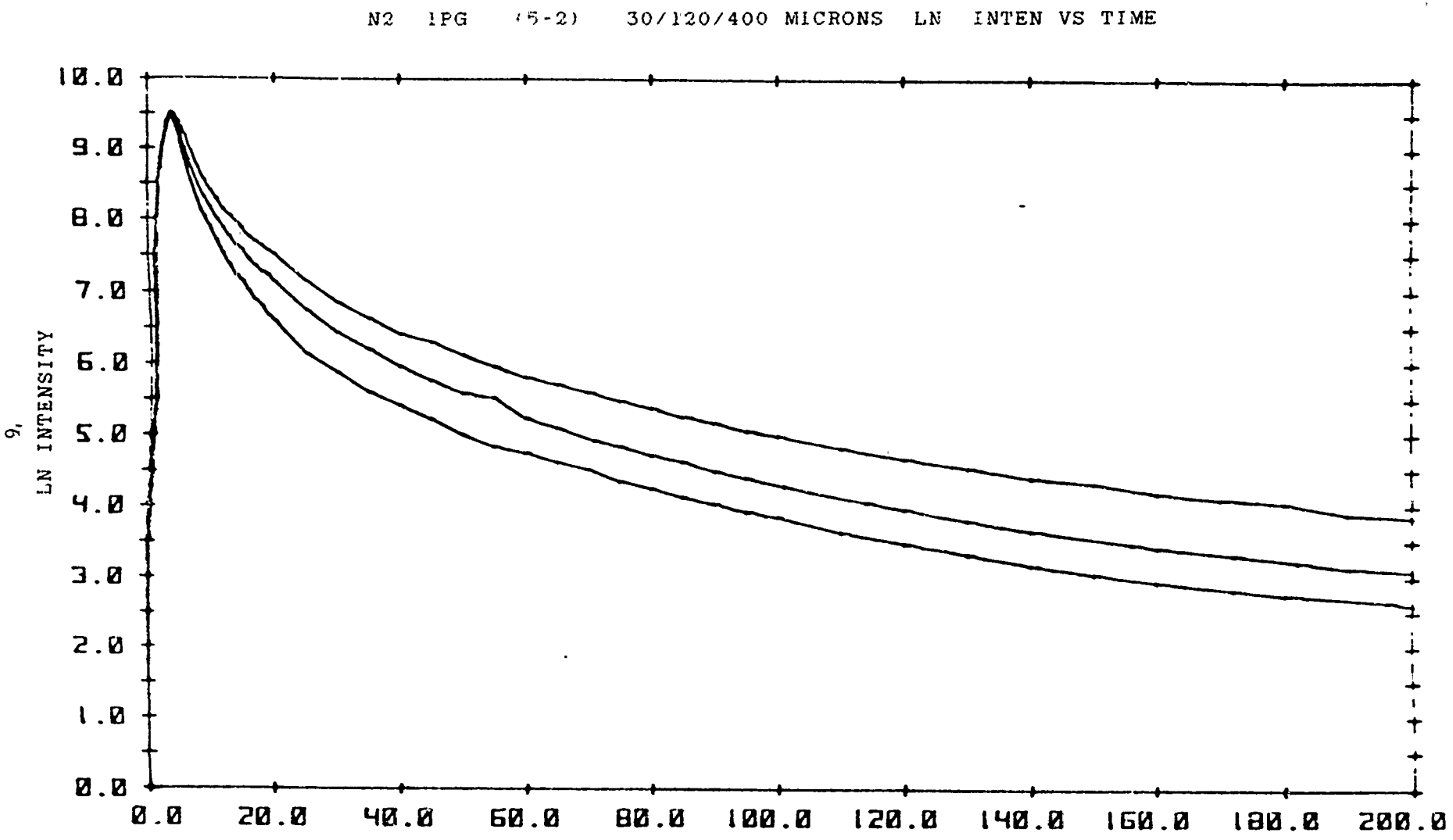
N2 1PG (5-2) 30/120/400 MICRONS LN INTEN VS TIME
LN INTENSITY
10.0
9.0
8.0
7.0
6.0
5.0
4.0
3.0
2.0
1.0
0.0
0.0
20.0
40.0
60.0
80.0
100.0
120.0
140.0
160.0
180.0
200.0
TIME (MICRO SEC)

Figure 2

emission profiles indicate the presence of long-term excitation enhancement as well. Although other mechanisms may, in fact, be principally responsible here, it would appear that the observed emission profiles point to the occurrence of long-term excitation enhancement as a significant contributor.

(3) The third effect that we find quite interesting is the observation of the marked impact on the nitrogen discharge spectrum of the variation of pulse repetition rate with all other parameters held constant. An example of the phenomenon is given in Figures 3 and 4 and the constant parameters are displayed on the figures (80 millitorr pressure, spectrum of the discharge at 3 μsec after the onset of the pulse, four sequences of the 1PG, $\Delta V = 1$ through 4). The Figure 3 trace was taken at a repetition rate of 5 Hz, the Figure 4 trace at 50 Hz.

The striking aspect of the grouping depicted is that the three sequences on the right seem relatively unaffected by the change in repetition rate while $\Delta V = 4$ is clearly much enhanced at the higher frequency. What is happening here is that the emission in $\Delta V = 4$ is primarily from the higher vibrational levels where the effect of repetition rate variation is most pronounced. At high rep rate there is a preferential excitation of the $B\ ^3\Pi_g$ vibrational levels approaching v=12. The preconditioned gaseous medium is responding in a different way to the pulse than that of the medium which has been permitted to relax. This is a non-linear effect which should have its parallel in the auroral excitation mechanism, particularly at the lower altitudes.

Our interpretation of this effect is that there is an energy carrier stored within the gaseous medium from pulse to pulse. It is reminiscent of

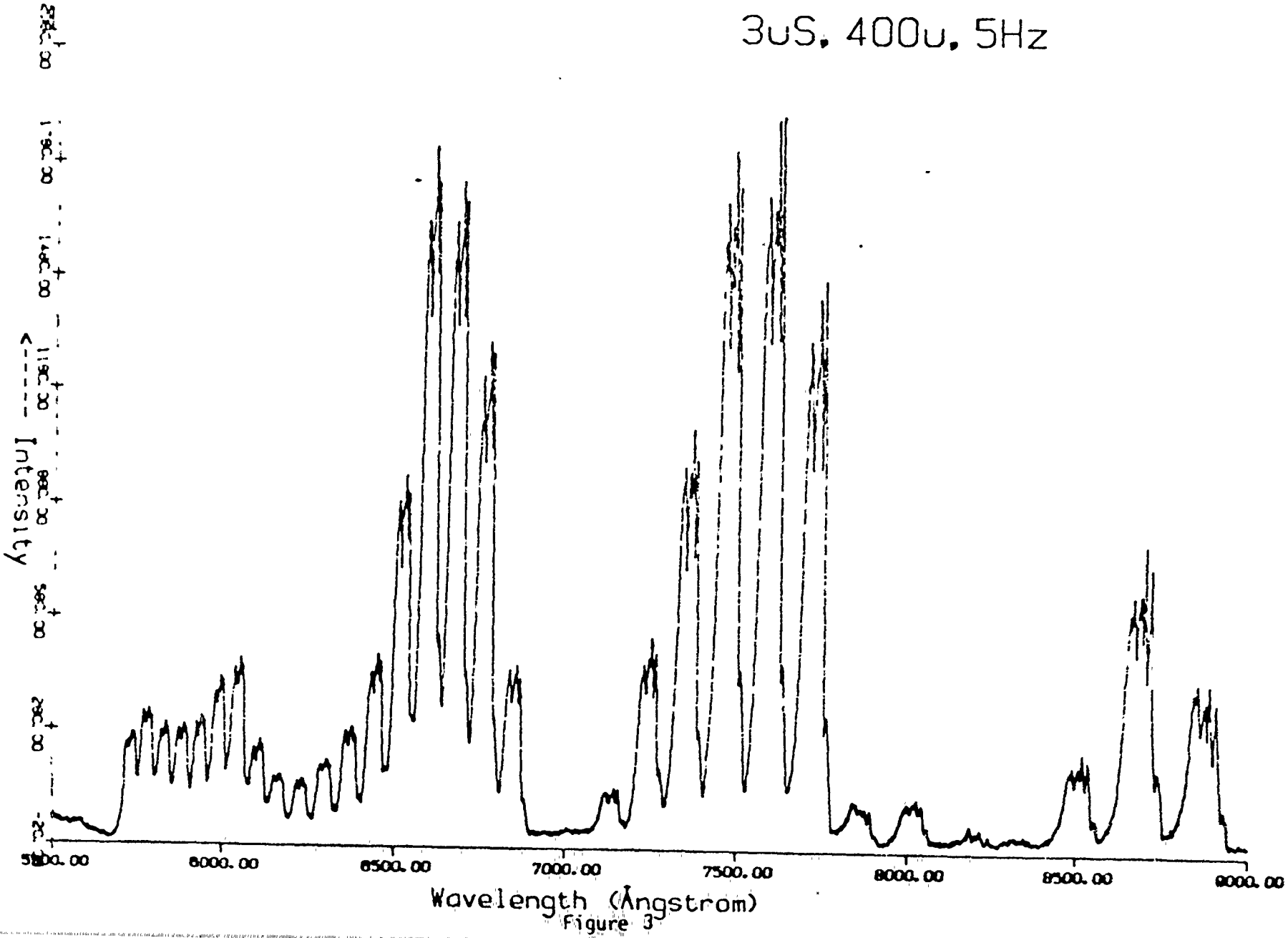
3uS, 400u, 5Hz
Intensity
5000.00
6000.00
6500.00
7000.00
7500.00
8000.00
8500.00
9000.00
Wavelength (Ångstrom)

Figure 3

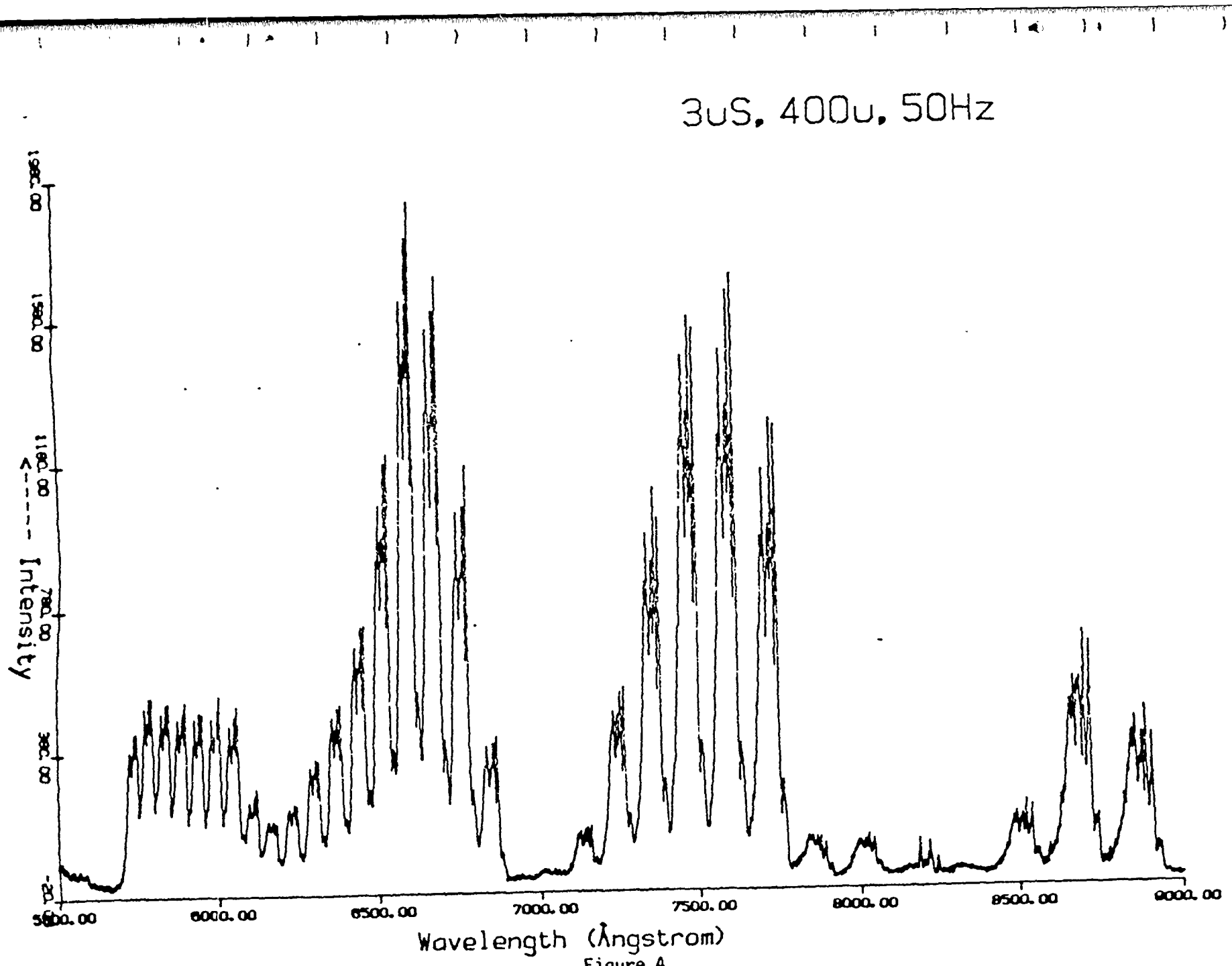
3uS, 400u, 50Hz
1980.00
1580.00
1180.00
780.00
380.00
-20.00
<----- Intensity
5500.00
6000.00
6500.00
7000.00
7500.00
8000.00
8500.00
9000.00
Wavelength (Ångstrom)

Figure 4

the preferential excitation of the higher levels in the Lewis-Rayleigh afterglow, and strongly suggests a transfer from the $A\ ^3\Sigma_u^+$ state. Recently, however, we have been considering a more basic storage mechanism comprising the vibrational excitation of the ground state, $X\ ^1\Sigma_g^+$. Preliminary modeling of the population trends in the $B\ ^3\Pi_g$ have been carried out by mapping ground state populations onto the B state via the Franck-Condon factors. The observed spectra have been related to enhanced ground state vibrational temperatures. Some of these results appear in Appendix A.

THE MOST RECENT INVESTIGATIONS

Since the experimentation and the compilation of the data presented in the paper of Appendix A, the emphasis in the program has been on an entirely new system of operation. The motivation for constructing the parallel system was two-fold. First, there is the matter of continuing concern that much of the data collected in the several laboratories now working on nitrogen may be system-dependent. The new system is very much different from the one previously described. Second, we have incorporated a number of technological enhancements into the new system and the results have been most gratifying.

The data aquisition section of the system consists of a network comprising an enhanced IBM PC XT, an EG&G PAR 4400 Signal Processing System, and a SPEX 0.22 meter spectrometer with a microprocessor-based programable scan controller. All calibration data (wavelength and intensity) is stored in the PC, while most of the data processing is performed by the 4400. The latter is primarily a super digital boxcar integrator. It provides real-time digitized and stored signals from two data channels simultaneously and supplies on-board reduction and analysis of the stored information. We are able to obtain immediate multiple exponential fits of the excitation and decay curves as well as both smoothing and background subtraction on a point-by-point basis. Time resolution is essentially infinite in terms of present experiments.

As an example of the uses to which this system has been put, we show the curves on the following page. The top curve is the raw signal, digitized and stored by the signal processing system, the middle curve is the signal with the light blocked out (we are working with a weak signal heavily distorted by

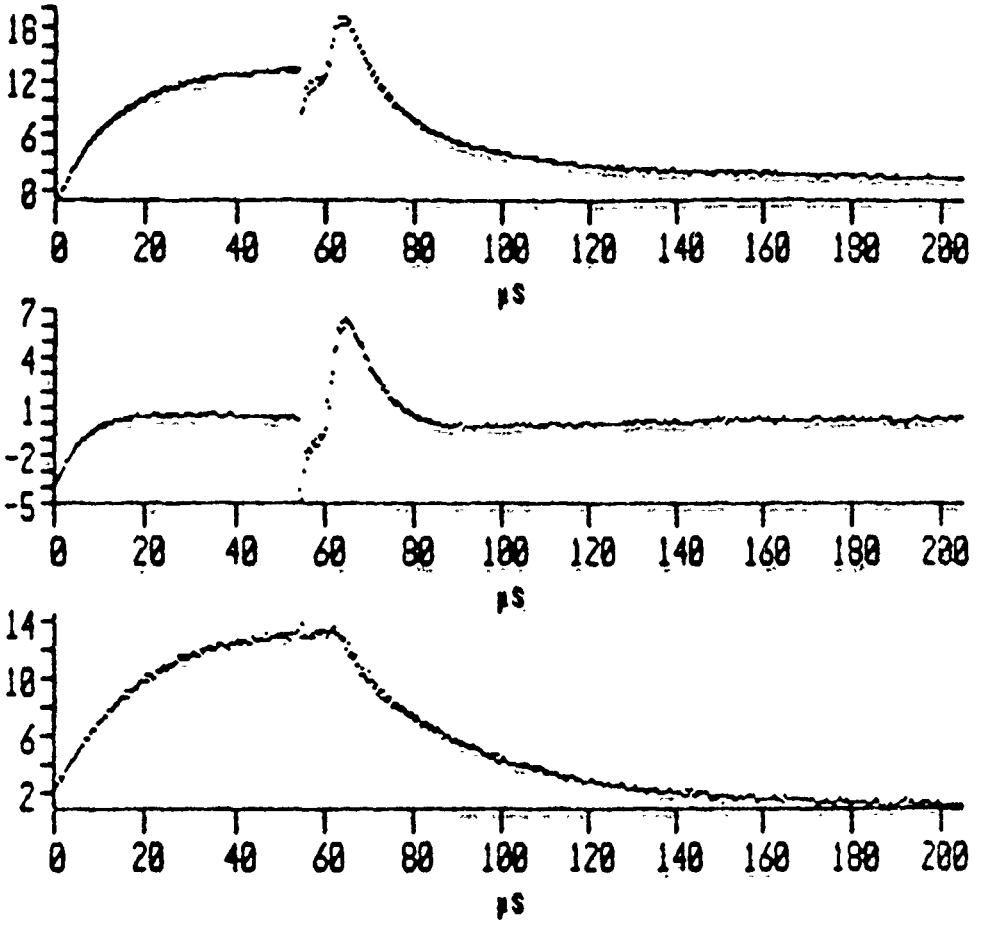
18
12
6
0
0 20 40 60 80 100 120 140 160 180 200
µS
7
4
1
-2
-5
0 20 40 60 80 100 120 140 160 180 200
µS
14
10
6
2
0 20 40 60 80 100 120 140 160 180 200
µS

electrical pickup), while the bottom curve is the difference curve representing the true excitation and decay trajectories for the v=0 level of the B state.

In deference to the question of obtaining data from a broader range of experimental environments, we have developed several low-current, low-power small-volume discharges in order to obtain spectra under conditions far removed from those of our big system. One discharge tube that we are using has the shape of an inverted (Π) with a discharge length of 4 in. and a diameter of 1 in. The current density in this tube is only one percent of that in the large-volume tube, namely 0.03 amps/cm^2 vs. 3.0 amps/cm^2 in the big tube. One of the more attractive features of the small tube systems is our ability to run them with discharge pulses of almost any width. Accordingly, we have been extending the pulse width upward and downward from the 4 μsec value which has been the staple of the large tube.

In the earlier experiments, we had been struck by the characteristic of the B $^3\Pi_g$ levels to increase their populations throughout the entire 4 μsec duration of the big tube current pulse while the C $^3\Pi_u$ populations begin to fall almost immediately after discharge onset. It was at first considered that the prolonged rise of the B $^3\Pi_g$ populations might be related to their relatively long lifetimes (5-10 μsec). However, the new system, with its highly variable pulse width, permits the aquisition of a much broader range of data and puts a whole new perspective on the population build-up phenomenon.

As the next figure shows, the B $^3\Pi_g$ continues to rise as long as the excitation pulse persists until some 150 μsec into the discharge, for this 1PG

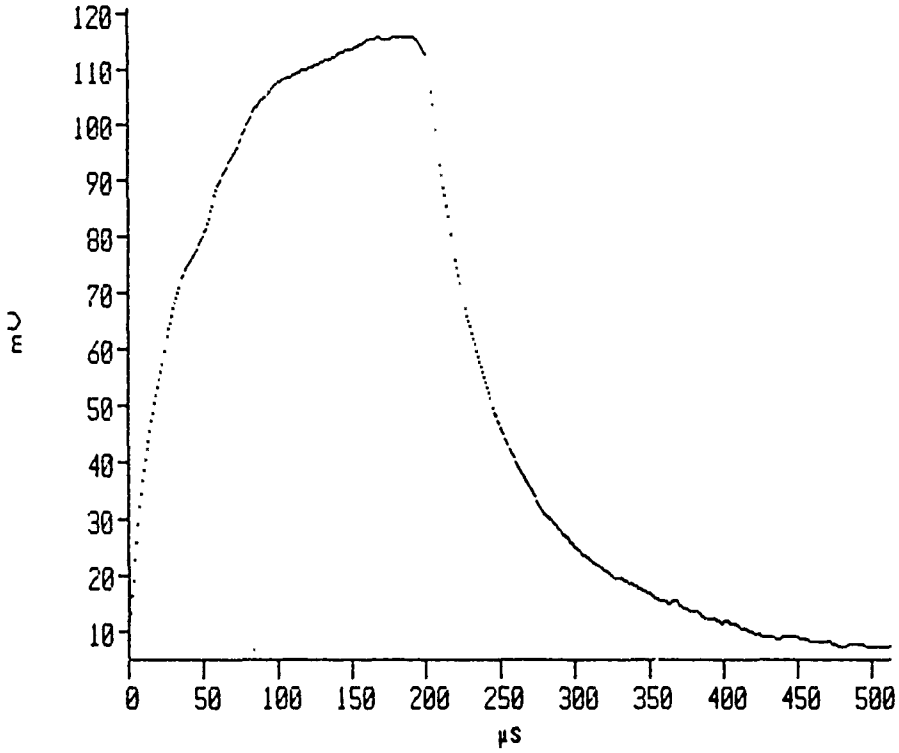
120
110
100
90
80
70
60
50
40
30
20
10
0
50
100
150
200
250
300
350
400
450
500
µS

1-0 band. Another important flexibility in the new system arises from the addition of infrared sensitive detectors, namely fast red-extended silicon diodes and cooled photomultiplier tubes with S1 photocathodes. Both of these detection devices allow observation of the 1PG 0-0 band and thus provide access to the v=0 level of the B state. The S1 photomultiplier has proven the most productive of the two thus far in that it permits real-time comparison of a large number of bands over a broad wavelength range. The results of the v=0 studies have been interesting, not to say startling.

A further enhancement of the system is an expanded capability of analyzing the data through curve fitting to a variety of functions, virtuallv in real time. Most advantageous for present purposes has been the fitting of the band decay curves to single and double exponentials.

The next six graphs illustrate the ability of the data aquisition system to provide incisive analysis of the time development of the spectroscopic features of present interest. In addition, these graphs demonstrate an important aspect of the 1PG population history, one not previously recognized.

The data of these curves come from either the 1PG 0-0 or the 1-0 band. Both discharges were struck in 300 mT of pure flowing nitrogen with pulse lengths of 4 μsec and a repetition rate of 1000 Hz. The boxcar integration mode here is that of the moving aquisition aperture which tracks the radiation of the spectral feature in time. The spectrometer does not scan, but acts as a narrow band filter centered on a particular nitrogen band. The pattern of graph presentation is 0-0 data, 0-0 curve fit, overlap of data and fit; 1-0 data, 1-0 curve fit, overlap. It is clear that these are excellent curve

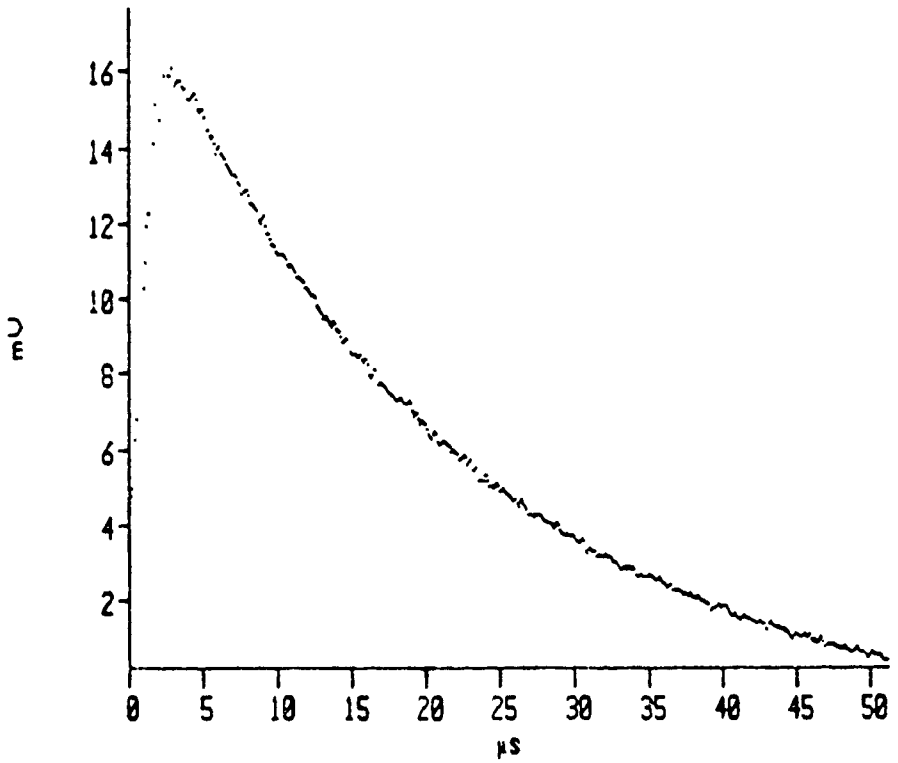

(0,0) 300U 1KHZ 4US PULSE_

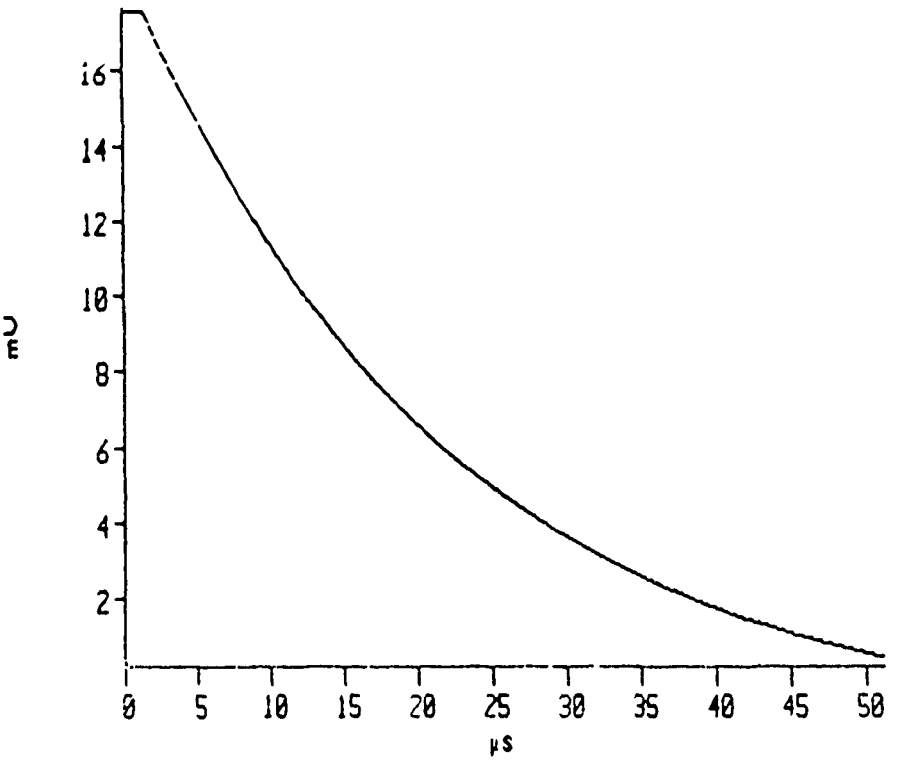
16
14
12
10
8
6
4
2
J
E
0
5
10
15
20
25
30
35
40
45
50
μs

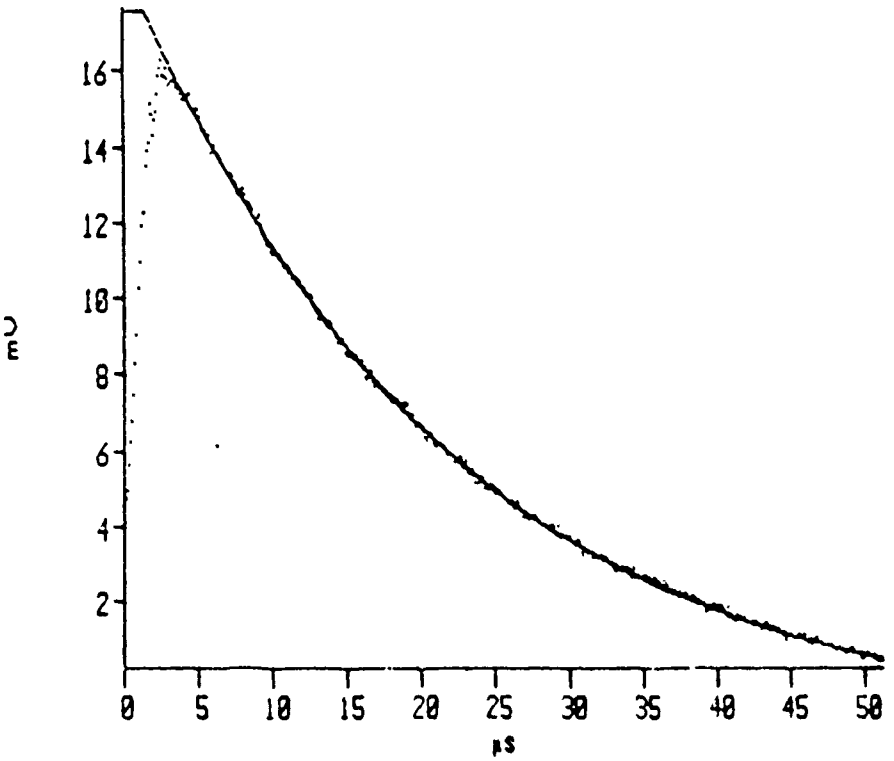

(0,0) 300U 1KHZ 40S PULSE_

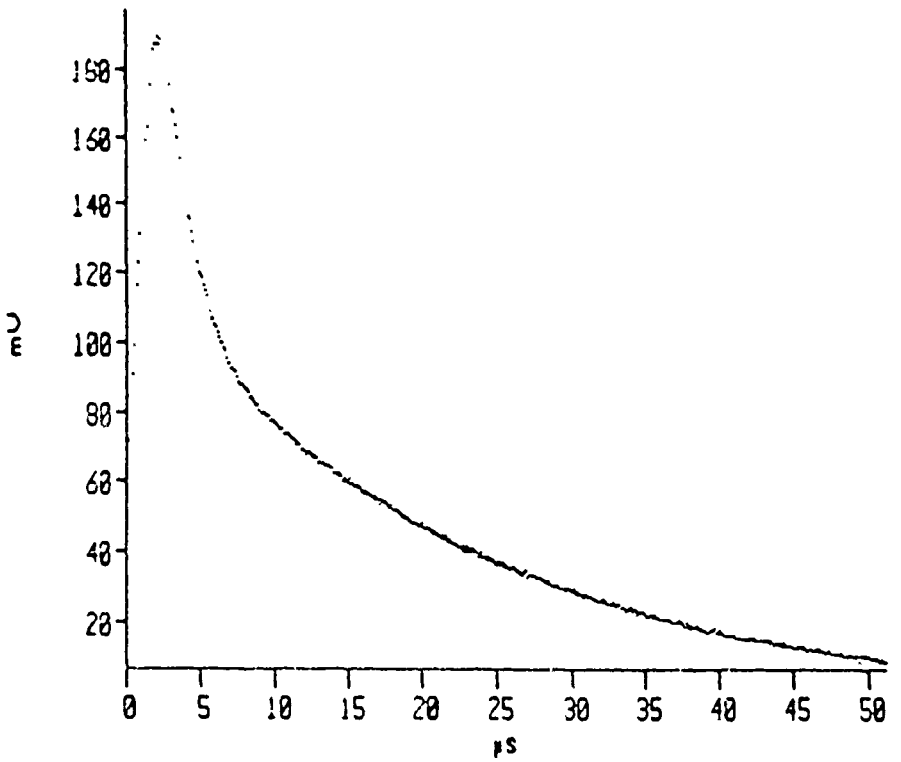

(1,0) 200U 1KHZ 4US PULSE_

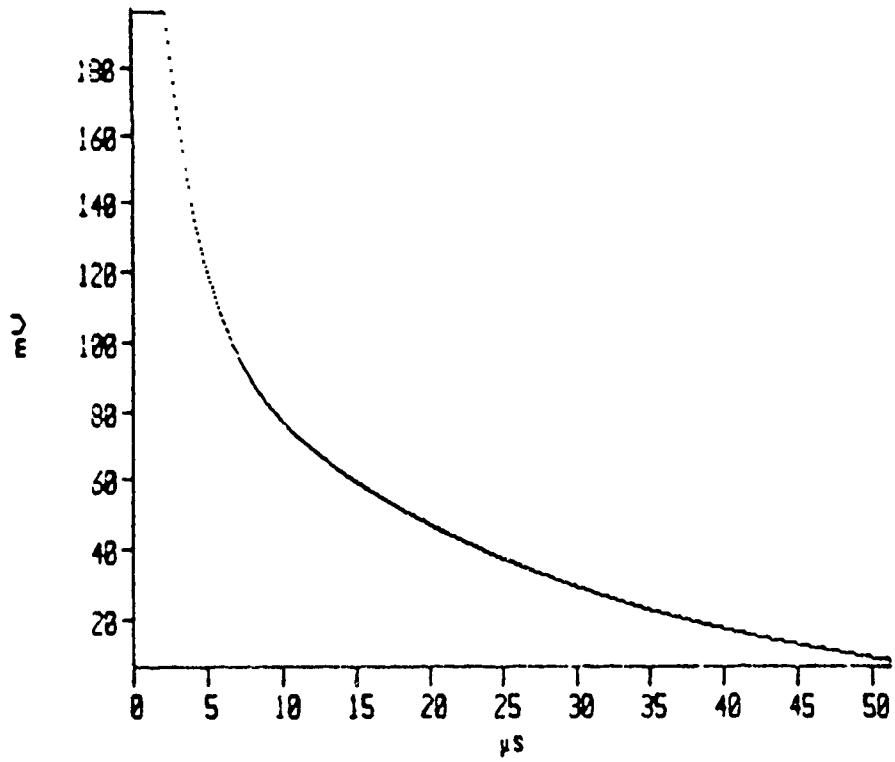
180
160
140
120
100
80
60
40
20
0
5
10
15
20
25
30
35
40
45
50
μs

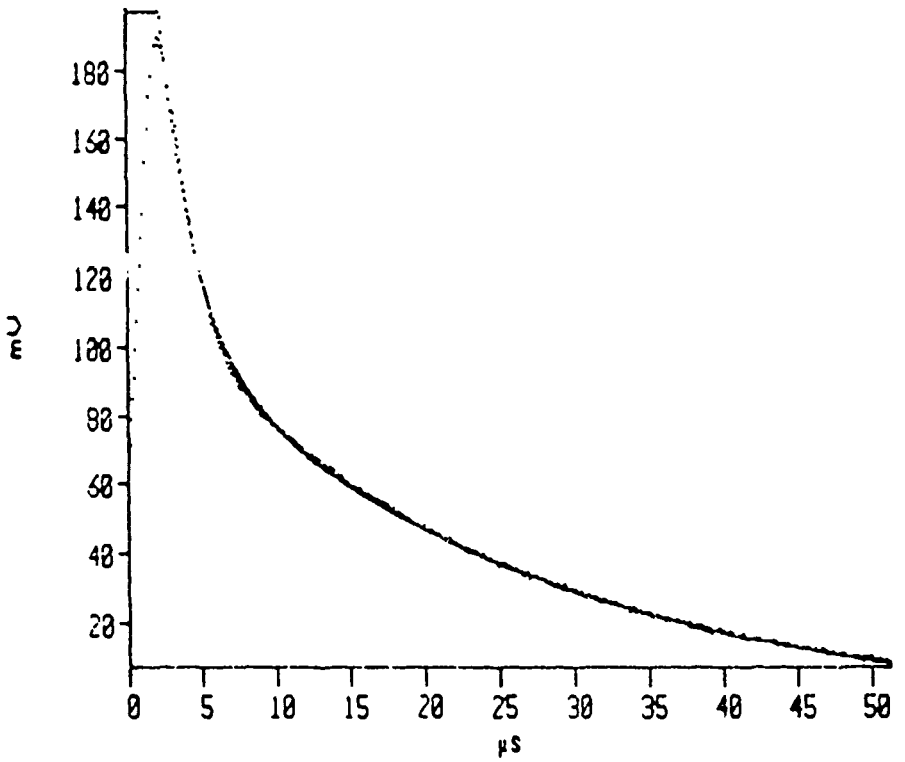

(1,0) 300U 1KHZ 4US PULSE_

fits. Less evident is the fact that the 0-0 band fits to a single exponential whereas the 1-0 fits to a double exponential.

$$I = e^{-t/21.4}$$

and

$$I = 2e^{-t/2.91} + e^{-t/25.6}$$

These are intensities as a function of the time in μsec. If we attempt to fit the 0-0 band to a double exponential, both exponents attain the same value. If we attempt to fit the 1-0 band to a single exponential, the overlap plot immediately demonstrates an obvious lack of agreement. Another mode of presentation for these decay data is applied in the next figure where the logarithm of the emission intensity of the 1-0 band is plotted against time. The two decay regions are sharply delineated and maintain remarkably constant decay coefficients within their time domains.

Our preliminary interpretation of these results is that the single exponential of the 0-0 band and the late (second) exponential of the 1-0 band arise from the same phenomenon. They contain both the radiative decay and the collisional components of the time development of the level populations. With increasing pressure, the late time decay constant is reduced. At 220u the 1-0 band decays with a 26 μsec time constant, whereas at 4 Torr the time constant is 6 μsec. The same pattern holds true for the 0-0 band. The time constant at the lower pressure is about 30 μsec; at the higher pressure it is about 7 μsec. This can be seen in the next four figures. There seems to be a collisional component to the late exponential decay.

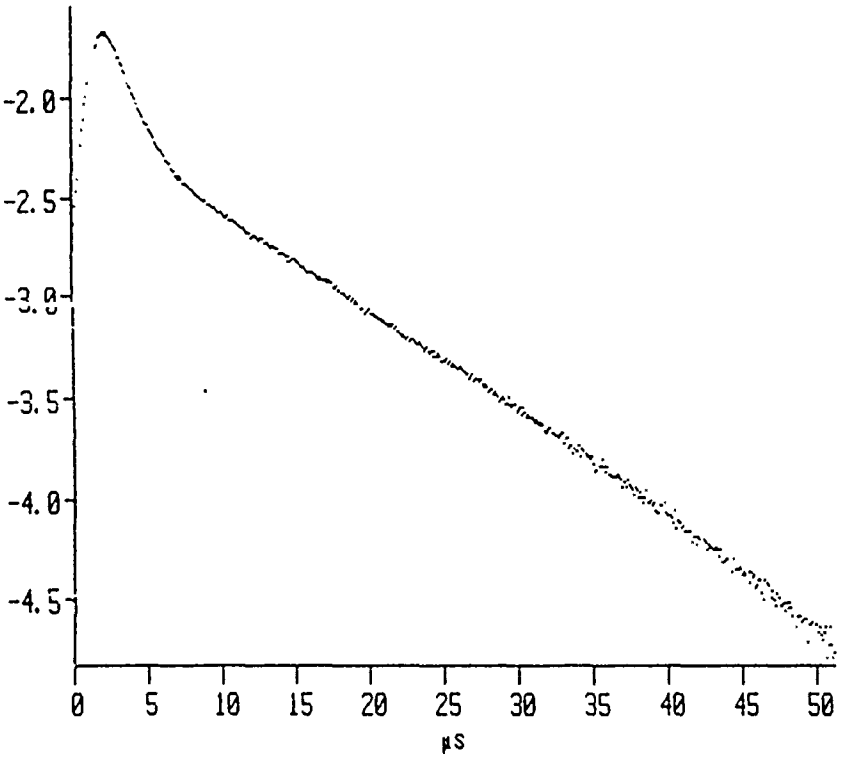
-2.0
-2.5
-3.0
-3.5
-4.0
-4.5
0
5
10
15
20
25
30
35
40
45
50
µS

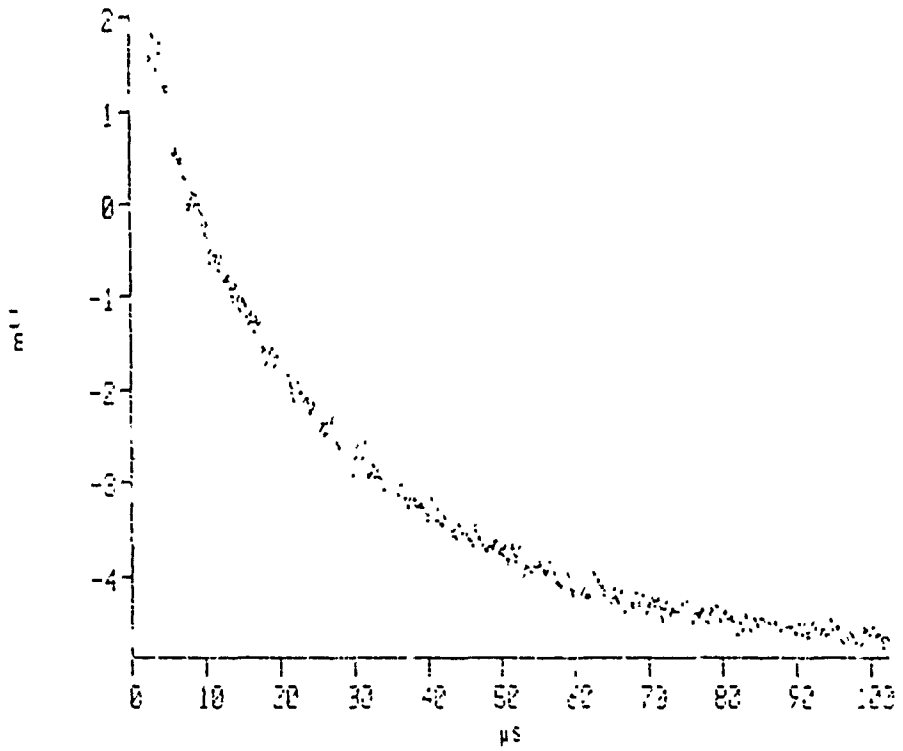

N2 4US PULSE 220U 1KHZ (0,0)_

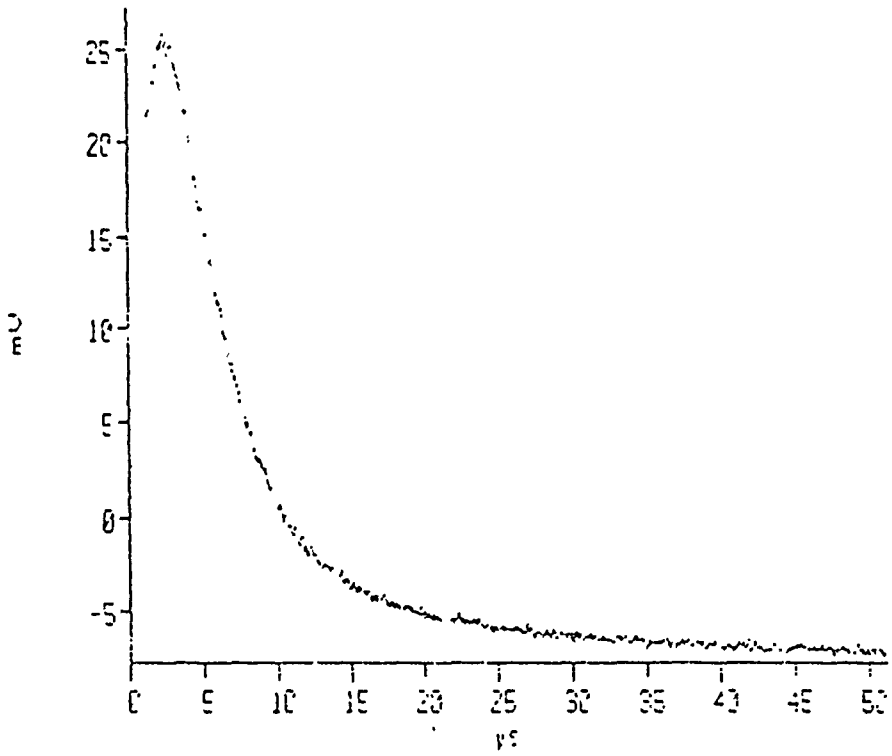

N2 1US PULSE 4T 1KHZ (0.0)_

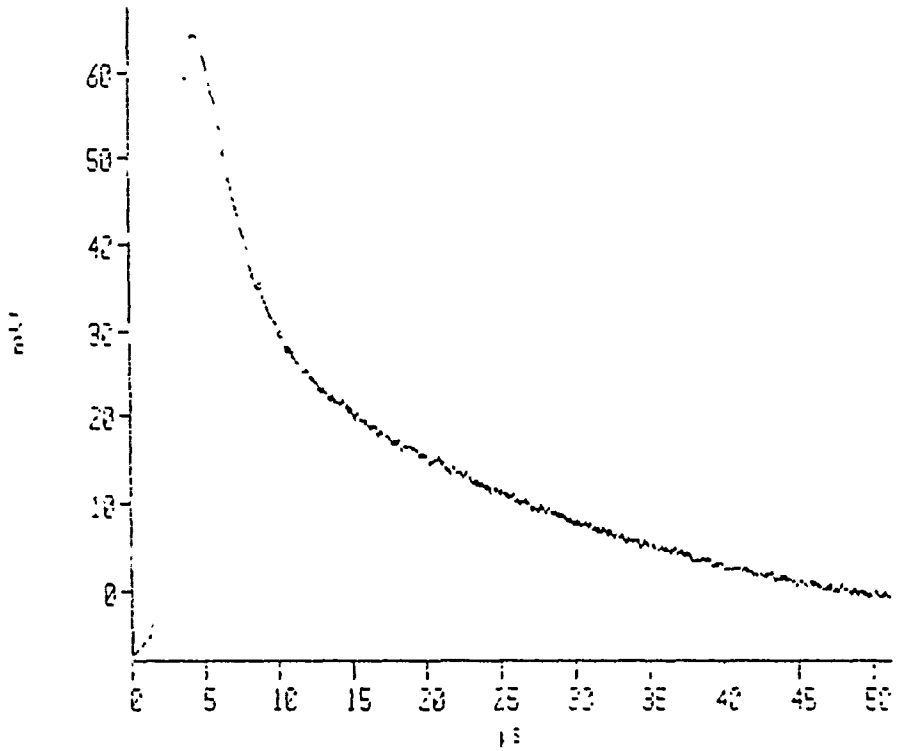

N2 4US PULSE 220U 1KHZ (1,0)_

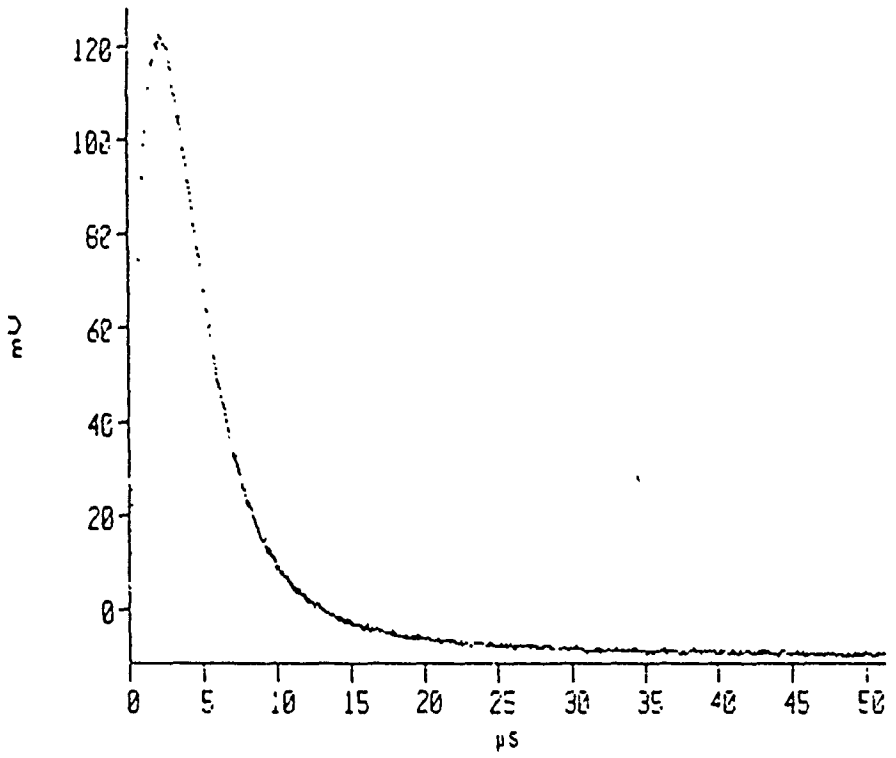

N2 1US PULSE 4T 1KHZ (1,0)_

What we find most interesting here is the fast exponential decay of the 1-0 band which is absent in the 0-0 decay. All low-lying levels of the $B\ ^3\Pi_g$ show the same dramatic decay following a short excitation pulse (except v=0) and for all of them the decay is faster than their radiative transition probabilities, more rapid than collisional transfer processes, and essentially independent of pressure.

We now surmise that what is manifested here is the effect of superradiance arising from an early population inversion between, for example, B(1) and W(0). It is deduced that these transitions remain superradiant until collisions have had time to equilibrate the population unbalance. The ~ 3 μsec decay rate during stimulated emission is largely an invariant, while the duration of the phenomenon is reduced as the discharge pressure rises. The probable superradiant transitions are indicated on the following potential curves. These are the infrared bands that we proposed in 1968 as having given rise to two groups of lines in McFarlane's early laser studies of condenser-pulsed nitrogen. The illustrated transitions were found to lase during the current pulse, but not in the afterglow. They are located between 5 and 6 microns wavelength.

The evidence in favor of associating the sharp depopulation trend of the $B\ ^3\Pi_g$ levels with stimulated emission we list, in order of increasing importance, as (a) the lack of correlation with collision frequency, (b) the occurrence in both discharge systems, (c) the circumstance that the superradiance takes place immediately following short pulses, but not after long pulses, and (d) the fact that the v=0 level follows an entirely different (longer) decay pattern during the same time domain. It should be pointed out that conditions

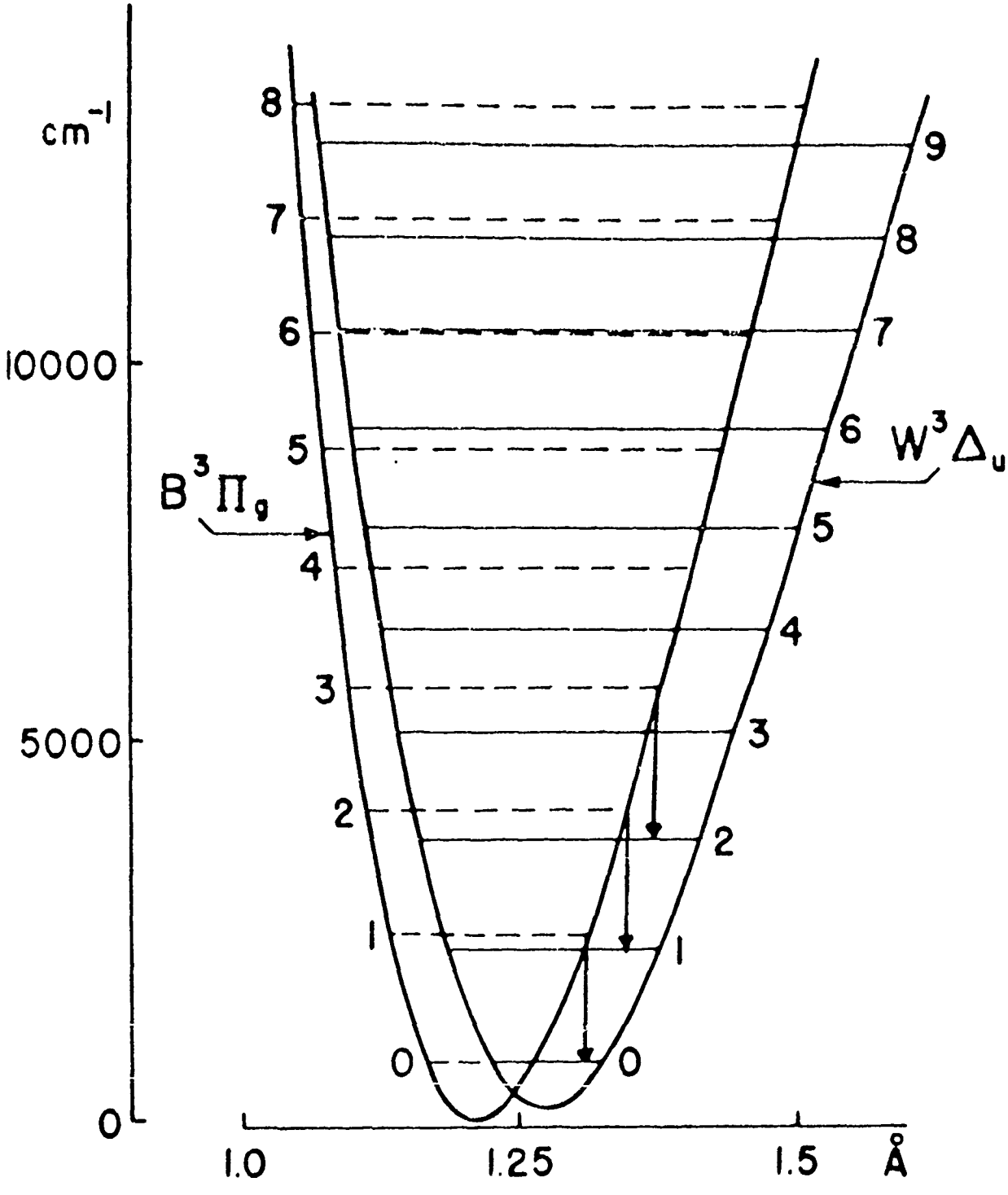
cm⁻¹
10000
5000
0
8
7
6
5
4
3
2
1
0
9
8
7
6
5
4
3
2
1
0
B³Πg
W³Δu
1.0
1.25
1.5
Å

in active auroral forms are quite conducive to the production of this type of superradiance since the medium is characterized by low collision frequency and minimal local water vapor absorption. The resultant lasing photons could not be expected to reach ground level, but should be observable at altitude in the form of short 6000 nm bursts.

As a corollary to the observation that the low-lying levels of the $B\ ^3\Pi_g$ become overpopulated with respect to those of the $W\ ^3\Delta_u$, we point out an aspect of the v=0 level that has not been recognized previously. It is that the v=0 level makes its way through the discharge pulse after starting with a population that generally is remarkably low. The point is illustrated in the next two figures. The first within the current pulse but with the 0-0 high. The second with the sample point set 2 μsec earlier so that 0-0 is low.

We have undertaken some studies of nitrogen excitation and decay processes in noble gas environments. The primary motivation here is to place the nitrogen molecule out of reach of its own kind and to permit it to collide only with monatomic particles. In our preliminary experiments, we have used 1% N_2 in helium and 1% N_2 in argon.

The next figure shows the spectrum of 1% N_2 in a 300 mT helium atmosphere at 35 μsec after a 40 μsec pulse. Essentially, there are two features here, the 0-0 band on the left and the 1-0 band on the right (our previous wavelength scale has been reversed). In other words, each sequence is represented almost entirely by its lowest member. This spectral structure is reminiscent of the early work of Carl Kenty who was also able to drive the vibrational population down the ladder in predominantly noble gas atmospheres.

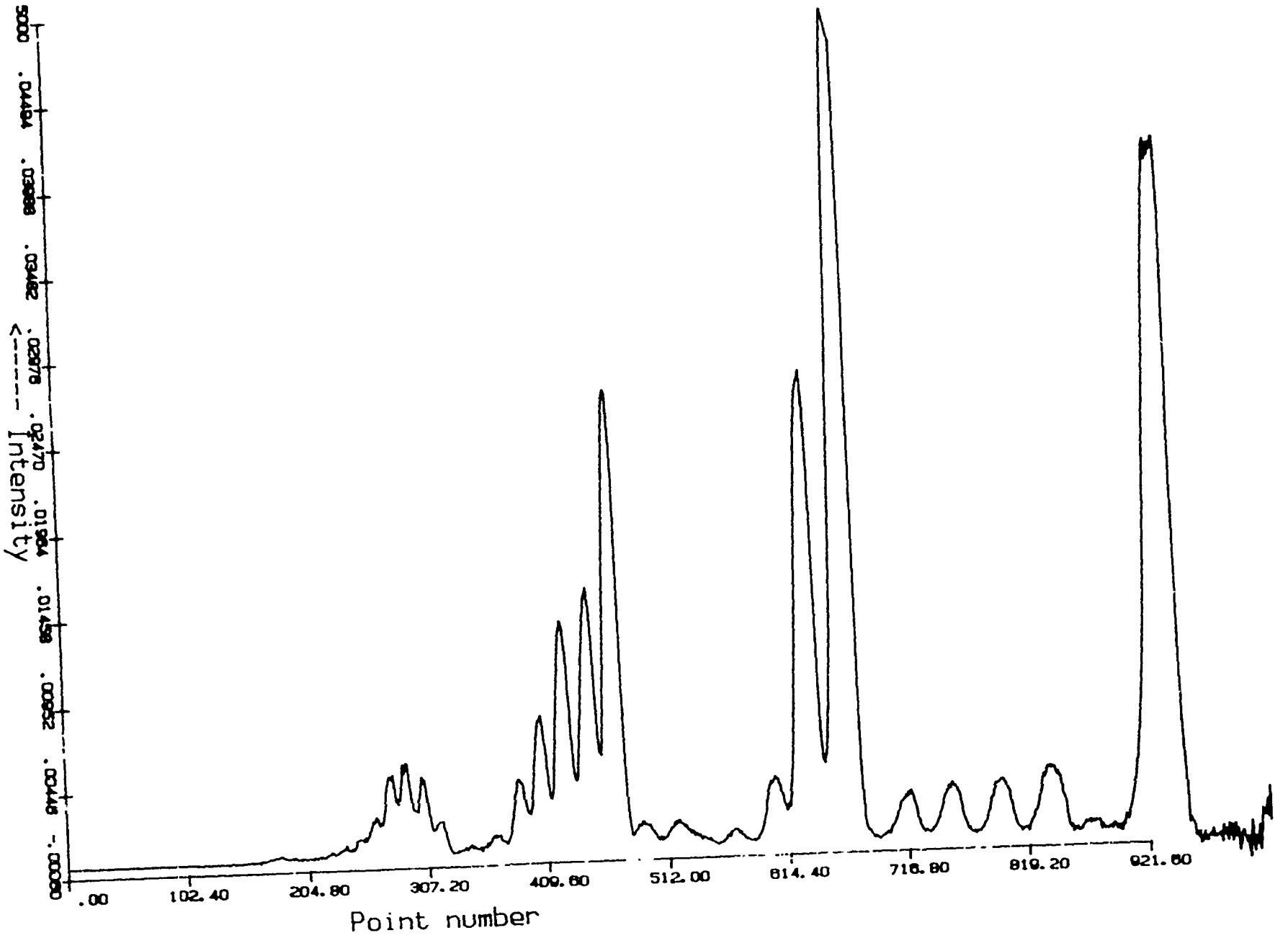
5000
.04484
.03888
.03482
.02878
.02470
.01964
.01458
.00952
.00446
-.00060
<------ Intensity
.00
102.40
204.80
307.20
409.60
512.00
614.40
716.80
819.20
921.60
Point number

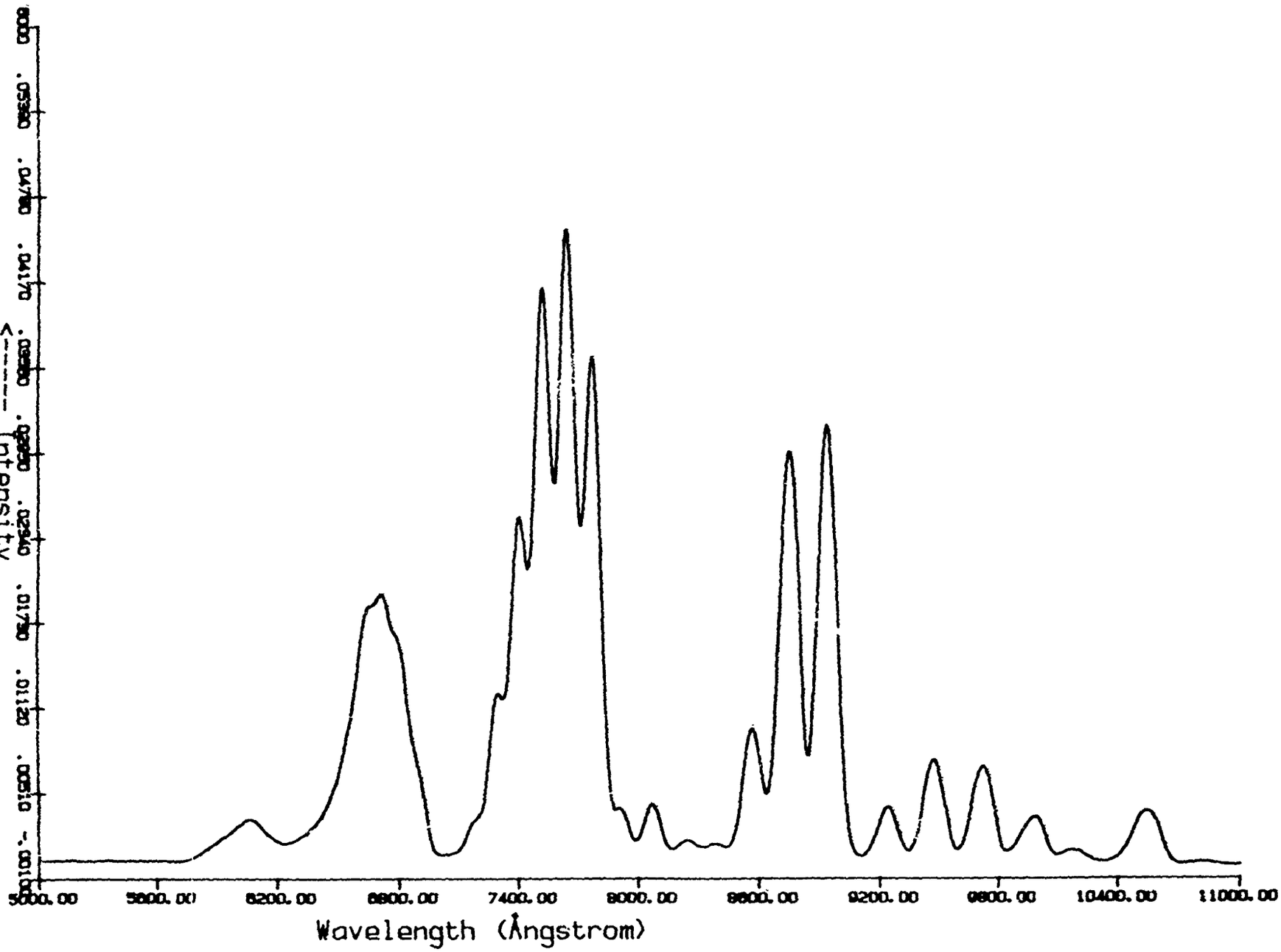
5000.00
5800.00
6200.00
6800.00
7400.00
8000.00
8600.00
9200.00
9800.00
10400.00
11000.00
Wavelength (Angstrom)
<----- Intensity

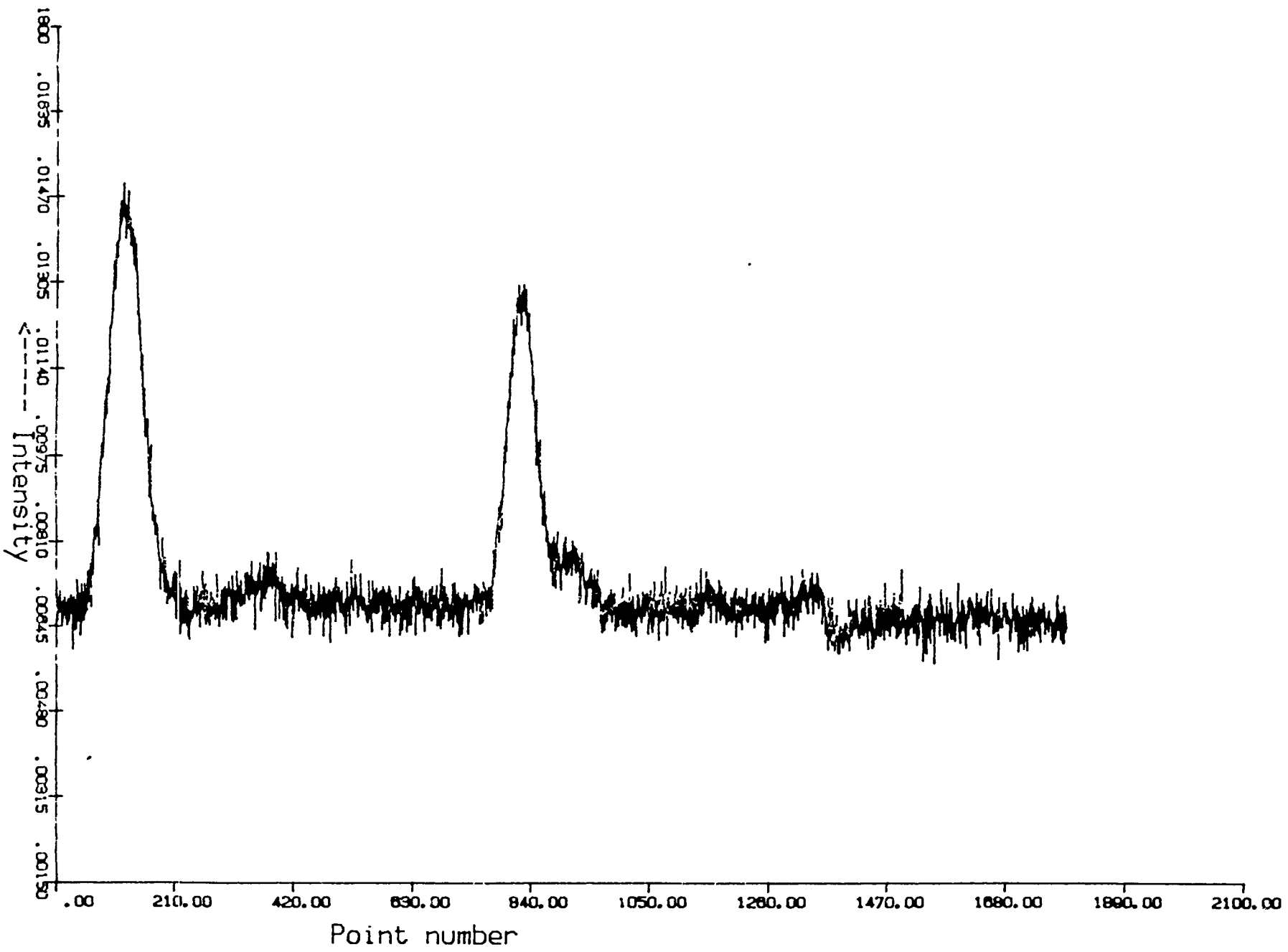
.01800
.01635
.01470
.01305
.01140
.00975
.00810
.00645
.00480
.00315
.00150
<------ Intensity
.00
210.00
420.00
630.00
840.00
1050.00
1260.00
1470.00
1680.00
1890.00
2100.00
Point number

Our understanding of the effect of the noble gas environment is quite fragmentary at this stage of the investigation, but we make the suggestion that it is not the special potency of rare gas collisions that impels the nitrogen population toward v=0. Rather, we believe that it is the absence of the secondary excitation mechanisms in the non-nitrogen atmosphere that precludes a continuing repopulation of the higher vibrational levels.

THE LEWIS-RAYLEIGH AFTERGLOW

The great majority of the effort in this program has been devoted to a study of the emission profiles of nitrogen molecules within a few tens of microseconds following direct excitation, since that time interval would seem to be most applicable to the auroral condition. On the other hand, the more long-lived emissions may well be of importance in the case, for example, of active auroral forms behind which decaying populations much exceed in volume the recently excited and less evolved emitters.

Perhaps the ultimate condition of aged excitation is that preceding the emission of the Lewis-Rayleigh afterglow, and it has been our intention from the beginning to attempt to follow the emission process in nitrogen through to the Lewis-Rayleigh stage. This has, indeed, proved possible recently with our upgraded equipment and we will discuss these experiments forthwith.

In general, we find that the LRA is most readily observable at higher pressures (of the order of 4 Torr) and at times of 20 μsec or more after the end of the current pulse. Prior to the time of the LRA, the higher vibrational levels of the B state become depopulated through collisional and radiative losses. In the LRA, however, the higher levels of the B, notably the levels near v=12, become "repopulated" by way of atomic recombination, and a new vibrational population distribution emerges. Spectra taken during the time domain of the LRA reveal bands of the Herman Infrared System as well.

The next three figures illustrate the development of the LRA. In all of these spectra, the pressure is 4 Torr, the pulse duration is 2 μsec, and the

repetition rate is 1 kHz. The first spectrum is taken 9 μsec after the end of the current pulse. An analysis of the population of the first 7 vibrational levels gives the following results. Note that the populations have been expressed in percentages.

vibrational level	percent population
0	54.7
1	25.8
2	15.4
3	1.8
4	1.1
5	0.66
6	0.50

The second spectrum is taken at approximately 100 μsec after the current pulse. The percentage average populations for each level are:

vibrational level	percent population
0	59.3
1	21.5
2	10.1
3	3.3
4	3.3
5	1.6
6	1.0

The third spectrum is taken at approximately 400 μsec after the current pulse.

vibrational level	percent population
0	52.6
1	22.1
2	13.5
3	4.2
4	3.8
5	1.9
6	1.8

As the time after the current pulse increases, the higher vibrational levels of the B state become repopulated, and the spectrum of the 1PG shifts in favor of the higher quantum numbers. We believe that this is the first time-resolved investigation of the LRA and of the development of the underlying populations into the long-time domain.

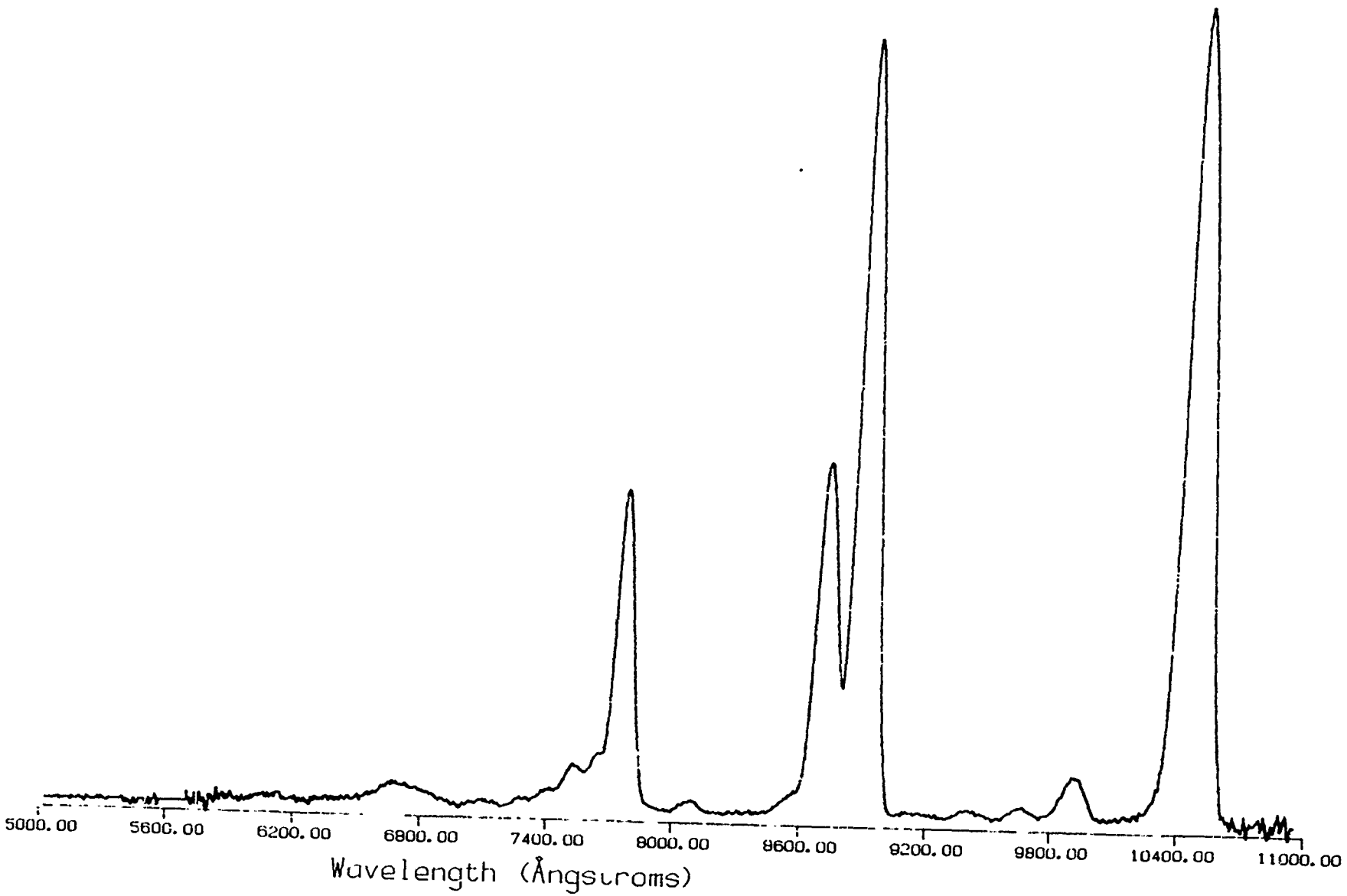
5000.00
5600.00
6200.00
6800.00
7400.00
8000.00
8600.00
9200.00
9800.00
10400.00
11000.00
Wavelength (Ångstroms)

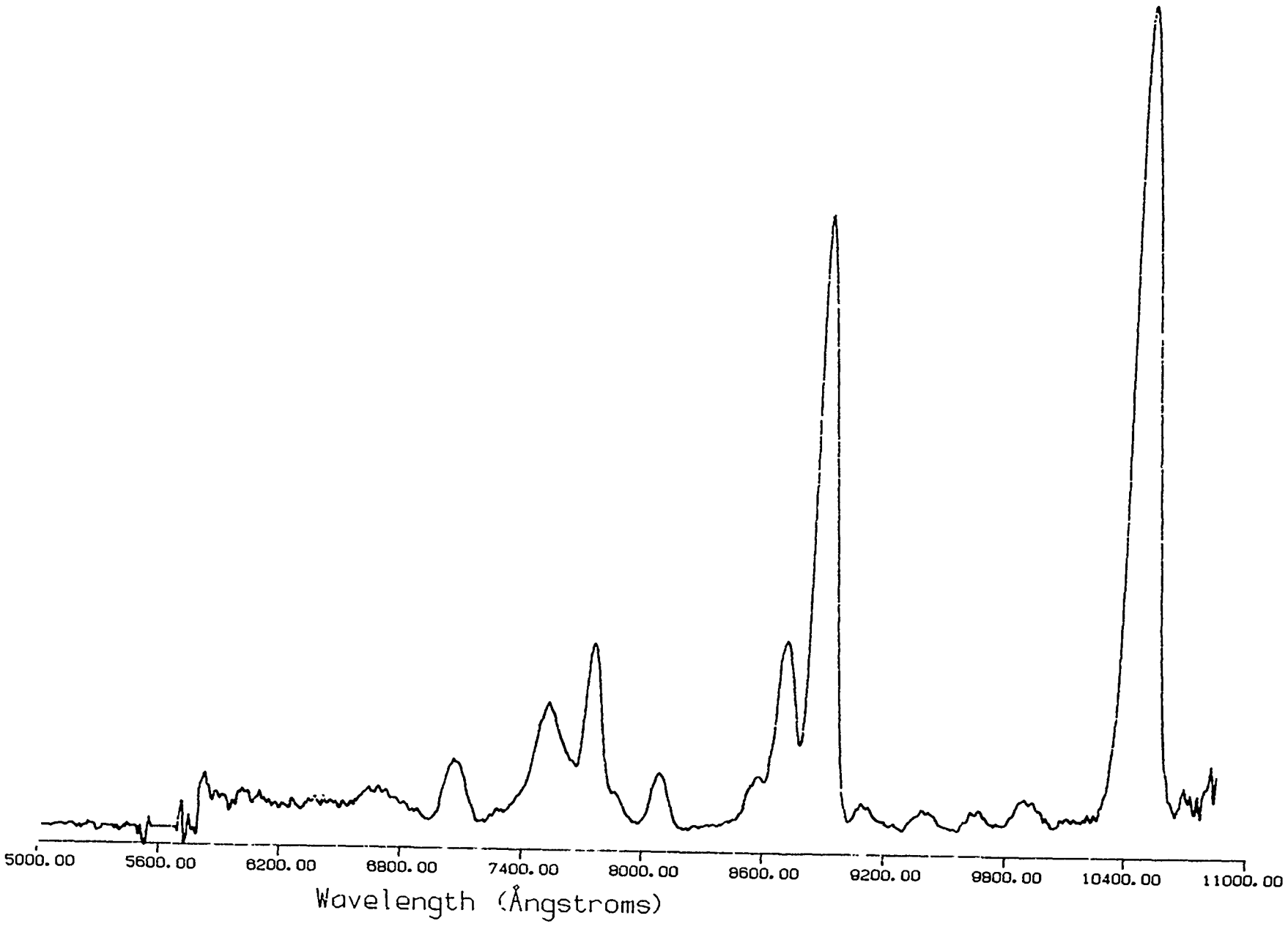
5000.00
5600.00
6200.00
6800.00
7400.00
8000.00
8600.00
9200.00
9800.00
10400.00
11000.00
Wavelength (Ångstroms)

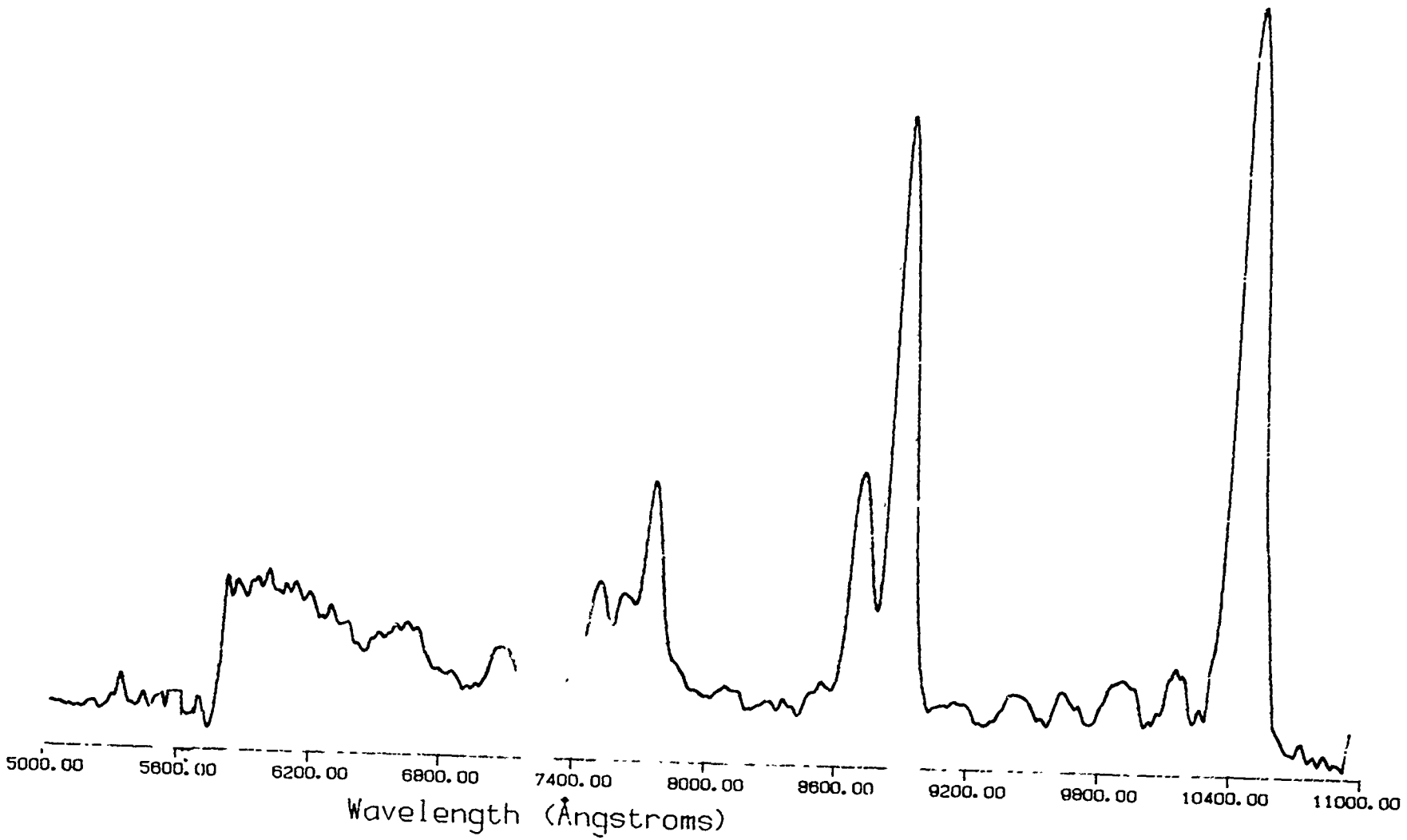
5000.00
5600.00
6200.00
6800.00
7400.00
8000.00
8600.00
9200.00
9800.00
10400.00
11000.00
Wavelength (Angstroms)

APPENDIX A

ABSTRACT

Title of Thesis: The Effect of Collisions and Plasma Preconditioning on the Vibrational Level Populations of Molecular Nitrogen

Jeff S Morrill, Master of Science, 1986

Thesis directed by: Dr. William Benesch, Professor
Institute for Physical Science
and Technology

Recent studies have shown the existence of an Intersystem Collisional Transfer Process that couples vibrational levels of adjacent electronic states. The present study has used a large volume, pulsed discharge to further our understanding of this process. Time-resolved spectroscopy has facilitated the analysis of the emission that occurs during and after the 4 microsecond excitation pulse. The primary spectrum of intrest has been the First Positive Group (1PG) of molecular Nitrogen. This spectrum reflects emission from the $B\,^3\Pi_g$ state of N_2.

The results have shown that dramatic changes in 1PG band intensities accompany the variation of experimental conditions. Specifically, the changes in the distribution of vibrational population in the $B\,^3\Pi_g$ state, are dependent largely on the number of collisions, regardless of pressure. A detailed analysis of these distributions during the first 20 microseconds is presented with the variation in pressure and frequency being from 50 to 400 microns and 5 to 50Hz, respectively. Other observations show that the emission from the vibrational levels of the $B\,^3\Pi_g$ state, continue long after expected, that is, relative to their natural lifetimes. The relationship between these observations and the Intersystem Collisional Transfer process is discussed.

Additional studies show that the initial $B\,^3\Pi_g$ state population distributions produced during the excitation pulse vary with pulse discharge frequency. Analysis of these initial populations gives strong indication the excitation is occuring from an elevated vibrational distribution within the ground state. Results imply that this ground state distribution is quasi-Boltzmann with vibrational temperatures of up to 2800 K.

THE EFFECT OF COLLISIONS AND PLASMA PRECONDITIONING ON THE VIBRATIONAL LEVEL POPULATIONS OF MOLECULAR NITROGEN

by
Jeff Stanley Morrill

Thesis submitted to the Faculty of the Graduate School
of the University of Maryland in partial fulfillment
of the requirements for the degree of
Master of Science
1986

TABLE OF CONTENTS

LIST OF TABLES

LIST OF FIGURES

LIST OF FIGURES

LIST OF FIGURES

PAGE

CHAPTER 4-SECTION (IV)

LIST OF FIGURES

LIST OF FIGURES

PAGE

APPENDIX A

CHAPTER 1 - HISTORICAL BACKGROUND and INTRODUCTION

The emission spectra of N_2 have been studied extensively in both the laboratory and in nature (Aurora). The initial studies, which started the determination of spectroscopic constants for N_2, began around the turn of the century.[1] This work has continued throughout the century and has extended into the present decade.[2] The spectra which have been studied are due to rovibronic transitions between pairs of electronic states. As a result of this work, researchers have compiled an extensive amount of information regarding the rotational, vibrational and electronic structure of the excited and ground states of the molecule N_2 and the ion N_2^+.

Recently, research has begun to focus on observations which indicate that collision induced transtions between quasi-isoenergetic levels of different electronic states can and do occur.[3-14] One of the spectra which researchers commonly observe in the study of this phenomnon is the First Positive Group (1PG). This corresponds to the transtion between the $B\,^3\Pi_g$ and the $A\,^3\Sigma_u^+$ states in the molecule. The 1PG comprises numerous vibrational bands which occur in the visible and extend into the infra red. This spectrum is of importance to the study of this phenomenon because of the proximity of the $B\,^3\Pi_g$ state to other excited electronic states of N_2 ($A\,^3\Sigma_u^+$, $B'\,^3\Sigma_u^-$, $W\,^3\Delta_u$, etc.; see figures 1 & 2). In this study we are able to detect changes in the relative intensity of the vibrational bands of the 1PG. Consequently, we are able to observe the redistrubution of excitation among these states. Further, when we follow the decay of a particular vibrational band, the effect of this redistribution on the population of the specific level is also observed. By changing the pressure of the system, the role of collisions in this redistribution can be determined.

Previous authors discussed this redistribution of excitation as a "secondary excitation process".[15] The term "afterglow" has also been used, and at times inconsistently.

POTENTIAL CURVES OF N2 & N2+

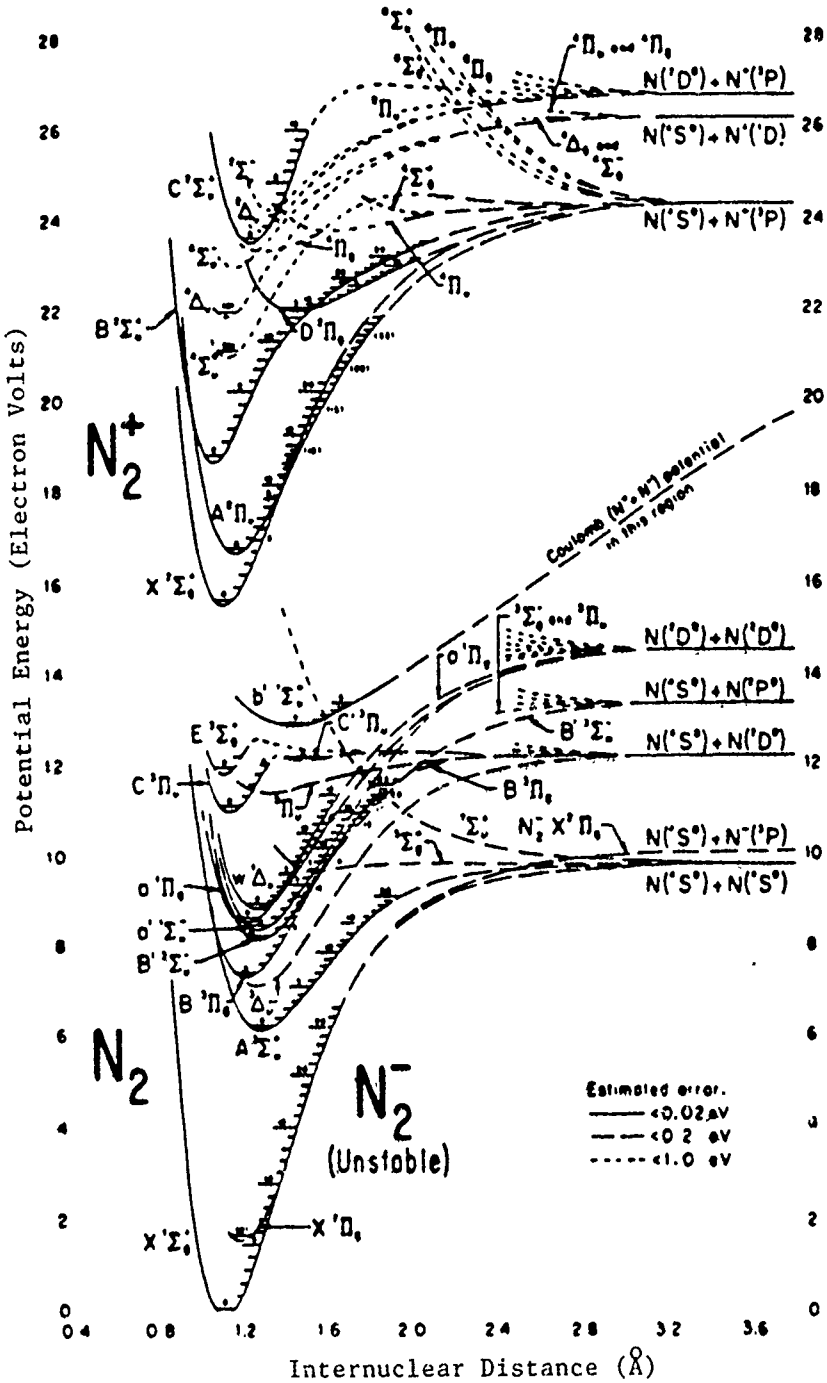

Figure 1

TRIPLET POTENTIALS

BETWEEN 6 & 12EV

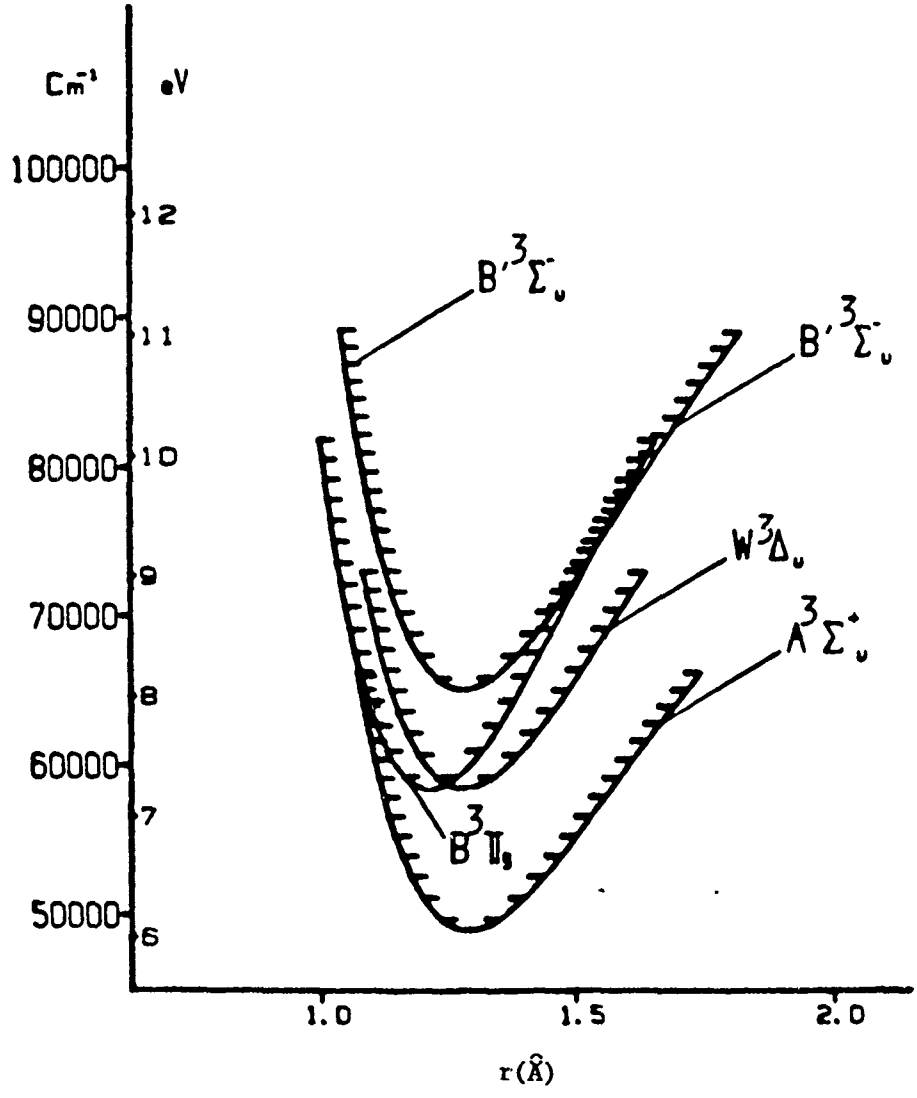

Figure 2

"Afterglow" has been used to distinguish between different regions in a long, flowing discharge where the entire length of the tube is not externally excited. The discharge region itself is referred to as the "glow". As the excited species flow down the tube, the spectra change. The region after the "glow" is called the "afterglow". This not a very rigorous definition and is used to cover a variety of experiments. One type of afterglow which is specific is the "Lewis-Rayleigh afterglow" (or L-R afterglow). This is due to the recombination of pairs of $N(^4S)$ atoms which form excited N_2 molecules. [16] The excited molecules which result are $B\,^3\Pi_g$ state molecules in the vibrational levels 10, 11 and 12. Consequently, the spectrum of an L-R afterglow is a 1PG spectrum which only shows emission from the high vibrational levels of the $B\,^3\Pi_g$ state.

In the past, the method used to generate the initial states associated with the observed transitions has generally been an electric discharge. Here, collisions between energetic electrons and N_2 molecules produce the myriad of states shown in figure 1. The extent to which each of these states is created is determined by the energy dependent cross-sections associated with each state and the energy distribution of electrons in the discharge.

Another method of excitation has involved electron beams. In this case electrons are emitted from a hot filament and then electrostatically focused and accelerated. This type of experiment has the advantage of being able to choose electrons of a specific energy with a certain bandwidth. The disadvantage with this type of experiment is that the system pressure must not exceed 10 to 100 millitorr.

Equipment of this type has also been used to measure the electron cross-sections mentioned above. Researchers studied these cross-sections as early as the 1920's and 30's[15] and continued into the 1960's and 70's. The most complete set of these cross-sections is given by Cartwright et al. in 1977.[17]

One of the earliest observations of the "secondary excitation process", mentioned above, was reported by Thompson and Williams in 1934[15]: at electron energies of 10.5 eV and greater "a red glow was seen to fill almost the whole of the collecting cylinder." This glow was the result of the 1PG. By looking down the length of the electron beam they were able to see that the emission was "spreading" away from the electron beam. The extent of this spreading from the beam was determined to be so great that the emission must be due a secondary excitation process.

Recent experiments have been more extensive than this earlier work. The work of Becker et al.[18] showed that the vibrational level populations of the $B\,^3\Pi_g$ state changed with discharge conditions, such as pressure and buffer gas. Electron beam studies by Shemansky and Broadfoot[19,20] and Shemansky[21] have shown that the decay of the vibrational levels of the $B\,^3\Pi_g$ state do not follow simple first order decay. Instead, emission from the levels of this state continue much longer than expected when we consider the natural lifetimes of these levels

In these latter studies the sole precursor for the so called "degenerate L-R afterglow"[20] was considered to be the $A\,^3\Sigma_u^+$ state. Other researchers have since shown that this is not the case.[14] This will be discussed further with the results of the present study.

The phenomenon of a long-time tail on the emission from the $B\,^3\Pi_g$ state has also been seen in experiments which monitor the emission from $B\,^3\Pi_g$ state molecules produced by a laser pulse. The authors of these Laser Induced Flourescence (LIF) studies have assumed that the decay curves can be expressed as sums of exponentials. This assumption has also been made by Shemansky. By dividing these curves into different time regions, they extracted the decay constants. These have been used to determine the rate constants for coupling the vibrational levels of the $B\,^3\Pi_g$ state with the levels of other excited electronic states. It has not been absolutely determined to which states and levels these

coupling constants apply.[5]

The most important result of LIF experiments is the emission from numerous levels that follows the pulsed laser excitation of a single level. In the work of Rotem and Rosenwaks the excitation of a specific vibrational level in the $B\ ^3\Pi_g$ state is followed not only by emission from the excited level, but also by emission from *lower* vibrational levels of the $B\ ^3\Pi_g$ state. In addition, and most important, emission also occurs from vibrational levels of overlapping electronic states which are energetically *adjacent* to the initially excited level.[8]

Other observations, using a DC discharge, have shown that adjacent vibrational level populations of overlapping electronic states are essentially equal if the pressure of the discharge is greater than about one torr. Benesch and Fraedrich have used this relationship to determine the transition probabilities of the infrared afterglow system ($B'\ ^3\Sigma_u^-$ to $B\ ^3\Pi_g$).[4]

All of these observations point to a collisional process which couples adjacent vibrational levels of overlapping electronic states. This process has been referred to by a number of names such as Resonance Collisional Transfer [14], Collisional Coupling [12] and Intersystem Collisional Transfer (ICT).[4, 7, 11] The term ICT will be used throughout this discussion.

In the present study we have used a large volume, pulsed-discharge tube with a 4 μs, high current, excitation pulse. This system has allowed time-resolved measurement of the vibrational level populations of the $B\ ^3\Pi_g$ state over the range of 0.5 to 200 μs. One of our initial observations in this study has been the different emission curves which arise from the decay of different excited states. A similar type of observation is of the long-time decay of specific vibrational bands of the 1PG. These two topics are discussed in sections II and III of the results.

A major objective of this study has been to measure the change in the vibrational population distribution in the B $^3\Pi_g$ state as a function of time during and after the current pulse. Preliminary studies in our laboratory have shown pressure and pulse-discharge frequency to be the two most significant discharge parameters regarding changes in the B $^3\Pi_g$ state vibrational distributions. Consequently, the major portion of data presented reflect the effect of these two parameters on the vibrational level populations of the B $^3\Pi_g$ state. The difference between these two parameters can be seen if we recognize the connection of collision frequency with pressure, and relaxation time with pulsed discharge frequency. This is discussed in section IV of the results.

Finally, the effect of discharge frequency on initial spectra will be discussed. This effect, known as "pre-conditioning", causes changes in the initial vibrational distribution in the B $^3\Pi_g$ state with changes in pulse-discharge frequency. The observed change appears to be associated with an increase in the vibrational temperature of the ground state. This process of "pre-conditioning" will be discussed in the last section of the results of this study.

In the next two chapters the discharge system and the experimental set up will be presented, followed by a discussion of some of the processes which occur in an electric discharge.

CHAPTER 2 - EXPERIMENT

The details of this experiment will be discussed in four parts; the light source, the spectrometer, the electronics and the system calibration. A block diagram of the system appears in figure 3.

LIGHT SOURCE

The light source used is a large volume, pulsed discharge tube which was designed and built at the University of Maryland. As shown in the block diagram (see figure 3), this discharge tube consists of a DC power supply, a high current supply and the discharge tube itself.

The DC power supply comprises a variac controlled AC step-up transformer capable of supplying 5 amps at 5 kV and a tube type rectifier (Fedral Telephone and Radio Corp., model CT-T-20208-A) used to generate the DC voltage. The specified output voltage is further regulated by a 4 μf/20 kV ballast capacitor.

The high current pulse supply is fairly simple in theory. Its main components are (1) an induction coil for doubling the input voltage, (2) a set of four, 1000 foot, coaxial cables (RG-8) used to store the charge for each current pulse and (3) a Thyratron (EG&G, HY-5) used to discharge the four coaxial cables through the discharge tube. A basic schematic diagram of the High Current Pulse Supply is shown in figure 4.

Once the cables are charged, a positive pulse is applied to the grid of the thyratron. This voltage pulse produces a discharge within the thyratron which connects the cables to the anode of the discharge tube. The resulting current pulse through the discharge tube, has a very sharp rise time (<1 μs). In order to shut off the thyratron a negative reflected wave must be generated by the discharge (the load). For this to happen the current must reach levels >300 amperes and the resistance the discharge tube must drop

Figure 3 - EXPERIMENT-BLOCK DIAGRAM

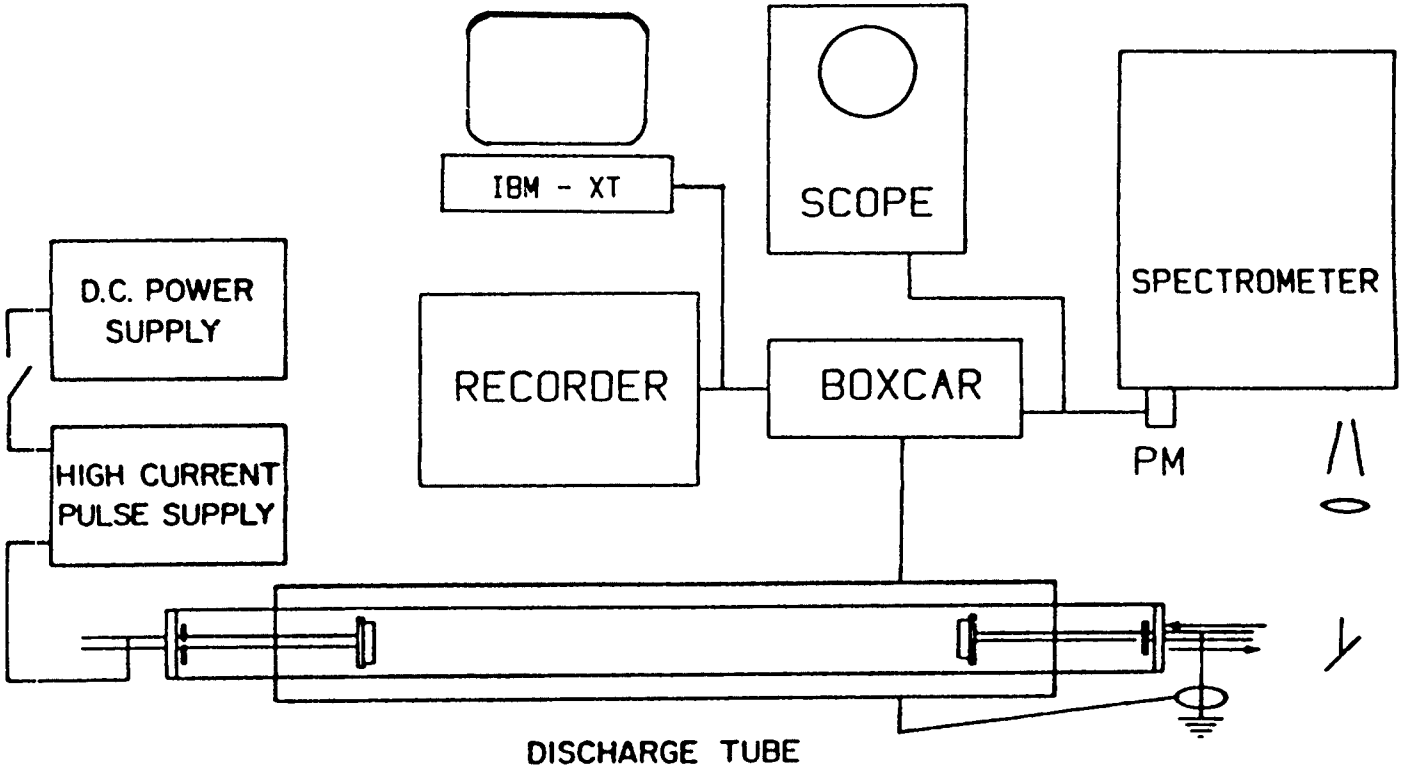

Figure 4 - **Schematic of High Current Pulse Supply**

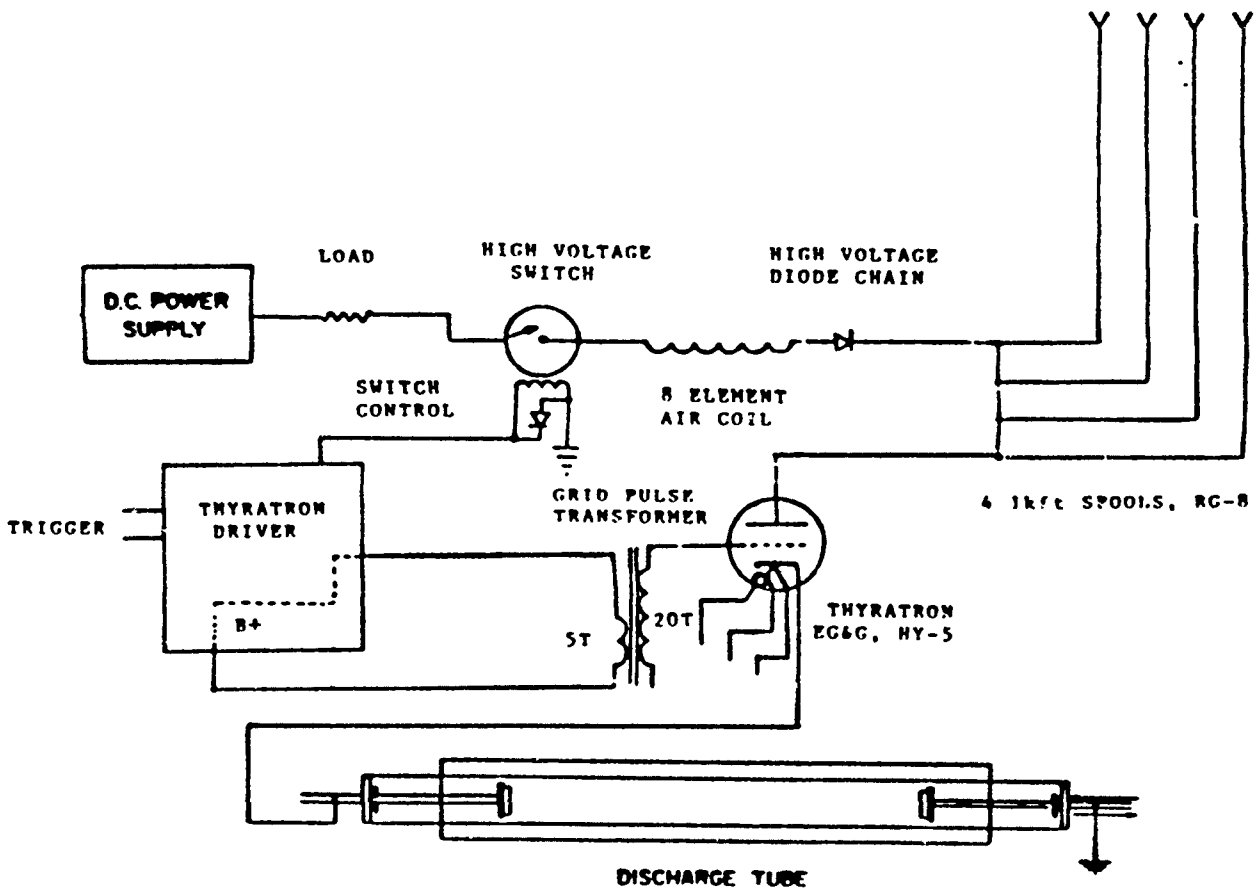

below a few ohms. When these conditions are met the current pulse produced is about 4 μs long. The effect of the negative reflected voltage is to change the polarity of the thyratron. This causes the discharge within the thyratron to cease, which in turn disconnects the cable from the anode of the discharge tube. This is necessary since the cables must be recharged for the next current pulse.[22,23]

If these conditions are not met the thyratron will "latch on". The result is a large surge of current through the discharge tube followed by blown fuses, tripped circuit breakers and often ruined electronic parts. In order to ensure the reproducibility in the current pulse necessary to prevent the thyratron from "latching on", 20 mesh granular Zinc is used as a cathode start up material. This material gives the cathode a vast array of rough edges from which electrons can emit and begin each discharge pulse. [23]

The light source itself is a glass tube 300 cm in length and 16 cm (ID) in diameter with Conical ends. There are also three 2.5 cm (ID) glass side arms mounted at various points along the length of the tube. The tube itself is mounted length wise in a plexiglas tank which contains water for cooling. The three side arms are approximately 18 cm in length and extend out of the top of the plexiglass tank. The central side arm is the exhaust of the discharge tube and the side arm at the cathode end of the tube is a port for measuring pressure.

The end pieces which cap either end of the tube are machined aluminum. These end pieces contain White cell mirrors and windows as well as electrical feed throughs for the electrodes.

The electrode assemblies are copper cylinders 12 cm in diameter, 0.25 cm thick and 3 cm high. These are welded to copper disks which are water cooled. The centers of these disks have been cut away so that light emitted along the axis of the discharge tube can be observed. Each of these assemblies is mounted on a two piece concentric copper shaft so that each electrode assembly extends into the tube about 50 cm. This positions the

electrodes directly below the two outer glass side arms.

Nitrogen gas is allowed to flow into the aluminum end piece at the cathode end of the tube. By varing the N_2 gas flow rate into the system and by throttling the exhaust, we are able to achieve the different system pressures. The flow rate is adjusted by use of a Brooks flow tube (model R215-D) with the flow rate measured in SCCM, (std. cc/minute@ 1psig). A set of two different sized valves are used to throttle the exhaust. The combination of these two valves allows us to maintain very good pressure control throughout the course of an experiment ($\pm$3%).

The pressure in the system was measured with a Vacuum General Capacitance Manometer (model CMT-01). This model reads pressure from 0.0001 to 1 torr with an error of 0.15 % of reading and was zeroed at less than 10^{-4} torr.

As mentioned, the current pulse produced by the system is approximately 4 μs long, regardless of the peak current, voltage, or pressure. The rise and fall time of the pulse becomes less sharp as the system is run at higher pressure. This tends to spread the current pulse at the base. An example of this is shown in figure 5.

Also shown in this figure are the voltage traces associated with the discharge at the indicated pressures of 50, 200 and 400 μ of N_2. One should note that in each photo the voltage trace shows a distinct plateau between 2 and 3 microseconds. The ratio of this plateau voltage to the peak current is taken to be the resistance of the discharge. Figure 6 shows that these values increase linearly with pressure. Assuming the gas is ideal, this indicates that the discharge resistance varies linearly with gas density as well.

Another trend which we see is that the peak current changes significantly with pressure. Here the observation is that for a given peak voltage the peak current decreases with increasing N_2 pressure. This is shown in figure 7. This observation

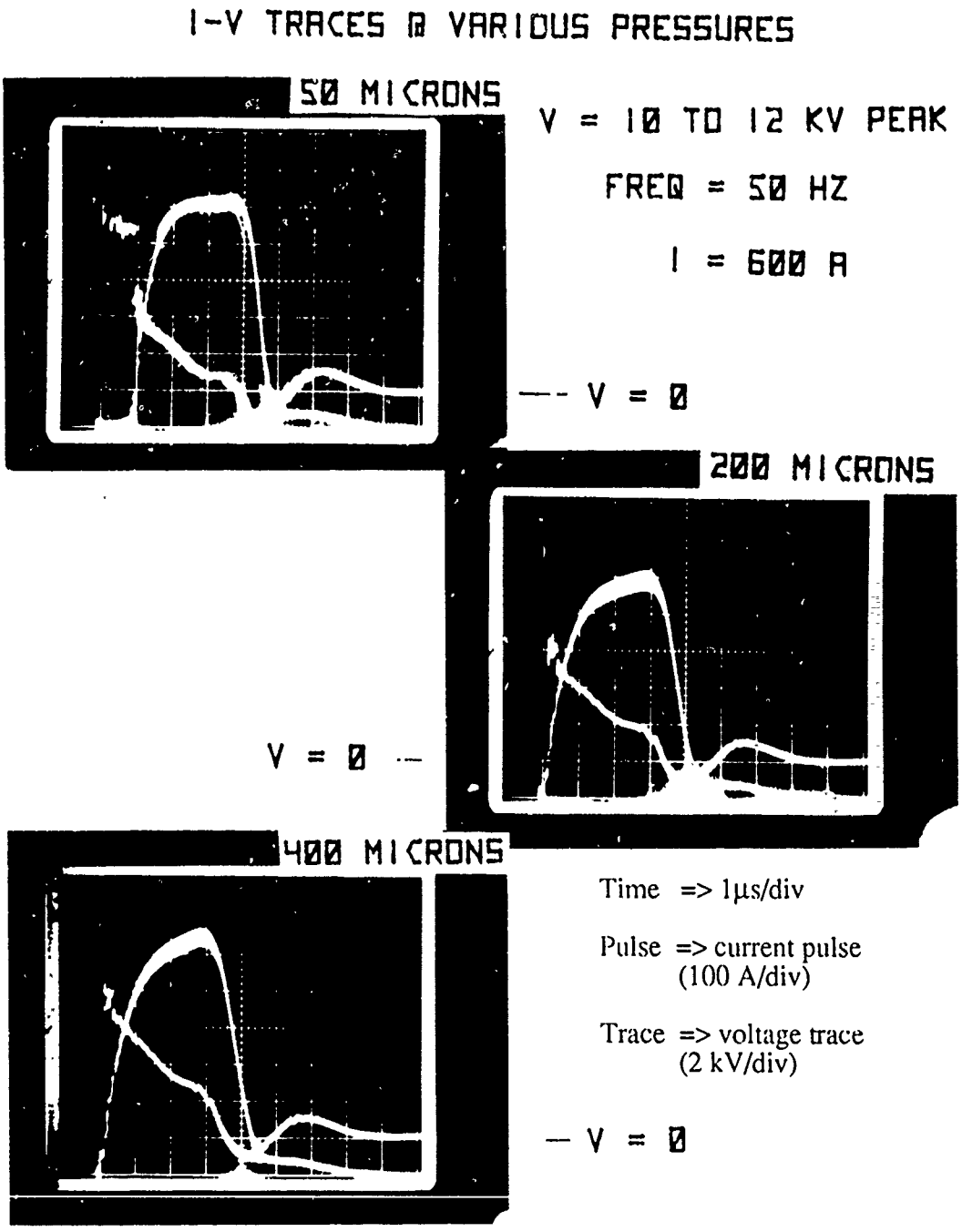
I-V TRACES @ VARIOUS PRESSURES
50 MICRONS
V = 10 TO 12 KV PEAK
FREQ = 50 HZ
I = 600 A
V = 0
200 MICRONS
V = 0
400 MICRONS
Time => 1μs/div
Pulse => current pulse (100 A/div)
Trace => voltage trace (2 kV/div)
V = 0

Figure 5 -

Figure 6 - DISCHARGE RESISTANCE(V/I) VS PRESSURE N2

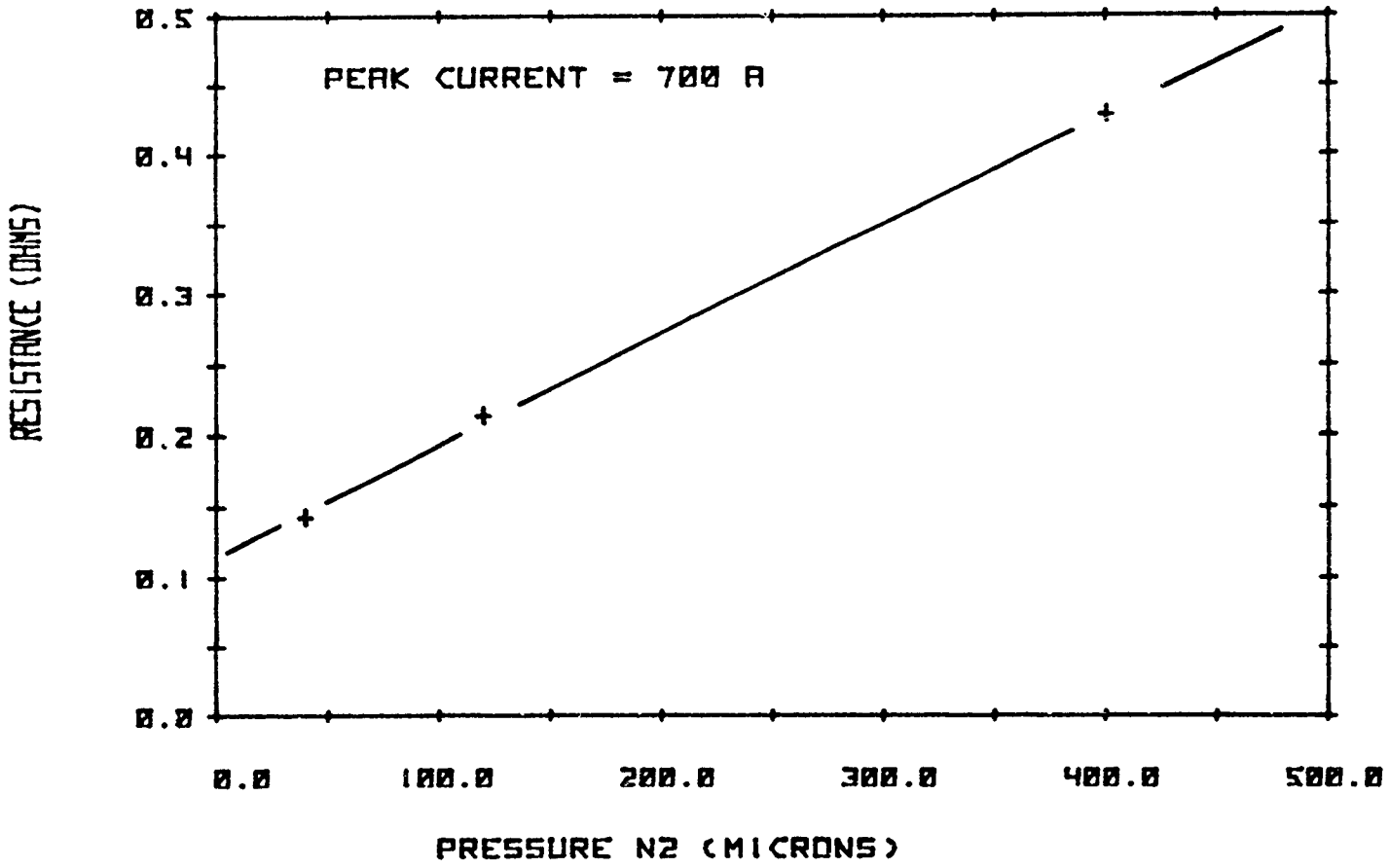

Figure 7 - PEAK DISCHARGE CURRENT VS PRESSURE N2

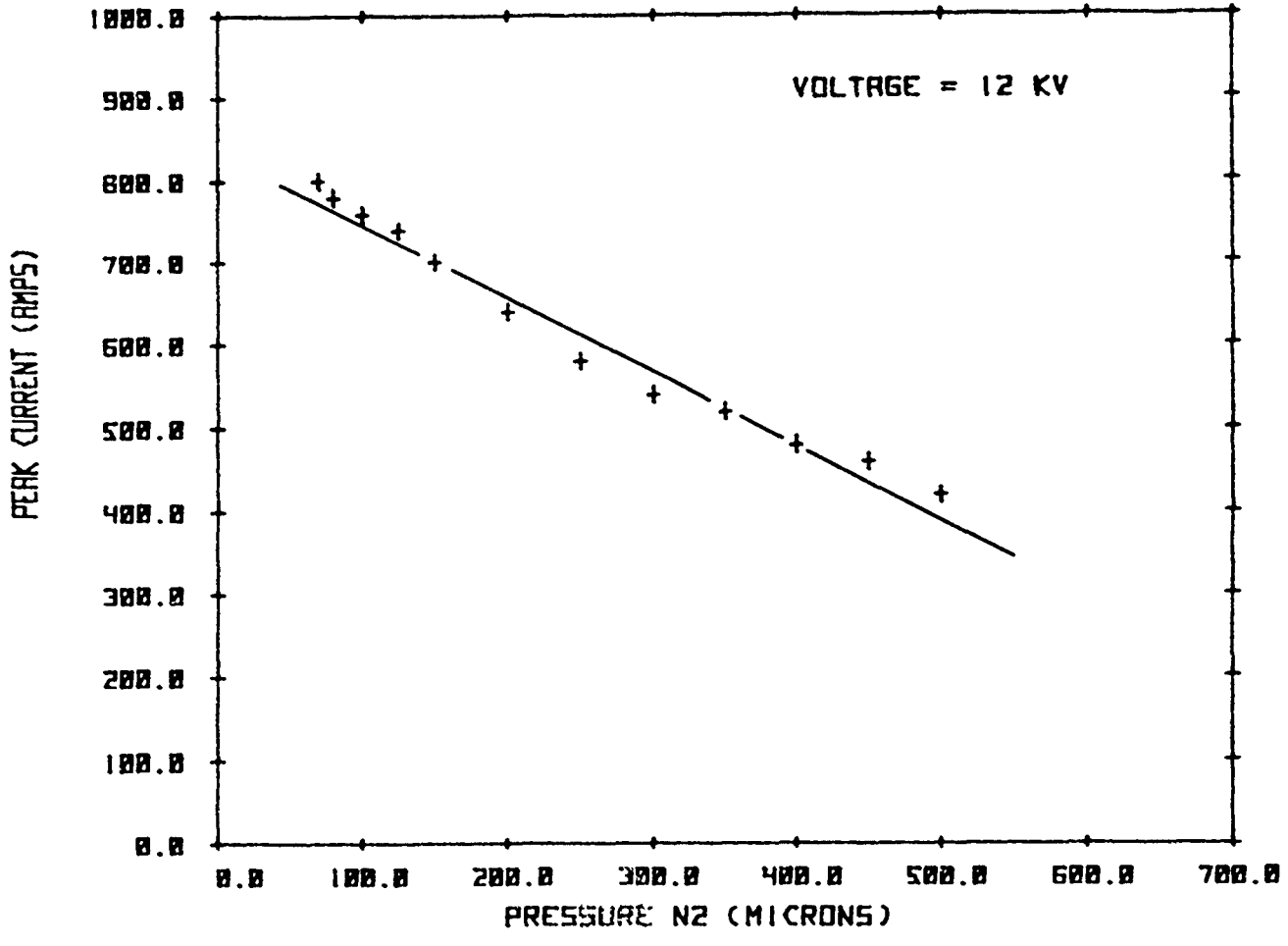

agrees with the observed increase in discharge resistance with increasing pressure.

SPECTROMETER

Light which is emitted along the axis of the discharge tube is focused on the entrance slit of a 2 meter spectrometer. The spectrometer is equipped with a 600 groves/mm, motor driven, grating. The grating drive is known as a "sine drive". The sine drive gets its name from the fact that linear movement of one component of the drive can be related to the sine of the angle through which the grating has moved.

In this system, the moving component is a metal plate which is driven by a finely machined, motor driven, lead screw. A lever arm is attached to the top of the main shaft, to which the grating is mounted and around which the grating turns. The tip of this arm rests against the metal plate of the sine drive. As the metal plate is driven by the lead screw, the lever arm is pushed foward which in turn causes the grating to rotate. The arrangement is set so that the linear displacement of the metal plate is directly proportional to the sine of the angular displacement of the grating.

The advantage of this system can be seen if we examine the grating (or Bragg) equation.

$$n\lambda = d\sin\theta$$

Here n is the order, λ is the wavelength, d is the line spacing of the grating and θ the angle of the grating normal with respect to the incident light. With a sine drive the $\sin\theta$ term can be replaced with a linear relationship, mX +b. Now the equation becomes,

$$n\lambda = (mX + b)$$

were X is the displacement of the metal plate, m a coefficient and b an initial offset.

In order to measure the position of the metal plate, we have fitted the sine drive with a digital shaft encoder. This shaft encoder is attached to a small output shaft on the sine drive. This shaft is connected to the lead screw through a series of gears. A shaft encoder gives a digital output for both the degree of rotation as well as the number of revolutions of the output shaft. The digital output of the shaft encoder is fed into a I/O board in an IBM-XT computer. Software converts the digital signals into numerical values. Shaft encoder values associated with the peaks in a spectrum of a standard lamp, were compared with the known wavelengths of those peaks. By doing so, we have determined the relationship between shaft encoder values and wavelength. This is discussed further in the calibration section of this chapter.

ELECTRONICS

As mentioned previously, light which is emitted along the axis of the discharge tube is focused on the entrance slit of the spectrometer. After the light is dispersed it is then focused on the exit slit of the spectrometer. There it is detected by a photomultiplier tube (Hamamatsu, type R-636). The photomultiplier tube is generally driven by a voltage of 900 to 1300 volts. The output feeds into a PAR 115 preamplifier (50 ohm termination, DC input) and preamplified 10 times. The preamp output is then fed to a PAR 160 Boxcar Integrator and an oscilliscope.

The Boxcar Integrator, which averages repeated waveforms, has been used in our study in two modes. In the first mode we set the spectrometer to a specific feature in the spectrum and the repeated pulse is fed into the Boxcar. By scanning along this pulse with the Boxcar gate, the Boxcar Integrator is able to reproduce this pulse on chart paper or as a computer file. An example is shown in figure 24. The Boxcar gate (or aperture) determines the portion of the waveform which the Boxcar amplifies. The gate is the small

spike which appears at 5 μs in figure 34a. The size of the Boxcar gate was generally 200ns as shown in figure 34a.

For the second mode, we have set the Boxcar gate at a specific time after the start of each current pulse. Here the spectrometer is scanned over a specified region of wavelength. The result in this case is a spectrum of the discharge characteristic of the position in time of the Boxcar gate (see figure 14).

In order to store and evaluate the large volume of data presented in this study it was necessary for us to incorporate an IBM-XT computer into the experiment. This was done by measuring the Boxcar output with an A-to-D converter which was read by the computer. When the spectrometer is scanning, the wavelength is determined by use of a shaft encoder. By using the digital output from the shaft encoder and the A-to-D converter, spectra from the Boxcar were stored as computer files. These were plotted and processed using software written specifically for this system. This greatly facilitated calibration and evaluation of the spectra.

WAVELENGTH CALIBRATION

In order to calibrate the spectrometer for wavelength we have taken the spectrum of a standard Mercury. This spectrum appears in figure 8. A wavelength calibration curve was generated by using the resulting list of measured intensities and associated shaft encoder values. The peaks in the measured intensities were identified by comparing spectra supplied by the manufacturer of the lamp with expanded versions of figure 8. This presented a bit of a challenge in that overlapping orders, which were excluded in the manufacturer's spectrum, were included in the calibration spectrum. As a consequence we were unable to use all peaks in the calibration since all peaks were not identified. The final set of data consisted of 39 pairs of values and covered a range of 10,000 Angstroms, not including zero order.

Figure 8 - Hg Wavelength Calibration Spectrum

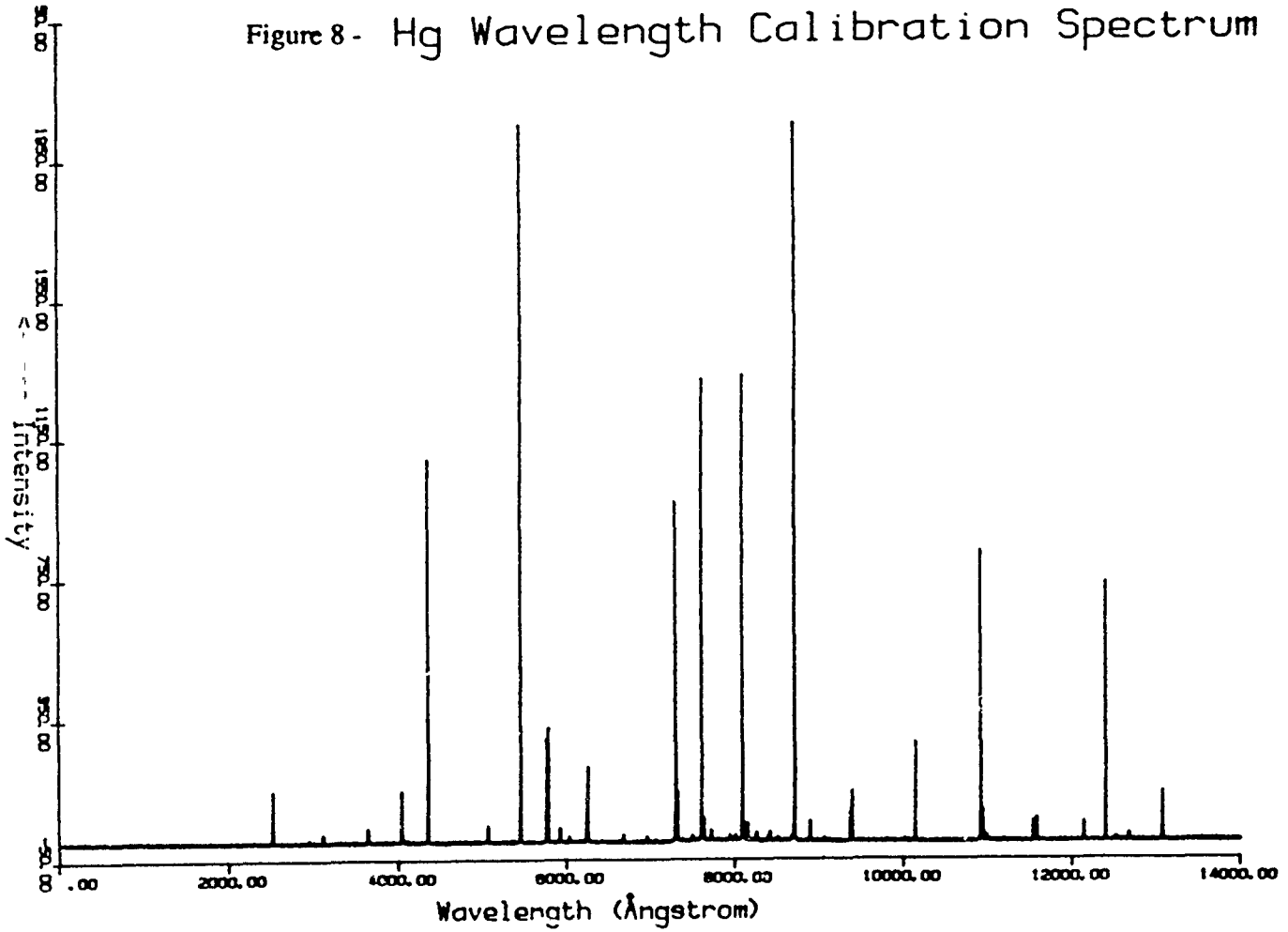

It was shown that by use of a sine drive the grating equation could be expressed as a linear function of displacement. In order to compensate for any inherent non-linearities in the drive system, we fit the calibration data to a second degree polynomial. The resulting polynomial has the following form:

$$\lambda = A + B(X) + C(X)^2,$$

were

$$X = \text{shaft encoder value},$$

$$A = -25.87,$$

$$B = 1.518,$$

$$C = 5.936 \times 10^{-7}$$

and

$$\lambda = \text{first order wavelength (Angstroms)}.$$

This equation is used in the routine which plots the spectra as well as the routine which evaluates the populations. This polynomial results from a leasts squares fit of the calibration data. The residuals are defined as the difference between the predicted value and the measured value. For the final set of data the residuals were on the order of $\pm$ 0.6A and no greater than $\pm$ 1.7A .

The resolution of the data collection system, for wavelength values in the 5000 A to 10,000 A range, is about 1.5 Angstroms/shaft encoder value. This is shown by the 1st degree coefficient (B = 1.518).

INTENSITY CALIBRATION

One of the major objectives of this study has been the measurement of the populations of the B $^3\Pi_g$ state as a function time at a number of different discharge conditions. In order to do so, the associated time resolved spectra must be corrected for the non-linear sensitivities of the spectrometer, photomultiplier, and focusing optics. This is

accomplished by use of a Black Body Oven at 1273 K ± 1 K (Barnes Engineering Co., model 11-201T). A spectrum was taken of the Black Body Oven put in place of the light source thus calibrating the entire optical system as a unit. The resulting spectrum was stored as a file and is shown in figure 9.

A computer program was used to generate a black body curve on the same wavelength scale as the calibration spectrum. This black body curve was produced using the equation,

$$M(\lambda) = \frac{2\pi hc(\lambda)^{-5}}{\exp(hc/\lambda kT) - 1},$$

where λ = wavelength (Angstroms). This quantity is referred to as the "spectral concentration of radiant exitance of wavelength λ."[24] The resulting black body curve was normalized so that its peak was unity. This puts the Black Body curve on a relative energy scale and is done merely for convenence. To determine the relative number of photons being emitted at a given wavelength, for a given temperature, the equation for $M(\lambda)$ must be divided by the energy per photon, $h\nu$ or hc/λ. The resulting curve is referred to as the photon flux curve.

The calibration curve results from the ratio of the photon flux curve to the Black Body spectrum. These computer files are plotted in figures 10 and 9, respectively. Since we have not sought absolute measurements, this calibration curve has been arbitrarily set equal to unity at ~8000 Angstroms. Calibration involves the point by point multiplication of spectra by this calibration curve. Since both the spectra and calibration curve are computer files, this multiplication takes place within a computer program. This converts these spectra from units of relative signal to relative numbers of photons. All spectra were zeroed and calibrated before analysis of the populations was performed. The calibration curve appears in figure 11.

Figure 9 - Black Body Spectrum @ 1273 K

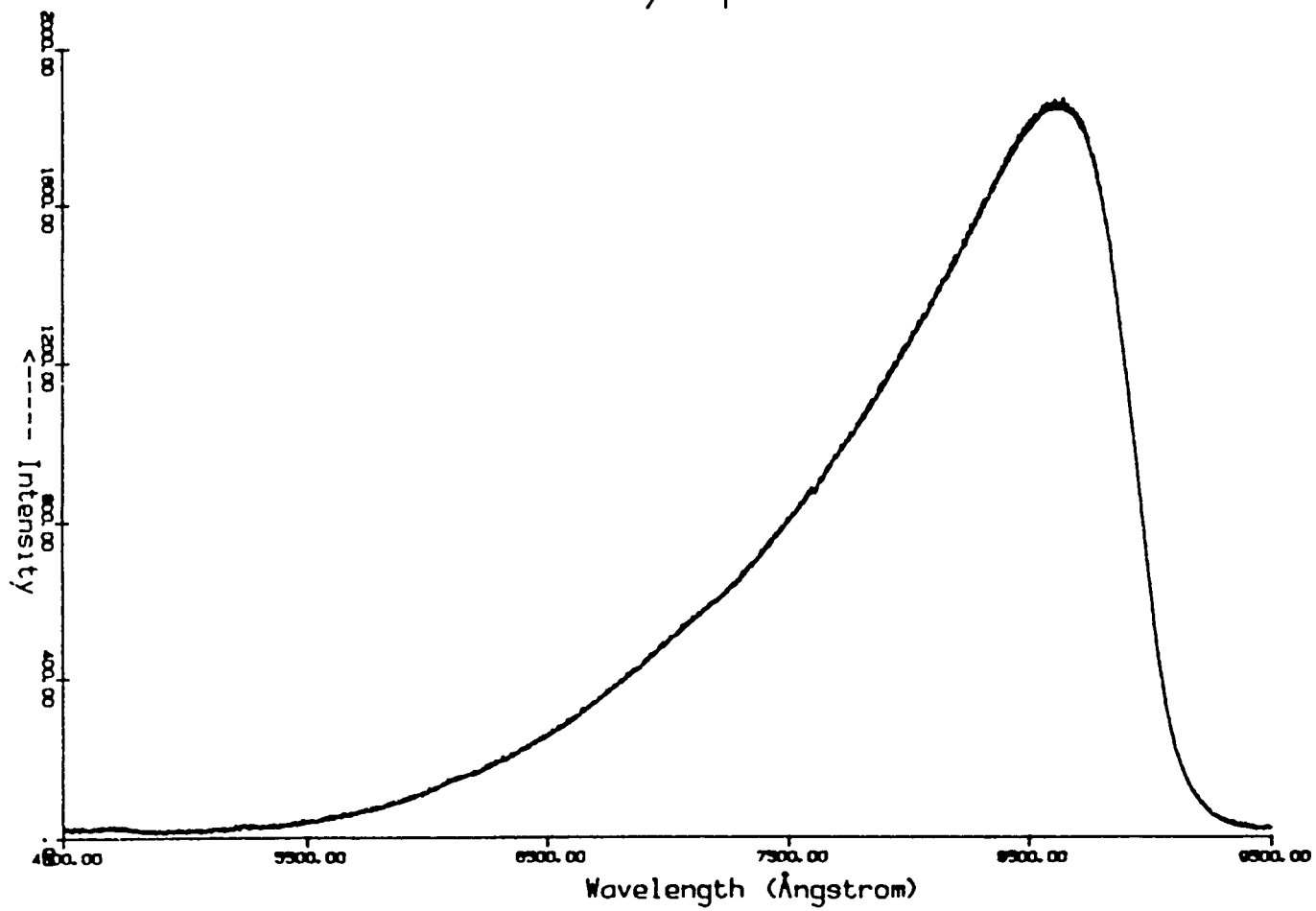

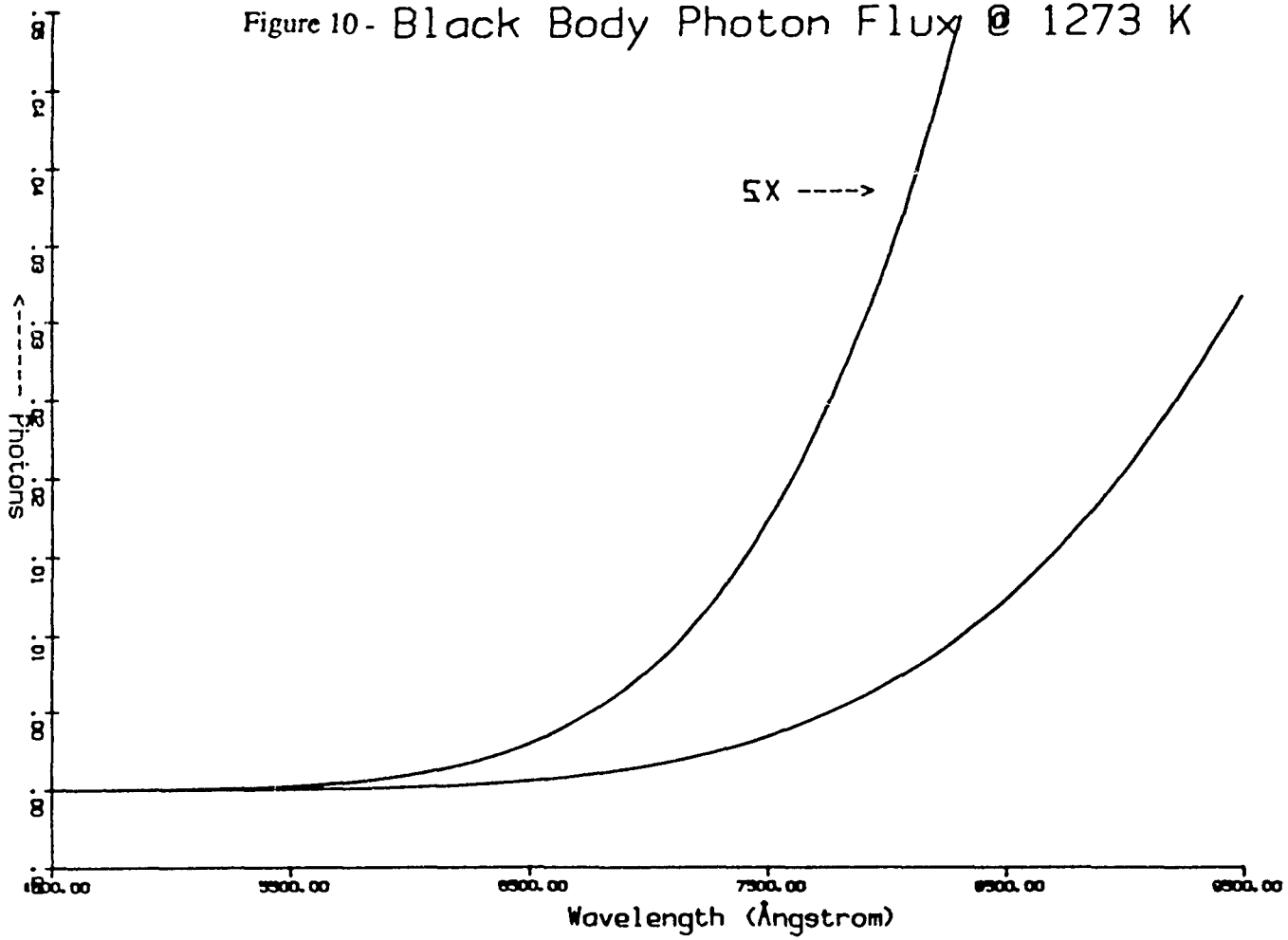
Black Body Photon Flux @ 1273 K
5X ---->
<------ Photons
Wavelength (Ångstrom)

Figure 10 -

Figure 11 - Calibration Curve for 1PG Spectra

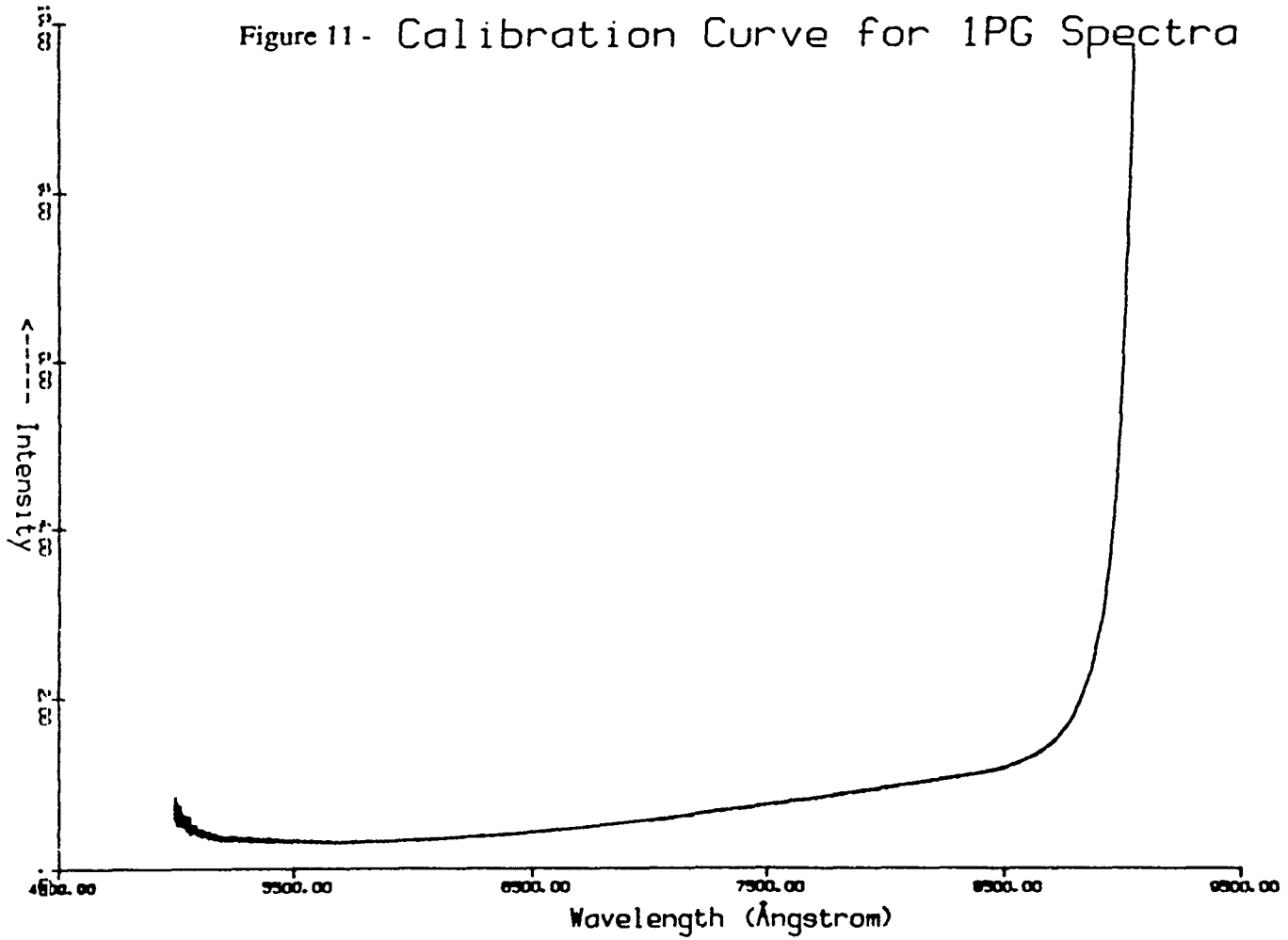

CHAPTER 3 - PROCESSES IN A DISCHARGE

In this section, brief reviews of some of the processes occuring in a discharge are presented. These processes are divided into two groups, primary and secondary excitation processes. In this discussion primary excitation processes are those which are due to excitation by energetic electrons in the discharge. These are the processes which occur during the current pulse but would be occuring continuously in a DC discharge. Secondary excitation processes are those which occur after the current pulse and are generally due to collisions involving excited species in the gas. These would also be occuring continuously in a DC discharge. The fact that these processes occur in two different time regimes in a pulsed discharge allows them to be studied separately. Using this separation and time resolved measurement, the effects of discharge parameters on both the initial excitation and subsequent relaxation can be independently observed. The following list is by no means complete, nor have all of these processes been examined in this study. They are presented both to reflect a review of the literature as well as address the complexity of the medium under study.

PRIMARY EXCITATION PROCESSES

I. Direct Electctron Excitation - This refers to the process where energetic electrons in a discharge excite a molecule from its initial electronic state to a final, higher energy, electronic state. The Born-Oppenheimer approximation is applied in this process. This states that during an electronic transtition the electronic rearrangement occurs much more rapidly than does the nuclear motion (rotation or vibration).

For cases where the final state in this transition is an attractive potential, two things happen. First, the vibrational distribution which results within a given potential, is largely governed by the overlap between the initial and final vibrational wavefunctions (Franck-Condon Principle). Second, the rotational distribution remains

virtually unchanged and initially reflects the rotational spacing of the initial electronic state.

The relative population of the various excited states depends on the energy dependent cross sections for these states as well as the electron energy distribution in the discharge.[17] The result of this process is the production of the various singlet and triplet states shown in figure 1.

II. Dissociation- For the case where final state produced by direct elctron excitation is a repulsive potential, the molecule will dissociate. The result of this process is the production of N atoms. [25]

III. Ionization - If the electron energies in the discharge are high enough, then ionization will occur. Again, the Franck-Condon Principle and the Born-Oppenheimer approximation apply. Therefore the rotational and vibrational distributions will behave as discussed under Direct Electron Excitation. [25]

The result of this process is the production of positive ions and electrons. These play an important role in the maintenance of the quasi-neutrality of the discharge. During the 4 microsecond current pulse (~700 amps) approximately $2x10^{16}$ electrons flow through a cross-section of the discharge tube. The amount of ionization which occurs will have to be large enough to balance electron loss processes and satisfy the relationship, N(ion) ~ N(electron). [26]

IV. Vibrational Excitation within the Ground State - Excitation of the first few vibrational levels in N_2 has been examined in a number of studies. Electron beam studies by Schultz[27] have shown that vibrational levels up to V = 8 are populated by electrons with energies in the range of ~1.5 to ~3.5 eV. The measured vibrational cross-sections oscillate as a function of energy. In addition, the peaks in these cross-sections occured at different energies for the different vibrational levels. These results complied with calculations based on a negative ion intermediate, N_2^-.

$$N_2(X\,^1\Sigma_g^+, V=0) + e^* \rightarrow [N_2^- (X\,^2\Pi_g, V=0)] \rightarrow$$
$$\rightarrow N_2(X\,^1\Sigma_g^+, V=1 \rightarrow 8) + e \quad (1)$$

It is not unreasonable to expect that as the levels greater than V=0 become populated, that vibrational excitation by electrons would occur from these levels also. Once produced, collisions between vibrationally excited molecules will tend to further populate the high vibrational levels of the ground state.

Massabieaux et al.[28] have presented results of calculations showing the expected ground state vibrational distributions as a function of residence time in a flowing N_2 discharge. These results indicate that, initially, as the residence time increases the distributions remain Boltzmann but with elevated vibrational temperatures. For longer residence times (15 to 50 ms) the distribution becomes less Boltzmann and shows the presence of a plateau or over-populated tail. This tail is from about V = 20 to V = 40. By over populated tail they mean that the high vibrational levels are populated to a larger extent than would be expected were the distribution Boltzmann and based on the population of the first few levels.

Other work by Anketell and Brochelhurst [29] show experimental results using a weak microwave discharge to excite the ground state vibrational levels. This was followed by subsequent RF excitation at various distances down a flow apparatus. Their data showed changes in the B $^3\Pi_g$ vibrational distribution which corresponds to direct electron excitation from a ground state vibrational distribution with an over populated tail An example of an over populated tail is shown in figure 12.

SECONDARY EXCITATION PROCESSES

I. Radiative Cascading - A number of transtions between excited states in N_2 are such that the lower state of one transition is the upper state for another transition. One

VIBRATIONAL DISTRIBUTIONS IN N2(X) STATE

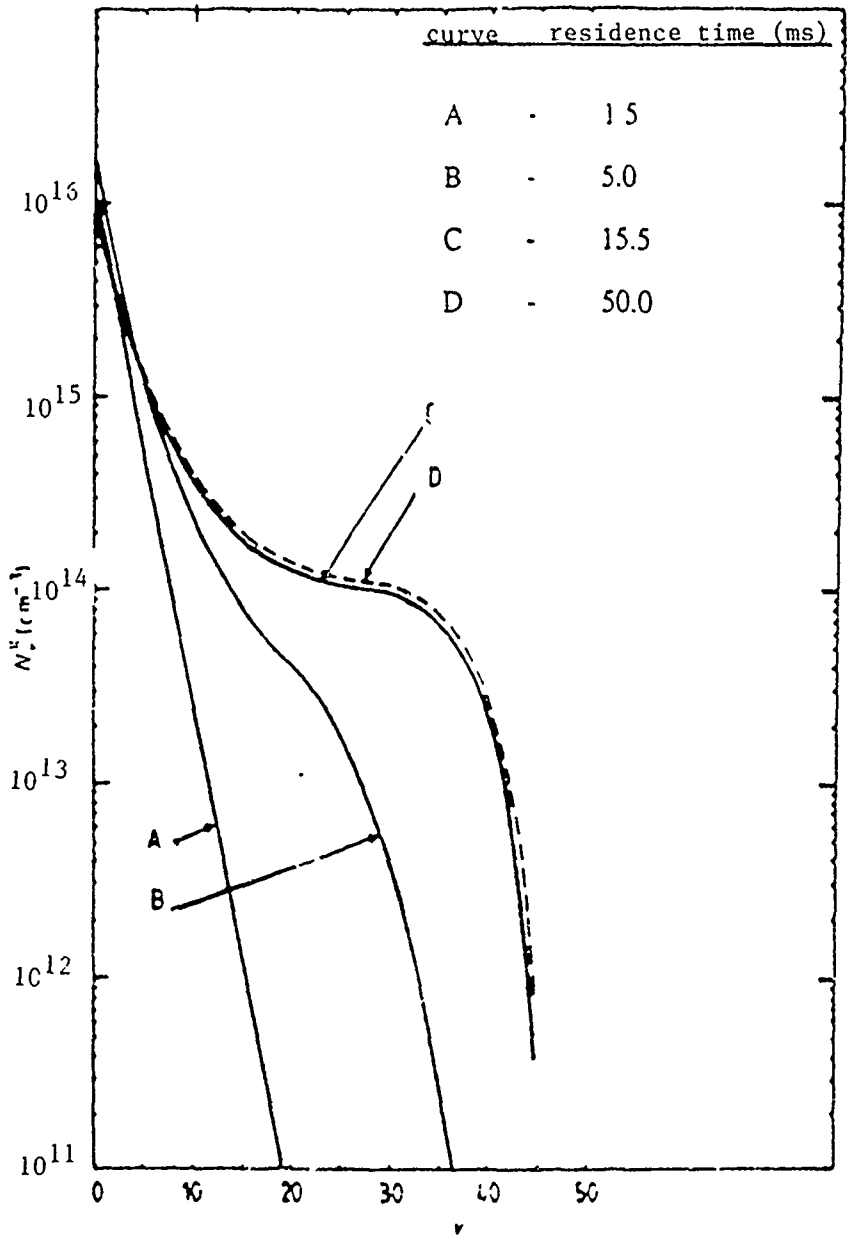

Figure 12 -

example is the 2PG ($C\ ^3\Pi_u$ -> $B\ ^3\Pi_g$), feeding the upper state of the 1PG ($B\ ^3\Pi_g$ -> $A^3\Sigma_u^+$). An important point in this case is that the 2PG does not feed all vibrational levels of the $B\ ^3\Pi_g$ state equally. Because the largest contibution is into the V = 0 thru 4 levels[30, 31], this cascade cannot be used as an explaination for the shape of the 1PG emission curves (see Results III). Basically the 1PG emission curves all have the same shape. If cascading from the $C\ ^3\Pi_u$ state had a significant effect, the 1PG emission curves of the lower vibrational levels of the $B\ ^3\Pi_g$ state, would have a different shape compared to those of the higher levels. This is not the case. This point will be discussed in more detail in the second section of the results.

II. Ion-Electron Recombination -The most important recombination process is dissociative recombination. This occurs when the incoming electron has sufficient energy to excite an electron in the ion onto a repulsive potential of the molecule. Then, in turn, the incoming electron is captured by an unoccupied molecular orbital of the resulting molecule. The molecule then dissociates along the repulsive potential: the result of this process is more N atoms. Recombination rate constants for N_2^+ are on the order of 10^{-7} cc/sec. This is about 10^{+5} times faster than for other recombination processes such as radiative recombination.[25]

III. N Atom Recombination - As shown above, there are a number of processes which contribute to the concentration of N atoms in the systems; Dissociation and Ion-Electron recombination. The N atom recombination process is reported to be a two body process below 1 torr. The mechanism which is reported is:

$$N(^4S) + N(^4S) \text{ --> } [\ N_2[\ ^5\Sigma_g^+\ )] \text{--> } N_2(B\ ^3\Pi_g, V=13) \qquad (2)$$

with a rate constant of,

$$k(2) = 1.6 \times 10^{-19} \text{ cc/ molecule-sec.}^{18}$$

There have been other mechanisms proposed which do not inculde the $N_2(\ ^5\Sigma_g^+\ )$ state but

rather the $N_2(A\,^3\Sigma_u^+)$ state.[21]

Regardless of the mechanism, as spectra are taken further from the discharge pulse, the effect of N atom recombination will become important in the 1PG. During this study no spectra were taken beyond 200 μs and it appears that recombination has had no significant contribution in these spectra. None-the-less, as spectra are taken at later times this process should become the predominant source of $B\,^3\Pi_g$ state molecules and consequently 1PG emission.

IV Energy Pooling - This term has been used in the literature to refer to the following types of reaction:

$$N_2(A\,^3\Sigma_u^+) + N_2(A\,^3\Sigma_u^+) \text{-----}>$$

$$\text{-----}> \quad N_2(C\,^3\Pi_u) + N_2(X\,^1\Sigma_g^+) \quad (3)$$

$$\text{-----}> \quad N_2(C'\,^3\Pi_u) + N_2(X\,^1\Sigma_g^+) \quad (4)$$

$$\text{-----}> \quad N_2(B\,^3\Pi_g) + N_2(X\,^1\Sigma_g^+) \quad (5)$$

The rate constants for these reactions are given by Hays and Oskam.[22] The values reported are,

$$k(3) = 2.5 \times 10^{-10} \text{ cc/molecule - sec}$$

$$k(4) = 2.5 \times 10^{-11} \text{ cc/molecule - sec}$$

$$k(5) = 1.1(+2/-0.5) \times 10^{-9} \text{ cc/molecule - sec}$$

An interesting point is that the total rate constant for loss of $A\,^3\Sigma_u^+$ state molecules, by these processes, is given as,

$$k(tot) = 1.4 \times 10^{-9} \text{ cc/molecules - sec}$$

$$= 1400 \text{ flHz/molecule}$$

Relative to other processes this rate constant appears very large. Nonetheless, the overall rate of this process is expected to be small due to the low concentration of $N_2(A^3\Sigma_u^+)$ molecules in the system.

V. Redistribution of Vibrational Energy in the Ground State - As mentioned in the section on primary excitation processes, collisions with low energy electrons can excite the first few vibrational levels of the ground state of N_2[27]

$$N_2(X\,^1\Sigma_g^+, V=0) + e^* \text{-----> } N_2(X\,^1\Sigma_g^+, V=1, 2, 3, 4 \text{ etc}) + e \quad (1)$$

Ensuing collisions between vibrationally excited $N_2(X\,^1\Sigma_g^+)$ molecules will extend this excitation to higher vibrational levels.[29, 33, 34]

$$N_2(X\,^1\Sigma_g^+, V_1>0) + N_2(X\,^1\Sigma_g^+, V_2>0) \text{--> } N_2(X, V = V_1 + 1) + N_2(X\,^1\Sigma_g^+, V = V_2 - 1) \quad (6)$$

The importance of this reaction will be discussed in the results section. The result of this reaction will be the redistribution of vibrational quanta in the ground state.

VI. Heavy Particle Reaction - As a result of an over populated tail in the vibrational distribution, excitation between states of the ion, N_2^+, has been postulated to occur via the following energy pooling reaction,[28]

$$N_2(X\,^1\Sigma_g^+, V>12) + N_2^+(X\,^2\Sigma_g^+) \text{---> } N_2(X\,^1\Sigma_g^+) + N_2^+(B\,^2\Sigma_u^+). \quad (7)$$

This mechanism could be one possibility for the behavior of the emission curve from the $N_2^+(B\,^2\Sigma_u^+)$ state (1NG) during the current pulse (see figure 30). Here the increase in collision frequency at increased pressure would cause reaction (7) to proceed more rapidly. This may explain why the end of the emission curve in figure 30 rises with pressure.

VII Intersystem Collisional Transfer - As mentioned in the introduction, numerous experimental observations have indicated the existence of a collisional process which couples adjacent vibrational levels of overlapping electronic states. In this study we examine the effects of this process on the vibrational level population of the $B\,^3\Pi_g$

state of N_2. This is not the only molecule which the study of this process has involved. Work by D. Katayama and co-workers has involved the collisional transfer of excitation between different states of N_2^+, CO^+ and CN.[35-38] In the present study the overlapping triplet states involved are the $A\ ^3\Sigma_u^+$, $B\ ^3\Pi_g$, $W\ ^3\Delta_u$, and the $B'\ ^3\Sigma_u^-$. These are shown in figure 2.

A number of basic observations regarding figure 2 should be noted. First, the $B\ ^3\Pi_g$ and $W\ ^3\Delta_u$ potentials overlap very well over the entire range of levels in the $B\ ^3\Pi_g$ state . (see figures 2 and 13). Second, levels in the $A\ ^3\Sigma_u^+$ state below V = 7 are not coupled to the $B\ ^3\Pi_g$ state. Finally, levels of the $B'\ ^3\Sigma_u^-$ state couple to the $B\ ^3\Pi_g$ state such that $B\ ^3\Pi_g(V+4) \sim B'\ ^3\Sigma_u^-(V)$. Another point to be noted in figure 2 is less obvious and basicly involves the fact that the minima in the different potentials occur at different internuclear separations. This effects the values of the Franck-Condon factors between the vibrational levels of the ground state with those of the excited states shown in figure 2. As mentioned before, the initial vibrational distributions which result from direct electron excitation are determined largely by these Franck-Condon factors. If excitation is occurring primarily from the V=0 level of the ground state the peaks in the excited state vibrational distributions are expected to be found at the following levels; $A\ ^3\Sigma_u^+$ (V=8), $B\ ^3\Pi_g$ (V=2), $W\ ^3\Delta_u$ (V=7) and $B'\ ^3\Sigma_u^-$(V=7).[39, 40]

Also mentioned above was the fact that the relative population of the various excited states is determined by the cross-sections associated with these states and the electron energy distribution in the discharge (current pulse). Consequently, the overall result of the direct electron excitation process is the production of excited molecules where the population of adjacent vibrational levels can be initially out of equilibrium.

Values of the expected equilibrium population ratios have been discussed by Benesch and Fraedrich.[4] The ratio of the populations of the $B\ ^3\Pi_g$ and $B'\ ^3\Sigma_u^-$ states was shown to be

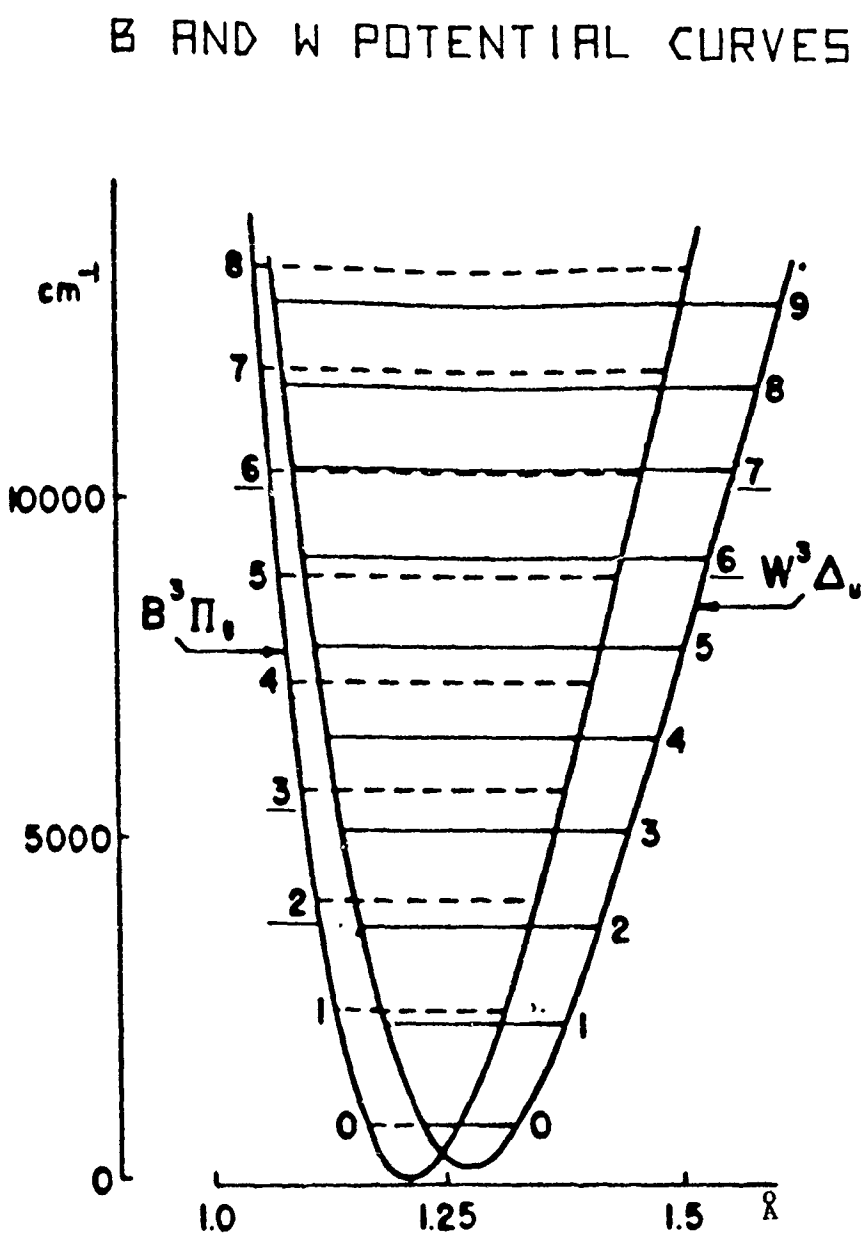

Figure 13 -

$$C = N(B'^3\Sigma_u^-)/N(B^3\Pi_g) = \frac{Q(B'^3\Sigma_u^-)}{Q(B^3\Pi_g)} \cdot \frac{g(B'^3\Sigma_u^-)}{g(B^3\Pi_g)} \quad (8)$$

where the g( )'s are the statistical weights,

$$g(B'^3\Sigma_u^-)/g(B^3\Pi_g) = 1/2 \text{ due to lambda doubling}$$

and

$$Q(B'^3\Sigma_u^-)/Q(B^3\Pi_g) \sim B(B^3\Pi_g)/B(B'^3\Sigma_u^-)$$

Here the Q( )'s are the rotational partition functions and the B( )'s are the rotational constants for the two states. Presumably this analysis would apply to the other excited states as well.

So what is expected to happen in our system is that first, the states in question are produced in ratios determined by the electron energy distributions and second the initial vibrational population distribution within these states are determined by the Franck-Condon factors. These populations continually emit according to their natural lifetimes. This represents an irreversible loss of excitation from a set of coupled vibrational levels. In addition, the collisions which occur during and after the production of these initial vibrational populations, will tend to shift the remaining populations toward values which reflect an equilibrium via the ICT process. This is in accordance with Le Chatelier's principle, in that the system has been prepared out of equilibrium and so tends to shift so as to bring itself back into equilibrium. This shifting of populations will be demonstrated in section(IV) of chapter 4.

Studies by Katayama et al. involving ICT between states of N_2^+, have shown evidence for certain selection or propensity rules for this process[3] . These rules involve changes in symmetry and rotational quantum number. The rule for symmetry changes was found to be,

$$S<\text{-->}S \quad A<\text{-->}A \text{ , but } S<\text{-}|\text{->}A \qquad (9)$$

For changes in rotational quantum number, their study showed a propensity rule of

$$\Delta J \sim 0 \qquad (10)$$

which was prefered to

$$\Delta E \sim 0 \qquad (11)$$

In discussions in our laboratory the spin slection rule

$$\Delta S = 0 \qquad (12)$$

is also considered to be strong but the role of transitions between the overlapping singlets and the $B\,^3\Pi_g$ state is not certain.

CHAPTER 4 - RESULTS (I) - SPECTRA

To begin the chapter on the results, a discussion of the spectrum studied is in order. As mentioned previously, the primary spectrum which we have observed is the 1PG ($B^3\Pi_g$ -->$A\,^3\Sigma_u^+$). An example appears in figure 14. Looking at this figure from left to right, we see four distinct sets of vibrational bands or sequences. They are the sequences δV = 4,3,2, and 1 respectively. Here, δV implies change in vibrational quantum number. An important point which one should notice about this spectrum is that different sequences feature different sets of vibrational levels in the $B\,^3\Pi_g$ state. Starting at the left, δV=4 shows bands due to V = 12 through 6, δV=3 shows V = 10 through 3, δV=2 shows V = 7 through 2, and δV=1 shows V = 3 through 1.

By looking at changes within a sequence, we are able to watch changes in the relative population within a given set of levels. Also, by observing relative intensities of different sequences, the behavior of different groups of levels can be observed. It must be kept in mind that these observations are only qualitative and that the important comparisions arise from the overall vibrational distributions. These distributions result when we analyse entire spectrum Still, the initial work in this study involved the spectra alone and so they warrant some consideration.

These observations show the role of collisions in producing similar distributions of band intensities. They also show features which would go largely unnoticed were one to look at the distributions only. In this section we discuss a number of these observations.

One of our first observations was of the change in the relative intensity of the (2-0) band of the δV=2 sequence. As spectra are taken at times further from the current pulse, the intensity of the (2-0) band increased relative to the other bands in the sequence (see figure 15 & 16). Our motivation for pursuing this observation came from spectra taken of

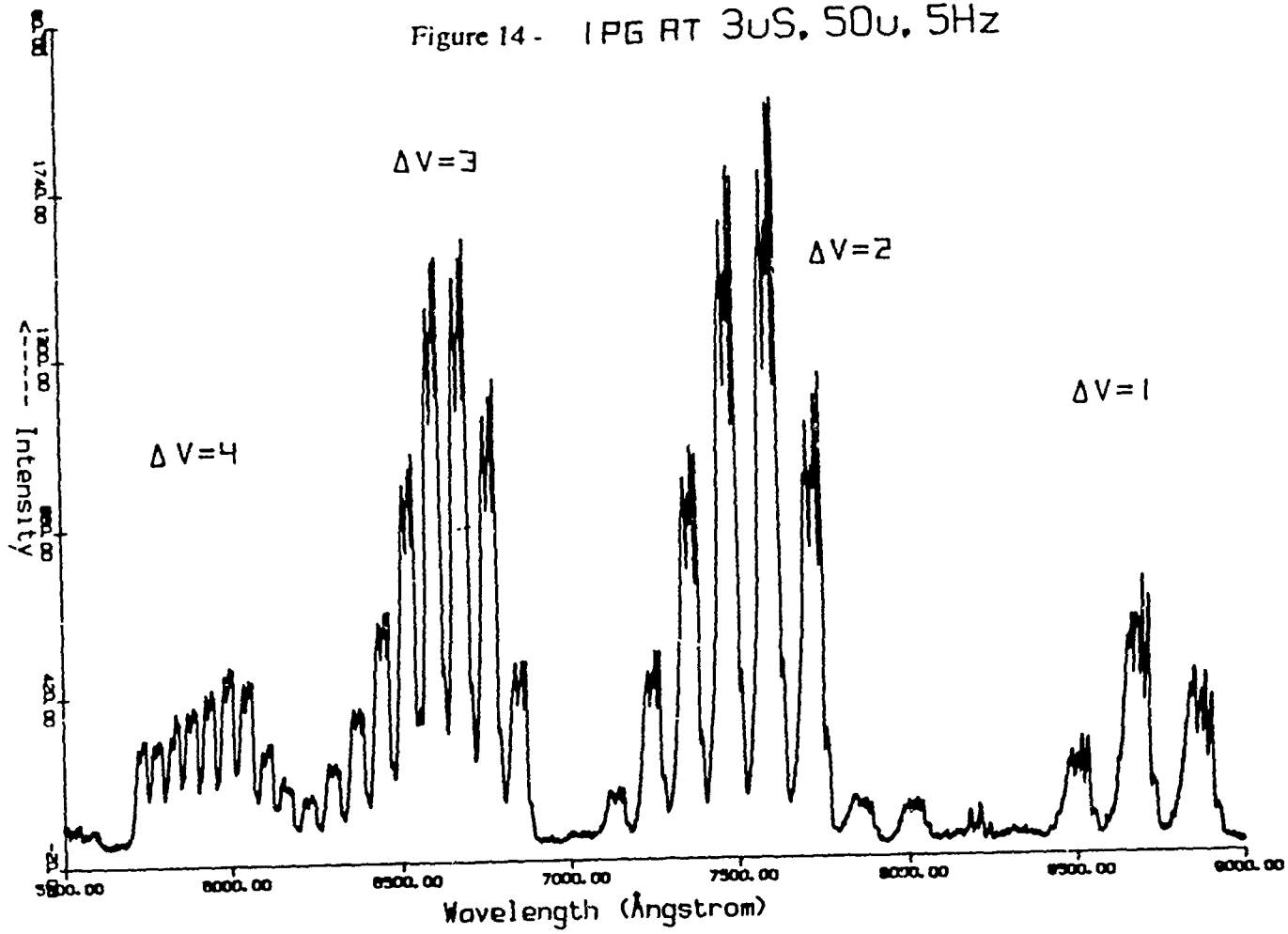

Figure 14 - IPG AT 3uS, 50u, 5Hz

Figure 15 - N2 IPG ΔV=2 400 MICRONS

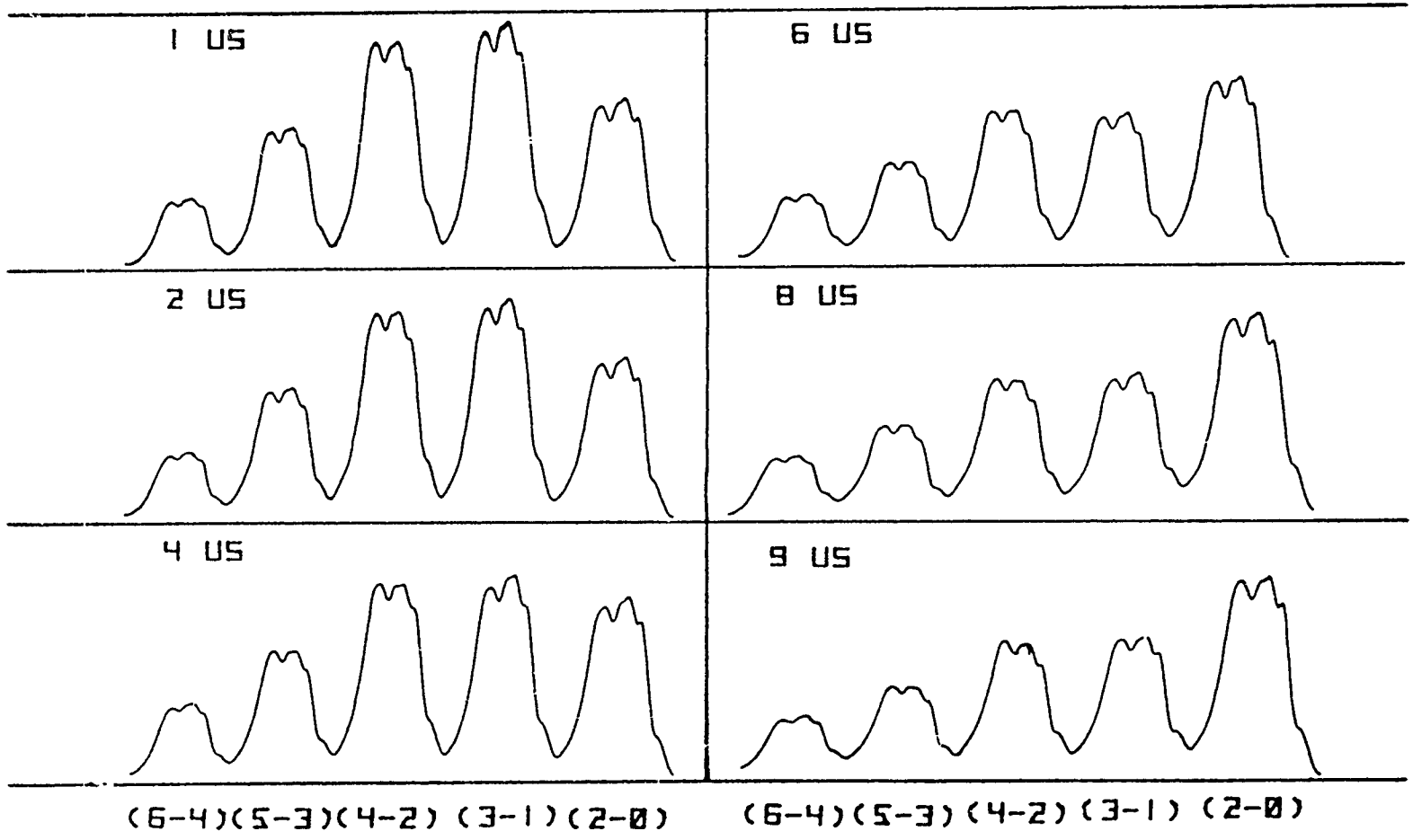

Figure 16 - N2 IPG ΔV=2 40 MICRONS

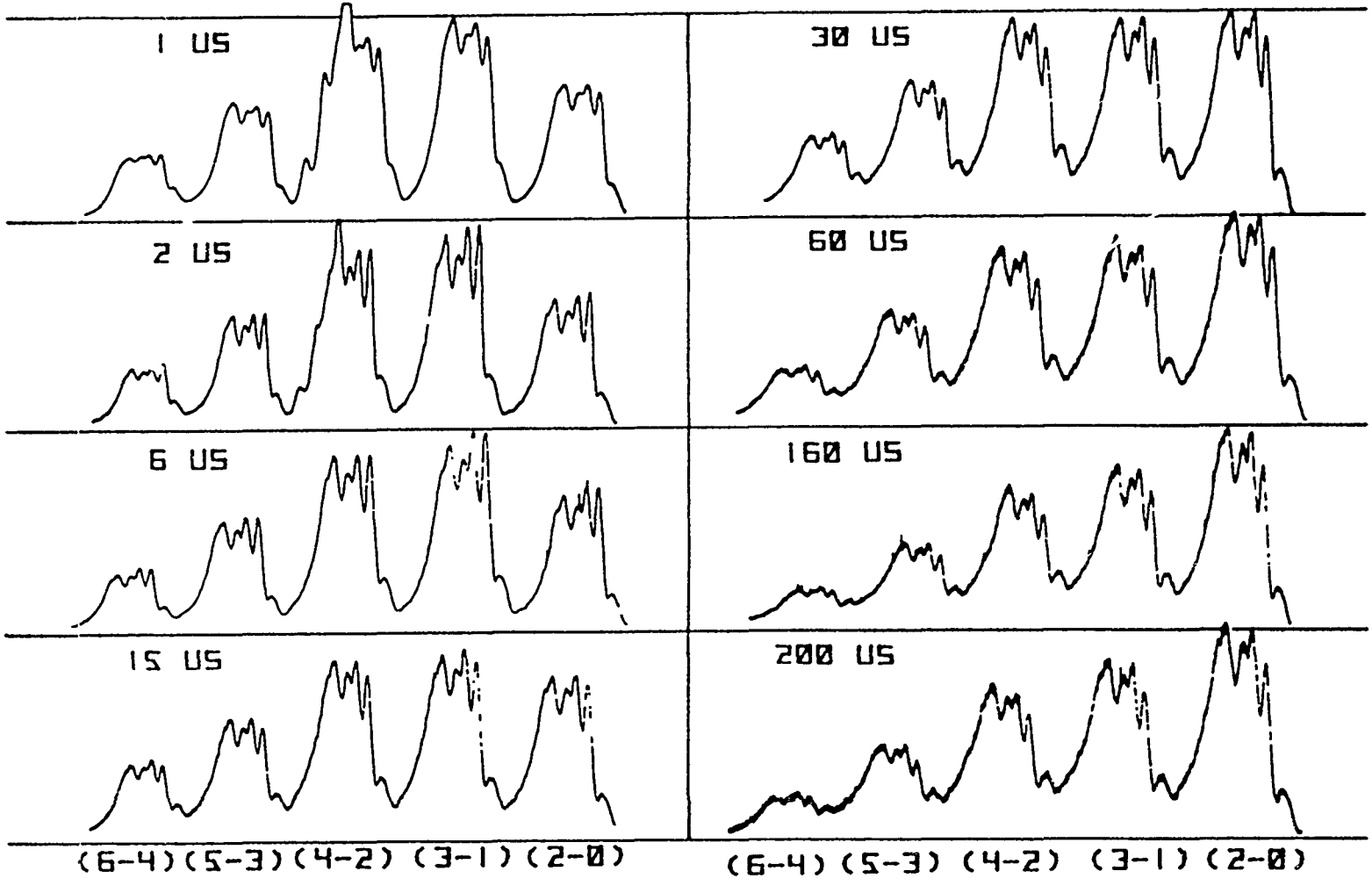

an RF discharge of N_2 These spectra showed that, as the pressure was increased the relative intensity of the (2-0) band increased as well (see figure 17). Our initial assumption was that this change was due to collisions. The time resolved pressure studies which were done have borne this out in part. There is a contribution due to the larger lifetimes of the lower levels but as we will see, collisions play the predominant role in the changes following the current pulse.

In figure 15, the $\delta V=2$ sequence has been observed from 1 to 9μs at 400 μ of N_2. The discharge frequency was ~5 Hz. This series of spectra show the increase in the relative intensity of the (2-0) band with increased time. The distribution does not change much between 8 and 9 μs, nor between 1 and 4 μs. The distributions in section (IV) (figure 48), show that the percent population for v = 2, 3, and 4 stablize at about 12 μs rather than 8 or 9 μs. Since the distribution doesn't change much during the first 4 μs of the current pulse, we will consider the salient collisions to be occuring between 4 and 12 μs. At 400 μ of N_2 with T = 300 K, the gas kinetic collision frequency is about 2.7 collisions/ μs. The number of collisions which have occured at the time of equilibrium is

$$(2.7\ \#/\ \mu s) \times (8\ \mu s) \sim 22 \text{ collisions}$$

For the case of $\delta V=2$ at 40 μ of N_2, a much larger amount of time is required to achieve this equilibrium distribution (figure 16). Here, the discharge frequency is ~35 Hz. From this figure, the equilibrium distribution appears to stabilize some where between 60 and 160 μs. Again from the results of section (IV) (figure 55), the distribution stabilizes at about 100 μs. The gas kinetic collision frequency at 40 μ is ~0.27 collisions/ μs, so the number of collisions required here is,

$$(0.27\ \#/\ \mu s) \times (\sim 96\ \mu s) \sim 26 \text{ collisions}$$

So from this we see that it takes about 24 collisions to reach this equilibrium

Figure 17 - RF DISCHARGE AT VARIOUS PRESSURES

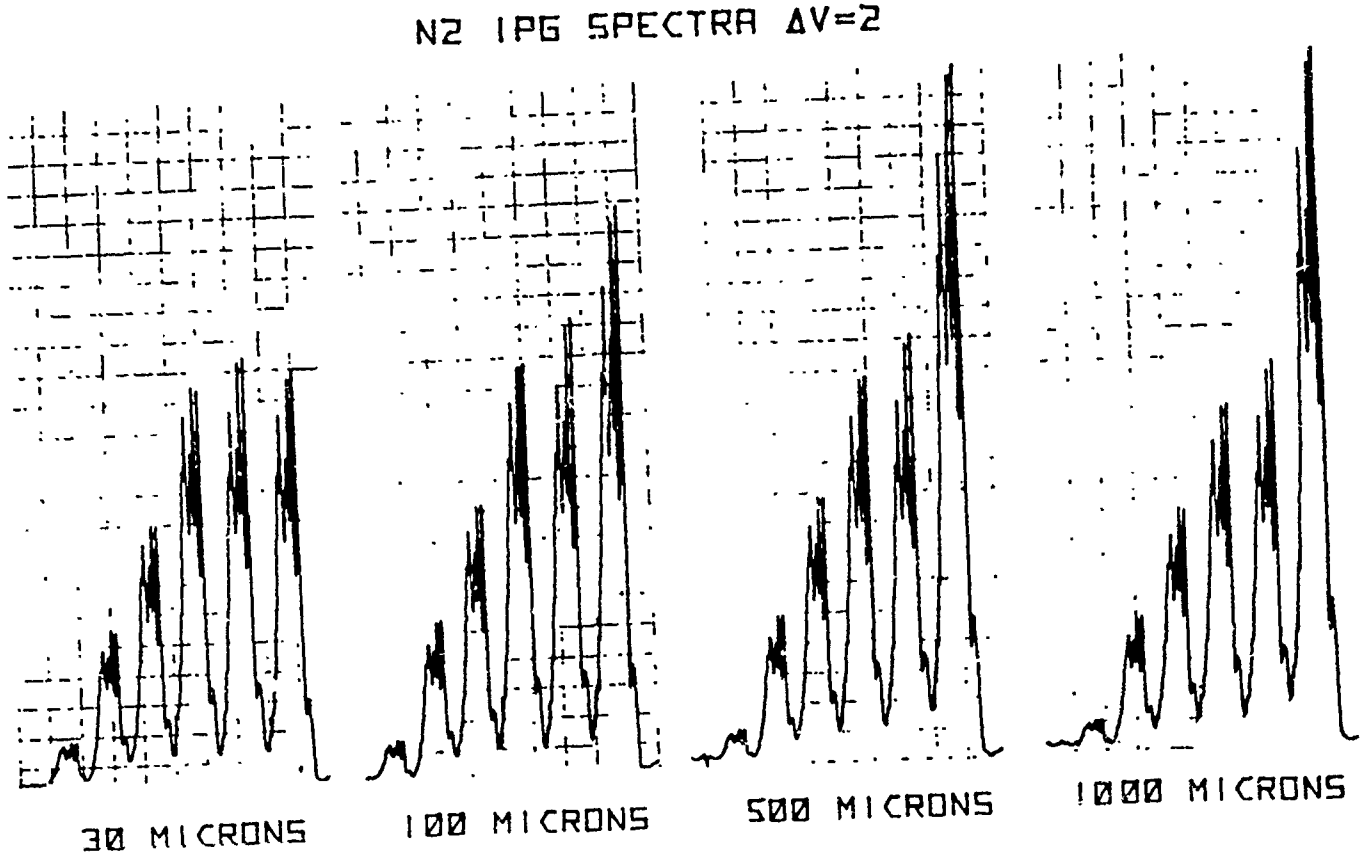

distribution of band intensities, regardless of the actual amount of time involved.

Another series of spectra involves the δV=3 sequence (figure 18). These spectra were taken at 40 μ and 35 Hz from 1 to 200 μs. Notice that as in the previous series, the distribution of band intensities remains largely unchanged between 60 and 200 μs. Also the initial and final distributions are virtually identical. In addition, between 6 and 30 μs the (7-4) and (6-3) bands increase relative to the other bands. This increase in the population of V = 6 and 7 is evidence for ICT from an adjacent electronic state. The proof, discussed in section (IV), is based on the observation that the peak in the percent population for V = 6 occurs at a constant number of gas kinetic collisions after the current pulse and is not time dependent.

A point which was not mentioned above is that the absolute intensities of the vibrtational bands of figures 15, 16, and 18 change with time. These three sets of spectra were taken so that the largest bands all had about the same peak intensity. In reality, these intensities increase for about 3 to 4 μs and then decay away. If we set the system at a constant gain and take spectra at 1 or 2 μs intervals, the overall 1PG spectrum can be seen for a given set of conditions. This is shown in figures 19, 20, and 21. These figures show the spectrum for the system run at 15 Hz and 150 μ of N_2, from 0.5 to 20 μs. It should be noted that this spectrum (figure 19) required about half a million pulses to produce.

It is difficult to extract much information directly from this spectrum. We are able to see the change in δV=2 which was just discussed (compare initial and final δV=2 sequences). Also there is an apparent change in the relative intensities of the δV=4 bands. The most important observation is that the changes in the relative band intensities occur at very different absolute intensities. This merely confirms the need for time resolved measurement in the study of a pulsed discharge of this type.

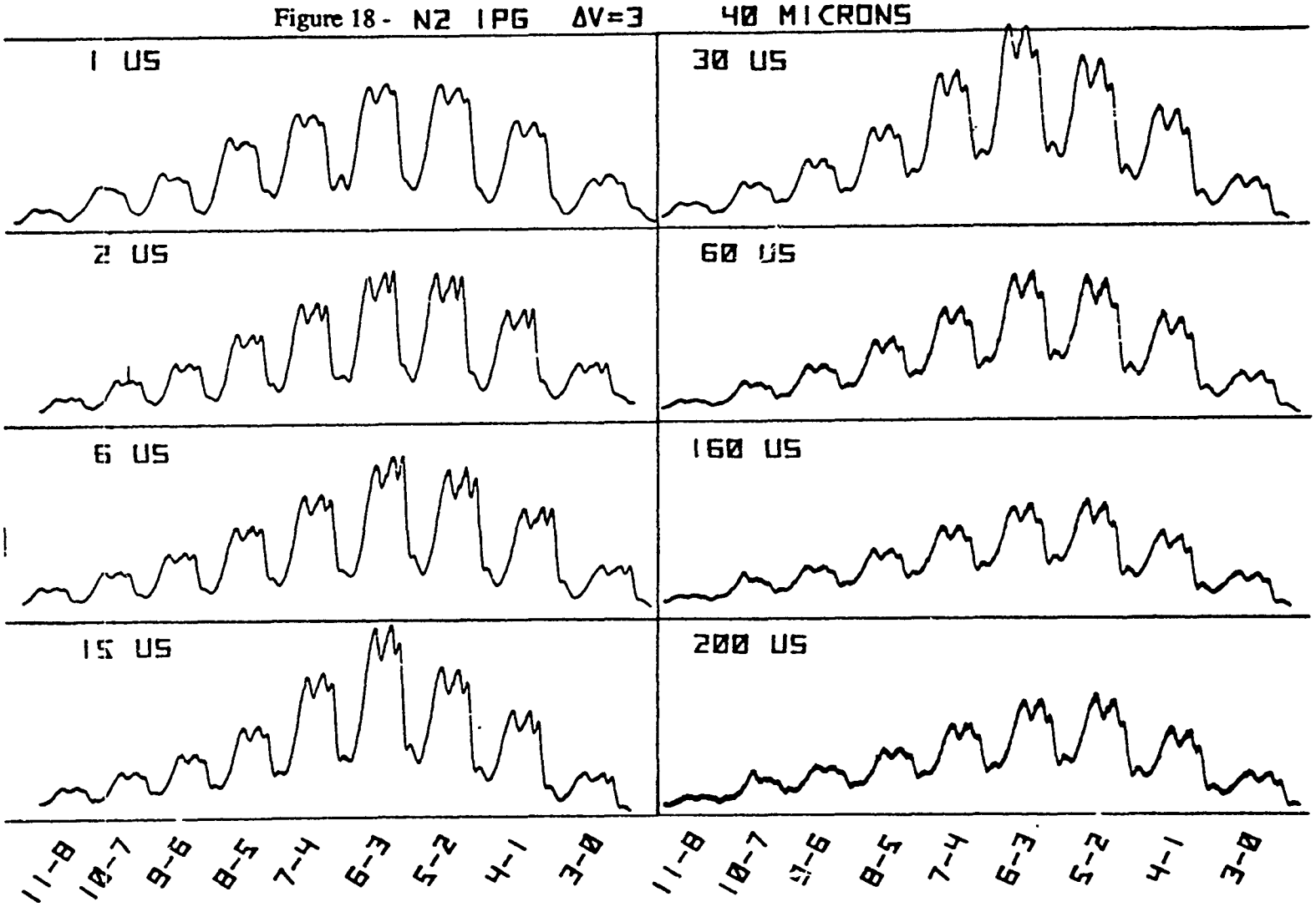
Figure 18 - N2 IPG ΔV=3 40 MICRONS
1 US
30 US
2 US
60 US
6 US
160 US
15 US
200 US
11-8
10-7
9-6
8-5
7-4
6-3
5-2
4-1
3-0

Figure 19 - 1PG @ 150u & 15Hz; 0 to 20us

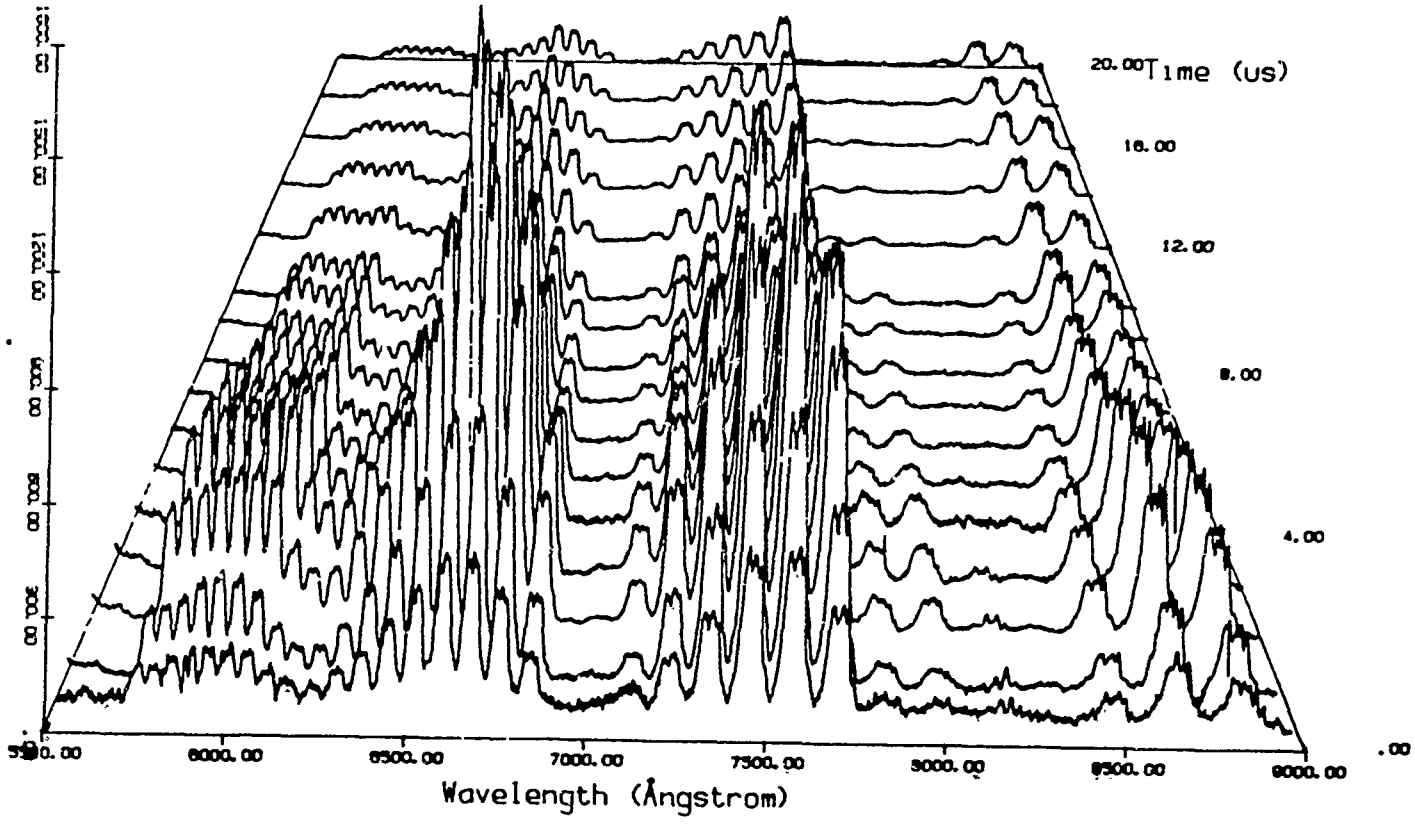

Figure 20 - 1PG @ 150u & 15Hz; 0 to 20us dV= 1.2

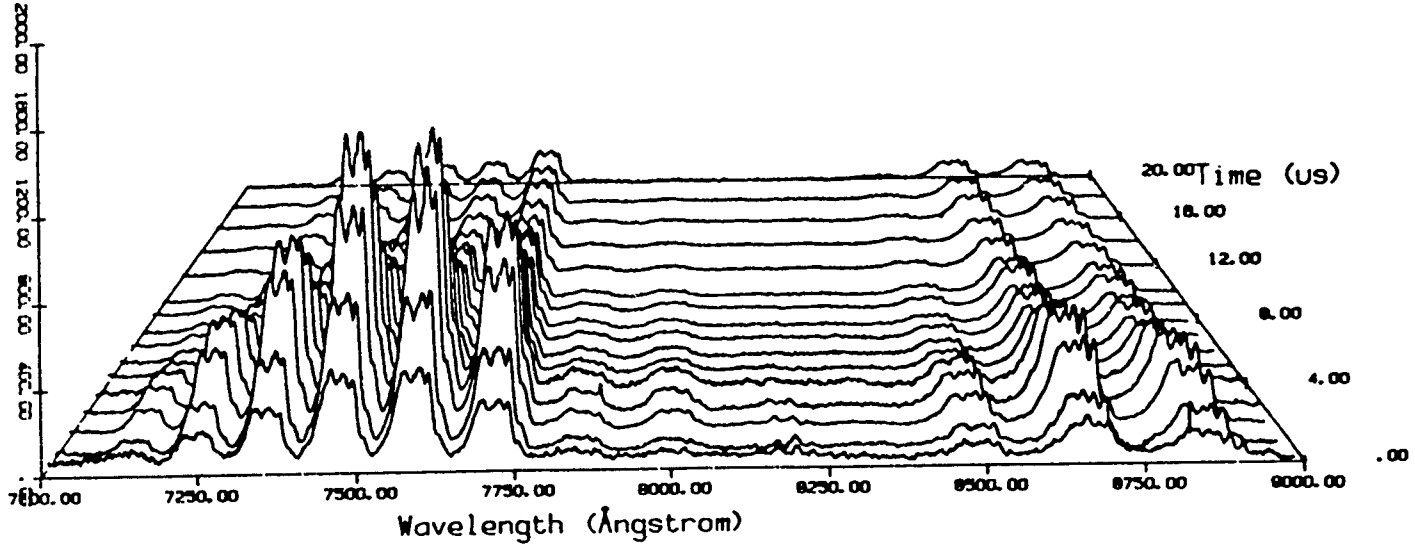

Figure 21 - 1PG @ 150u & 15Hz; 0 to 20us dV= 3.4

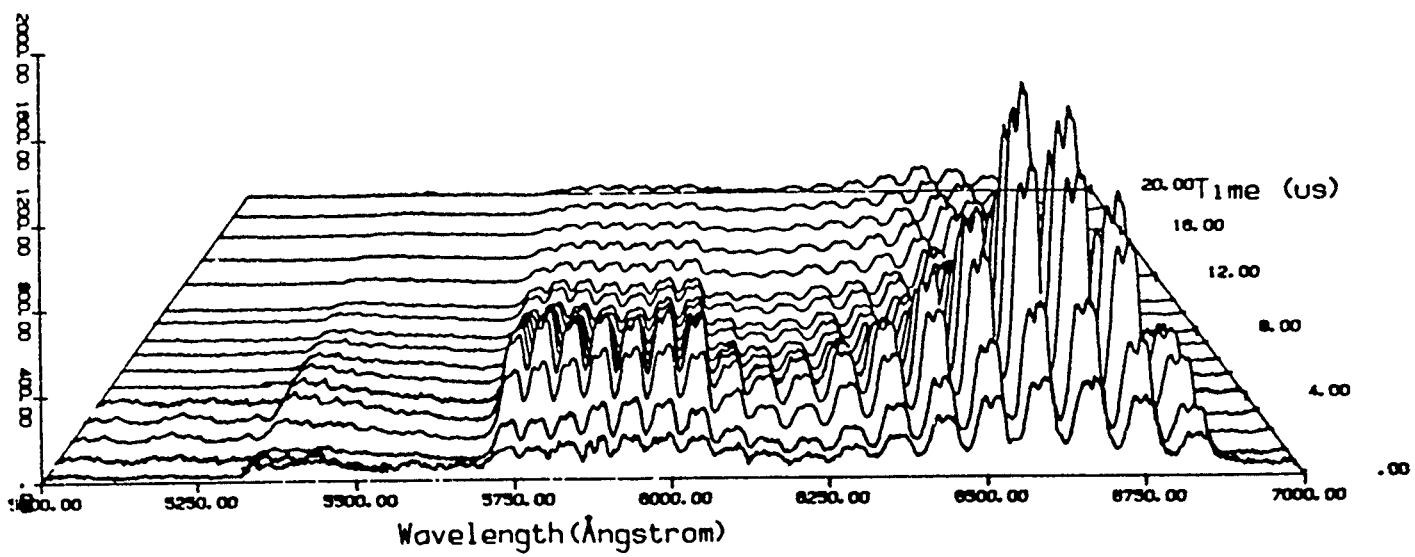

To extract information from these spectra, we have measured the percent populations from the individual spectra for each time and they are plotted in figure 22. This figure shows the distinct increase in the percent population for V = 2 which was shown in the δV=2 sequences discussed above. Also, there is a peak in the distribution for V = 6 as was seen in the increase in the (6-3) band in the δV=3 sequences. We will discuss plots of this type in greater detail in section (IV) of chapter 4. They are presented here so that their relationship with the spectra will be clear.

One final series of spectra will be discussed, the δV=4 sequence in figure 23. This is perhaps the most significant observation made in this study. In the last two frames of this figure there is a large spike in the short wavelength (left) side of the (10-6) band. Returning to figure 18, this spike appears in the (10-7) band as well. In the original spectrum, these bands are of similar intensity. Consequently, this spike is of a similar magnitude for both bands. The (10-6) band at 160 μs, is characteristically different then the other bands present. The width of these bands is produced by emission from a rotational distribution at the V = 10 level. Clearly this distribution is distinctly different from those of the other levels. At 160 μs all these levels are being fed by a secondary excitation process (see chapter 4 - section III). Understanding the source of additional population would greatly clarify this process.

An interesting experiment would be the observation of emission from the levels, $B'^3\Sigma_u^-$ (V=6) or $W^3\Delta_u$ (V=11). These are the vibrational levels which are adjacent to $B^3\Pi_g$ (V=10) and so are are possible coupling partners. If the above feature is due to ICT from one of these two states, bands which arise from these levels would show an uncharacteristic depression in the band shape; the band would have a hole in it. The (6-3) and (6-4) bands of the $B'^3\Sigma_u^-$ to $B^3\Pi_g$ system (IRA) are possible candidates. Both have large transition probablities (~10^6 Hz) though they appear at wavelengths near 10,000 A.[4] This could make them difficult to detect at this time after the pulse. There also might be interference

Figure 22 -

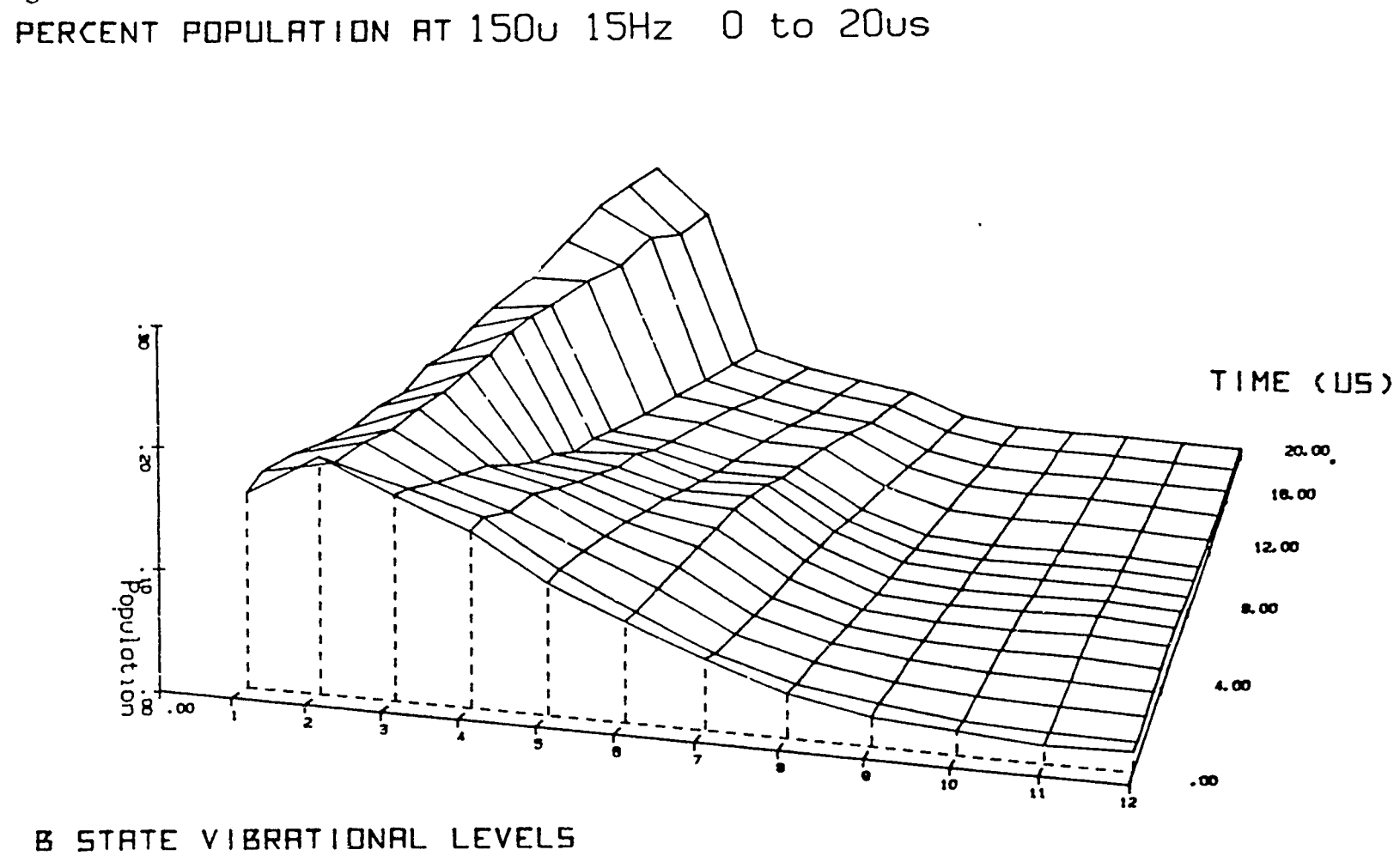
PERCENT POPULATION AT 150u 15Hz 0 to 20us
TIME (US)
20.00
16.00
12.00
8.00
4.00
.00
Population
.80
.40
.00
1
2
3
4
5
6
7
8
9
10
11
12
B STATE VIBRATIONAL LEVELS

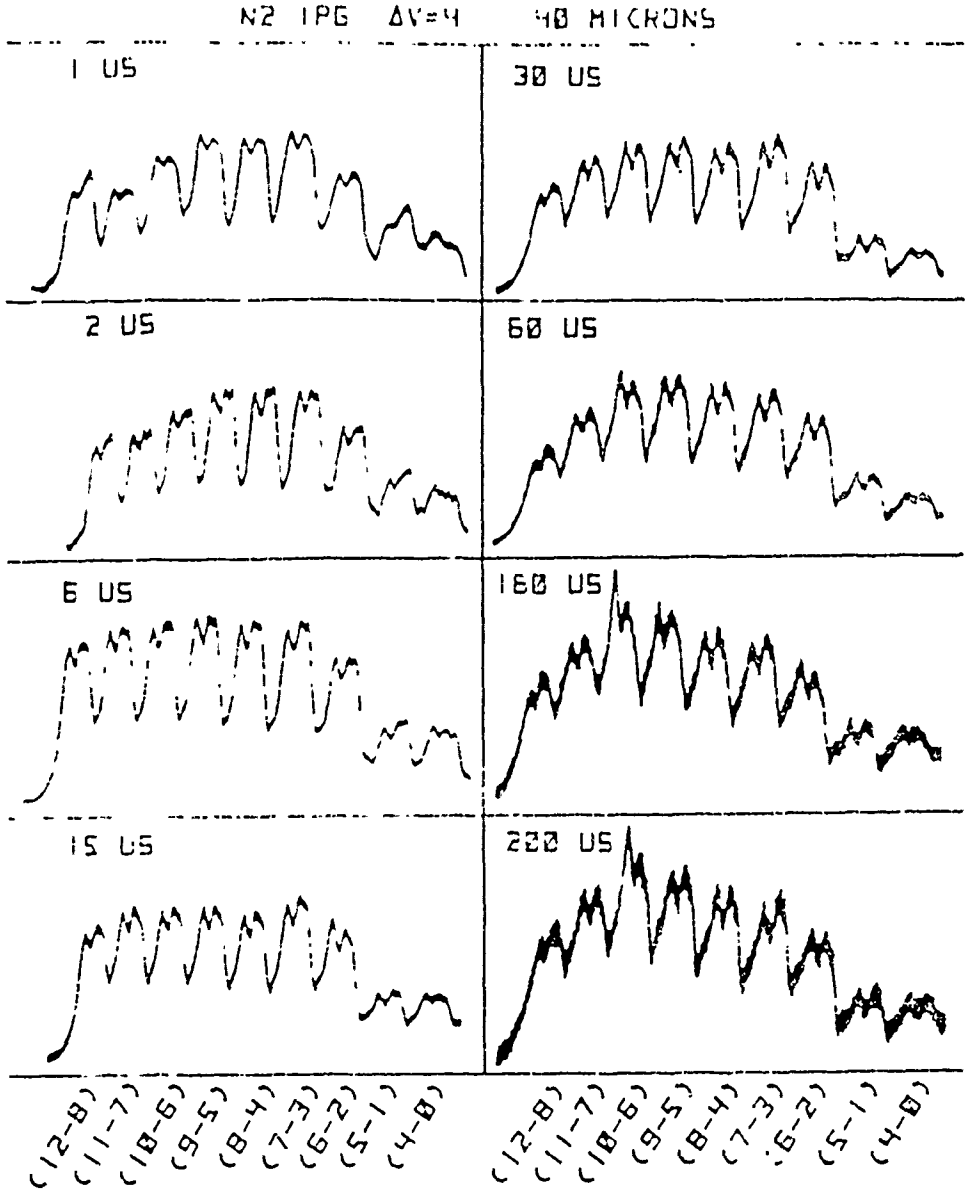
N2 IPG ΔV=4 40 MICRONS
1 US
30 US
2 US
60 US
6 US
180 US
15 US
220 US
(12-8)
(11-7)
(10-6)
(9-5)
(8-4)
(7-3)
(6-2)
(5-1)
(4-0)

Figure 23 -

with 1PG bands in this region. Regardless, the above feature is pervasive in the data of this study. Consequently, it is the result of a dominant process at work in these experiments and is therefore an important component in the events which produce the results of this study.

CHAPTER 4 - RESULTS (II) - EMISSION CURVES

One of the distinctive features of the pulsed discharge is the shape of the emission curves produced by three of the emission systems of N_2 and N_2^+. Three examples are shown in figures 24, 25 and 26. In these figures the spectrometer is tuned to a specific band in the spectrum and the repeated light pulse is observed as a funtion of time. These data were all taken with the Boxcar Integrator and a strip chart recorder. They were then fit to the scales as shown. The discharge frequency for all three emission curves is 35 Hz and the system pressure was 400 μ of flowing N_2. The above figures correspond to the 1PG (1-0) band, 2PG (0-3) band and the 1NG (0-2) band respectively. As discussed previously the 1PG is due to the ($B\,^3\Pi_g$ --> $A\,^3\Sigma_u^+$) transtion in the molecule, N_2. The 2PG arises from the transition ($C\,^3\Pi_u$ --> $B\,^3\Pi_g$) in the molecule, and the 1NG results from the transition ($B\,^2\Sigma_u^+$ -> $X\,^2\Sigma_g^+$) in the ion, N_2^+. 1NG and 2PG spectra are not shown.

As illustrated in these figures, each transition yields a unique emission curve or emission pulse. The primary difference between these three curves is the position of the peak; the 2PG at ~1 to 2 μs, the 1NG at ~ 3 μs and the 1PG at ~3 to 3.5 μs. More accurate measurements with the oscilliscope show that the 2PG pulse peaks at ~1 μs (figure 27). Further observations show that this distinctive behavior is relatively invariant with pressure for the 1PG and 2PG. The behavior of the 1NG, on the other hand, varies dramatically as a function of pressure. These observations are seen in figures 28, 29 and 30.

Regarding the 1NG emission pulse, a possible explanation could be associated with the increase in the plateau voltage with increases in pressure (figure 5). The rise in the end of the 1NG emission pulse with increasing pressure could reflect direct electron excitation of ground state molecular ions generated during the first two microseconds of the current pulse. This explanation is more likely than the one based on a heavy particle

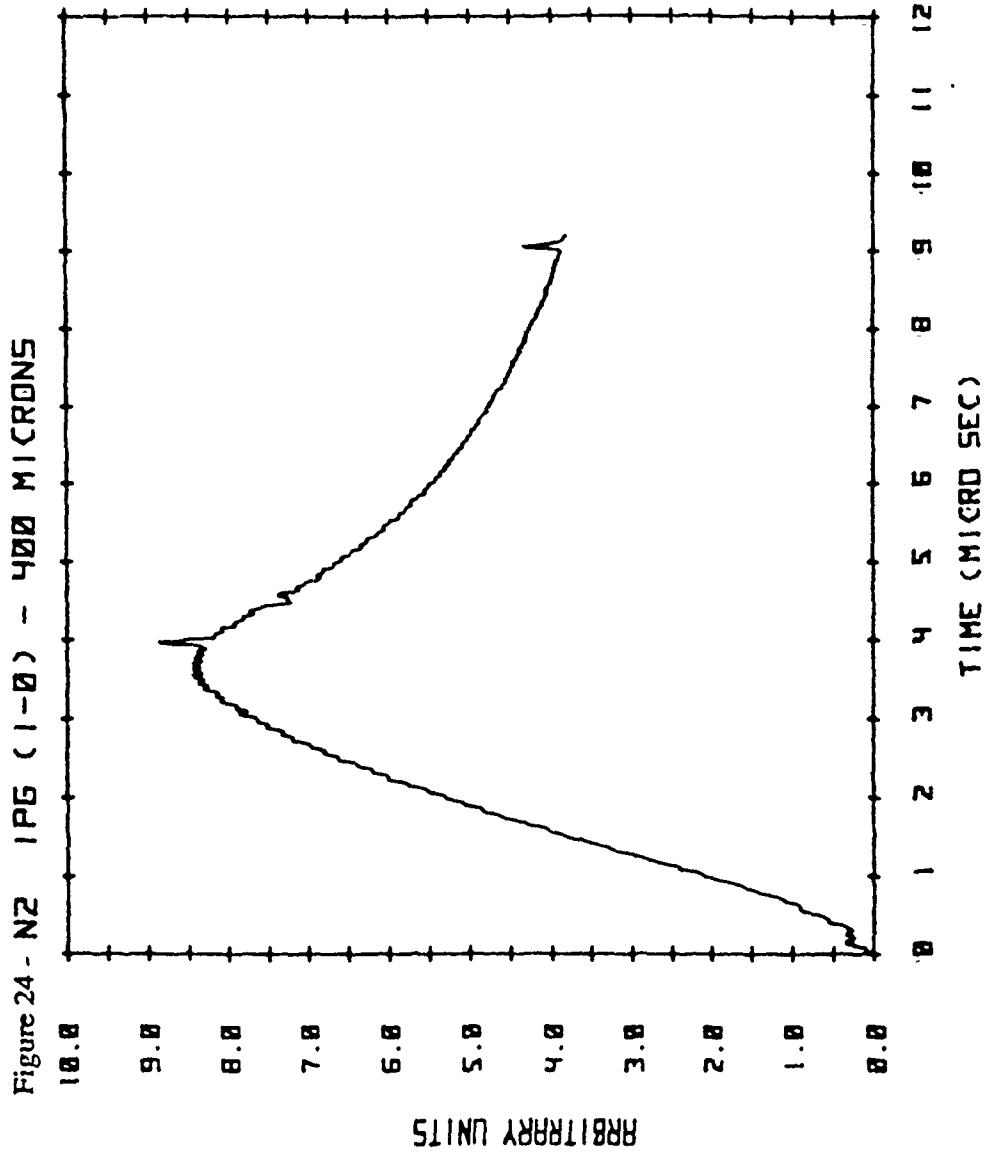
IPG EMISSION PULSE
N2 IPG (1-0) - 400 MICRONS
ARBITRARY UNITS
10.0
9.0
8.0
7.0
6.0
5.0
4.0
3.0
2.0
1.0
0.0
0 1 2 3 4 5 6 7 8 9 10 11 12
TIME (MICRO SEC)

Figure 24 -

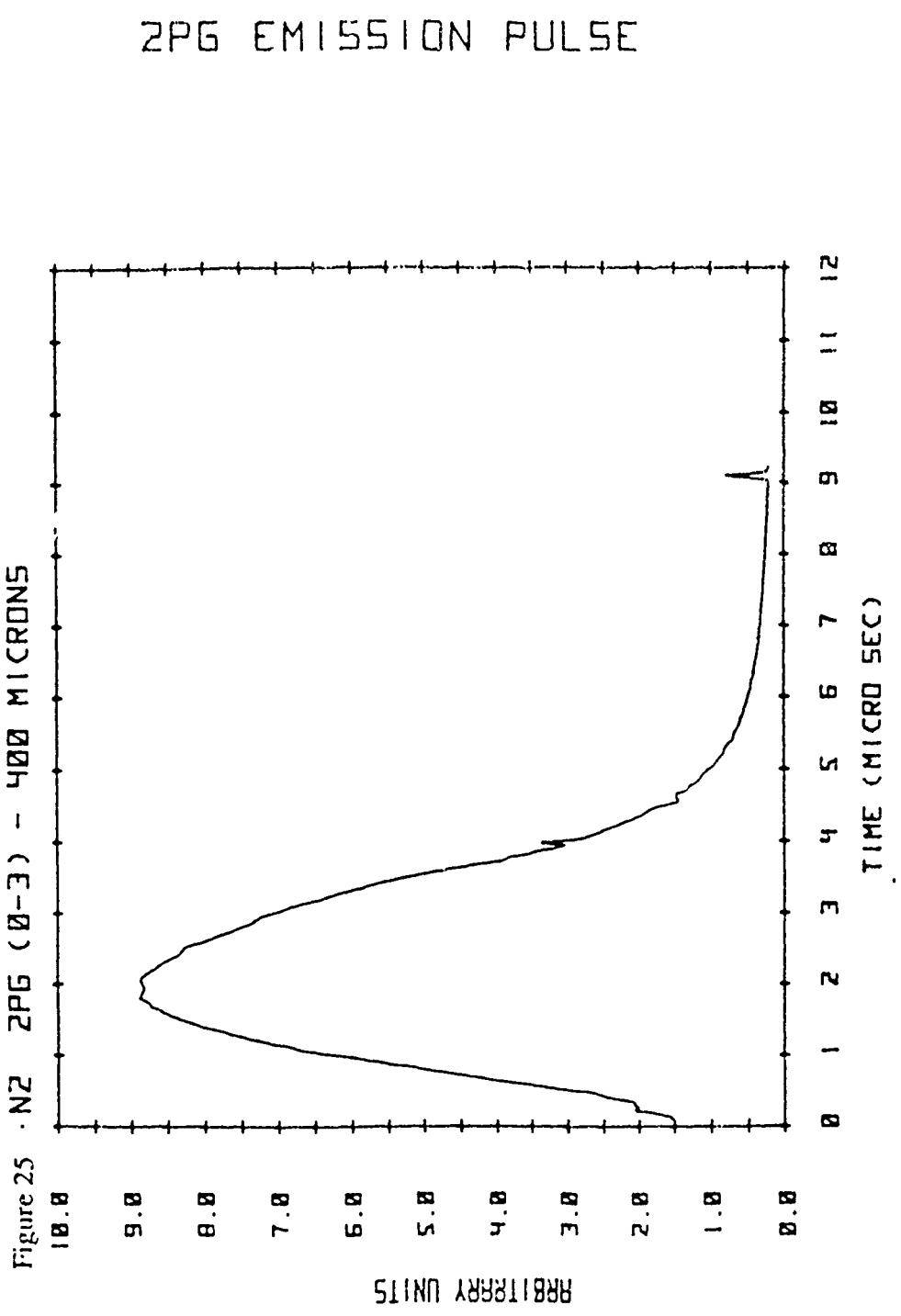
2PG EMISSION PULSE
N2 2PG (0-3) - 400 MICRONS
ARBITRARY UNITS
10.0
9.0
8.0
7.0
6.0
5.0
4.0
3.0
2.0
1.0
0.0
0 1 2 3 4 5 6 7 8 9 10 11 12
TIME (MICRO SEC)

Figure 25

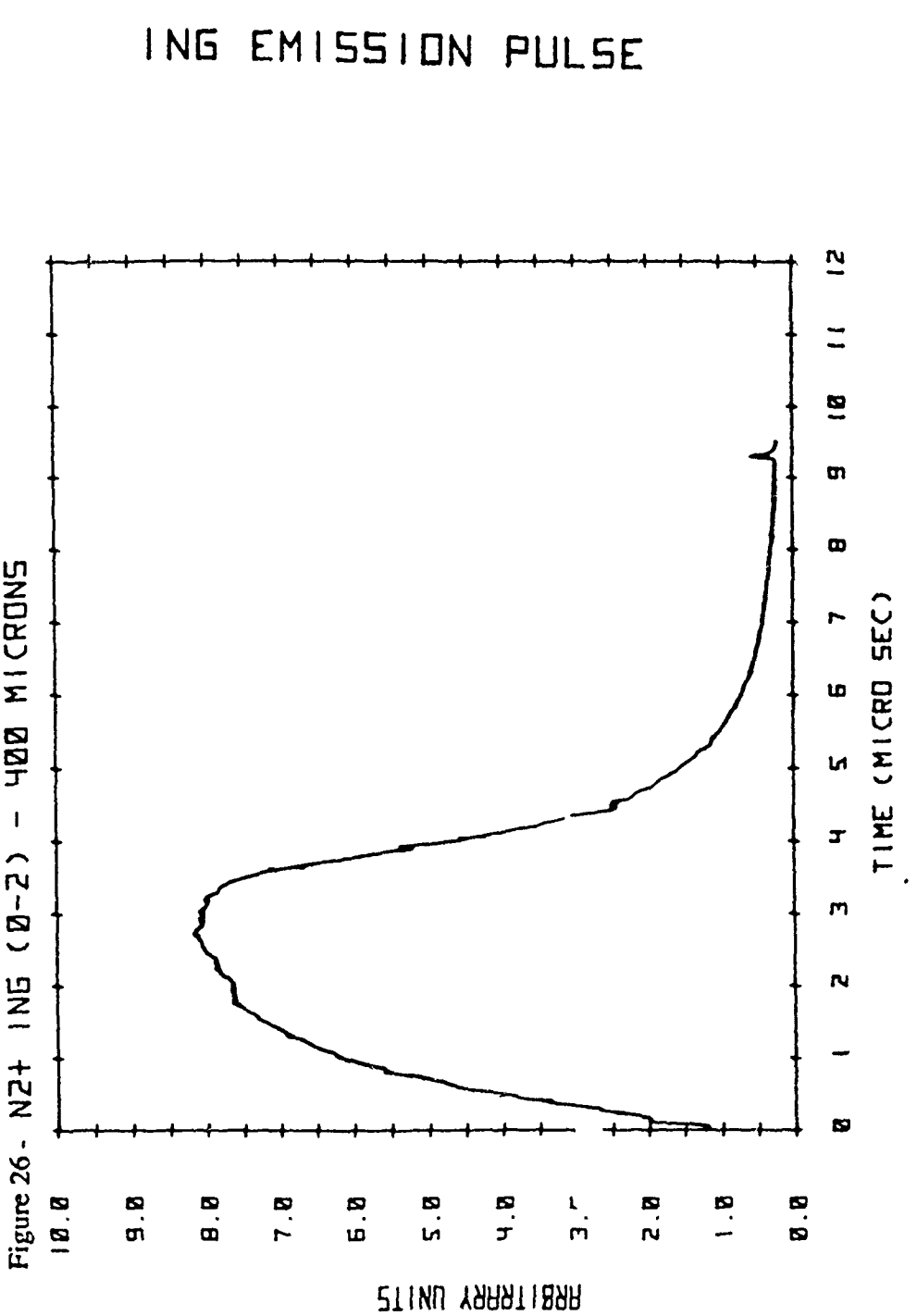

Figure 26- N2+ ING (0-2) - 400 MICRONS

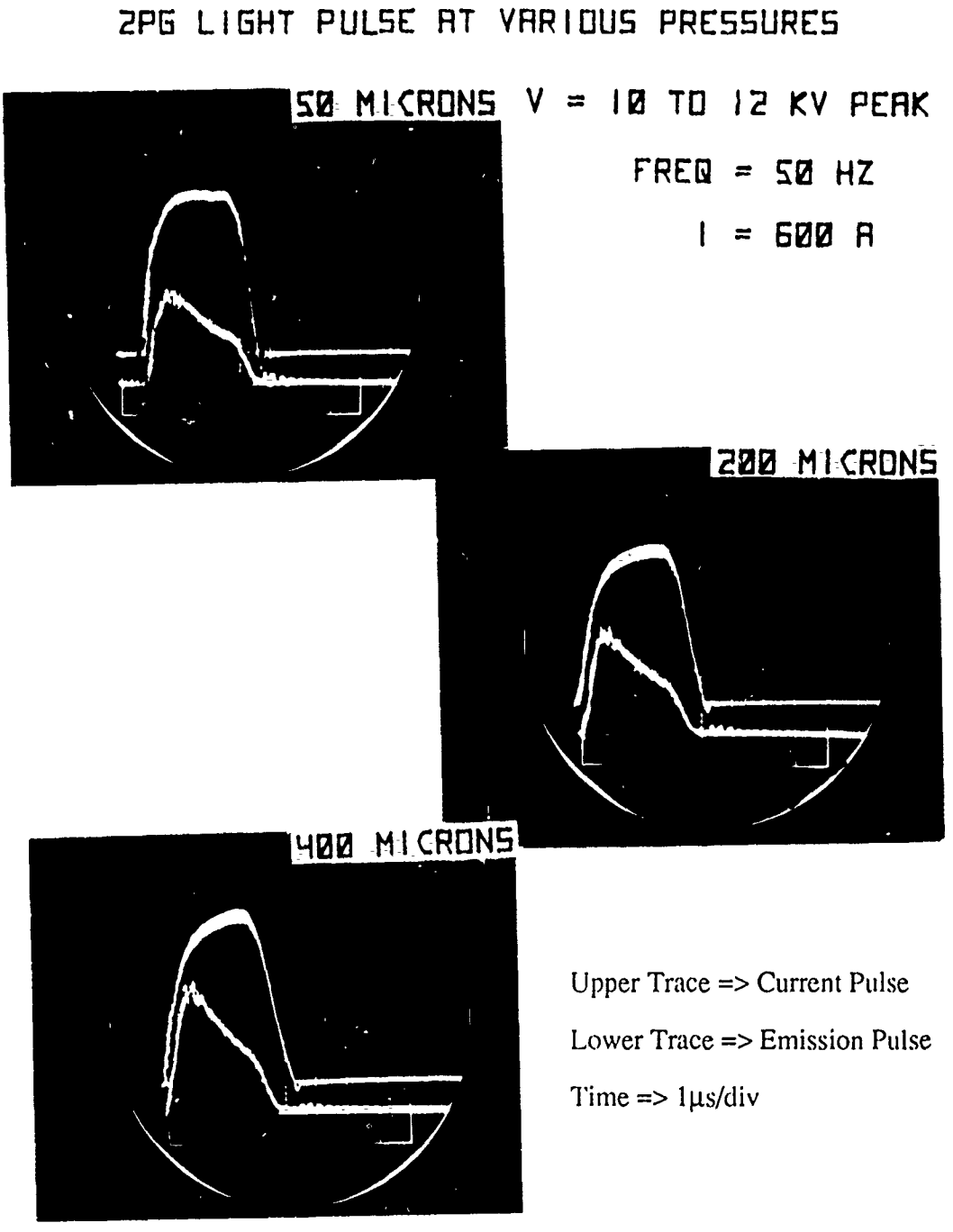
2PG LIGHT PULSE AT VARIOUS PRESSURES
50 MICRONS V = 10 TO 12 KV PEAK
FREQ = 50 HZ
I = 600 A
200 MICRONS
400 MICRONS
Upper Trace => Current Pulse
Lower Trace => Emission Pulse
Time => 1μs/div

Figure 27

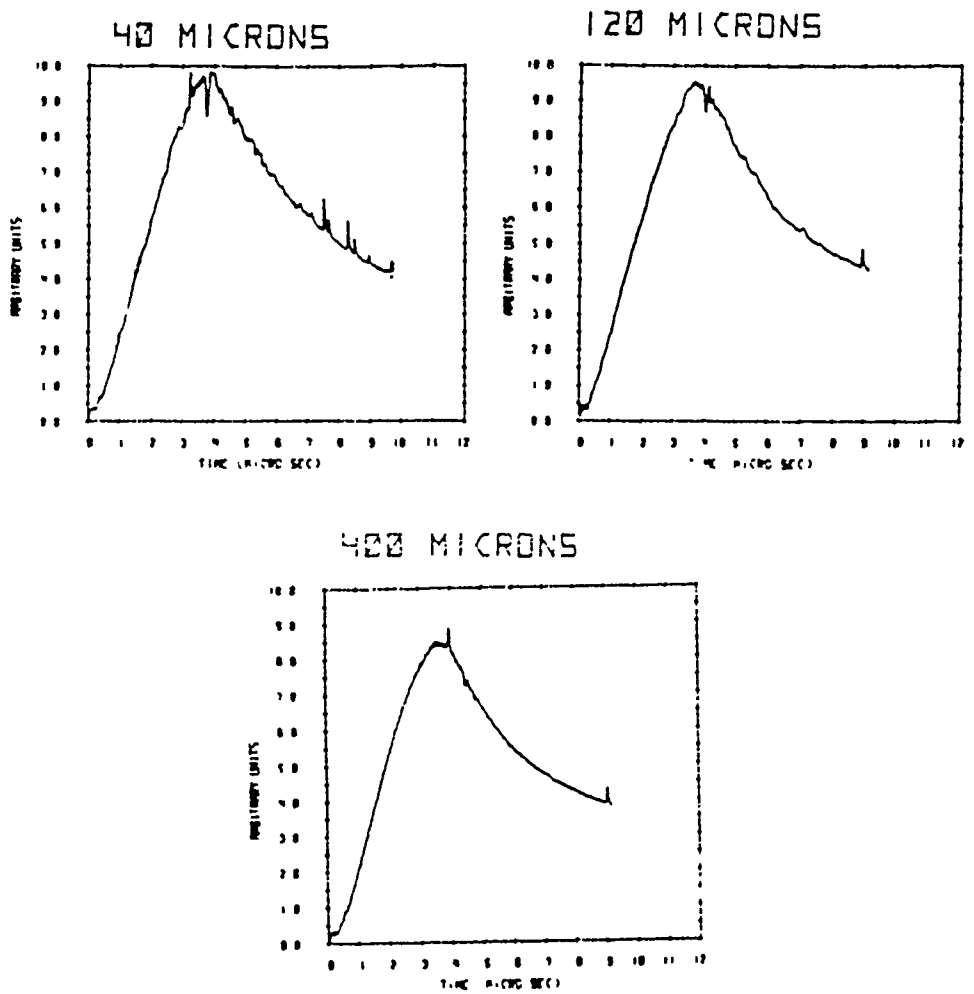
IPG EMISSION PULSE
N2 IPG (1-0)
40 MICRONS
120 MICRONS
400 MICRONS

Figure 28

2PG EMISSION PLATE

N2 2PG (0-3)

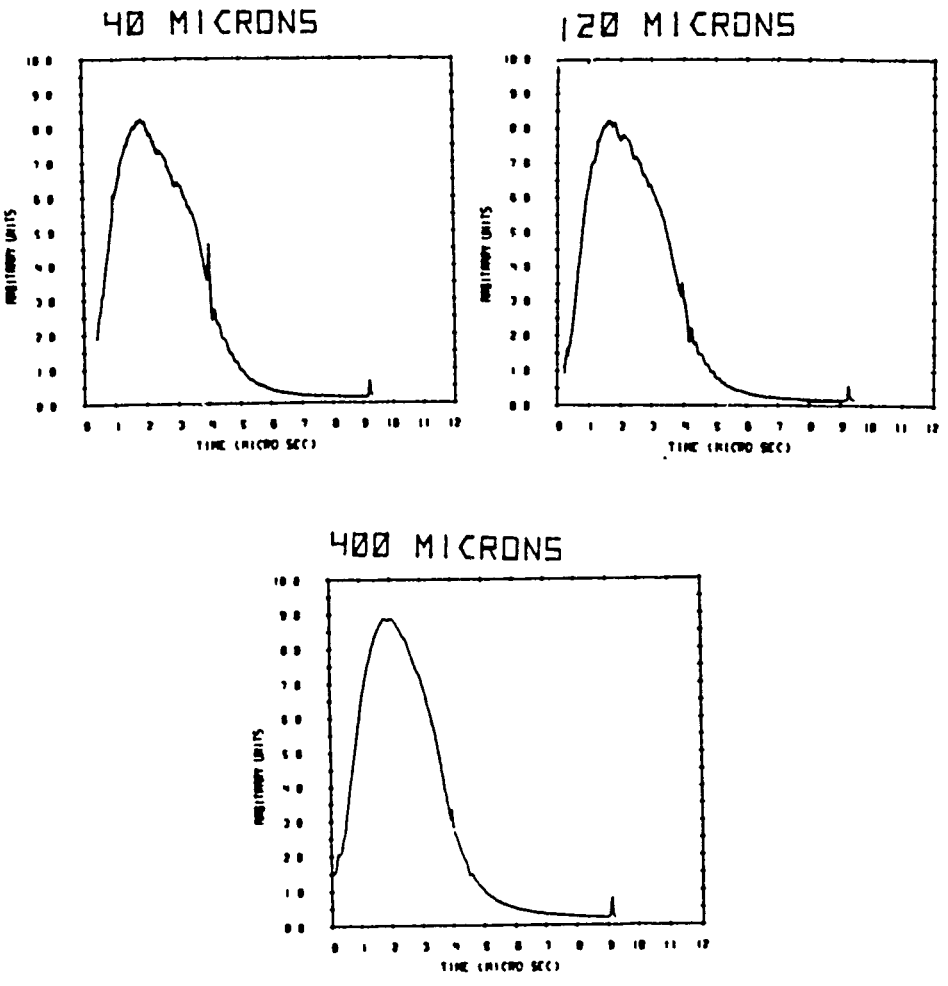

Figure 29

ING EMISSION PULSE

N2+ ING (0-2)

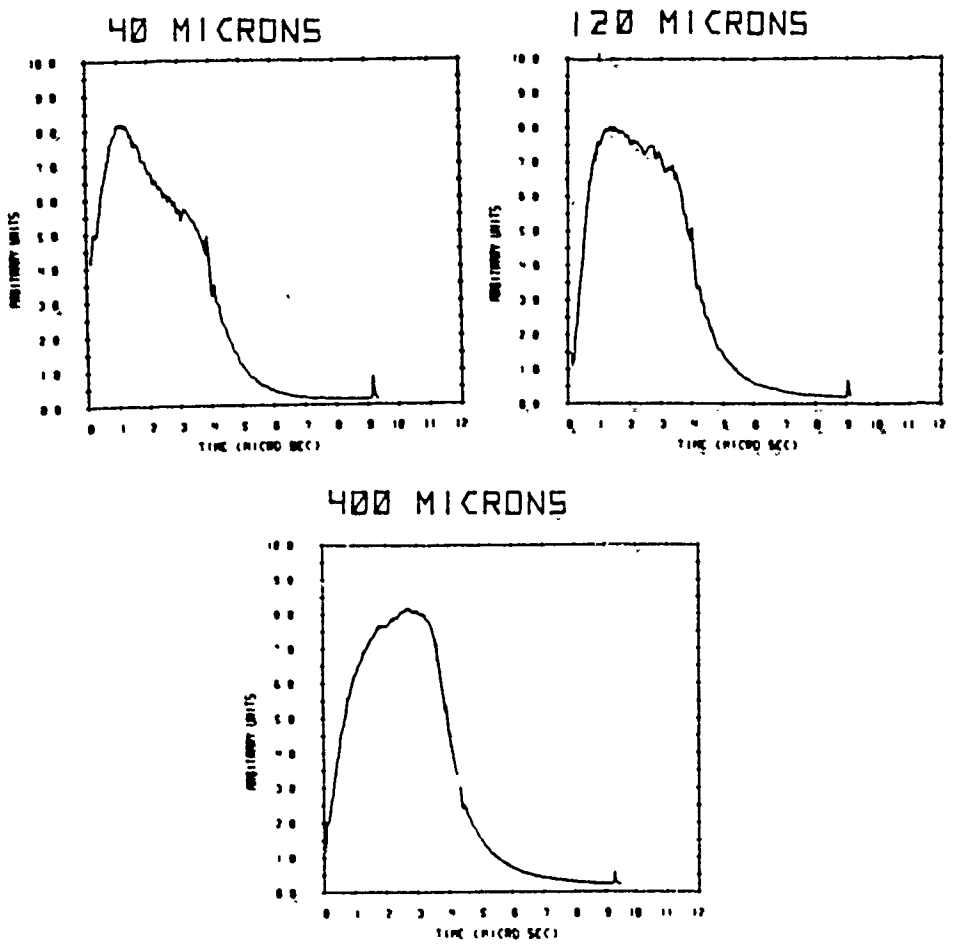

Figure 30

reaction as proposed in chapter 3. A study of the 1NG emission pulse as a function of frequency as well as pressure should distinguish between these two processes. This is due to the varying amount of vibrationally excited molecules present at different frequencies (see chapter 3 and chapter 4 - section 5).

If we consider the 1PG and 2PG, there are a number of important relationships and distinctions between them. First, the 2PG emission appears to follow the drop in the voltage during the current pulse. This is seen when we compare the 2PG emission pulse of figure 27 with the voltage trace of figure 16. Note that the majority of the voltage drop occurs within the first two microseconds. One microsecond is the point where the 2PG emission peaks, and is then followed by a slow decay. However, if excitation of the $C\,^3\Pi_u$ state stopped at 1 μs, the decay would be much more rapid than shown. This is expected since the lifetime of the $C\,^3\Pi_u$ state is on the order of 40 to 50 ns.[19] Therefore, given the data of figure 25 and 27, excitation must still be occurring after 1 μs.

In comparison the 1PG curve peaks at approximately 3.5 μs, near the end of the current pulse. The question which arises is, why does emission from the 1PG continue to rise all through the current pulse whereas 2PG emission drops rapidly during most of the same pulse?

A possible explanation arises from the fact that 2PG emission represents cascading into the the upper state of the 1PG. Consequently, one can argue that the 1PG curves peak later in the current pulse due to cascading from the $C\,^3\Pi_g$ state. This is unlikely, however, since the 2PG feeds the lower vibrational levels of the $B\,^3\Pi_g$ state preferentially.[30, 31] Data used to produce the long time decay curves of the next section, show that emission from vibrational levels 1, 2, 5, 8 and 12 of the $B\,^3\Pi_g$ state, all peak at approximately 3.5 μs. This implies that although cascading may have an effect on the leading edge of some 1PG emission curves, it cannot cause them *all* to peak near the end of the current pulse.

A second difference between the $B\,^3\Pi_g$ and $C\,^3\Pi_u$ states is the lifetimes associated with their vibrational levels: 0.044 to 0.048 μs ($C\,^3\Pi_u$, V=0 thru 4) and 8.9 to 4.6 μs ($B^3\Pi_g$, V=0 thru 12), respectively.[19] This shows the $B\,^3\Pi_g$ state lifetimes to be roughly two orders of magnitude greater than that of the $C\,^3\Pi_u$ state. Presumably, the effect of the larger lifetimes of the $B\,^3\Pi_g$ state would tend to spread the emission pulse over a larger amount of time. An analysis based on the different lifetimes of these states is presented in appendix A.

Finally, an other process which could be responsible for the continued rise in the $B^3\Pi_g$ state emission pulse is collisional coupling from adjacent vibrational levels of the $A\,^3\Sigma_u^+$, $B\,^3\Sigma_u^-$ and $W\,^3\Delta_u$ states. In this case molecules which are initially excited into these states would be coupled into the $B\,^3\Pi_g$ state by collisions. This would require the initial population of the vibrational levels of these states to be larger than those of the $B\,^3\Pi_g$ state. Collisional coupling would then cause the population to flow into the $B\,^3\Pi_g$ state. This type of process would not be possible for the $C\,^3\Pi_u$ state since it has no nearby state with which it could collisionally couple. Unfortunately, we have not made direct measurements of the vibrational level populations of these adjacent states. This makes it difficult to gauge the effect of collisional coupling from these levels during the course of the current pulse.

For a complete explanation of the observed $B\,^3\Pi_g$ state emission curves, the inclusion of all three of the above processes would be necessary. This would require a full set of emission curves from the 13 observed $B\,^3\Pi_g$ state vibrational levels, taken at various pressures and frequencies. These traces would need to be of greater accuracy than the present data since slight changes in the position of the peak or the initial decay after the end of the current pulse, would be significant indicators of the predominant processes which are taking place in this time regime. Other required information would be the

relative populations of the $C\,^3\Pi_u$ state vibrational levels, which one would need to determine the component of the $B\,^3\Pi_g$ state populations due to cascade. Also, some estimate or measurememt of $A\,^3\Sigma_u^+$, $B\,^3\Sigma_u^-$ and $W\,^3\Delta_u$ state populations would be required as well.

To sum up, the above results for the 1PG and 2PG show only slight changes with pressure. Nonetheless, these are significant and would be important in a more complete analysis. Second, due to the proximity of the $B\,^3\Pi_g$ state to other electronic potentials and its role as the recipient in the 2PG cascade, emission from $B\,^3\Pi_g$ state vibrational levels necessarily shows the effects of multiple processes ocurring within the current pulse.

CHAPTER 4 - RESULTS (III) - LONG TIME DECAY CURVES

In figures 35 thru 39, the decay of specific bands of the 1PG have been followed at three different pressures; 30, 120 and 400 μ of N_2. Again, all curves were taken at 35 Hz. The 1PG bands shown are (1-0), (2-0), (5-2), (8-4) and (12-8). These bands are generally free from overlap of other 1PG bands with the exception of (2-0). Table 1 indicates the estimated amount of overlap and the overlap band. These estimates are based on the ratio of populations at 4 μs (50 μ, 32 Hz) and the ratio of the transtion probabilities of the measured and overlap bands. Since the percent populations of the upper levels decrease with time, these values of percent overlap will also decrease.

TABLE 1 - LONG-TIME TAIL OVERLAP BANDS

BAND	OVERLAP BAND		% OVERLAP @ 4 μs
	(1-0)	(6-6)	~4%
	(2-0)	(8-7)	~12%
	(5-2)	(12-10)	~6%
	(8-4)	-	~0%
	(12-8)	-	~0%

Note that in the following figures, the intensity is on a natural log scale so a decrease of one unit on the y-axis corresponds to a drop of 1/e in intensity. Each curve was collected as a number of chart recordings with each of the charts overlapping other charts as necessary. In general we have taken data from these charts at the following intervals;

Figure 35 - N2 IPG (1-0) 30/120/400 MICRONS LN INTENSITY VS TIME

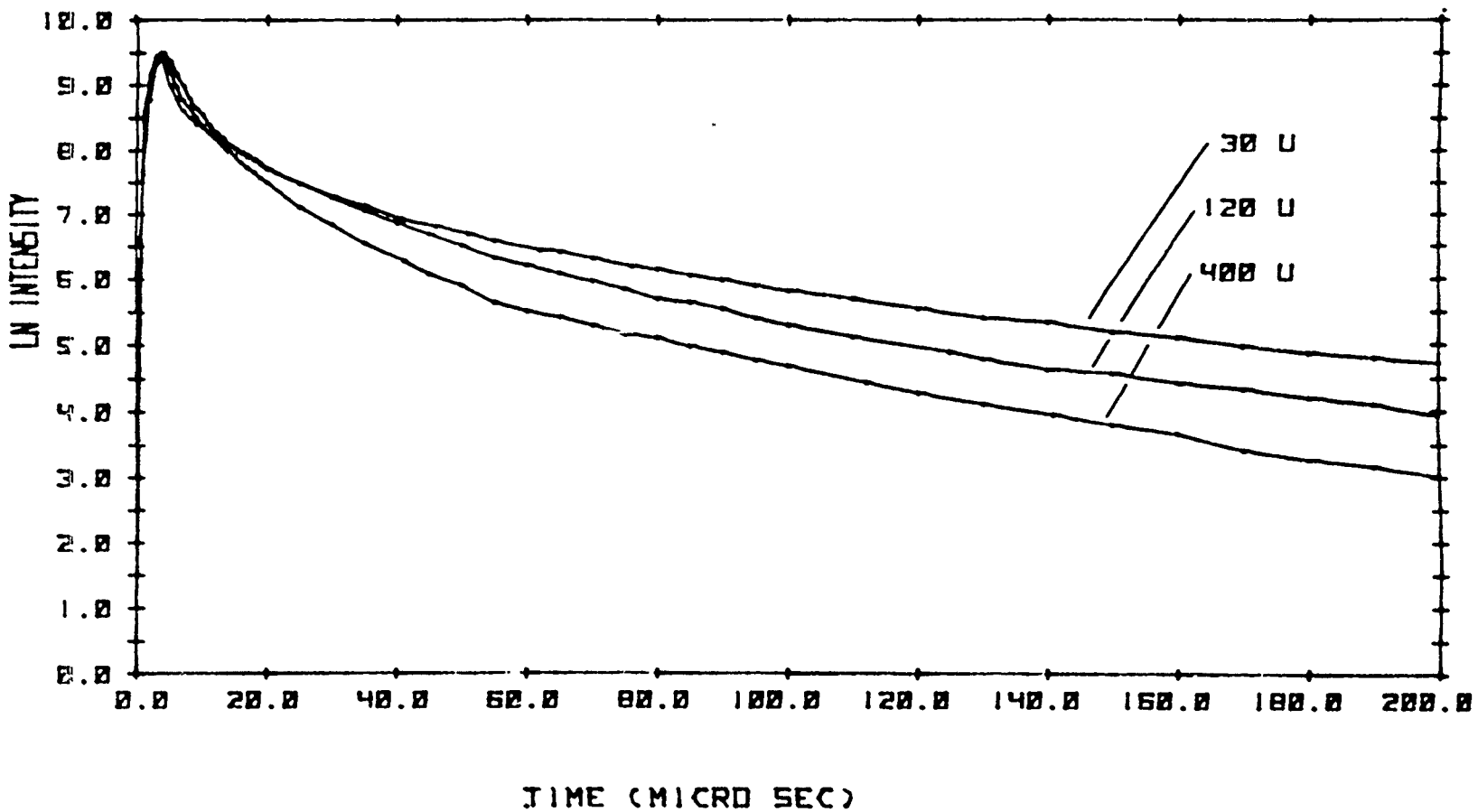

Figure 36 - N2 IPG (2-0) 30/120/400 MICRONS LN INTENSITY VS TIME

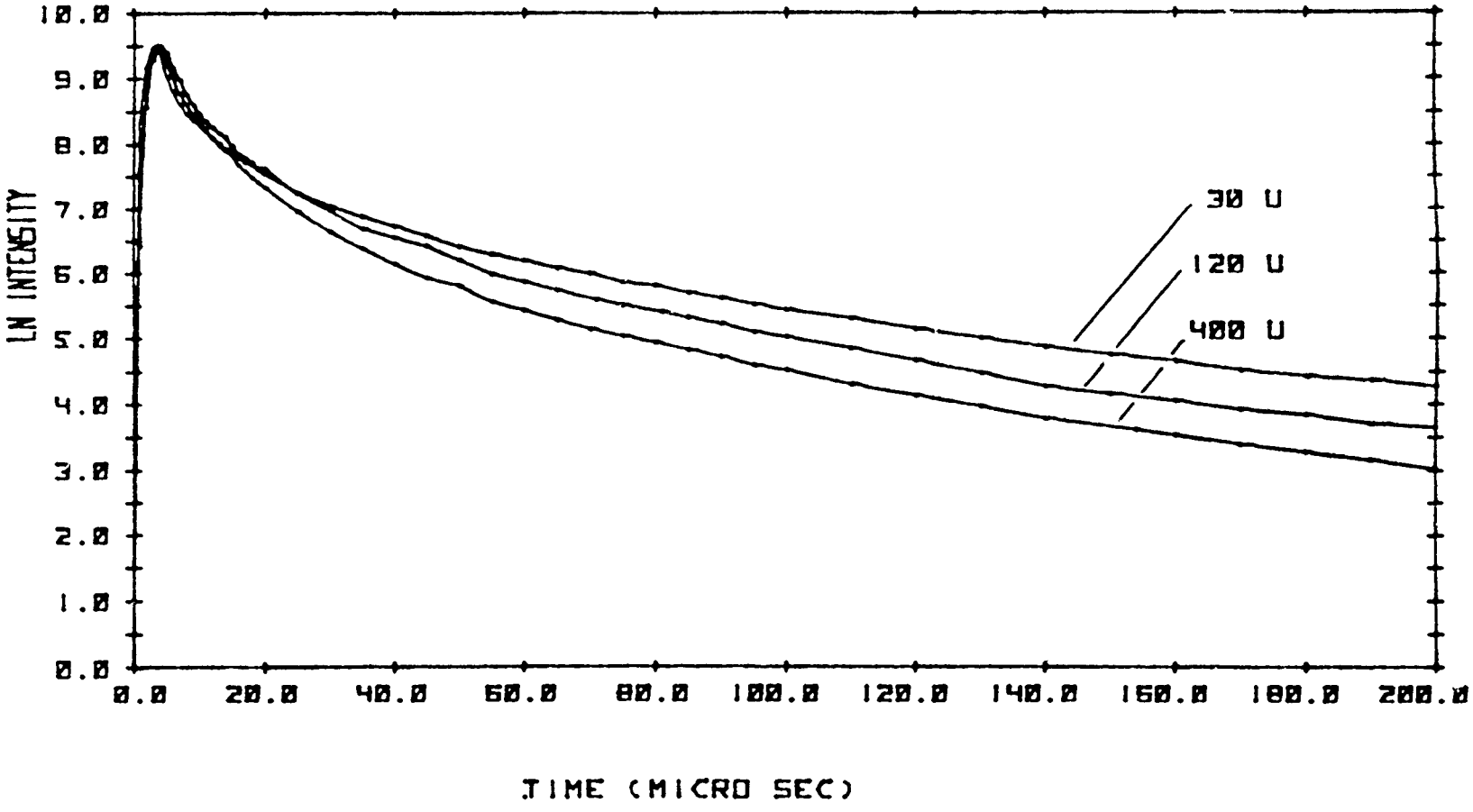

Figure 37 - N2 IPG (S-2) 30/120/400 MICRONS LN INTENSITY VS TIME

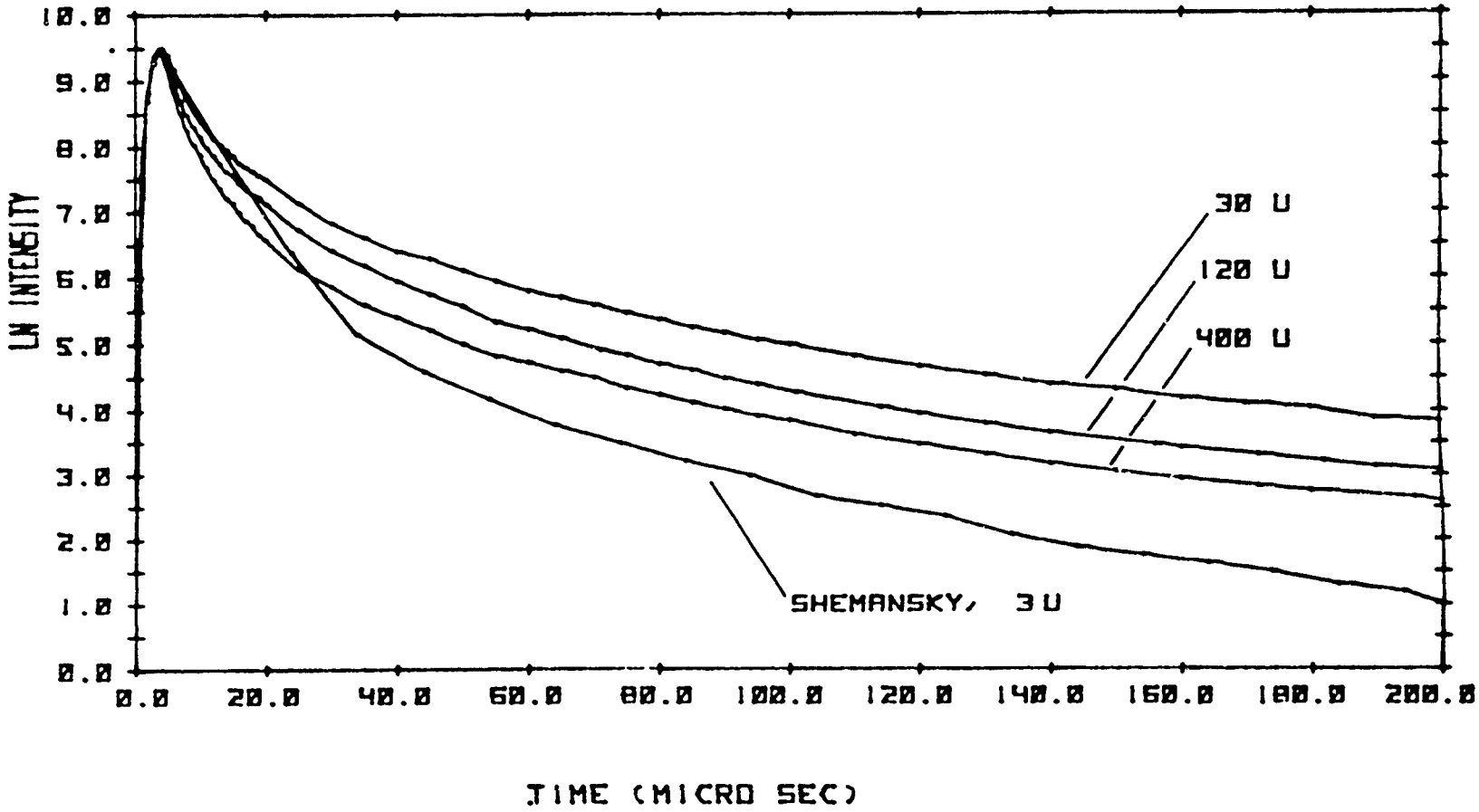

Figure 38 - N2 IPG (8-4) 30/120/400 MICRONS LN INTENSITY VS TIME

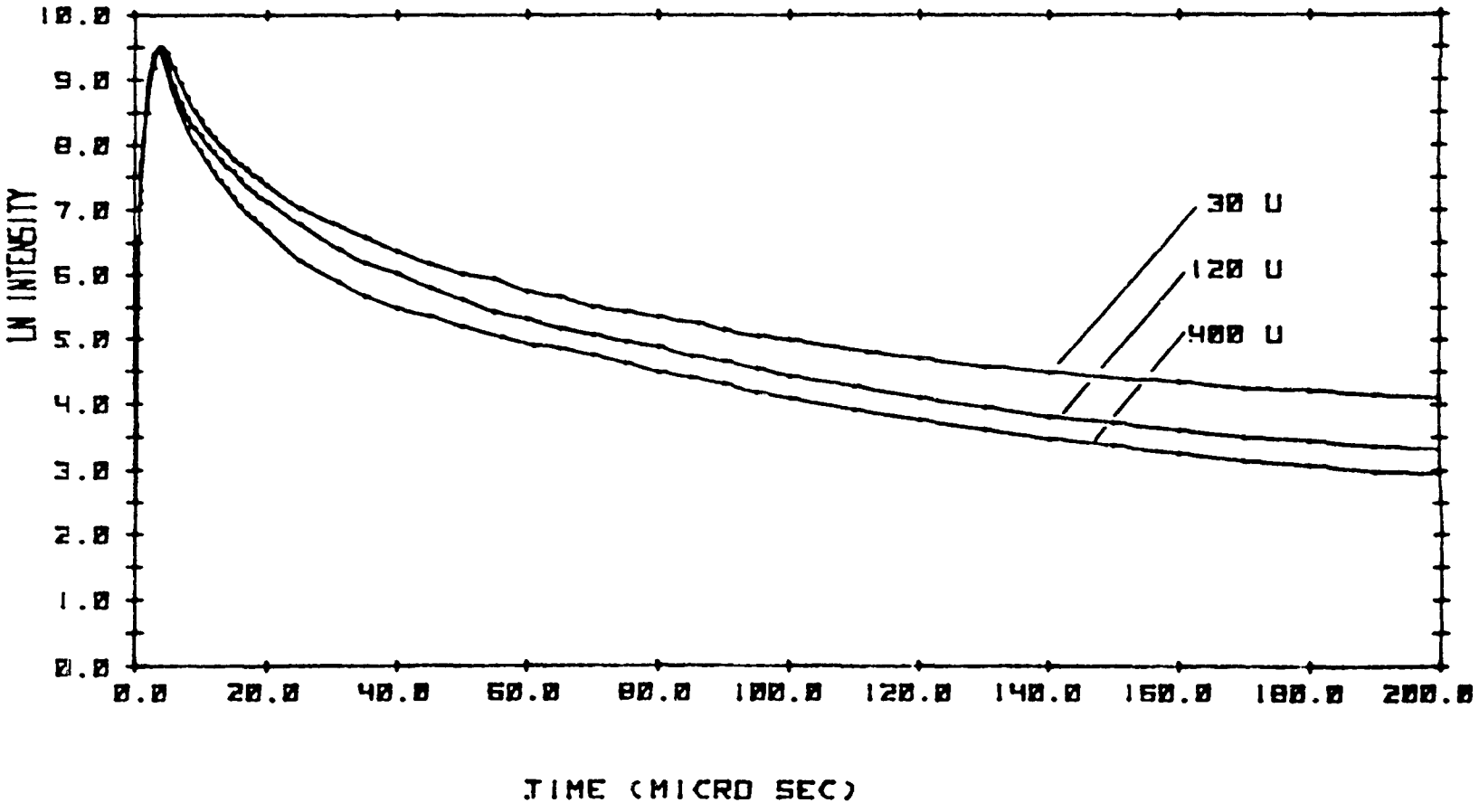

Figure 39 - N2 IPG (12-8) 30/120/400 MICRONS LN INTENSITY VS TIME

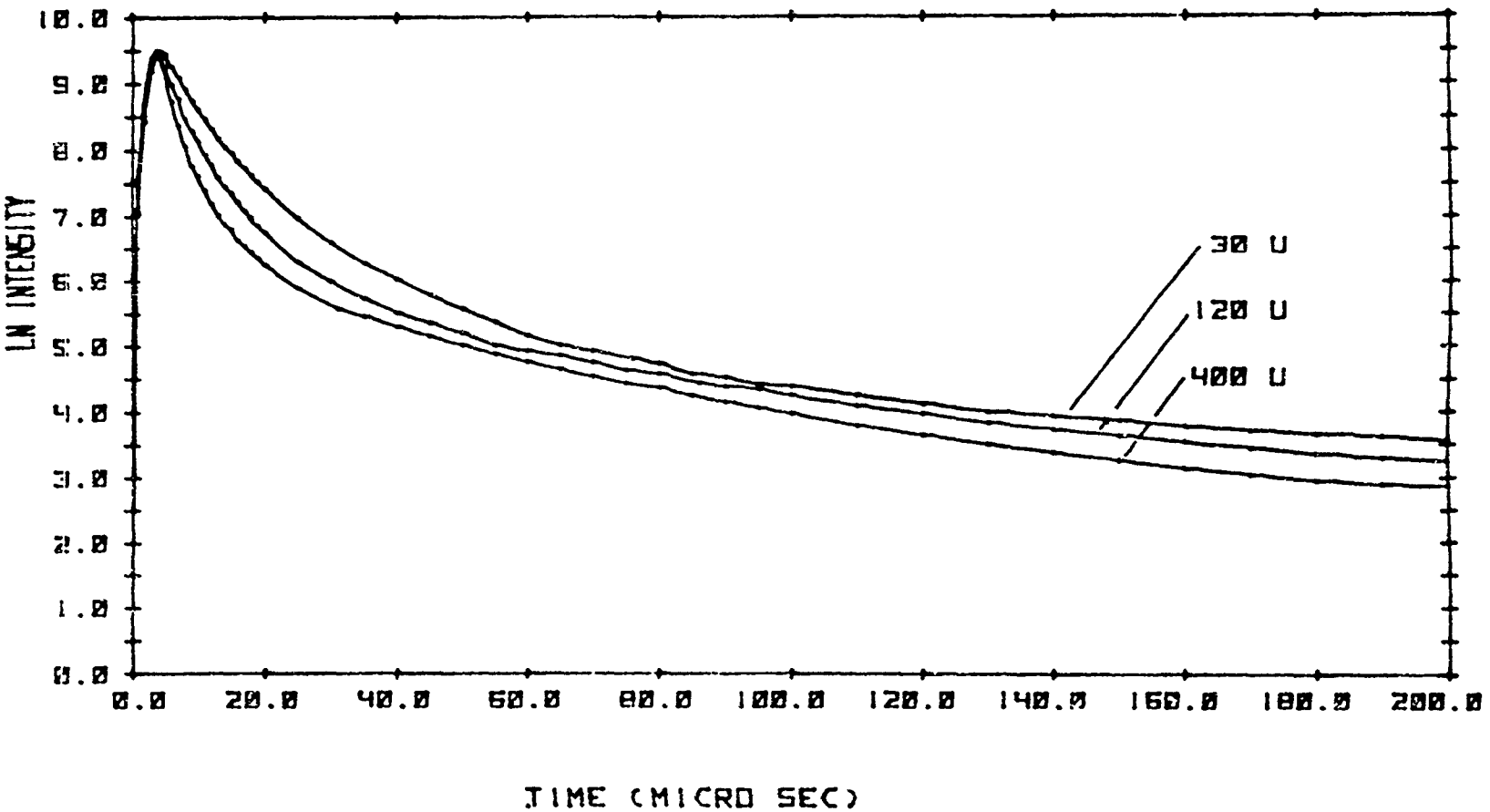

SET	TIME RANGE
1	0 to 20 μs (δt = 1 μs)
2	10 to 50 μs (δt = 2 or 5 μs)
3	15 to 100 μs (δt = 5 μs)
4	80 to 200 μs (δt = 10 μs)

For a given curve, we calculated multiplication factors for the normalization of each chart to a common scale. The resulting curves were then scaled to the same peak value. The data for these curves appear in tables 2 thru 6. The scaling factors and std. dev. appear in table 7.

These curves show a number of interesting and significant trends. First, for each set of curves, the initial slope increases with pressure. Since these curves are on a natural log scale, these slopes are the apparent lifetime of the indicated $B\,^3\Pi_g$ state vibrational level. Consequently, these results show a decrease in the apparent lifetime of these levels with increasing pressure.

This trend of increasing slope with increasing pressure is clearly evident for three of the five figures shown; V = 5, 8, and 12. In the case of V =1 and 2, the curves for 120 μ and 400 μ cross (figure 35 and 36). Regardless, if we consider only the initial slopes, the general trend is for the apparent lifetimes to decrease with increasing pressure.

Another very striking feature of these curves is the level to which the intensity drops before the curves begin their long time behavior. The behavior seen is that as we decrease the pressure, the decay curves remain at higher values when this long time tail begins.

The third point to be noted involves the slope of the long-time tail as a function of

TABLE 7 - SCALING FACTORS AND STANDARD DEVIATIONS FOR LONG-TIME TAIL DATA

Band Set	Pressure (microns) 30	120	400
(1-0) 1 to 2	30.09	47.74	79.04
(1 to 3)	0.443	2.77	1.79
2 to 3	-----	15.25	26.70
	-----	0.381	1.82
3 to 4	9.168	11.98	18.48
	0.145	0.262	0.650
(2-0) 1 to 2	44.03	63.62	100.2
(3 to 1)	0.832	3.50	2.13
2 to 3	-----	20.38	32.13
	-----	2.07	2.89
3 to 4	8.293	14.07	23.09
	0.218	0.182	0.850
(5-2) 1 to 2	59.94	119.1	200.7
(1 to 3)	0.690	1.34	7.18
2 to 3	-----	32.95	48.26
	-----	0.826	2.75
3 to 4	10.12	21.34	21.84
	0.1918	0.364	0.990
(8-4) 1 to 2	63.46	115.0	161.1
(1 to 3)	2.16	3.05	13.2
2 to 3	-----	29.44	48.37
	-----	1.94	0.996
3 to 4	12.16	19.40	19.24
	0.295	0.291	1.09
(12-8) 1 to 2	79.82	144.5	188.2
(1 to 3)	2.30	9.06	3.29
2 to 3	36.23	45.25	31.83
	1.45	2.37	1.98
3 to 4	19.18	18.84	13.02
	0.879	0.430	0.257

upper entries - scaling factor lower entries - standard deviation

pressure. Other studies[21] have expressed these curves as a sum of expontials. This form assumes that the processes contributing to the decay are first order. Considering this assumption valid for our system, time constants for these curves were calculated between 100 and 200 μs. These were determined even though the data showed some curvature. The values obtained are shown in table 8. The present results do not show a dramatic change in the long-time slope with changes in pressure. The long-time decay constants do tend to increase as the pressure is increased (see table 8).

As mentioned in the introduction, similar behavior in decay curves has been seen in past studies.[21] For comparison, Shemansky's data are plotted in figure 37 with the present data. This figure is for the (5-2) band whereas Shemansky's data are for the (5-3) band. Regardless, both correspond to decay of the V = 5 of the $B\,^3\Pi_g$ state.

Shemansky's experiment differed from the present study in that he used an electron beam. His source was reported to have a "0.5 eV half width at 10 eV." [21] The electron energy for this data was given as 11 eV and at a pressure of 3 μ of pure N_2. This was a pulsed experiment with an electron beam pulse length of 10 μs and a total period of 210 μs. This corresponds to a frequency of approximately 4800 Hz (~5 kHz).

If we compare Shemansky's data with the present study we see that, first, the initial decay component for emmision from a given level increases with pressure as seen in this study (the lifetime decreases with increasing pressure). Next, the point where Shemansky's long time behavior begins, occurs at a much lower relative intensity than in this study. This is at odds with the present results where the point of crossover, to long time behavior, occurs at *lower* intensity for *higher* pressure. Finally, the decay constants associated with the long-time behavior of Shemansky's curves changes dramatically with pressure. The trend in his results is for these decay constants to *decrease* with *increasing* pressure. The present results, on the other hand, show no dramatic change with

TABLE 8 - LONG-TIME TAIL DECAY CONSTANTS

Pressure ->	10μ (Shemansky)	30μ (Present Study)	120μ	400μ
Vibrational Level	Upper value / Lower value	Decay constant (MHz) / Apparent Lifetime(μs)		
0	---- / ----	---- / ----	---- / ----	---- / ----
1	9E-3 / 111	11E-3 / 91	13E-3 / 78	17E-3 / 61
2	7E-3 / 250	12E-3 / 83	14E-3 / 72	14E-3 / 69
3	4E-3 / 250	---- / ----	---- / ----	---- / ----
4	5E-3 / 200	---- / ----	---- / ----	---- / ----
5	4E-3 / 250	11E-3 / 88	12E-3 / 83	12E-3 / 83
6	9E-3 / 111	---- / ----	---- / ----	---- / ----
7	4E-3 / 250	---- / ----	---- / ----	---- / ----
8	5E-4 / 2000	8.6E-3 / 116	11E-3 / 90	12E-3 / 87
9	4E-4 / 2500	---- / ----	---- / ----	---- / ----
10	7E-3 / 143	---- / ----	---- / ----	---- / ----
11	7E-3 / 143	---- / ----	---- / ----	---- / ----
12	4E-3 / 250	8.1E-3 / 123	10E-3 / 99	11E-3 / 88

pressure and the trend is for these decay constants to increase with increasing pressure.

An important difference between the present experiment and any low energy beam experiment involves the production of vibrationally excited molecules by electrons. In light of the value of the electron beam energy used to generate the excited electronic states, $E \geq 10$ eV (see table 9), very little vibrational excitation will occur. This is because the cross-sections for vibrational excitation by electrons peaks between 1.5 and 3.5 eV.[27] Also, in a beam experiment, the region of the chamber being excited is usually a small fraction of the total volume. Consequently, any vibrationally excited molecules which do result, would not tend to raise the vibrational temperature of the gas.

The present experiment offers two differences when compared to a beam experiment. First, the excited species which result are produced by a distribution of energetic electrons. This tends to produce species with a wide range of energy content relative to the ground state. This includes vibrationally excited ground state molecules. Second, approximately 2/3 of the entire volume of the chamber is excited during each pulse. As a result excited species do not diffuse out of the field of view as was the case with Shemansky's experiment. One effect, of these two differences, is that the vibrational temperture of the gas appears to become elevated under certain conditions. We will discuss this later in more detail (see chapter4 - section V).

Other pulsed discharge experiments by Hays and Oskam show evidence for the following two reactions,[32]

$$N_2(A\,^3\Sigma_u^+) + N_2(A\,^3\Sigma_u^+) \text{---> N2}(B\,^3\Pi_g,\ C\,^3\Pi_u,\ \text{or}\ C'\,^3\Pi_u) + N_2(X\,^1\Sigma_g^+)^* \quad (1)$$

and

$$N_2(A\,^3\Sigma_u^+) + N_2(X\,^1\Sigma_g^+)^* \text{--> } N_2(A\,^3\Sigma_u^+, V>7) + N_2(X\,^1\Sigma_g^+) \text{-->}$$
$$\text{--> } N_2(B\,^3\Pi_g) + N_2(X\,^1\Sigma_g^+) \qquad (2)$$

TABLE 9 - ELECTRON CROSS-SECTIONS AND PERCENT POPULATION BETWEEN 11 AND 12 eV

Energy	Electronic States - Cross-Sections (1E16 cm^2)							
	A	B	W	B'	a'	a	w	C
11	0.148	0.278	0.166	0.055	0.045	0.099	0.071	---
11.5*	0.160	0.289	0.190	0.065	0.054	0.120	0.085	0.073
12	0.171	0.299	0.213	0.074	0.062	0.140	0.099	0.146

Energy	Electronic States - Ratio to B State							
	A	B	W	B'	a'	a	w	C
11	0.53	1	0.60	0.20	0.16	0.36	0.26	---
11.5	0.55	1	0.66	0.22	0.19	0.41	0.29	0.25
12	0.57	1	0.71	0.25	0.21	0.47	0.33	0.49

Energy	Electronic States - Percent Population							
	A	B	W	B'	a'	a	w	C
11	17	32	19	6.4	5.1	12	8.4	---
11.5	15	28	19	6.2	5.3	12	8.1	7.0
12	14	25	18	6.2	5.2	12	8.2	12

* => Based on extrapolated values between 11 and 12 eV.

where $N_2(X\,^1\Sigma_g^+)^*$ is a vibrational excited ground state molecule.

The first reaction is undoubtedly occuring in beam experiments as well as ours. The second reaction, on the other hand, would only be expected to be occuring in our system.

As mentioned, other results of this study (chapter 4-section V) have shown that the apparent vibrational temperature increases under most conditions. Table 10 lists the estimated vibrational temperature and concentration of ground state molecules with $V \geq 7$, expected for the conditions used for the long time curves. The ground state level, V=7 was chosen since it represents the minimum energy required to excite the V=5 level of the $B\,^3\Pi_g$ state from the V=3 level of the $A\,^3\Sigma_u^+$ state. The V=3 level of the $A\,^3\Sigma_u^+$ state has the largest Franck-Condon overlap with the V=5 level of the $B\,^3\Pi_g$ state.

The estimated values of this table shows that as the pressure increases, the density of ground state molecules with $V \geq 7$ decreases, within the errors of the measurments of section V. These values were estimated by fitting a straight line through a plot of the log of the measured concentrations vs pressure. We have taken the estimated values from this linear fit.

Returning to figure 37, a possible explaination for the difference between our result and Shemansky's is that, as the concentration of vibrationally excited molecules decreases (going to higher pressure), the curves of this study approach Shemansky's low pressure data. His experiment is expected have been generally free of vibrationally excited molecules so his results can be viewed as a baseline for the effect of this excited species.

This explanation does not account for the effect of the difference in pressure on these two sets of data. Nor does it address Intersystem Collisional Transfer (ICT) between the $B\,^3\Pi_g$ state and other states, besides $A\,^3\Sigma_u^+$, which is necessarily occuring. It is difficult for us to estimate the effect of ICT in the above decay curves. It is

TABLE 10 - Measured and Estimated Amounts of [N2*(X)]

P[μ]	Z[#/μs]	density [#/cc]	Tv[K]	fraction in V>7	N2(X)* [#/cc]
400	2.7	1.287E16	1980	6.60E-6	8.49E10
			±64	+2.8E-6	+3.6E10
				-2.1E-6	-2.6E-10
200	1.3	6.435E15	2100	1.31E-5	8.43E10
			±29	+.14E-5	+0.90E10
				-.14E-5	-0.90E10
50	0.3	1.609E15	2540	9.16E-5	1.47E11
			±102	+3.9E-5	+0.62E11
				-2.9E-5	-0.46E11
			----- ESTIMATED VALUES -----		
400	2.7	1.28E16	1920	4.5E-6	5.8E10
120	0.8	3.86E15	2220	2.3E-5	9.0E10
30	0.2	9.65E14	2620	1.2E-4	1.12E11

Values of T_v where taken from table -- for the case of 32 Hz discharge frequency and the above pressures.

obvious that $B^3\Pi_g$ state molecules are being produced by some secondary process long after the initial excitation pulse. Once the $B^3\Pi_g$ state molecules are produced, the population will tend to redistribute itself amongst the adjacent states. This should have the effect of extending the apparent lifetime. What the above long-time data shows is apparent liftimes of 60 to 80 μs, or a factor of about 10 greater than the natural lifetimes. It is doubtful that ICT alone could increase the lifetimes by this amount. Consequently, these decay curves probably represent the effects of other processes as well. These processes are most likely reactions (1) and (2) above.

In order to disentangle the effects of reactions (1) and (2) above, as well as the role of ICT, further data is required. The present results show that a decrease in the concentration of vibrationally excited molecules coincide with a more rapid decrease in the intensity, as a function of time. Unfortunately in these figures, this decrease in concentration occurs with an increase in pressure and so collision frequency. Changes in collision frequency will undoubtly effect the rates at which these processes occur.

This decrease in vibrationally excited molecules can also be achieved at a constant pressure by a decrease in pulse discharge frequency. Therefore, the role of vibrationally excited molecules would best be shown if we examine decay curves taken at constant pressure and over a wide range of discharge frequencies. We would expect a trend similar to that of the present data, but it would not show the effect of the variation in collision frequency which makes the above curves difficult to interpret. It would, however, clarify the role of vibrationally excited molecules in the production of $B^3\Pi_g$ state, upon which these results appear to depend.

Tables 2 through 6. The pressure at which the curves were taken appear at the top of each pair of columns. The left column of each pair is the time in micro-seconds and the right column is the natural log of the intensity. All curves have been normalized to 9.5 at the peak.

Table 2 - N2 DECAY CURVES - DATA
(1-0) BAND

30 MICRONS		120 MICRONS		400 MICRONS	
0	0	0	0	0	0
1	7.63	1	8.51	1	7.69
2	8.78	2	9.16	2	8.92
3	9.34	3	9.45	3	9.42
3.75	9.46	3.75	9.5	3.75	9.5
4	9.5	4	9.36	4	9.48
5	9.37	5	8.99	5	9.22
6	9.17	6	8.8	6	8.99
7	9	7	8.62	7	8.78
8	8.81	8	8.51	8	8.67
9	8.65	9	8.4	9	8.52
10	8.56	10	8.36	10	8.39
11	8.41	11	8.28	11	8.29
12	8.29	12	8.2	12	8.19
13	8.21	13	8.13	13	8.09
14	8.1	14	8.07	14	7.99
15	8.04	15	8.02	15	7.93
16	7.98	16	7.97	16	7.82
17	7.93	17	7.91	17	7.74
18	7.86	18	7.87	18	7.67
19	7.8	19	7.81	19	7.58
20	7.72	20	7.73	20	7.51
25	7.49	25	7.5	25	7.12
30	7.29	30	7.27	30	6.85
35	7.14	35	7.06	35	6.56
40	6.95	40	6.87	41	6.29
46	6.82	45	6.69	45	6.08
51	6.7	50	6.52	50	5.91
55	6.59	55	6.33	55	5.65
62	6.45	60	6.22	60	5.52
65	6.42	65	6.09	65	5.43
70	6.32	70	5.97	70	5.3
76	6.2	75	5.85	75	5.16
80	6.15	80	5.7	80	5.11
85	6.06	85	5.65	85	4.98
90	5.99	90	5.55	90	4.89
95	5.9	95	5.41	95	4.78
100	5.82	100	5.3	100	4.69
110	5.7	110	5.12	112	4.44
120	5.55	125	4.89	120	4.28
130	5.41	130	4.79	130	4.11
140	5.34	140	4.63	141	3.95
150	5.19	150	4.57	150	3.8
160	5.11	160	4.43	160	3.67
170	4.98	170	4.34	170	3.42
180	4.88	180	4.21	180	3.28
190	4.81	190	4.11	190	3.18
200	4.73	200	3.94	200	3.02

Table 3 - N2 DECAY CURVES - DATA
(2-0) BAND

30 MICRONS		120 MICRONS		400 MICRONS	
0	0	0	0	0	0
1	6.43	1	8.36	1	7.47
2	8.57	2	9.16	2	8.84
3	9.28	3	9.48	3	9.41
3.75	9.45	3.5	9.5	3.75	9.5
4	9.5	4	9.41	4	9.48
5	9.4	5	9.03	5	9.25
6	9.16	6	8.81	6	9
7	8.98	7	8.62	7	8.78
8	8.78	8	8.47	8	8.62
9	8.61	9	8.36	9	8.46
10	8.47	10	8.29	10	8.36
11	8.35	11	8.19	11	8.23
12	8.26	12	8.09	12	8.11
13	8.17	13	8.02	13	7.99
14	8.11	14	7.93	14	7.9
15	7.99	15	7.89	15	7.83
16	7.85	16	7.8	16	7.68
17	7.79	17	7.72	17	7.59
18	7.72	18	7.68	18	7.49
19	7.61	19	7.63	19	7.42
20	7.54	20	7.62	20	7.34
25	7.26	25	7.25	25	6.97
30	7.05	30	6.98	30	6.66
35	6.89	35	6.7	35	6.4
40	6.74	40	6.57	40	6.15
45	6.59	45	6.43	45	5.93
50	6.42	50	6.21	50	5.81
55	6.3	55	5.99	55	5.56
60	6.2	60	5.87	60	5.44
65	6.08	65	5.74	65	5.29
70	6	71	5.59	70	5.15
75	5.86	75	5.51	75	5.04
80	5.81	81	5.41	80	4.94
85	5.7	85	5.32	85	4.83
90	5.62	90	5.23	90	4.73
95	5.52	95	5.1	95	4.6
100	5.44	100	5.02	100	4.53
110	5.31	110	4.85	110	4.31
120	5.15	120	4.67	120	4.14
130	5.01	130	4.49	130	3.98
140	4.87	140	4.28	140	3.79
150	4.76	150	4.16	154	3.62
160	4.66	160	4.05	160	3.54
170	4.53	170	3.93	170	3.4
180	4.44	180	3.85	180	3.29
190	4.38	190	3.71	190	3.17
200	4.28	200	3.65	200	3.03

Table 4 - N2 DECAY CURVES - DATA
(5-2) BAND

30 MICRONS		120 MICRONS		400 MICRONS	
0	0	0	0	0	0
1	5.51	1	7.56	1	7.4
2	8.71	2	8.81	2	8.86
3	9.27	3	9.39	3	9.39
3.75	9.48	3.75	9.5	3.75	9.5
4	9.5	4	9.49	4	9.47
5	9.4	5	9.28	5	9.18
6	9.19	6	9	6	8.82
7	8.95	7	8.71	7	8.52
8	8.74	8	8.5	8	8.27
9	8.55	9	8.31	9	8.05
10	8.4	10	8.17	10	7.9
11	8.28	11	8.01	11	7.71
12	8.14	12	7.89	12	7.53
13	8.05	13	7.76	13	7.38
14	7.97	14	7.64	14	7.23
15	7.88	15	7.58	15	7.15
16	7.76	16	7.45	16	7.01
17	7.7	17	7.36	17	6.89
18	7.64	18	7.28	18	6.81
19	7.57	19	7.24	19	6.68
20	7.52	20	7.14	20	6.6
25	7.15	25	6.75	25	6.14
30	6.85	30	6.43	30	5.88
35	6.63	35	6.2	35	5.6
40	6.41	40	5.96	40	5.42
45	6.3	45	5.76	45	5.23
50	6.12	50	5.58	50	5.01
55	5.96	55	5.35	55	4.84
60	5.81	60	5.24	60	4.75
65	5.71	65	5.11	65	4.62
70	5.6	71	4.93	70	4.52
75	5.48	75	4.85	75	4.36
80	5.38	80	4.72	80	4.26
85	5.26	85	4.63	85	4.14
90	5.18	90	4.5	90	4.04
95	5.07	95	4.41	95	3.93
100	5	101	4.29	100	3.86
110	4.83	114	4.07	110	3.64
120	4.68	120	3.97	120	3.49
130	4.55	130	3.81	130	3.34
140	4.41	140	3.66	140	3.19
150	4.33	156	3.48	150	3.06
160	4.2	160	3.43	160	2.95
170	4.12	172	3.33	172	2.84
180	4.06	182	3.23	180	2.77
190	3.9	190	3.15	196	2.67
200	3.85	200	3.09	200	2.61

Table 4b - N2 DECAY CURVES - DATA
SHEMANSKY 95-3) BAND
3 MICRONS

4	9.5
14	7.89
24	6.4
34	5.16
44	4.61
54	4.2
64	3.79
74	3.51
84	3.23
94	3
104	2.69
114	2.54
124	2.37
134	2.08
144	1.9
154	1.77
164	1.65
174	1.51
184	1.32
194	1.21
200	1.03

Table 5 - N2 DECAY CURVES - DATA
(8-4) BAND

30 MICRONS	
0	0
1	7.11
2	8.51
3	9.2
3.75	9.49
4	9.5
5	9.42
6	9.19
7	8.95
8	8.74
9	8.53
10	8.4
11	8.24
12	8.12
13	7.99
14	7.91
15	7.78
16	7.7
17	7.64
18	7.53
19	7.48
20	7.38
25	7.03
30	6.8
35	6.59
40	6.37
45	6.17
50	6.02
55	5.94
60	5.74
65	5.67
70	5.51
75	5.44
80	5.35
86	5.26
90	5.14
95	5.05
100	4.99
112	4.81
120	4.71
130	4.58
140	4.5
152	4.39
160	4.35
170	4.25
180	4.22
190	4.15
200	4.1

120 MICRONS	
0	0
1	7.73
2	8.8
3	9.39
3.75	9.5
4	9.48
5	9.26
6	8.91
7	8.66
8	8.43
9	8.27
10	8.16
11	8.01
12	7.9
13	7.78
14	7.66
15	7.59
16	7.47
17	7.36
18	7.28
19	7.19
20	7.13
25	6.79
31	6.4
35	6.19
40	6.03
45	5.8
50	5.63
55	5.43
60	5.32
65	5.17
70	5.07
75	4.96
80	4.88
85	4.74
90	4.66
95	4.55
100	4.43
110	4.28
120	4.1
130	3.96
140	3.81
150	3.72
160	3.61
170	3.51
180	3.45
190	3.37
200	3.32

400 MICRONS	
0	0
1	7.3
2	8.88
3	9.39
3.75	9.5
4	9.46
5	9.1
6	8.77
7	8.48
8	8.26
9	8.04
10	7.92
11	7.75
12	7.59
13	7.45
14	7.33
15	7.19
16	7.06
17	6.96
18	6.88
19	6.79
20	6.69
25	6.23
31	5.89
35	5.68
40	5.49
45	5.36
50	5.2
56	5.03
61	4.9
65	4.86
70	4.76
75	4.63
80	4.49
85	4.41
90	4.31
95	4.18
100	4.09
110	3.92
120	3.76
130	3.62
140	3.48
150	3.38
160	3.26
170	3.15
180	3.08
190	2.99
200	2.95

Table 6 - N2 DECAY CURVES - DATA
(12-8) BAND

30 MICRONS		120 MICRONS		400 MICRONS	
0	0	0	0	0	0
1	7.05	1	7.7	1	7.65
2	8.42	2	8.93	2	8.83
3	9.19	3	9.33	3	9.38
4	9.47	3.75	9.5	3.75	9.5
4.25	9.5	4	9.48	4	9.47
5	9.45	5	9.24	5	9.15
6	9.26	6	8.99	6	8.74
7	9.1	7	8.78	7	8.37
8	8.93	8	8.48	8	8.08
9	8.75	9	8.29	9	7.77
10	8.61	10	8.14	10	7.61
11	8.47	11	7.94	11	7.4
12	8.32	12	7.79	12	7.2
13	8.17	13	7.59	13	7.02
14	8.06	14	7.47	14	6.89
15	7.97	15	7.36	15	6.81
16	7.84	16	7.23	16	6.64
17	7.74	17	7.09	17	6.55
18	7.63	18	6.98	18	6.44
19	7.53	19	6.86	19	6.36
20	7.43	20	6.76	20	6.26
25	6.98	25	6.3	25	5.9
30	6.6	30	6	31	5.58
35	6.28	35	5.73	35	5.47
40	6.04	40	5.52	40	5.31
45	5.78	45	5.36	45	5.16
50	5.57	50	5.21	50	5.02
55	5.38	55	5.02	55	4.89
60	5.17	60	4.93	60	4.77
65	5.02	65	4.86	65	4.65
70	4.93	70	4.76	70	4.54
76	4.82	75	4.64	75	4.44
80	4.74	80	4.58	80	4.37
85	4.58	86	4.44	85	4.25
90	4.53	90	4.39	90	4.16
95	4.42	95	4.34	95	4.07
100	4.39	100	4.25	100	3.98
110	4.36	110	4.1	110	3.8
120	4.13	120	3.98	120	3.65
130	4.01	130	3.84	130	3.51
140	3.94	140	3.73	140	3.38
150	3.88	150	3.64	150	3.27
160	3.78	160	3.54	160	3.15
170	3.72	170	3.45	170	3.05
180	3.66	180	3.36	180	2.95
190	3.62	190	3.3	190	2.89
200	3.56	200	3.25	200	2.86

CHAPTER 4 - RESULTS (IV) - POPULATION PLOTS

The major body of data which we will present involves the change in time of the vibrational populations of levels 1 thru 12 of the $B\ ^3\Pi_g$ state. These data make up a matrix of pressure and frequency conditions at which the discharge was run. The conditions are,

Pressures => 50, 200, 400 μs

Frequencies => 5, 15, 32, 50 Hz

Current => 600 amps peak

Therefore, each of the resulting data sets are elements of a 3x4 matrix composed of the above conditions.

1PG spectra covering the sequences $\delta V = 1,2,3,4$ were taken at times from 0.5 to 200 μs. The time ranges and intervals are listed below.

TIME RANGE	INTERVAL
0 to 10 μs	1 μs
10 to 20 μs	2 μs
40 to 200 μs	40 μs

An example of one of these spectra appears in figure 14.

Spectra from 0.5 to 20 μs were taken for each combination of pressure and discharge frequency above, at constant photomultiplier tube (PMT) voltage. In order to optimize the signal at 3 μs we were required to vary the PMT voltage for each set of conditions. Later we normalized the results to the same relative population scale by a set of spectra taken at 3 μs and each of the above sets of conditions. This set of scaling spectra were all taken with the same PMT voltage. The results of this procedure showed that the overall intensity of these scaling spectra increased with increasing pressure. This is shown by the increase in the scaling factors with increasing pressure (table 24). This

implies that the total number of excited molecules in the tube is increasing with pressure as well. The fractional excitation, however, does decrease with increasing pressure. This is found from the ratio of the scaling factors to the density, for the three pressures.

The following collection of tables and plots result from about 300 spectra. All were calibrated with the calibration curve discussed in chapter 2. The populations were determined from the spectra using a computer program that integrated band intensities over a constant wavenumber region around the band origin of each vibrational band considered. A total of 26 bands were analyzed from each spectrum with the resulting populations of each level reflecting the average of at least two bands, except for V = 1 and 12. The transition probabilities and band orgins of Shemansky and Broadfoot[19] were used to correct for overlapping bands and determines the populations. These values appear in table 11. The upper entries are the band origins in Angstroms and the lower entries are the transition probabilities in Hz.

The resulting populations appear in tables 12 thru 23 and figures 40 thru 51. These tables and figures appear at the end of this section. In the tables, the left hand column is the time when the spectrum was taken. All time values are relative to the start of the current pulse. The top row of numbers indicate the vibrational level of the $B\,^3\Pi_g$ state. For a given time, there are two entries for each vibrational level. The upper entry is the population of the level relative to all other populations shown in the table. As mentioned, steps were taken to put all results on a common scale. This makes the upper entries relative to populations in all other tables, within the error of the conversion factors (table 24). So, by relative population we mean that there is a multiplication factor, which has not been determined, which would convert the upper entries from relative populations to absolute densities of $B\,^3\Pi_g$ state molecules at the indicated vibrational

IPG TRANSITION PROBABILITIES

	0	1	2	3	4	5	6	7	8	9	10	11	12	13	$\sum A_{ij}$	Extrapolated
0	104690	123166	148945	187191	250829	375220									1.12+5	1.12+5
	6.95+4	3.56+4	1.12+4	2.47+3	3.97+2	4.24+1										
1	88834	101790	118781	142017	175693	229829	325037								1.28+5	1.29+5
	8.72+4	4.12+2	1.85+4	1.48+4	5.69+3	1.40+3	2.27+2									
2	77120	86953	99057	114709	115721	165388	210198	286714	444176						1.42+5	1.43+5
	4.84+4	6.17+4	1.25+4	2.68+3	1.05+4	7.29+3	2.71+3	6.39+2	8.87+1							
3	68583	76058	85160	96477	110920	29974	156241	194732	256487	371562	660899				1.54+5	1.54+5
	1.07+4	7.73+4	2.17+4	2.85+4	7.97+2	1.88+3	6.33+3	1.68+3	1.24+3	2.57+2	2.54+1					
4	61731	67721	74844	83447	94038	107384	124706	148066	180248	232028	319329	504316			1.62+5	1.64+5
	1.39+3	3.02+4	8.36+4	1.54+3	2.94+4	7.84+3	1.93+2	1.52+3	3.74+3	1.84+3	5.44+2	9.03+1				
5	56216	61141	66887	73675	81810	91729	104077	119859	140712	169515	211822	279934	407563		1.72+5	1.73+5
	7.12+1	5.08+3	5.26+4	6.86+4	3.02+3	1.91+4	1.52+4	1.13+3	1.02+3	2.81+3	2.13+3	8.95+2	2.24+2			
6		55816	60567	66080	72550	80244	89538	100976	115382	134059	159207	194838	249140	341700	1.78+5	1.81+5
		3.71+2	1.19+4	7.09+4	4.38+4	1.58+4	7.10+3	1.76+4	5.11+3		1.40+3	1.91+3	1.17+3	4.24+2		
7			55427	60009	65297	71465	78744	87456	98060	111231	128007	156074	180351	224342	1.81+5	1.88+5
			1.07+3	2.14+4	8.10+4	2.03+4	2.88+4	5.09+2	1.43+4	9.39+3	1.12+3	2.31+2	1.26+3	1.22+3		
8				55049	59467	64539	70418	77704	85474	95111	107369	122474	141917	167811	1.82+5	1.95+5
				2.34+3	3.25+4	8.15+4	4.94+3	3.50+4	1.38+3	8.11+3	1.15+4	3.73+3	9.33+1	4.62+2		
9				50922	54680	58919	63801	69405	75921	83583	92714	103764	117391	134566	1.82+5	2.01+5
				7.77+1	4.29+3	4.38+4	7.31+4		1.28+4	7.66+3	2.44+3	1.04+4	6.47+3	1.17+3		
10					50682	54320	58425	63088	68426	74589	81776	90253	100389	112689	1.78+5	2.07+5
					1.59+2	6.92+3	5.38+4	5.86+4	1.99+3	2.44+4	1.54+4		6.96+3	7.95+3		
11						50448	53970	57925	62193	67477	73305	80045	87918	97210	1.65+5	2.13+5
						2.82+2	1.01+4	6.11+4	4.14+4	1.33+4	1.38+4	2.09+4	1.58+3	2.98+3		
12							50221	53628	57436	61717	66556	72066	78385	85688	1.60+5	2.18+5
							4.49+2	1.38+4	6.49+4	2.48+4	2.37+4	4.86+3	2.19+4	6.03+3		

Table 11

TABLE 24 - SCALING FACTORS FOR POPULATION TABLES

Frequency(Hz)	Pressure (μ) 50	200	400
5	0.360 0.033 (9.2%)	0.742 0.073 (9.8%)	0.893 0.192 (22%)*
15	0.325 0.040 (12.3)	0.736 0.078 (10.6)	1.000 0.207 (21%)*
32	0.327 0.068 (14%)	0.699 0.068 (9.7%)	0.872 0.082 (9.4%)
50	0.337 0.043 (13%)	0.709 0.076 (11%)	0.864 0.098 (11%)
Average - S.D. - as % -	0.337 0.009 (1%)	0.722 0.012 (1.5%)	0.907 0.036 (4%)

N.B. -- Upper entries are scaling factors
-- Middle entries are the average standard deviation from the scaling spectra
-- Lower entries are the standard deviation as percent of the factor

* --- These factors were scaled up to 600Amps peak from 450 and 500 Amps respectively. Factors for scaling these to 600Amps were gotten from spectra at 450 and 500Amps at 32Hz. The standard deviations for these two values are the sum the average standard deviation from the two spectra.

levels.

The errors associated with the populations in tables 12 thru 23 have not been listed. These errors are the probable error which results from the standard deviation in the population of a given level. The standard deviation reflects the spread in the measured band intensities used to determine the population of a given level. The probable error is defined as ~0.67 x (Std. Dev.) and the range of probable errors for the above populations was generally 5 to 15%.

The lower entries in these tables are the percent of the total population for vibrational levels 1 thru 12 at the indicated time. These percentages are the values that are plotted in figures 40 thru 51. In these figures the time scale (0 to 20 μs) is the axis at the right side of each figure and the horizontial axis is the vibrational quantum number of the $B\ ^3\Pi_g$ state. The vertical axis is the percent relative population (lower entry in corresponding table).

In order to understand these plots a point of comparison is necessary. Figure 52 shows the effects of the variation of lifetimes of the different levels on a decaying vibrational distribution. The axes of this figure are as above. The first line, at t = 1 μs, is the initial distribution from 15 Hz and 150 μ. This figure shows that as the distribution decays the precent population of the lower vibrational levels increases because of their longer lifetimes. There is however none of the structure which is evident in all of the experimental distributions. Regardless, we do see the trend that causes band intensities of the lower levels (V = 1,2) to increase with time. This type of effect was shown in the spectral series of the first section of this chapter.

This trend, of the lower levels having an increase in the percent population with increasing time, implies that the decay of molecules in lower levels occurs more slowly than from the higher levels This type of behavior is expected because of the decrease in lifetime with increasing vibrational level. This characteristic rise in the percent

Figure 52 - PERCENT POPULATION / Effect of LIFETIME only

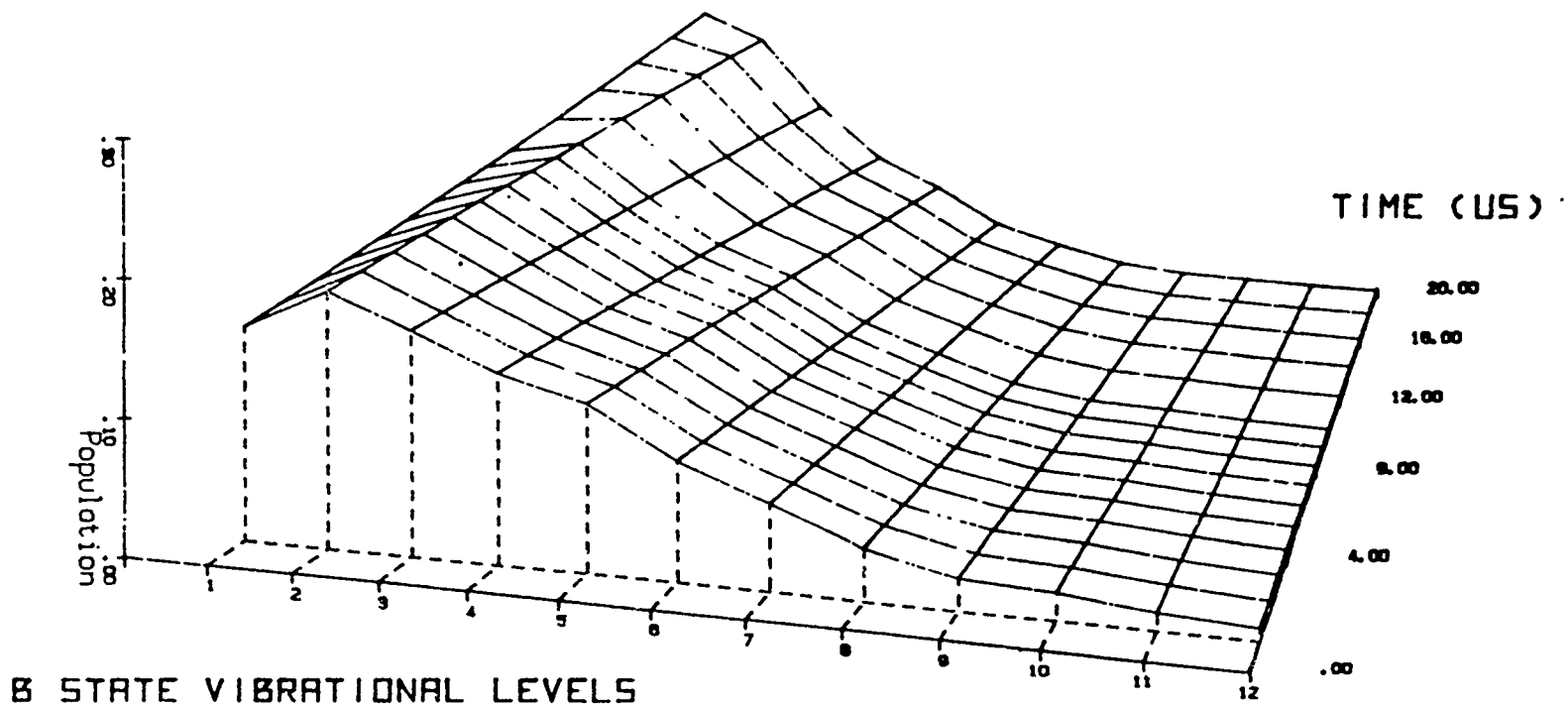

population of the lower levels can be seen in all the experimental population plots. The major difference is seen when comparing plots of different pressures. For higher pressures, a larger increase in the precent population of the lower V levels has occured by 20 μs.

Longer time plots show that for all conditions the distributions are almost identical for times between 100 and 200 μs. This will be referred to as a "long time equilibrium" and is shown in figures 53 to 64 (these figures appear at the end of this section). The distributions at 120 μs for these 12 figures appears in tables 25, 26, and 27. Looking back to the 0 to 20 μs plots we see that the greater the pressure the greater the progress toward this "long time equilibrium" at 20 μs. Another point to be noticed about the 0 to 20 μs plots is that, at a given pressure the degree of progress toward this "long time equilibrium" at 20 μs, decreases with increased discharge frequency (see figures 40 to 51).

A number of other features in the 0 to 20 μs plots are notable and appear to varying degrees in all plots. First there is a bump or rise in the plots associated with V = 6. Notice that its position in time varies with pressure. Table 28 shows the measured time at which the peak occurs in the percent population for V = 6, for all sets of conditions. In general the distribution does not change drastically during the 4us of the current pulse. To determine the actual time to the peak in V = 6, 4 μs is subtracted from the measured time. These times are the middle entries in table 28. Averaging these times for plots of identical pressure yields the following values,

400 μ ~ 1.0 μs

200 μ ~ 2.25 μs

50 μ ~ 7.8 μs

TABLE 25 - PERCENT POPULATION AT 120 μs

50μ, 5 TO 50Hz

Vibrational Level	Frequency (Hz) 5	15	32	50
1	33.1 ----	32.4 ----	32.7 ----	31.9 ----
2	25.1 ±0.1	24.5 ±0.8	24.1 ±0.8	23.7 ±1.1
3	11.5 ±1.1	11.5 ±1.4	11.3 ±0.9	11.7 ±0.9
4	7.6 ±0.4	7.8 ±0.4	8.2 ±0.5	8.7 ±0.7
5	6.4 ±0.5	6.4 ±1.5	6.5 ±1.2	6.8 ±1.0
6	4.8 ±0.5	5.0 ±0.5	5.1 ±0.4	5.1 ±0.4
7	3.3 ±0.4	3.5 ±0.5	3.5 ±0.4	3.6 ±0.3
8	2.1 ±0.02	2.3 ±0.2	2.3 ±0.2	2.4 ±0.2
9	1.9 ±0.1	2.0 ±0.1	2.0 ±0.02	1.9 ±0.1
10	1.9 ±0.04	1.9 ±0.01	1.8 ±0.01	1.8 ±0.01
11	1.4 ±0.02	1.4 ±0.1	1.4 ±0.08	1.3 ±0.06
12	0.9 ---	1.0 ---	1.0 ---	0.9 ---

TABLE 26 - PERCENT POPULATION AT 120 μs

200μ, 5 TO 50Hz

Vibrational Levels	Frequency (Hz) 5	15	32	50
1	33.9 ----	34.7 ----	36.4 ----	35.9 ----
2	25.7 ±2.1	24.9 ±2.2	25.3 ±1.9	24.4 ±2.0
3	10.0 ±0.7	10.1 ±1.1	9.7 ±0.9	9.7 ±0.9
4	7.5 ±0.4	7.4 ±0.4	7.3 ±0.4	7.7 ±0.8
5	6.2 ±1.2	6.3 ±1.3	6.0 ±1.0	6.4 ±1.1
6	5.1 ±0.5	5.2 ±0.4	4.7 ±0.3	5.1 ±0.4
7	3.0 ±0.4	3.0 ±0.3	2.9 ±0.3	3.1 ±0.3
8	2.0 ±0.2	2.1 ±0.2	1.9 ±0.1	2.1 ±0.2
9	1.8 ±0.1	1.9 ±0.06	1.7 ±0.05	1.8 ±0.08
10	2.1 ±0.06	2.0 ±0.01	1.8 ±0.01	1.7 ±0.03
11	1.5 ±0.2	1.5 ±0.2	1.3 ±0.1	1.3 ±0.2
12	0.9 ---	0.9 ---	0.8 ---	0.8 ---

TABLE 27 - PERCENT POPULATION AT 120 μs

400μ, 5 TO 50Hz

Frequency (Hz)

Vibrational Level	5	15	32	50
1	36.5 ----	37.3 ----	33.5 ----	33.6 ----
2	25.7 ±2.2	26.6 ±2.5	24.0 ±1.4	23.3 ±1.2
3	9.7 ±1.0	9.3 ±0.7	10.6 ±1.4	10.6 ±1.9
4	7.0 ±0.5	6.9 ±0.3	7.5 ±0.5	7.7 ±0.7
5	6.0 ±1.0	5.8 ±0.7	6.6 ±1.7	6.6 ±1.5
6	4.8 ±0.4	4.6 ±0.4	5.3 ±0.5	5.3 ±0.5
7	2.8 ±0.2	2.5 ±0.2	3.5 ±0.7	3.6 ±0.6
8	1.8 ±0.1	1.7 ±0.2	2.2 ±0.2	2.3 ±0.2
9	1.7 ±0.06	1.5 ±0.06	2.0 ±0.04	2.1 ±0.06
10	1.9 ±0.03	1.7 ±0.0	2.0 ±0.04	2.0 ±0.01
11	1.2 ±0.07	1.2 ±0.1	1.6 ±0.2	1.7 ±0.2
12	0.8 ---	0.7 ---	1.1 ---	1.1 ---

TABLE 28 - TIMES TO PEAK IN V=6 (PERCENT POPULATION)

Frequency(Hz)	Pressure(μ) and Collision Frequency(#/μs) 50μ 0.33#/μs	200μ 1.3#/μs	400μ 2.7#/μs
5	12 8 (9.42)	6 2 (9.26)	4/6 0/2 (8.7/8.7)
15	12 8 (9.34)	7 3 (9.72)	5 1 (9.44)
32	9/14 5/10 (9.2/9.2)	6 2 (9.36)	5 1 (9.41)
50	12 8 (9.48)	6 2 (9.45)	5 1 (9.41)
Average Time (μs)	7.8	2.25	1.0
S.D.	0.89	0.29	0.35
Average Number of Collisions	2.6	3.0	2.7
S.D.	0.30	0.38	0.95

N.B. -- Upper entries are actual time after start of current pulse
-- Middle entries are the time after the end of current pulse
-- Lower entries are the value of percent population of V = 6 at the peak

-- The average number of collisions is the product of the average time after the end of the current and the collision frequency

The product of these times and the collision frequency for the corresponding pressures determine the number of gas kinetic collisions which have occured at the time peak.

These values are,

400 μ => 2.7 collsions

200 μ => 3.0 collisions

50 μ => 2.6 collisions

Average => 2.8 collisions

So, it appears that for all conditions of this experiment 2.5 to 3.0 collisions are required to produce the peak in this feature in the $B\ ^3\Pi_g$ state vibrational distribution. This feature reflects the number of collisions necessary to equilibrate the populations of the V = 6 level of the $B\ ^3\Pi_g$ state with the V = 7 level of the $W\ ^3\Delta_u$ state via the ICT process. It should be noted that in general, the overall distributions are similar at the times where the peak in V=6 occurs. Consequently, the position of the peak in V=6 has not been effected by drastic changes in the percent populations of other (lower) levels.

The role of collisional coupling between the $B\ ^3\Pi_g$ and $W\ ^3\Delta_u$ states was considered by Benesch[7] in the explanation of the red lower border of B-type Aurora. Specifically, he discussed the implications of the 85 Km turn-on altitude for this phenomenon. A result of this discussion was the the estimation of the rate constant for coupling from the vibrational levels 6,7 and 8 of the $W\ ^3\Delta_u$ state to the adjacent levels of the $B\ ^3\Pi_g$ state (v=5,6,and 7). The analysis was based souly on the temperature and collision frequency at this altitude and the lifetimes of the above levels of the $W\ ^3\Delta_u$ state. The resulting value was,

$$k(W\ ^3\Delta_u \rightarrow B\ ^3\Pi_g) = 1.3 \times 10^{-10}\ \text{cc/s-molecule}$$

Measurement of the reverse reaction was done by Rotem and Rosenwaks. Their work produced a value very similar to that estimated by Benesch. This was an LIF experiment which generated only $B\,^3\Pi_g$ state molecules and monitored the subsequent decay. Loss of $B^3\Pi_g(V=6)$ molecules, by collisions, had a measured rate constant of,[5]

$$k(B\,^3\Pi_g \rightarrow W\,^3\Delta_u) = 1.08 \times 10^{-10}\ cc/s\text{- molecule}$$

Their results implied that the ICT process was occuring with the $W\,^3\Delta_u(V=7)$ level.

Another point of Benesch's discussion, and the one which is important here, is the remark noting that 85 Km reflects a collision frequency of approximately "2 collision per radiative lifetime" of the V = 6 thru 8 levels of the $W\,^3\Delta_u$ state. He considered this to be sufficient to divert the excitation from the ($W\,^3\Delta_u \rightarrow B\,^3\Pi_g$) system to the ($B\,^3\Pi_g \rightarrow A^3\Sigma_u^+$) system." [7] Due to the time resolved nature of the present study the progress of the collisional coupling of these two levels, $B\,^3\Pi_g(V = 6)$ and $W\,^3\Delta_u(V = 7)$, can be directly observed. The above analysis indicates that approximately 2.5 to 3 collisions are required to couple these levels, in close agreement with the estimate of Benesch.

The fact that the percent population rises for $B\,^3\Pi_g(V = 6)$ implies that the absolute populations of $B\,^3\Pi_g(V = 6)$ and $W\,^3\Delta_u(V = 7)$ are initially out of equilibrium. In order to estimate the initial population of these two levels, we must make an assumption about the amounts of these two states initially produced in the discharge. Computer studies done in our laboratory have indicated that the production rate ratio of W-to-B is generally about 0.65. If it is also assumed that excitation occurs from the V = 0 of the ground, $N_2(X\,^1\Sigma_g^+)$, state then the distribution into these two levels is governed largely by the Franck-Condon factors (FCF) between $N_2(X\,^1\Sigma_g^+, V=0)$ and these levels. The resulting populations will be given by,

$$N(W,7) = FCF(W,7) * Ratio(W:B)$$
$$= (0.1050) * (0.65)$$
$$= 0.070$$

$$N(B,6) = FCF(B,6) * Ratio(B:B)$$
$$= (0.06587)* (1.0)$$
$$= 0.066,$$

where N( ) is the relative population of the indicated level.

These values represent a difference of ~15% relative to N(W,7). An additional factor which will increase the differences in these amounts is the lifetimes of the two levels. In appendix A, it is shown that an increase in the lifetime results in a larger fraction of the total population, remaining at the end of the excitation pulse. The lifetime of the $W\,^3\Delta_u(V=7)$ level is ~54 μs[41] whereas that of the $B\,^3\Pi_g(V=6)$ level is ~5.5 μs.[19] This would further tend to increase the relative amount of $W\,^3\Delta_u(V=7)$ at times just after the current pulse. From the above two points we see reason to expect that excitaion which originated in $W\,^3\Delta_u(V = 7)$ would be collisional coupled into $B\,^3\Pi_g(V = 6)$ via the ICT process.

Other evidence for collisional coupling into the $B\,^3\Pi_g(V=6)$ level is shown in the low pressure data (50 μ) for the decay of V=6 between 5 and 8 μs. The population appears to be falling slightly less rapidly than expected considering the natural lifetime, 5.5 μs.

Another feature which becomes more predominant with increased pressure is the break or trough at V = 3. The values for the percent population do not go through a definite minimum. Consequently, it is difficult to determine the number of collisions necessary for achieving an equilibrium, presumably with V = 3 of the $W\,^3\Delta_u$ state. Regardless the above analysis can be discussed. If the expected populations of the two levels are

estimated, we see similar compliance with the present results. Proceeding as before,

$$N(W,3) = FCF(W,3) * Ratio(W:B)$$
$$= (0.04383)* (0.65)$$
$$= 0.028$$
$$N(B,3) = FCF(B,3) * Ratio(B:B)$$
$$= (0.1907) * (1.0)$$
$$= 0.19.$$

In this case the population of the $B\,^3\Pi_g(V = 3)$ level is estimated to be much larger than the $W\,^3\Delta_u(V = 3)$ level so that a flow of excitation into the $W\,^3\Delta_u(V = 3)$ level is expected. Again if we look at the low pressure data for these plots they show that between 5 and 8 μs the decay of V = 3 is occuring more rapidly than expected from the natural lifetime of 6.5 μs.[19]

Unfortunately if this analysis is extended to $B\,^3\Pi_g(V = 2)$ the results do not appear, at first, to comply with the observed changes in the percent population plots. Here, the estimated populations of the two levels are

$$N(W,2) = (2.295E\text{-}2) * (0.65)$$
$$= 1.49E\text{-}2$$
$$N(B,2) = (1.954E\text{-}1) * (1.0)$$
$$= 1.95E\text{-}1$$

which is a difference of about twelve times, $B\,^3\Pi_g$ greater then $W\,^3\Delta_u$. So it would be expected that the flow would be from $B\,^3\Pi_g(V = 2)$ to $W\,^3\Delta_u(V = 2)$. Looking at the plots

of percent population this does not appear to be the case.

This example is important in that more precise r , of the ICT process (and other processes that contribute to these results) would have to compare predicted values with the percent populations and, more important, with the relative populations (upper entries in tables 12 thru 23). Doing this for $B\,^3\Pi_g(V=2)$ of the low pressure data between 5 and 8 μs, we see that the relative population is falling more rapidly than predicted by a lifetime of 7.0 μs, except for the 50 Hz data. In the 50 Hz case the population seems to follow the lifetime quite well. A comparison of values from tables 12 thru 15 with predicted values is shown in table 29.

The range of errors indicated in table 29 are the probable errors of the measured populations, mentioned above. The errors for the estimated values at 8 μs are determined from the errors of the 5 μs values. For the 5 Hz data, the estimated V=2 population is well above the measured value. The 15 Hz estimate is within the limits of error and the 32 Hz estimate is just outside the limits of error.

So from this it appears that the relative population of $B\,^3\Pi_g(V = 2)$ is generally falling more rapidly than expected given the lifetime of the level, even though some values are on the edge of the limits of error. This *is* in compliance with the example above for $B\,^3\Pi_g(V = 2)$ comparing the estimated populations of the $B\,^3\Pi_g$ and $W\,^3\Delta_u$ levels. This exercise should serve notice to the reader on the pitfalls of the use of plots of percent populations. Ultimately the comparision of these results with model results will have to be made with the relative populations. This does not reduce the value of the plots of percent population in that the structure which is evident there is not as apparent in 3-D plots of the relative values.

Returning to the example of $B\,^3\Pi_g(V = 3)$ there has been data showing a similiar trough at this level. The data of Benesch and Fraedrich[14] show the populations of the $B\,^3\Pi_g$ state and the $B'\,^3\Sigma_u^-$ state, (see figure 2). Their data appears in figure 65 and is from

TABLE 29 - ESTIMATED POPULATIONS OF V = 2 AT 8μs FOR 50μ, 5 TO 50Hz

	Frequency (Hz)			
TIME(μs)	5	15	32	50
5	.613E4 ±.41E3	.476E4 ±.22E3	.505E4 ±.20E3	.458E4 ±.32E2
8	.353E4 ±.71E2	.281E4 ±.15E3	.301E4 ±.14E3	.308E4 ±.19E3
8(est)	.399E4 ±.27E3	.310E4 ±.15E3	.329E4 ±.13E3	.298E4 ±.13E3

$dt = 3\mu s$

and $\exp(-3/7) = 0.651$

observations of the positive column of a DC discharge. The important feature to note is the overlap of $B\,^3\Pi_g(V = 4)$ with $B'\,^3\Sigma_u^-(V = 0)$. In general the overlap of vibrational levels between these two states is $B\,^3\Pi_g(V + 4) = B'\,^3\Sigma_u^-(V)$. What is significant in figure 65 is the observation that the vibrational distribution of the $B^3\Pi_g$ state vibrational levels above V = 3, is enhanced by the presence of the levels of the $B'^3\Sigma_u^-$ state.

The evidence of collisional coupling between $B'\,^3\Sigma_u^-$ and $B\,^3\Pi_g$, beyond the obvious trough at V=3, is less striking in this study and it appears in a different set of vibrational levels. There is a rise in the percent population plot for 200 μ and 5 Hz for V = 9 thru 12. This is shown in figure 66.

An estimate of the $B'\,^3\Sigma_u^-$ vibrational distribution due to direct electron excitation from the ground state (with a ground state vibrational temperature of 300 K) is shown in figure 67. This distribution peaks in the region of V = 6 thru 8 in the $B'\,^3\Sigma_u^-$ state. This corresponds to the V = 10 to 12 in the $B\,^3\Pi_g$ state. As shown in figure 66 this is the region which shows an increase in the percent population during the early microseconds after the current pulse.

Estimating the population of the vibrational levels $B\,^3\Pi_g(V = 11)$ and $B'\,^3\Sigma_u^-(V = 7)$ the following values result. In this case the estimated production rate ratio between $B^3\Pi_g$ and $B'^3\Sigma_u^-$ is approxiamtely, B:B' ~ 6

$$N(B,11) = FCF(B,11) * Ratio(B:B')$$
$$= (2.918E\text{-}3) * (6)$$
$$= 1.75E\text{-}2$$

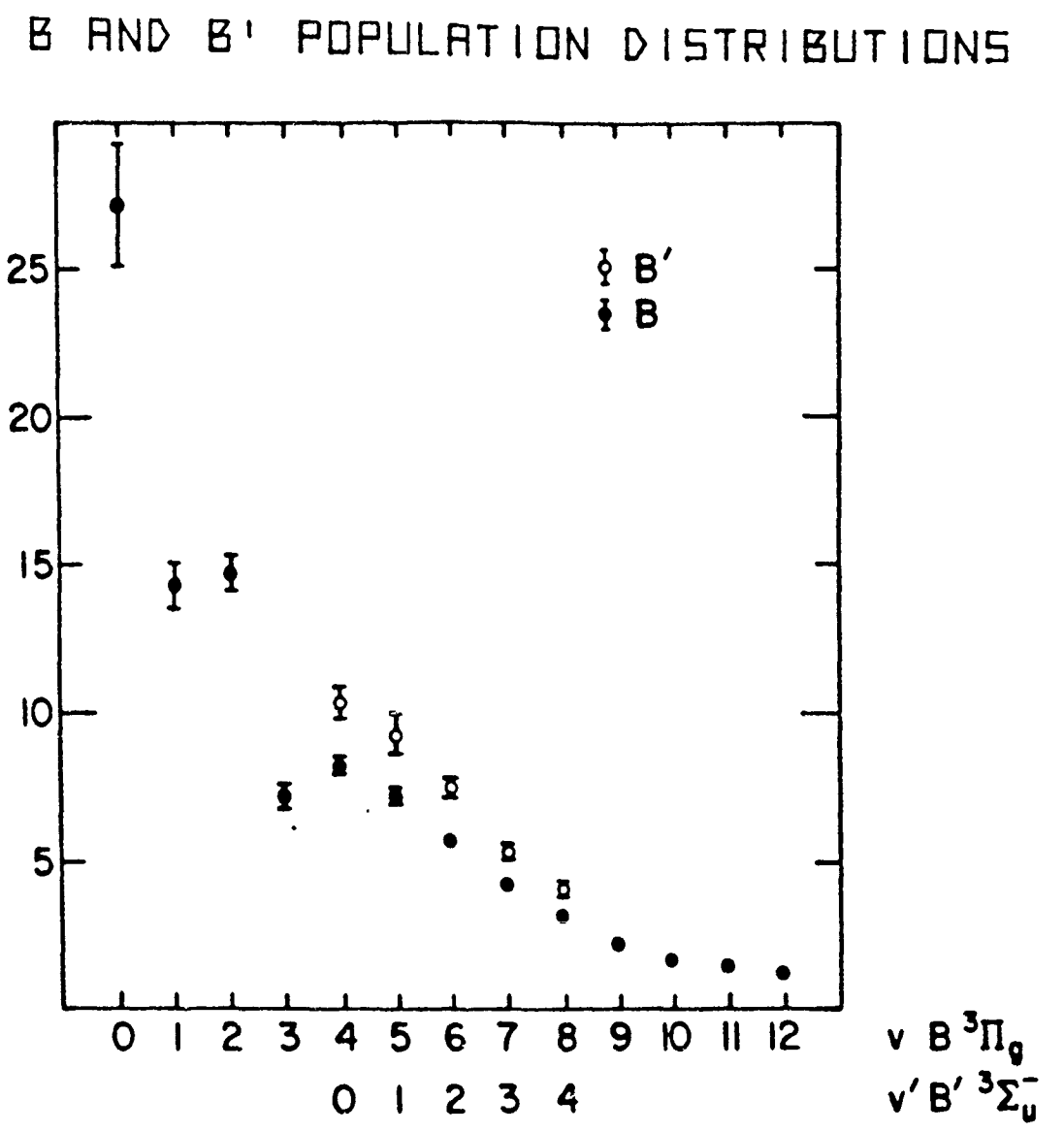
B AND B' POPULATION DISTRIBUTIONS
25
20
15
10
5
B'
B
0 1 2 3 4 5 6 7 8 9 10 11 12
v B $^3\Pi_g$
0 1 2 3 4
v' B' $^3\Sigma_u^-$

Figure 65 -

Figure 66 -

PERCENT POPULATION AT 200u 5Hz 0 to 20uS V = 8 to 12

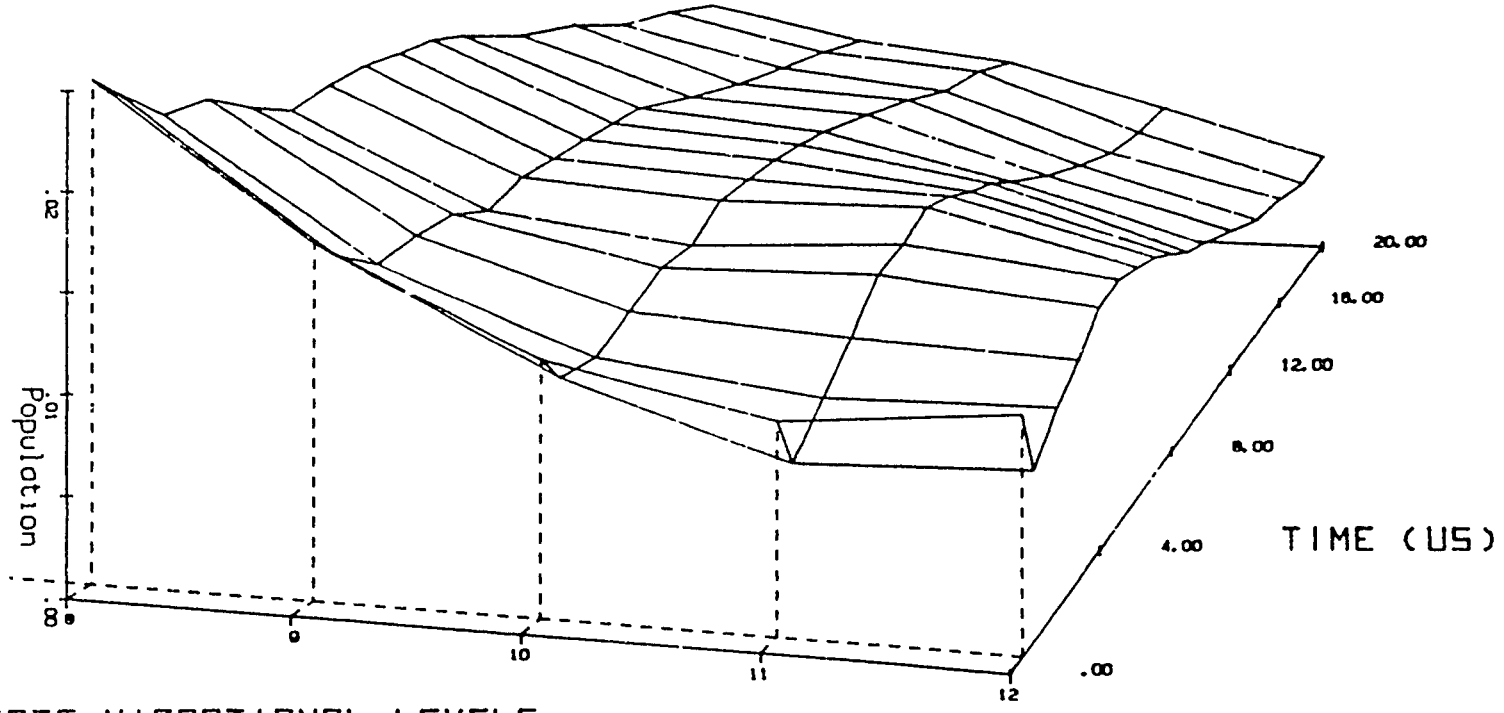

B STATE VIBRATIONAL LEVELS

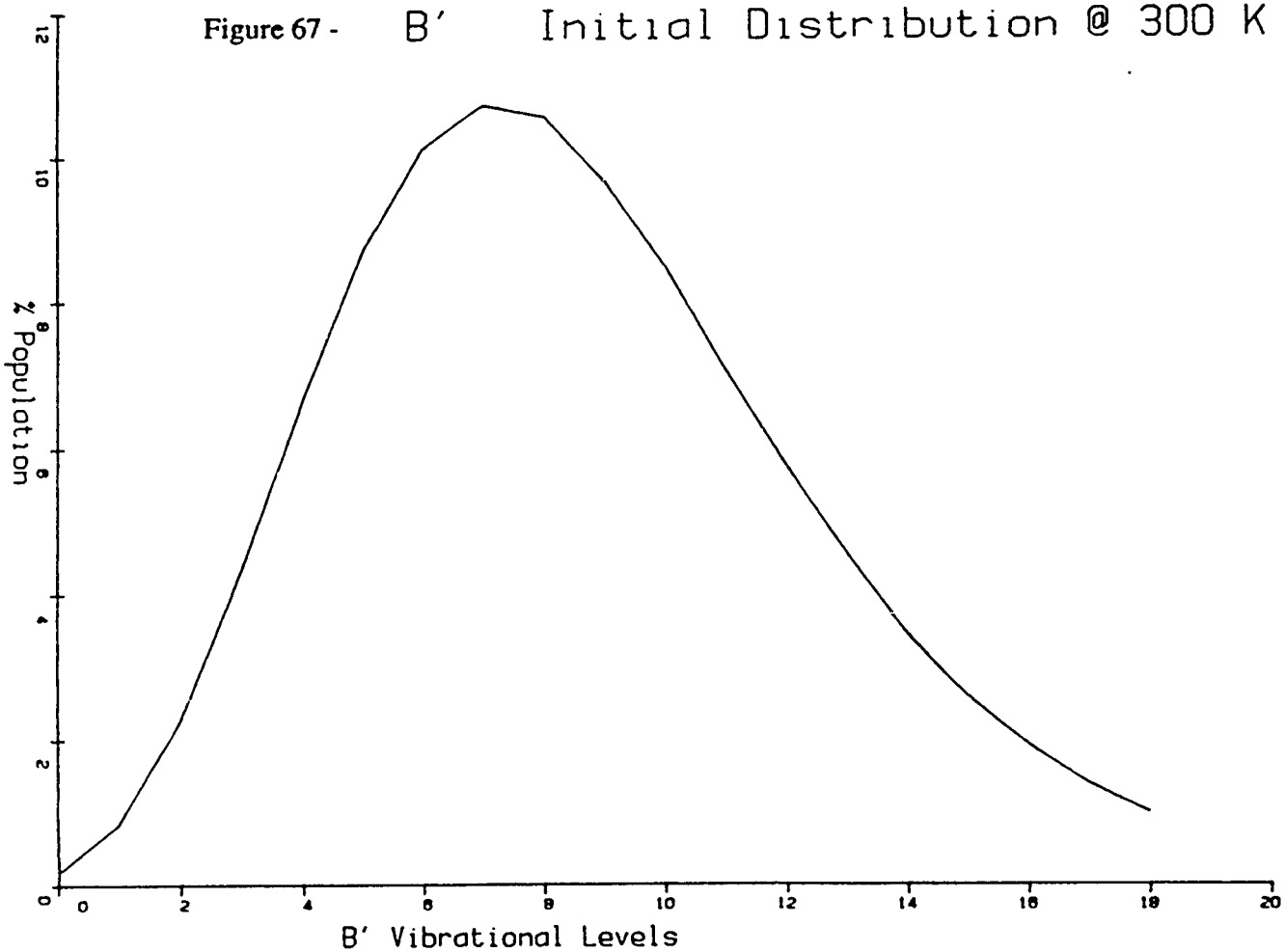
B' Initial Distribution @ 300 K
% Population
0
2
4
6
8
10
12
0
2
4
6
8
10
12
14
16
18
20
B' Vibrational Levels

Figure 67 -

$$N(B',7) = FCF(B',7) * Ratio(B':B')$$
$$= (0.1047) * (1.0)$$
$$= 1.047E\text{-}1$$

This estimates the $B'\,^3\Sigma_u^-(V=7)$ level to be populated about 6 times greater than the $B^3\Pi_g(V=11)$ level. By examining the relative populations of V = 9 through 12 between 5 an 8 μs (table 16), we see that in this case these levels are decaying *less* rapidly than expected using the natural lifetimes of these levels. The results appear below in table 30. Here too, the range of errors shown are the probable errors of the measured populations, with the errors for the estimated values taken from the 5 μs data. In this table only the estimated and measured values for V = 10 at 8 μs lie outside the limits of error. For V = 9 and 11 the limits of error overlap by 24% and 36% of total error, respectively. Even though the error bars overlap, none of the estimated values fall within the limits of error of the measured values. So again, within the limits of the above approximation and present data, we see evidence pointing to Intersystem Collisional Transfer and the source and recepient of transfered excitation.

The above discussion has used approximate values of excitation rate ratios for the $B'^3\Sigma_u^-$ and $W^3\Delta_u$ states. Also, simply comparing pairs of measured populations from these tables is far from a complete treatment of this data set. A complete analysis would require the measurement of the electron energy distribution during the course of the current pulse, for each set of conditions. This would allow an accurate determination of the excitation rates for the individual states. Also the effect of discharge frequency on the initial distributions would need to be accounted for. This effect will be discussed in the next section. Finally, with this additional information, a set of master equations could be written coupling the vibrational levels of the $A\,^3\Sigma_u^+$, $B'\,^3\Sigma_u^-$, and $W\,^3\Delta_u$ state

TABLE 30 - ESTIMATED POPULATION OF V = 9 --> 12 AT 8μs FOR 200μ, 5Hz

		TIME(μs)		
LIFETIME (μs)	VIBRATIONAL LEVEL	5	8	8(est)
5.0	9	.179E4 ±143	.110E4 ±77	.0982E4 ±79
4.8	10	.163E4 ±65	.105E4 ±63	.0872E4 ±35
4.7	11	.170E4 ±85	.0957E4 ±48	.0898E4 ±45
4.6	12	.136E4 ---	.0659E4 ---	.0708E4 ---

with those of the $B\ ^3\Pi_g$ state. By fitting the results of these equations to the data of this section, ICT rate constants could be determined. Even without this type of modeling, these data sets show evidence for ICT durning the early times following the current pulse.

Populations of B3IIg Levels Table 12
50u & 5Hz from 0 to 20us in N2

time (us) v' ---------->

		1	2	3	4	5	6	7	8	9	10	11	12
.500	.	.120E+01	.168E+01	.132E+01	.107E+01	725.	561.	347.	218.	145.	113.	79.4	69.4
	.	16.1	22.4	17.7	13.6	9.70	7.51	4.65	2.92	1.94	1.51	1.06	.928
1.00	.	.287E+01	.375E+01	.339E+01	.265E+01	.188E+01	.147E+01	998.	557.	407.	287.	223.	173.
	.	15.4	20.1	18.2	14.2	10.1	7.88	5.35	2.98	2.18	1.54	1.19	.925
2.00		563E+01	.712E+01	.661E+01	.541E+01	.388E+01	.279E+01	.165E+01	982	657.	459.	343.	327.
	.	15.7	19.9	18.4	15.1	10.8	7.77	4.61	2.74	1.83	1.28	.957	.912
3.00	.	.673E+01	.875E+01	.828E+01	.664E+01	.478E+01	.344E+01	.199E+01	.114E+01	785.	580.	462.	423.
	.	15.5	19.9	18.8	15.1	10.9	7.82	4.53	2.60	1.78	1.32	1.05	.962
4.00		622E+01	.767E+01	.693E+01	.554E+01	.414E+01	.313E+01	.179E+01	.109E+01	766.	610.	514.	451.
	.	16.0	19.7	17.8	14.3	10.7	8.07	4.60	2.79	1.97	1.57	1.32	1.16
5.00	.	.495E+01	.613E+01	.534E+01	.431E+01	.320E+01	.251E+01	.143E+01	812.	602.	467.	441.	393.
	.	16.2	20.0	17.5	14.1	10.5	8.19	4.69	2.66	1.97	1.53	1.44	1.29
6.00	.	.390E+01	.492E+01	.404E+01	.327E+01	.248E+01	.207E+01	.119E+01	632.	478.	397.	375.	341.
	.	16.2	20.4	16.8	13.6	10.3	8.58	4.94	2.62	1.98	1.65	1.56	1.42
7.00	.	.334E+01	.418E+01	.321E+01	.266E+01	.199E+01	.169E+01	986.	531.	391.	320.	317.	286.
	.	16.8	21.0	16.1	13.4	9.96	8.52	4.96	2.67	1.97	1.61	1.59	1.44
8.00	.	.296E+01	.353E+01	.264E+01	.215E+01	.157E+01	.143E+01	799.	426.	331.	273.	265.	236.
	.	17.8	21.3	15.9	12.9	9.43	8.60	4.81	2.57	1.99	1.65	1.60	1.43
9.00	.	.266E+01	.307E+01	.220E+01	.188E+01	.141E+01	.134E+01	751.	388.	293.	246.	242.	216.
	.	18.1	20.9	14.9	12.8	9.56	9.15	5.12	2.64	2.00	1.67	1.65	1.47
10.0	.	.226E+01	.277E+01	.185E+01	.154E+01	.119E+01	.116E+01	682.	342	252.	216.	218.	185.
	.	18.0	21.9	14.6	12.1	9.36	9.16	5.37	2.67	1.99	1.70	1.72	1.46
12.0	.	.186E+01	.227E+01	.139E+01	.123E+01	947.	960.	559.	275.	204.	174.	172.	146.
	.	18.3	22.3	13.7	12.1	9.30	9.43	5.49	2.70	2.00	1.71	1.69	1.34
14.0	.	.172E+01	.197E+01	.115E+01	997.	780.	787.	473.	238.	182	157	149.	117
	.	19.7	22.6	13.2	11.4	8.94	9.03	5.42	2.73	2.09	1.80	1.71	1.34
16.0	.	.145E+01	.170E+01	907.	790.	638.	648.	391.	196.	145	128	117.	90.0
		20.1	23.6	12.6	11.0	8.86	9.00	5.43	2.72	2.01	1.77	1.63	1.25
18.0	.	.133E+01	.148E+01	767.	679.	541.	546	325	171	125	109	98.8	78.3
		21.3	23.7	12.2	10.9	8.68	8.77	5.21	2.75	2.01	1.76	1.59	1.13
20.0	.	.126E+01	.137E+01	734.	616.	499	485.	300	160	122	108	90.6	66.4
	.	21.6	23.6	12.6	10.6	8.60	8.35	5.16	2.75	2.11	1.85	1.56	1.14

Populations of B3IIg Levels Table 13
50u & 15Hz from 0 to 20us in N2
time (us) v' ---------->

		1	2	3	4	5	6	7	8	9	10	11	12
.500		979	133E+04	.100E+04	842.	606.	472.	308.	196	131.	102.	66.2	65.0
	.	16.0	21.8	16.4	13.8	9.94	7.74	5.05	3.21	2.15	1.67	1.09	1.07
1.00	.	.225E+04	.283E+04	.247E+04	.198E+04	.143E+04	.109E+04	606.	413.	254.	201.	133.	132.
	.	16.3	20.6	17.9	14.4	10.3	7.88	4.39	2.99	1.91	1 46	.961	.955
2.00	.	.445E+04	.536E+04	.494E+04	.403E+04	.299E+04	.222E+04	.140E+04	865.	605.	443.	333.	293.
	.	15.9	19.2	17.7	14.4	10.7	7.94	5.03	3.10	2.17	1.59	1.19	1.05
3.00	.	.562E+04	.688E+04	.631E+04	.518E+04	.384E+04	.288E+04	.178E+04	.110E+04	790.	590.	468.	420.
	.	15.7	19.2	17.6	14.4	10.7	8.04	4.97	3.08	2.20	1.64	1.30	1.17
4.00	.	.515E+04	.584E+04	.519E+04	.424E+04	.320E+04	.248E+04	.150E+04	945.	701.	530.	440.	400.
	.	16.8	19.1	16.9	13.9	10.5	8.09	4.90	3.09	2.29	1.73	1.44	1.31
5.00	.	.408E+04	.476E+04	.406E+04	.329E+04	255E+04	.204E+04	.122E+04	724.	554.	442.	393.	357.
	.	16.7	19.5	16.6	13.5	10.4	8.34	4.99	2.96	2.27	1.81	1.61	1.46
6.00	.	.328E+04	.388E+04	.318E+04	.265E+04	.203E+04	.171E+04	.102E+04	592.	461.	376.	342.	311.
	.	16.5	19.6	16.1	13.4	10.2	8.64	5.13	2.98	2.32	1.90	1.72	1.57
7.00	.	.282E+04	.332E+04	.258E+04	.216E+04	.168E+04	.147E+04	869.	491.	383.	319.	295.	267.
	.	16.9	20.0	15.5	12.9	10.1	8.84	5.21	2.95	2.30	1.92	1.77	1.60
8.00	.	.241E+04	.281E+04	.211E+04	.178E+04	.139E+04	.127E+04	754.	412.	322.	272.	254.	226.
	.	17.2	20.1	15.0	12.7	9.92	9.06	5.39	2.94	2.30	1.94	1.81	1.61
9.00	.	.217E+04	.250E+04	.180E+04	.151E+04	.120E+04	.114E+04	681.	362.	286.	244.	229.	201.
	.	17.6	20.3	14.6	12.3	9.74	9.22	5.52	2.94	2.32	1.98	1.86	1.63
10.0		196E+04	.222E+04	.153E+04	.130E+04	.104E+04	.101E+04	609	320.	253.	217.	207.	179.
		18.0	20.5	14.1	12.0	9.58	9.29	5.62	2.95	2 33	2.00	1.91	1.65
12.0	.	.165E+04	.187E+04	.121E+04	.103E+04	833.	834.	521.	269.	211.	183.	173.	145.
	.	18.5	20.9	13.5	11.5	9.33	9.34	5.84	3.01	2.36	2.05	1.94	1.63
14.0	.	.139E+04	.154E+04	920.	803	650.	664.	414.	214	167	145.	131.	106.
	.	19.4	21.6	12 9	11.2	9 19	9.29	5.79	2.99	2.33	2 02	1.83	1.48
16.0	.	.136E+04	.143E+04	845.	705	588.	589.	382.	200.	157.	136.	123.	93.9
	.	20.6	21.7	12.8	10.7	8.89	8.91	5.77	3.03	2 37	2.06	1 86	1.42
18.0	.	.114E+04	.119E+04	651.	577.	479.	470.	297	161.	125	107.	93.0	67.7
	.	21.3	22.2	12.1	10.8	8.93	8.76	5.53	3.01	2 33	1 99	1.73	1 26
20.0	.	.105E+04	.108E+04	577.	502	421.	406.	256.	144.	112.	96.0	81 8	58.2
		21.9	22.5	12 1	10.5	8.82	8.50	5.35	3.02	2 34	2 01	1.71	1 22

Populations of B3IIg Levels Table 14
50u & 32Hz from 0 to 20us in NZ
time (us) v' ----------)

		1	2	3	4	5	6	7	8	9	10	11	12
.500		109E+04	.126E+04	995	779.	579.	461.	330.	216.	161.	128.	96.7	84.1
		17.7	20.4	16.1	12.6	9.37	7 46	5.34	3.50	2.60	2.07	1.56	1.36
1.00	.	338E+04	.331E+04	266E+04	.214E+04	.166E+04	.133E+04	922	680	518.	429.	327.	270.
		19.2	18.7	15.1	12.2	9.44	7 57	5.23	3.85	2.94	2.43	1.85	1.53
2.00	.	483E+04	.557E+04	484E+04	.401E+04	.301E+04	.230E+04	.149E+04	.100E+04	795.	601.	452.	395.
	.	16.5	19.0	16.5	13.7	10.3	7.85	5.00	3.43	2.71	2.05	1.54	1.35
3.00	.	586E+04	.685E+04	.597E+04	.495E+04	.379E+04	.295E+04	.188E+04	.127E+04	902.	756.	598.	536.
	.	16.1	18.8	16.4	13.6	10.4	8.12	5.16	3.50	2 70	2.08	1.64	1.47
4.00	.	.535E+04	.588E+04	.499E+04	.413E+04	.325E+04	.262E+04	.162E+04	.107E+04	854	696.	592.	521.
	.	16.9	18.6	15.8	13.1	10.3	8.29	5.14	3.38	2.71	2.21	1.88	1 65
5.00	.	.455E+04	.505E+04	.419E+04	.348E+04	.275E+04	.226E+04	.140E+04	900.	724.	596.	520.	463.
	.	16.9	18.8	15.6	12.9	10.2	8.42	5.22	3.35	2.69	2.21	1.93	1.72
6.00	.	.383E+04	.418E+04	.328E+04	.272E+04	.212E+04	.182E+04	.109E+04	651.	523.	435.	392.	358.
	.	17.9	19.5	15.3	12.7	9.91	8.50	5.10	3.04	2 44	2.03	1.83	1.67
7.00	.	.317E+04	.350E+04	.266E+04	.222E+04	.179E+04	.159E+04	961.	570.	464.	388.	356.	315.
	.	17.6	19.5	14.8	12.3	9.93	8 86	5.35	3.17	2.58	2.16	1.98	1.75
8.00	.	.272E+04	.301E+04	.216E+04	.185E+04	.149E+04	.137E+04	83J.	479.	385.	329.	301.	270.
	.	17.3	19.0	14.2	12.2	9.79	9 03	5.49	3.15	2.53	2.16	1.98	1.77
9.00	.	.244E+04	.264E+04	.186E+04	.160E+04	.130E+04	.124E+04	760.	422	344.	297.	274.	234.
	.	18.2	19.7	13 9	11.9	9.72	9.23	5.66	3.15	2.57	2.21	2.04	1.75
10.0	.	.222E+04	.238E+04	.161E+04	.137E+04	.113E+04	.109E+04	684	383.	311	268.	246.	212.
	.	10.6	20.0	13.5	11.5	9.49	9.17	5.75	3.21	2.61	2.25	2.07	1.78
12.0	.	.194E+04	.198E+04	.126E+04	.108E+04	890	887.	546	2°9	253	206.	187.	162.
	.	20.0	20.5	13.0	11.2	9.21	9 17	5.65	3.09	2.1b	2.13	1.93	1.68
14.0	.	.166E+04	.166E+04	.104E+04	922.	781.	772	505.	27?.	232	203	183.	144
		19.8	19.9	12 4	11.0	9 31	9 2%	6.02	3 30	2 77	2 42	2 18	1.71
16.0	.	.155E+04	.166E+04	944.	831.	696.	691	440.	243	191	166	148	116
	.	21.3	21.4	12.1	10 7	8.94	8 87	5.65	3 13	2 46	2 13	1 90	1 49
18.0	.	.144E+04	.147E+04	827.	728.	618.	598.	357.	220	174	149	127	98 5
		21.1	21.4	12.1	10.6	9.03	8.74	5.22	3.21	2 54	2.17	1 86	1 44
20.0		.120E+04	.117E+04	643.	556.	472.	448	294.	166	131	110	94 0	69 0
	.	22.4	21.9	12.0	10.4	8.82	8 37	5.46	3 10	2 46	2 06	1 77	1 30

Populations of B3IIg Levels Table 15
50u & 50Hz from 0 to 20us in NZ

time (us) v' ---------->

		1	2	3	4	5	6	7	8	9	10	11	12
.500	.	.108E+04	.134E+04	920.	826.	612.	508	373.	281.	212	177.	123.	123.
	.	16.5	20.4	14.0	12.5	9.30	7 72	5.67	4.26	3 22	2.68	1.87	1.87
1.00	.	.300E+04	.341E+04	.263E+04	.232E+04	.176E+04	.140E+04	975.	717	545.	428.	327.	316.
	.	16.8	19.1	14.8	13 0	9.88	7.87	5.47	4.02	3.05	2.40	1.84	1.77
2.00	.	.502E+04	.575E+04	.504E+04	429E+04	.334E+04	.263E+04	.181E+04	.127E+04	983.	783.	610.	526
	.	15.7	17.9	15.7	13.4	10.4	8.21	5.64	3.95	3.07	2.44	1.90	1.64
3.00	.	.590E+04	.699E+04	.614E+04	.520E+04	.407E+04	.322E+04	.215E+04	.149E+04	.117E+04	934.	750.	659.
	.	15.3	18.1	15.9	13.4	10.5	8.32	5.56	3.86	3.04	2.41	1.94	1.70
4.00	.	.586E+04	.586E+04	.519E+04	.443E+04	.342E+04	.276E+04	.175E+04	.128E+04	980.	805.	646.	593.
	.	17.4	17.5	15.5	13.2	10.2	8.23	5.21	3.81	2.92	2.40	1.92	1.77
5.00	.	.426E+04	.458E+04	.380E+04	.314E+04	.254E+04	.217E+04	.137E+04	905.	755.	636.	550.	492.
	.	16.9	18.2	15.1	12.5	10.1	8.62	5.42	3.59	2.99	2.52	2.18	1.95
6.00	.	.367E+04	.387E+04	.310E+04	.267E+04	.216E+04	.185E+04	.119E+04	762.	637.	528.	478.	424.
	.	17.2	18.1	14.5	12.5	10.1	8.68	5.57	3.57	2.98	2.48	2.24	1.99
7.00	.	.335E+04	.361E+04	.279E+04	.236E+04	.195E+04	.173E+04	.107E+04	661.	536.	460.	424.	375.
	.	17.4	18.7	14.4	12.2	10.1	8.96	5.54	3.42	2.77	2.38	2.20	1 94
8.00	.	.285E+04	.308E+04	.230E+04	.197E+04	.162E+04	.150E+04	906.	539.	435.	376.	347.	310.
	.	17.6	19.0	14.2	12.1	9.97	9.22	5.58	3.32	2.68	2.32	2.14	1.91
9.00	.	.259E+04	.271E+04	.193E+04	.168E+04	.138E+04	.131E+04	807.	464.	381.	324.	306.	266.
		18.3	19.1	13.7	11 9	9.76	9.28	5.70	3.28	2.69	2.29	2.16	1.88
10.0	.	.231E+04	.240E+04	.162E+04	.143E+04	.118E+04	.115E+04	699.	394.	327.	278.	256.	229.
	.	10.8	19.6	13.2	11.6	9.60	9.35	5.70	3.22	2.67	2.27	2.09	1.86
12.0		.185E+04	.197E+04	.126E+04	.111E+04	925	930.	572.	318.	259.	226.	209.	177.
	.	18.9	20.1	12.8	11.4	9 43	9.48	5.83	3.24	2.64	2.31	2.13	1.81
14.0	.	.151E+04	.149E+04	949.	850.	741.	723.	477.	270.	218.	184.	170.	140.
	.	19.5	19.3	12.3	11.0	9.59	9.36	6.18	3.50	2.82	2.38	2.21	1.81
16.0	.	.132E+04	135E+04	813.	738.	620.	613.	405.	221.	178.	154.	138.	114
	.	19.9	20.2	12.2	11.1	9.30	9 19	6.08	3.32	2 67	2 32	2.07	1 71
18.0	.	.121E+04	.115E+04	674.	596.	512.	507.	348.	201.	162	146	124	96.5
	.	21.1	20.1	11.8	10.4	8.95	8.86	6.08	3.50	2 82	2.55	2 17	1 68
20.0	.	833.	954.	540.	490.	422.	409.	271.	161.	123.	105.	89 6	26 5
	.	18.8	21.6	12.2	11.1	9.54	9.24	6.13	3.64	2 78	2 37	2.03	595

Populations of B3IIg Levels Table 16
Z00u & 5Hz from 0 to Z0us in NZ

time (us) v' ---------->

		1	2	3	4	5	6	7	8	9	10	11	12
.500	.	.592E+04	.692E+04	.627E+04	.500E+04	.360E+04	.258E+04	.156E+04	868.	602.	425.	348.	311.
	.	17.2	20.1	18.2	14.5	10.5	7.51	4.54	2.52	1.75	1.24	1.01	.904
1.00	.	.139E+05	.172E+05	.164E+05	.135E+05	.936E+04	.665E+04	.370E+04	.209E+04	.141E+04	944.	644.	609.
	.	16.1	19.9	19.0	15.6	10.9	7.71	4.29	2.42	1.64	1.09	.747	.706
2.00	.	.269E+05	.361E+05	.322E+05	.269E+05	.187E+05	.139E+05	.698E+04	.385E+04	.258E+04	.186E+04	.164E+04	.147E+04
	.	15.5	20.9	18.6	15.6	10.8	8.00	4.03	2.23	1.49	1.07	.945	.848
3.00	.	.298E+05	.422E+05	.366E+05	.317E+05	.224E+05	.169E+05	.855E+04	.453E+04	.313E+04	.243E+04	.228E+04	.193E+04
	.	14.7	20.8	18.1	15.7	11.1	8.36	4.22	2.23	1.55	1.20	1.13	.952
4.00	.	.257E+05	.342E+05	.265E+05	.232E+05	.169E+05	.130E+05	.674E+04	.336E+04	.249E+04	.211E+04	.215E+04	.174E+04
	.	16.2	21.5	16.7	14.6	10.6	8.70	4.24	2.11	1.57	1.33	1.35	1.10
5.00	.	.206E+05	.284E+05	.182E+05	.161E+05	.118E+05	.108E+05	.530E+04	.242E+04	.179E+04	.163E+04	.170E+04	.136E+04
	.	17.2	23.6	15.2	13.4	9.84	9.01	4.41	2.02	1.49	1.35	1.41	1.13
6.00		.170E+05	.223E+05	.130E+05	.118E+05	.889E+04	.862E+04	.429E+04	.195E+04	.149E+04	.141E+04	.142E+04	.104E+04
	.	18.2	24.0	13.9	12.6	9 54	9.26	4.60	2.09	1.60	1.51	1.52	1.11
7.00	.	.153E+05	.195E+05	.102E+05	.939E+04	.716E+04	.719E+04	.358E+04	.167E+04	.127E+04	.121E+04	.117E+04	833.
	.	19.5	24.9	13.1	11.9	9.13	9.17	4.56	2.13	1.62	1.55	1.49	1.06
8.00	.	.138E+05	.171E+05	.820E+04	.755E+04	.585E+04	.591E+04	.300E+04	.143E+04	.110E+04	.105E+04	957.	659.
	.	20.7	25.6	12.4	11.3	8.77	8.86	4.50	2.14	1.66	1.58	1.43	.988
9.00	.	.131E+05	.153E+05	.706E+04	.631E+04	.490E+04	.497E+04	.253E+04	.126E+04	982.	933.	821.	529.
	.	22.2	26.0	12.0	10.7	0.48	0.46	4.31	2.15	1.67	1.59	1.40	.900
10.0		112E+05	.129E+05	.564E+04	.499E+04	.390E+04	.391E+04	.198E+04	.102E+04	817	763.	636.	415.
	.	23.3	26.7	11.7	10.4	8.10	8.13	4.12	2.11	1.69	1.59	1.32	.862
12.0	.	.105E+05	.113E+05	.475E+04	.400E+04	.313E+04	.304E+04	.155E+04	817.	663.	631.	489.	308.
	.	25.5	27.4	11.5	9.71	7 60	7 39	5 75	1 98	1.61	1.53	1.19	747
14.0	.	.940E+04	.955E+04	.396E+04	.318E+04	.246E+04	232E+04	.119E+04	659.	532	507.	371.	220
	.	27.4	27.8	11.5	9.26	7.16	6.75	3.45	1 92	1.55	1 48	1.08	641
16.0		.828E+04	.802E+04	.331E+04	.253E+04	.199E+04	.178E+04	918	513	434	398.	286.	169
		28.9	28.0	11.6	8.84	6.95	6.21	3.21	1.79	1.52	1 39	.999	590
18.0		739E+04	.688E+04	.271E+04	.202E+04	.160E+04	140E+04	716.	424.	362	355	238	129
	.	30.5	28.4	11.2	8.36	6.61	5.79	2.96	1 75	1 49	1 39	982	533
20.0	.	.706E+04	.621E+04	.250E+04	.177E+04	.141E+04	.119E+04	617.	371.	320	290.	221.	118
	.	32.0	28.1	11.3	8.03	6.40	5.40	2.79	1.68	1 45	1 31	1.00	.534

Populations of B3IIg Levels Table 17
200u & 15Hz from 0 to 20us in N2
time (us) v' ---------->

		1	2	3	4	5	6	7	8	9	10	11	12
.500	.	.483E+04	.575E+04	.549E+04	.506E+04	.378E+04	.306E+04	.193E+04	.131E+04	957.	667.	525.	555.
		14.2	17.0	16.2	14.9	11.1	9.01	5.70	3.85	2.82	1.97	1.55	1.64
1.00	.	.103E+05	.124E+05	.113E+05	102E+05	.745E+04	.530E+04	.312E+04	.193E+04	.136E+04	930.	633.	576.
	.	15.7	18.9	17.2	15.5	11.4	8.10	4.77	2.95	2.08	1.42	.968	.881
2.00	.	.228E+05	.292E+05	.269E+05	.229E+05	.167E+05	.123E+05	.658E+04	.396E+04	.265E+04	.192E+04	.164E+04	.142E+04
	.	15.3	19.6	18.0	15.4	11.2	8.28	4.42	2.62	1.78	1.29	1.10	.956
3.00	.	.316E+05	.416E+05	.347E+05	.296E+05	.215E+05	.165E+05	.854E+04	.474E+04	.345E+04	.265E+04	.241E+04	.205E+04
	.	15.9	20.9	17.4	14.8	10.8	8.29	4.28	2.38	1.73	1.33	1.21	1.03
4.00	.	.248E+05	.325E+05	.254E+05	.224E+05	.167E+05	.157E+05	.681E+04	.356E+04	.274E+04	.229E+04	.220E+04	.180E+04
	.	16.0	21.0	16.4	14.4	10.8	8.82	4.40	2.30	1.77	1.48	1.42	1.16
5.00	.	.191E+05	.246E+05	.167E+05	.149E+05	.114E+05	.103E+05	.516E+04	.248E+04	.193E+04	.175E+04	.176E+04	.140E+04
	.	17.1	22.1	15.0	13.3	10.3	9.27	4.63	2.23	1.73	1.57	1.58	1.26
6.00	.	.152E+05	.194E+05	.113E+05	.105E+05	.821E+04	.797E+04	.394E+04	.182E+04	.143E+04	.133E+04	.135E+04	.100E+04
	.	18.2	23.3	13.6	12.5	9.84	9.56	4.72	2.18	1.72	1.59	1.62	1.20
7.00	.	.137E+05	.170E+05	.899E+04	.868E+04	.692E+04	.696E+04	.342E+04	.155E+04	.123E+04	.118E+04	.113E+04	821.
	.	19.2	23.7	12.6	12.1	9.67	9.72	4.77	2.17	1.71	1.65	1.57	1.15
8.00		.126E+05	.149E+05	.725E+04	.671E+04	.539E+04	.546E+04	.277E+04	.131E+04	.101E+04	977.	904.	631.
	.	21.0	24.9	12.1	11.2	9.00	9.11	4.62	2.19	1.74	1.63	1.51	1.05
9.00	.	.106E+05	.123E+05	.567E+04	.536E+04	.429E+04	.444E+04	.227E+04	.110E+04	879.	867.	742.	490.
	.	21.6	25.1	11.6	11.0	8.76	9.06	4.63	2.24	1.80	1.73	1.52	1.00
10.0	.	.109E+05	.119E+05	.535E+04	.487E+04	.401E+04	.397E+04	.204E+04	.106E+04	847.	779.	668.	433.
	.	23.3	25.5	11.4	10.4	8.56	8.48	4.35	2.25	1.81	1.66	1.43	.925
12.0	.	.936E+04	.907E+04	.384E+04	.314E+04	.259E+04	.244E+04	.129E+04	742.	605	582	440.	270.
	.	27.2	26.4	11.2	9.13	7.52	7.11	3.76	2.16	1.76	1.69	1.28	784
14.0	.	.937E+04	.909E+04	.385E+04	.314E+04	.259E+04	.245E+04	.130E+04	744	607.	584.	442.	271.
	.	27.2	26.4	11.2	9.12	7.52	7.11	3.77	2.16	1.76	1.70	1.28	.787
16.0	.	.799E+04	.769E+04	.306E+04	.251E+04	.199E+04	.184E+04	941.	541	438	405	310.	195
	.	28.6	27.5	11.0	8.98	7.12	6.60	3.37	1 94	1.57	1.45	1 11	695
18.0	.	.734E+04	.667E+04	.271E+04	.206E+04	.170E+04	.148E+04	781.	468.	397	356.	256.	136
	.	30.1	27.4	11.1	8.46	6.97	6.06	3.21	1.93	1 63	1.46	1.05	.558
20.0	.	.677E+04	.591E+04	.240E+04	.177E+04	.145E+04	.123E+04	675	403	340.	322.	228	12
	.	31.3	27.3	11.1	8.17	6.71	5.70	3.12	1.86	1 57	1.49	1 05	580

Populations of B3IIg Levels Table 18
200u & 32Hz from 0 to 20us in N2
time (us) v' ---------->

		1	2	3	4	5	6	7	8	9	10	11	12
.500	.	.502E+04	578E+04	.502E+04	455E+04	.325E+04	.239E+04	.157E+04	981.	699.	595.	370.	107.
	.	16.4	18.9	16.4	14 9	10.6	7.81	5.14	3.20	2.28	1.94	1.21	1.33
1.00	.	.154E+05	.168E+05	.140E+05	.121E+05	.889E+04	.660E+04	.398E+04	.253E+04	.176E+04	.123E+04	874.	839.
	.	18.1	19.7	16 4	14.3	10.5	7.77	4.68	2.98	2.07	1 45	1.03	.988
2.00	.	.259E+05	.303E+05	.258E+05	.221E+05	.164E+05	.128E+05	.729E+04	.453E+04	.339E+04	.250E+04	.215E+04	.178E+04
	.	16.7	19.5	16.7	14.3	10.6	8.24	4.70	2.92	2.19	1.61	1.39	1.15
3.00	.	.292E+05	.360E+05	.296E+05	.255E+05	.195E+05	.151E+05	.843E+04	.500E+04	.379E+04	.300E+04	.267E+04	.217E+04
	.	16.3	20.0	16.4	14.2	10.8	8.37	4.69	2.78	2.11	1.67	1.48	1.21
4.00	.	.260E+05	.305E+05	.228E+05	.202E+05	.157E+05	.127E+05	.687E+04	.381E+04	.305E+04	.259E+04	.240E+04	.185E+04
	.	17.5	20.5	15.4	13.6	10.6	8.57	4.63	2.57	2.06	1.75	1.62	1.25
5.00	.	.189E+05	.229E+05	.147E+05	.131E+05	.106E+05	.950E+04	.499E+04	.249E+04	.197E+04	.182E+04	.177E+04	.138E+04
	.	18.2	22.0	14.1	12.6	10.2	9.12	4.79	2.39	1.89	1.74	1.70	1.32
6.00		.158E+05	.187E+05	.108E+05	.998E+04	.810E+04	.779E+04	.409E+04	.207E+04	.165E+04	.155E+04	.149E+04	.111E+04
	.	19.0	22.5	13.0	12.0	9.75	9.38	4.92	2.50	1.99	1.87	1.79	1.33
7.00	.	.153E+05	.168E+05	.865E+04	.809E+04	.652E+04	.640E+04	.337E+04	.165E+04	.133E+04	.120E+04	.114E+04	818.
	.	21.4	23.5	12.2	11.4	9.15	9.00	4.73	2.31	1.87	1.69	1.61	1.15
8.00	.	.129E+05	.143E+05	.706E+04	.650E+04	.542E+04	.541E+04	.290E+04	.147E+04	.116E+04	.108E+04	981.	689.
	.	21.6	23.9	11.8	10.8	9.05	9.04	4.84	2.45	1.94	1.81	1.64	1.15
9.00		.120E+05	.128E+05	.602E+04	.558E+04	.466E+04	467E+04	.247E+04	.128E+04	104E+04	954.	835.	574.
	.	22.7	24.2	11.4	10.5	8.82	8.83	4.66	2.42	1.97	1.80	1.58	1.09
10.0	.	.112E+05	.119E+05	.526E+04	.485E+04	.403E+04	.398E+04	.213E+04	.116E+04	923	867.	708.	482.
		23.5	25.1	11.1	10.2	8.49	8 38	4.47	2.43	1 94	1 82	1.49	1.01
12.0	.	.100E+05	.998E+04	.430E+04	.378E+04	.314E+04	.303E+04	.159E+04	899.	730.	675.	525.	332.
	.	25.8	25.6	11 0	9.68	8.05	7.76	4.07	2.30	1 87	1.73	1.35	851
14.0		.893E+04	.866E+04	.351E+04	.308E+04	.253E+04	.228E+04	.120E+04	702	587	515	383.	225
	.	27.4	26.5	10.8	9.43	7.76	7.00	3.67	2.15	1.80	1.58	1.17	.690
16.0	.	.829E+04	.769E+04	.318E+04	.261E+04	.215E+04	.190E+04	.103E+04	612.	513	455.	346	209
		28.6	26.5	11.0	9.00	7.41	6.56	3.57	2 11	1.77	1 57	1.19	722
18.0		.740E+04	.664E+04	268E+04	.215E+04	.178E+04	.153E+04	841.	503	409	381	280	157
	.	29.9	26.8	10.8	8.68	7.18	6.17	3.40	2 03	1.65	1 54	1 13	635
20.0	.	.680E+04	.588E+04	.236E+04	.188E+04	.151E+04	.129E+04	697.	427	361	330	238	137
	.	31.0	26.9	10.8	8.57	6.89	5.87	3.18	1 95	1 65	1.50	1 09	625

Populations of B3IIg Levels Table 19
200u & 50Hz from 0 to 20us in NZ
time (us) v' ---------->

		1	2	3	4	5	6	7	8	9	10	11	12
.500		.499E+04	.578E+04	.510E+04	.436E+04	.326E+04	.255E+04	.168E+04	.117E+04	888.	668.	532.	464.
		15.9	18.4	16.2	13.9	10.4	8.11	5.34	3.71	2.83	2.12	1.69	1.48
1.00		.108E+05	.115E+05	.912E+04	.795E+04	.597E+04	.463E+04	.298E+04	.206E+04	.152E+04	.115E+04	849.	784.
		18.2	19.3	15.4	13.4	10.1	7.81	5.03	3.48	2.56	1.94	1.43	1.32
2.00	.	.278E+05	.275E+05	.216E+05	.218E+05	.162E+05	.120E+05	.697E+04	.464E+04	.361E+04	.272E+04	.214E+04	.194E+04
	.	15.5	18.7	16.7	14.8	11.0	8.18	4.74	3.16	2.46	1.85	1.46	1.32
3.00	.	.302E+05	.356E+05	.305E+05	.262E+05	.200E+05	.153E+05	.877E+04	.557E+04	.423E+04	.333E+04	.292E+04	.242E+04
	.	16.3	19.3	16.5	14.1	10.8	8.29	4.74	3.01	2.29	1.80	1.58	1.31
4.00	.	.165E+05	.198E+05	.155E+05	.137E+05	.109E+05	.900E+04	.488E+04	.287E+04	.231E+04	.196E+04	.183E+04	.147E+04
	.	16.4	19.7	15.4	13.6	10.8	8.92	4.84	2.85	2.29	1.94	1.81	1.45
5.00	.	.124E+05	.149E+05	.101E+05	.908E+04	.741E+04	.676E+04	.364E+04	.195E+04	.158E+04	.141E+04	.138E+04	.108E+04
	.	17.3	20.7	14.1	12.7	10.3	9.43	5.07	2.72	2.20	1.96	1.92	1.51
6.00	.	.106E+05	.121E+05	.729E+04	.664E+04	.553E+04	.528E+04	.288E+04	.147E+04	.121E+04	.110E+04	.106E+04	820.
	.	18.9	21.6	13.0	11.9	9.89	9.45	5.15	2.63	2.16	1.96	1.90	1.47
7.00	.	.977E+04	.113E+05	.616E+04	.573E+04	.479E+04	.472E+04	.260E+04	.132E+04	.107E+04	.100E+04	941.	695.
	.	19.5	22.6	12.3	11.4	9.54	9.42	5.18	2.64	2.14	2.00	1.88	1.38
8.00	.	.852E+04	.954E+04	.508E+04	.485E+04	.386E+04	.391E+04	.223E+04	.109E+04	883.	819.	761.	554.
	.	20.2	22.7	12.1	11.5	9.17	9.29	5.30	2.59	2.10	1.95	1.81	1.32
9.00	.	.802E+04	.862E+04	.421E+04	.382E+04	.326E+04	.323E+04	.178E+04	926.	753.	692.	615.	432.
	.	22.1	23.7	11.6	10.5	8.97	8.87	4.88	2.55	2.07	1.90	1.69	1.19
10.0		.750E+04	.784E+04	.375E+04	.340E+04	.289E+04	.282E+04	.154E+04	840.	679.	628.	542.	361.
	.	22.9	23.9	11.4	10.4	8.80	8.60	4.71	2.56	2.07	1.91	1.65	1.10
12.0	.	.649E+04	.658E+04	.299E+04	.267E+04	.226E+04	.215E+04	.118E+04	673.	550	494.	391.	255.
		24.3	24.7	11.2	9.99	8.48	8.07	4.42	2 52	2 06	1.85	1.46	.956
14.0	.	.595E+04	.574E+04	.248E+04	.219E+04	.182E+04	.168E+04	917.	553.	447.	398.	307.	183.
	.	26.3	25.3	10.9	9.65	8.03	7.42	4.05	2.44	1.97	1.76	1.35	.808
16.0	.	.537E+04	.494E+04	.214E+04	.182E+04	.152E+04	.133E+04	713	436.	368	329.	250.	140.
	.	27.8	25.5	11.0	9.39	7.84	6.88	3.68	2.25	1 90	1.70	1 29	.721
18.0		.476E+04	.442E+04	189E+04	.157E+04	130E+04	.113E+04	631	390	317	294	230	134
	.	27.9	25.9	11.1	9.19	7.63	6.60	3.70	2.29	1.86	1.72	1.35	.788
20.0	.	.656E+04	.579E+04	.243E+04	.195E+04	.164E+04	.135E+04	759.	470.	389.	336.	252.	136
	.	29.7	26.2	11.0	8.82	7.43	6.11	3 44	2 13	1.76	1.52	1.14	.616

Populations of B3IIg Levels Table 20
400u & 5Hz from 0 to 20us in NZ
time (us) v' ---------->

		1	2	3	4	5	6	7	8	9	10	11	12
.500	.	710E+04	.857E+04	.795E+04	.656E+04	.457E+04	.358E+04	.203E+04	.113E+04	744.	523.	376.	386.
		16.3	19.7	18.3	15.1	10.5	8.23	4.66	2.59	1.71	1.20	.863	.888
1.00		.108E+05	.175E+05	161E+05	.138E+05	.967E+04	.696E+04	.363E+04	.194E+04	.125E+04	835.	662.	616.
		12.9	20.8	19.5	16.4	11.5	8.28	4.31	2.31	1.49	.993	.787	.733
2.00	.	.303E+05	.430E+05	.373E+05	.326E+05	.223E+05	.170E+05	.844E+04	.418E+04	.283E+04	.213E+04	.194E+04	.179E+04
	.	14.9	21.1	18.3	16.0	10.9	8.34	4.14	2.05	1.39	1.05	.954	.878
3.00	.	.386E+05	.583E+05	.453E+05	.394E+05	.278E+05	.212E+05	.995E+04	.471E+04	.330E+04	.267E+04	.267E+04	.214E+04
	.	15.1	22.8	17.7	15.4	10.8	8.27	3.89	1.84	1.29	1.04	1.04	.836
4.00	.	.335E+05	.473E+05	.321E+05	.291E+05	.207E+05	.177E+05	.803E+04	.372E+04	.278E+04	.252E+04	.259E+04	.194E+04
		16.6	23.4	15.9	14.4	10.2	8.74	3.98	1.84	1.38	1.25	1.28	.959
5.00		.270E+05	.371E+05	.193E+05	.174E+05	.130E+05	.118E+05	.546E+04	.243E+04	.197E+04	.187E+04	.185E+04	.128E+04
	.	19.2	26.4	13.7	12.4	9.23	8.42	3.89	1.73	1.40	1.33	1.32	.911
6.00		.218E+05	.284E+05	.129E+05	.118E+05	.897E+04	.900E+04	.412E+04	.185E+04	.146E+04	.145E+04	.131E+04	846.
	.	21.0	27.3	12.4	11.4	8.62	8.72	3.96	1.77	1.40	1.40	1.26	.817
7.00	.	.213E+05	.253E+05	.105E+05	.906E+04	.697E+04	.710E+04	.324E+04	.153E+04	.122E+04	.120E+04	.100E+04	634.
	.	23.9	28.4	11.8	10.2	7.82	7.97	3.64	1.72	1.37	1.35	1.12	.712
8.00	.	.202E+05	.221E+05	.895E+04	.741E+04	.583E+04	591E+04	.279E+04	.140E+04	.114E+04	.111E+04	914.	563.
	.	25.8	28.2	11.4	9.47	7.45	7.55	3.57	1.79	1 45	1.42	1.17	.719
9.00	.	.186E+05	.198E+05	.766E+04	.616E+04	.485E+04	475E+04	.221E+04	.115E+04	936.	889	697.	418.
	.	27.4	29.0	11.2	9.04	7.12	6.98	3.24	1.69	1.37	1.31	1.02	.613
10.0	.	.174E+05	.173E+05	.660E+04	.509E+04	.401E+04	386E+04	.182E+04	951	806.	765.	590.	331.
	.	29.3	29.0	11.1	8.55	6.74	6.48	3.06	1.60	1.35	1.29	.991	.557
12.0	.	.147E+05	.134E+05	.510E+04	.364E+04	.284E+04	.264E+04	.123E+04	681.	592.	555.	411.	213.
	.	32.0	29.1	11.1	7.91	6.17	5.74	2.68	1 48	1.29	1.21	.893	.464
14.0	.	.125E+05	.108E+05	.404E+04	.280E+04	.220E+04	.193E+04	945	526.	458.	434.	331.	156.
	.	33.7	29.1	10.8	7.52	5.92	5 19	2.54	1.41	1.23	1.17	.890	.420
16.0		.108E+05	.903E+04	.327E+04	.223E+04	173E+04	.147E+04	733.	424	380.	371.	281.	169.
	.	35.0	29.2	10.6	7.23	5.59	4.75	2.37	1 37	1.23	1.20	.909	.546
18.0		.942E+04	.751E+04	.269E+04	.176E+04	.135E+04	.114E+04	585.	524	290.	278.	207.	115.
	.	36.7	29.3	10.3	6.87	5.28	4.47	2.28	1.27	1.13	1.09	.800	.449
20.0	.	.870E+04	.658E+04	.225E+04	.149E+04	.118E+04	954	484	282	247.	246	198.	97.0
	.	38.3	29.0	9.91	6.56	5.20	4.20	2.13	1.24	1.09	1.08	.872	.427

Populations of B3IIg Levels Table 21
400u & 15Hz from 0 to 20us in N2
time (us) v' ---------->

		1	2	3	4	5	6	7	8	9	10	11	12
.500		.981E+04	.120E+05	.108E+05	.950E+04	.683E+04	.507E+04	.304E+04	.188E+04	.132E+04	933.	726.	647.
	.	15.7	19.3	17.2	15.2	10.9	8.10	4.86	3.01	2.11	1.49	1.16	1.03
1.00	.	.289E+05	.336E+05	.289E+05	.244E+05	.179E+05	.132E+05	.778E+04	.470E+04	.342E+04	.241E+04	.187E+04	.165E+04
		17.1	19.9	17.1	14.5	10.6	7.83	4.61	2.79	2.03	1.43	1.11	.980
2.00	.	.516E+05	.67[illegible]E+05	.573E+05	.493E+05	.365E+05	.280E+05	.145E+05	.819E+04	.612E+04	.473E+04	.427E+04	.373E+04
	.	15.5	20.4	17.3	14.9	11.0	8.43	4.37	2.47	1.84	1.43	1.29	1.12
3.00	.	.577E+05	.779E+05	.597E+05	.536E+05	.407E+05	.326E+05	.162E+05	.866E+04	.662E+04	.539E+04	.507E+04	.401E+04
	.	15.7	21.2	16.2	14.6	11.0	8.86	4.40	2.35	1.80	1.47	1.38	1.09
4.00	.	.485E+05	.641E+05	.410E+05	.374E+05	.292E+05	.259E+05	.123E+05	.599E+04	.482E+04	.431E+04	.423E+04	.317E+04
		17.3	22.8	14.6	13 3	10.4	9.21	4.36	2.13	1.72	1.54	1.51	1.13
5.00	.	.350E+05	.466E+05	.240E+05	.224E+05	.181E+05	.176E+05	.812E+04	.307E+04	.309E+04	.297E+04	.280E+04	.193E+04
	.	18.7	25.0	12.9	12.0	9.69	9.43	4.35	2.08	1.66	1.59	1.50	1.04
6.00	.	.317E+05	.393E+05	.179E+05	.165E+05	.134E+05	.135E+05	.639E+04	.302E+04	.242E+04	.232E+04	.212E+04	.140E+04
	.	21.2	26.2	11.9	11.0	8.93	8.99	4.26	2.01	1.62	1.55	1.41	.936
7.00	.	.295E+05	.340E+05	.145E+05	.129E+05	.106E+05	.10[illegible]E+05	.565E+04	.252E+04	.204E+04	.197E+04	.164E+04	.105E+04
	.	23.4	26.9	11.4	10.2	8.36	8.44	3.99	1.99	1.61	1.56	1.30	.828
8.00	.	.280E+05	.303E+05	.126E+05	.106E+05	.879E+04	.870E+04	.423E+04	.218E+04	.182E+04	.175E+04	.140E+04	862.
	.	25.2	27.2	11.3	9.53	7.90	7.82	3.80	1.96	1.64	1.58	1.26	.775
9.00	.	.256E+05	.266E+05	.106E+05	.864E+04	.708E+04	.692E+04	.335E+04	.177E+04	.146E+04	.139E+04	.109E+04	646.
		26.9	27.9	11.1	9.08	7.45	7.28	3.52	1.86	1.53	1.46	1.14	.679
10.0		.253E+05	.245E+05	.101E+05	.772E+04	.636E+04	.604E+04	.304E+04	.167E+04	.143E+04	.134E+04	.107E+04	625.
	.	28.3	27.4	11.3	8.66	7.13	6.78	3.42	1.87	1.61	1.50	1.20	.701
12.0	.	.212E+05	.195E+05	.750E+04	.558E+04	.459E+04	.419E+04	.212E+04	.115E+04	973.	957.	735.	415.
	.	30.7	28.3	10.9	8.09	6.66	6.07	3.08	1.67	1.41	1.39	1.07	.602
14.0	.	.185E+05	.161E+05	.605E+04	.433E+04	.343E+04	.304E+04	.153E+04	865	759	682.	527.	293.
	.	33.0	28.7	10.8	7.71	6.11	5.42	2.73	1.54	1.35	1.21	.938	.522
16.0	.	.161E+05	.135E+05	.487E+04	.348E+04	.281E+04	.236E+04	.123E+04	712	620	584.	448.	244.
	.	34.3	28.8	10.4	7.41	5.97	5.02	2.62	1 52	1.32	1.24	.953	.520
18.0	.	.143E+05	.116E+05	.413E+04	.279E+04	.223E+04	.188E+04	986	547.	501.	474.	366.	195.
		35.8	28.9	10.3	6.99	5.57	4.71	2 47	1.37	1.25	1.19	.917	.487
20.0	.	.126E+05	.989E+04	.332E+04	.233E+04	.187E+04	.152E+04	735	435	407.	374.	271.	186.
	.	37.1	29.2	9.78	6.86	5.50	4.49	2.17	1.28	1.20	1.10	.800	.547

Populations of B3IIg Levels Table 22
400u & 32Hz from 0 to 20us in NZ
time (us) v' ------------>

		1	2	3	4	5	6	7	8	9	10	11	12
.500	.	762E+04	.937E+04	.821E+04	.682E+04	.512E+04	.379E+04	.234E+04	.146E+04	.103E+04	721.	563.	553.
		16.0	19.7	17.2	14.3	10.7	7.97	4.92	3.06	2.17	1.52	1.18	1.16
1.00	.	.177E+05	.222E+05	.196E+05	.168E+05	.127E+05	.959E+04	.569E+04	.371E+04	.269E+04	.196E+04	.163E+04	.143E+04
	.	15.3	19.2	16 9	14.5	11.0	8.29	4.92	3.21	2.32	1.70	1.41	1.23
2.00	.	.386E+05	.498E+05	.418E+05	.369E+05	.281E+05	.214E+05	.116E+05	.685E+04	.519E+04	.407E+04	.369E+04	.297E+04
	.	15.4	19.8	16.7	14.7	11.2	8.54	4.63	2.73	2.07	1.62	1.47	1.18
3.00	.	.454E+05	.568E+05	.446E+05	.393E+05	.303E+05	.245E+05	.130E+05	.737E+04	.579E+04	.486E+04	.448E+04	.350E+04
	.	16.2	20.3	15.9	14.0	10.8	8.76	4.65	2.63	2.07	1.74	1.60	1.25
4.00		.376E+05	.469E+05	.319E+05	.288E+05	.232E+05	.201E+05	.102E+05	.537E+04	.439E+04	.388F+04	.371E+04	.280E+04
	.	17.2	21.4	14.6	13.2	10.6	9.18	4.67	2.45	2.01	1.77	1.70	1.28
5 00	.	.291E+05	.345E+05	.186E+05	.176E+05	.145E+05	.139E+05	.687E+04	.332E+04	.262E+04	.242E+04	.223E+04	.178E+04
	.	19.9	23.4	12.6	11.9	9.80	9.44	4.65	2.25	1.77	1.64	1.51	1.20
6.00	.	.240E+05	.272E+05	.135E+05	.123E+05	.104E+05	.103E+05	.530E+04	.273E+04	.222E+04	.208E+04	.183E+04	.126E+04
	.	21.2	24.1	11.9	10.9	9.18	9.14	4.68	2.41	1.96	1.84	1.61	1.11
7.00	.	.230E+05	.251E+05	.116E+05	.103E+05	.871E+04	.840E+04	.436E+04	.230E+04	.187E+04	.174E+04	.145E+04	968.
	.	23.1	25.2	11.6	10.3	8.72	8.41	4.37	2.30	1.87	1.75	1.45	.969
8.00	.	.208E+05	.218E+05	.959E+04	.846E+04	.707E+04	.683E+04	.350E+04	.191E+04	.156E+04	.142E+04	.116E+04	718.
	.	24.5	25.7	11.3	9.98	8.34	8.05	4.12	2.25	1.84	1.67	1.36	.847
9.00	.	.195E+05	.195E+05	.851E+04	.719E+04	.604E+04	.567E+04	.293E+04	.164E+04	.137E+04	.123E+04	967.	590.
	.	25.9	26.0	11.3	9.57	8.04	7.54	3.90	2.18	1.83	1.64	1.29	.785
10.0	.	.179E+05	.174E+05	.734E+04	.613E+04	.508E+04	.463E+04	.241E+04	.138E+04	.116E+04	.105E+04	805.	471.
	.	27.2	26.5	11.2	9.33	7.72	7.05	3.66	2.10	1.77	1.59	1.22	.717
12.0	.	.159E+05	.144E+05	.607E+04	.473E+04	.391E+04	.347E+04	.183E+04	.107E+04	921.	818.	627.	353.
	.	29.3	26.7	11.2	8.74	7.28	6 41	3.38	1.98	1.70	1.51	1.16	.651
14.0	.	.134E+05	.119E+05	.474E+04	.369E+04	.307E+04	.259E+04	.130E+04	840	710.	645.	497.	283.
	.	30.7	27.1	10.8	8.42	7.02	5.92	3.16	1.92	1.69	1.47	1.14	.646
16.0	.	.984E+04	.940E+04	.415E+04	.299E+04	.245E+04	.202E+04	.108E+04	661.	573.	517.	369.	221.
	.	28.7	27.4	12.1	8.73	7.16	5.88	3.16	1 93	1.67	1.51	1.08	.646
18.0	.	.110E+05	.906E+04	.386E+04	.261E+04	.214E+04	.175E+04	.101E+04	610.	552.	505.	392.	228.
	.	32.6	26.9	11.5	7.74	6.35	5.18	2.98	1.81	1.64	1.50	1.16	.677
20.0	.	.953E+04	.763E+04	.314E+04	.216E+04	.178E+04	.148E+04	840.	495.	441.	406.	320.	186.
	.	33.5	26.8	11.1	7.66	6.25	5.20	2.96	1.74	1.55	1.43	1.12	.654

Populations of B3IIg Levels Table 23
400u & 50Hz from 0 t 20us in NZ
time (us) v' ---------->

		1	2	3	4	5	6	7	8	9	10	11	12
.500		.723E+04	.843E+04	.774E+04	.702E+04	.503E+04	.391E+04	.249E+04	.163E+04	.118E+04	858.	646.	603.
		15.5	18.0	16.6	15.0	10.7	8.37	5.31	3.49	2.53	1.83	1.38	1.29
1.00	.	.195E+05	.224E+05	.180E+05	.160E+05	.120E+05	.886E+04	.532E+04	.363E+04	.273E+04	.207E+04	.144E+04	.124E+04
	.	17.2	19.8	15.9	14.2	10.6	7.83	4.70	3.20	2.42	1.83	1.27	1.09
2.00	.	.400E+05	.487E+05	.409E+05	.354E+05	.276E+05	.216E+05	.123E+05	.761E+04	.590E+04	.469E+04	.406E+04	.335E+04
	.	15.9	19.3	16.2	14.0	11.0	8.55	4.87	3.02	2.34	1.86	1.61	1.33
3.00	.	.553E+05	.683E+05	.537E+05	.471E+05	.378E+05	.306E+05	.173E+05	.104E+05	.819E+04	.688E+04	.612E+04	.492E+04
	.	16.0	19.7	15.5	13.6	10.9	8.83	4.98	2.99	2.36	1.99	1.77	1.42
4.00	.	.700E+05	.484E+05	.345E+05	.302E+05	.251E+05	.217E+05	.120E+05	.674E+04	.553E+04	.488E+04	.449E+04	.350E+04
	.	16.9	20.4	14.6	12.7	10.6	9.17	5.05	2.84	2.33	2.06	1.89	1.48
5.00		.314E+05	.357E+05	.216E+05	.195E+05	.167E+05	.156E+05	.857E+04	.457E+04	.373E+04	.328E+04	.312E+04	.236E+04
	.	10.9	21.5	13.0	11.7	10.0	9.41	5.16	2.75	2.24	1.98	1.88	1.42
6.00	.	.233E+05	.257E+05	.136E+05	.127E+05	.111E+05	.108E+05	.586E+04	.318E+04	.262E+04	.239E+04	.212E+04	.150E+04
	.	20.3	22.4	11.9	11.0	9.63	9.37	5.10	2.77	2.28	2.08	1.84	1.31
7.00	.	.203E+05	.220E+05	.109E+05	.101E+05	.874E+04	.851E+04	.463E+04	.261E+04	.212E+04	.195E+04	.163E+04	.110E+04
	.	21.5	23.2	11.5	10.7	9.25	9.00	4.90	2.76	2.25	2.07	1.73	1.16
8.00	.	.191E+05	.196E+05	.926E+04	.847E+04	.732E+04	.700E+04	.381E+04	.222E+04	.184E+04	.167E+04	.134E+04	892.
	.	23.2	23.7	11.2	10.3	8.87	8.48	4.61	2.69	2.23	2.03	1.62	1.08
9.00	.	.177E+05	.177E+05	.807E+04	.718E+04	.622E+04	.582E+04	.314E+04	.190E+04	.156E+04	.142E+04	.109E+04	696.
	.	24.4	24.4	11.1	9.90	8.59	8.03	4.33	2.62	2.15	1.95	1.50	.959
10.0	.	.165E+05	.156E+05	.731E+04	.593E+04	.514E+04	.468E+04	.264E+04	.156E+04	.131E+04	.118E+04	930.	675.
	.	26.0	24.6	11.5	9.34	8.10	7.37	4.16	2.46	2.07	1.85	1.46	1.06
12.0	.	.140E+05	.129E+05	.575E+04	.457E+04	.393E+04	.345E+04	.191E+04	.118E+04	994	876.	670.	520.
	.	27.5	25.4	11.3	9.01	7.75	6.80	3.77	2.32	1.96	1.73	1.32	1.02
14.0	.	.123E+05	.112E+05	.486E+04	.381E+04	.321E+04	.272E+04	.154E+04	953.	803.	709.	538.	304.
	.	28.6	26.1	11.3	8.89	7.50	6.34	3.59	2.22	1.87	1.65	1.25	.709
16.0	.	.107E+05	.937E+04	.400E+04	.314E+04	.262E+04	.218E+04	.125E+04	790.	676.	591.	454.	263.
	.	29.7	26.0	11.1	8.72	7.27	6.04	3.47	2.19	1.88	1.64	1.26	.731
18.0	.	.103E+05	.835E+04	.362E+04	.268E+04	.228E+04	.182E+04	.107E+04	679.	577.	516.	417.	233.
	.	31.8	25.6	11.1	8.22	6.99	5.59	3.30	2.08	1.77	1.58	1.28	.716
20.0	.	.803E+04	.673E+04	.262E+04	.215E+04	.173E+04	.138E+04	781	512.	424.	397.	290.	157.
	.	31.9	26.7	10.4	8.53	6.87	5.47	3.10	2.03	1.68	1.57	1.15	.624

Figure 40 -

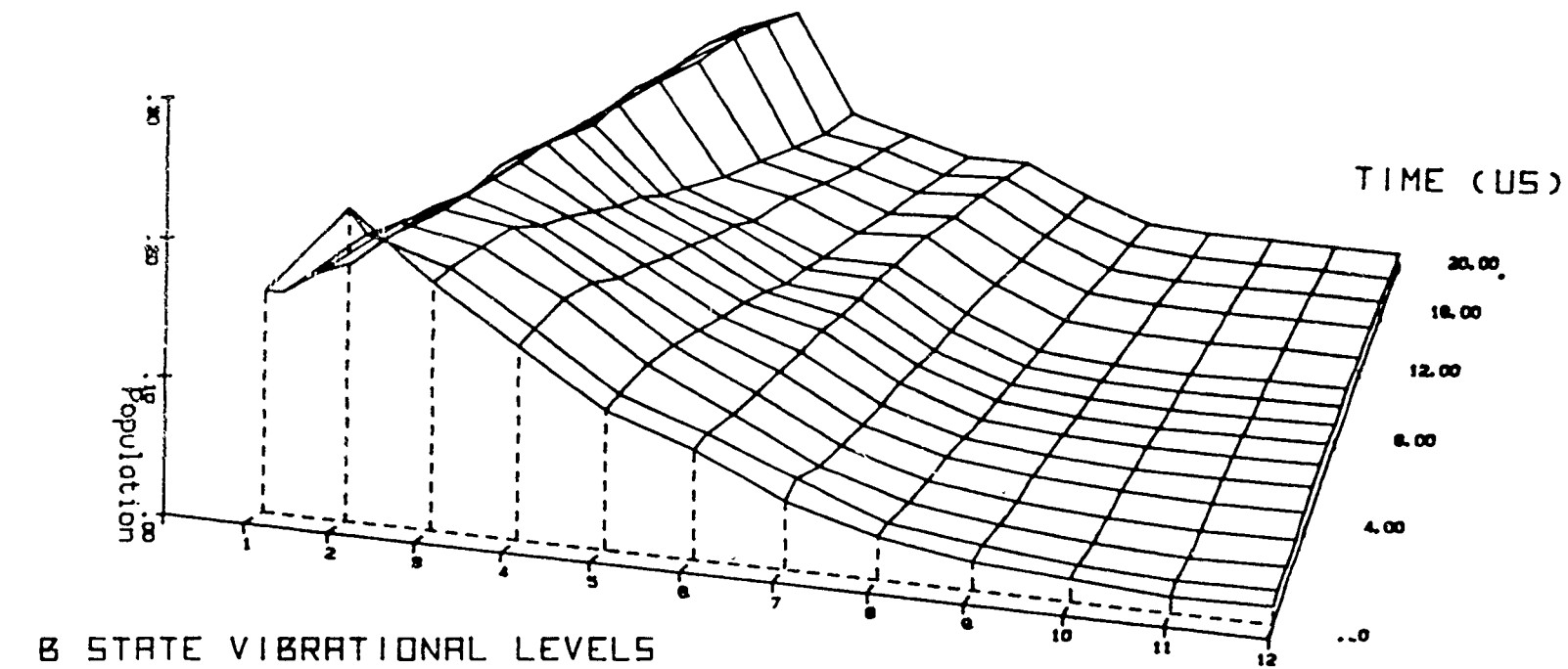
PERCENT POPULATION AT 50u 5Hz 0 to 20uS
TIME (US)
20.00
16.00
12.00
8.00
4.00
.0
Population
B STATE VIBRATIONAL LEVELS
1
2
3
4
5
6
7
8
9
10
11
12

Figure 41 -
PERCENT POPULATION AT 50u 15Hz 0 to 20uS

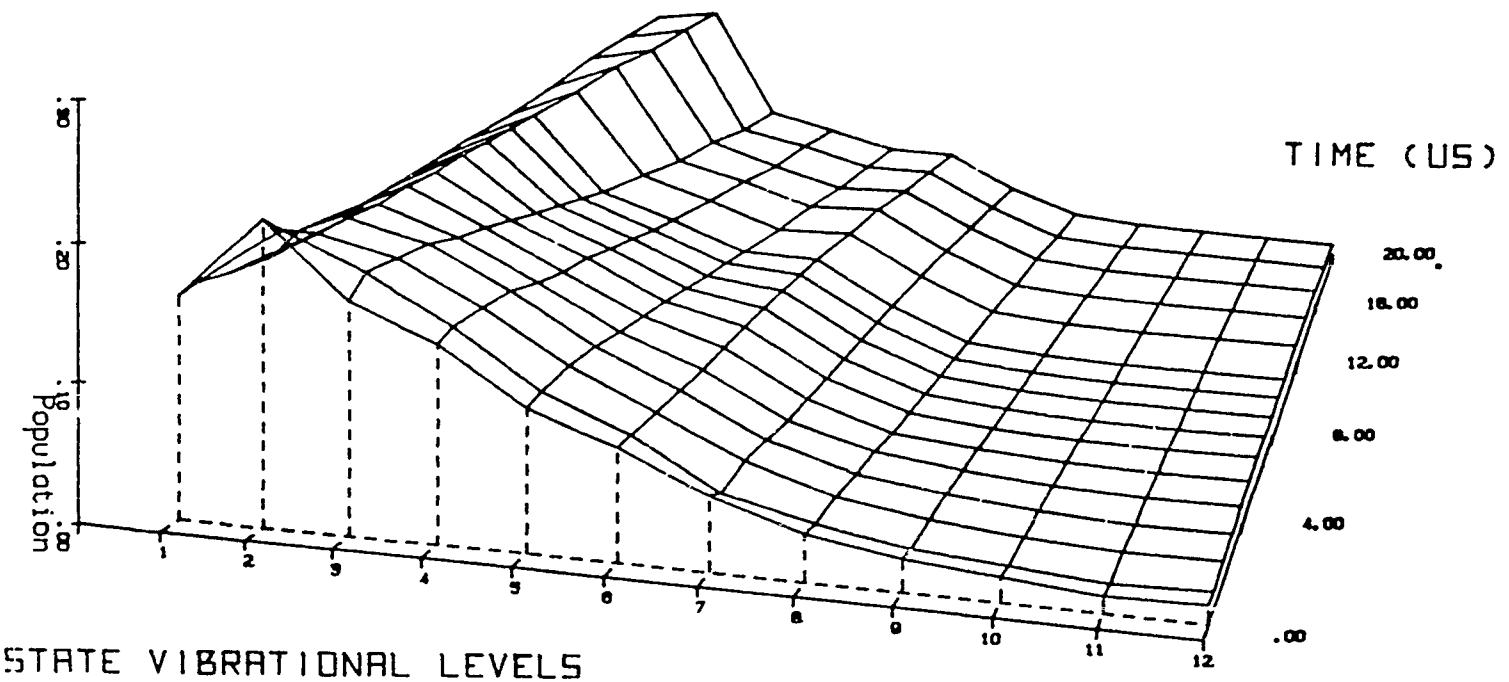

Figure 42 -
PERCENT POPULATION AT 50u 32Hz 0 to 20uS

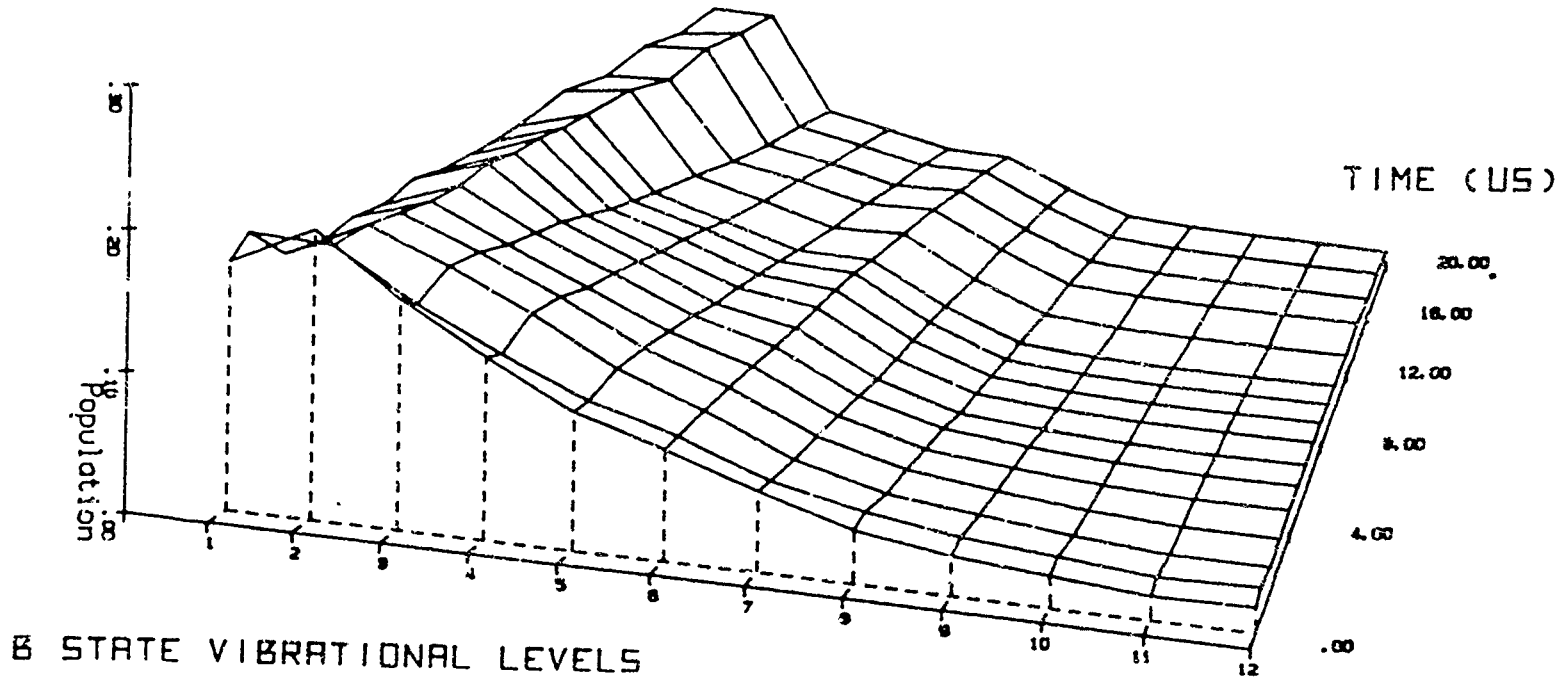

Figure 43 -
PERCENT POPULATION AT 50u 50Hz 0 to 20uS

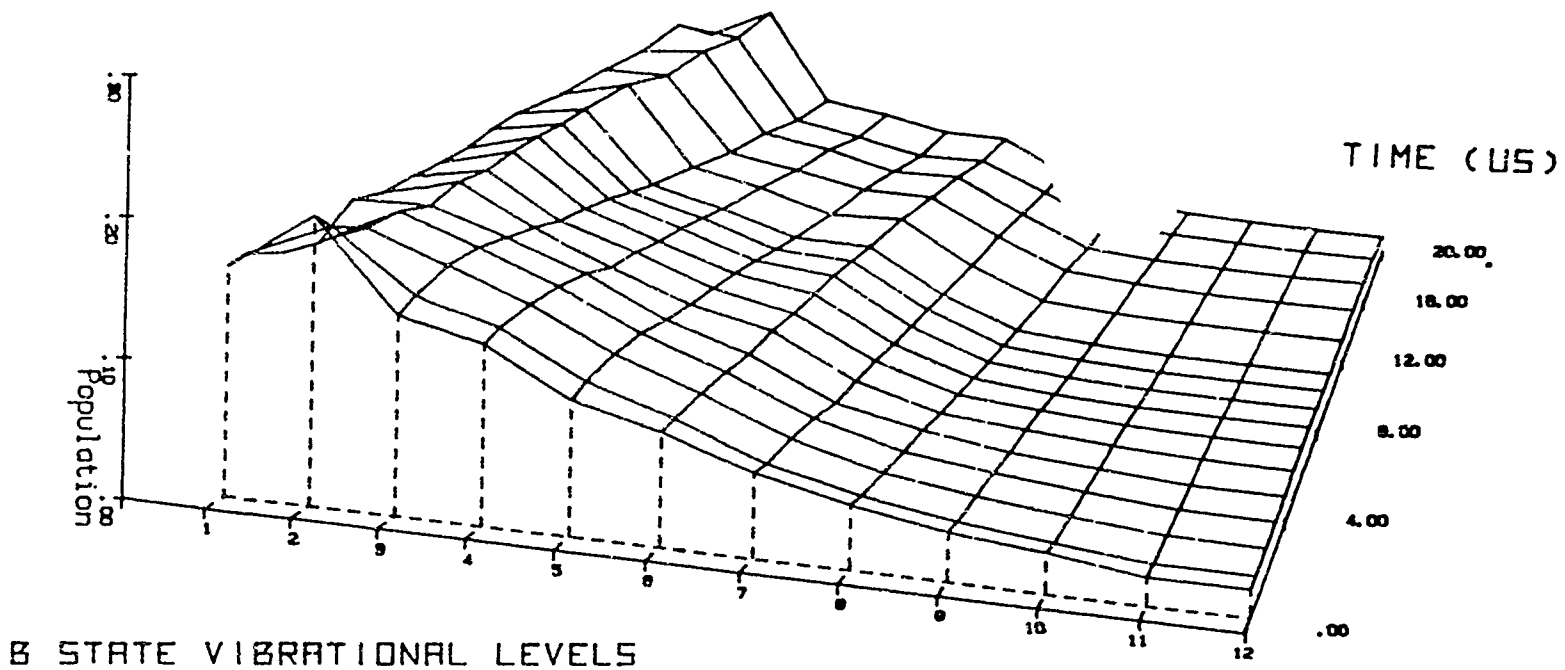

Figure 44 -

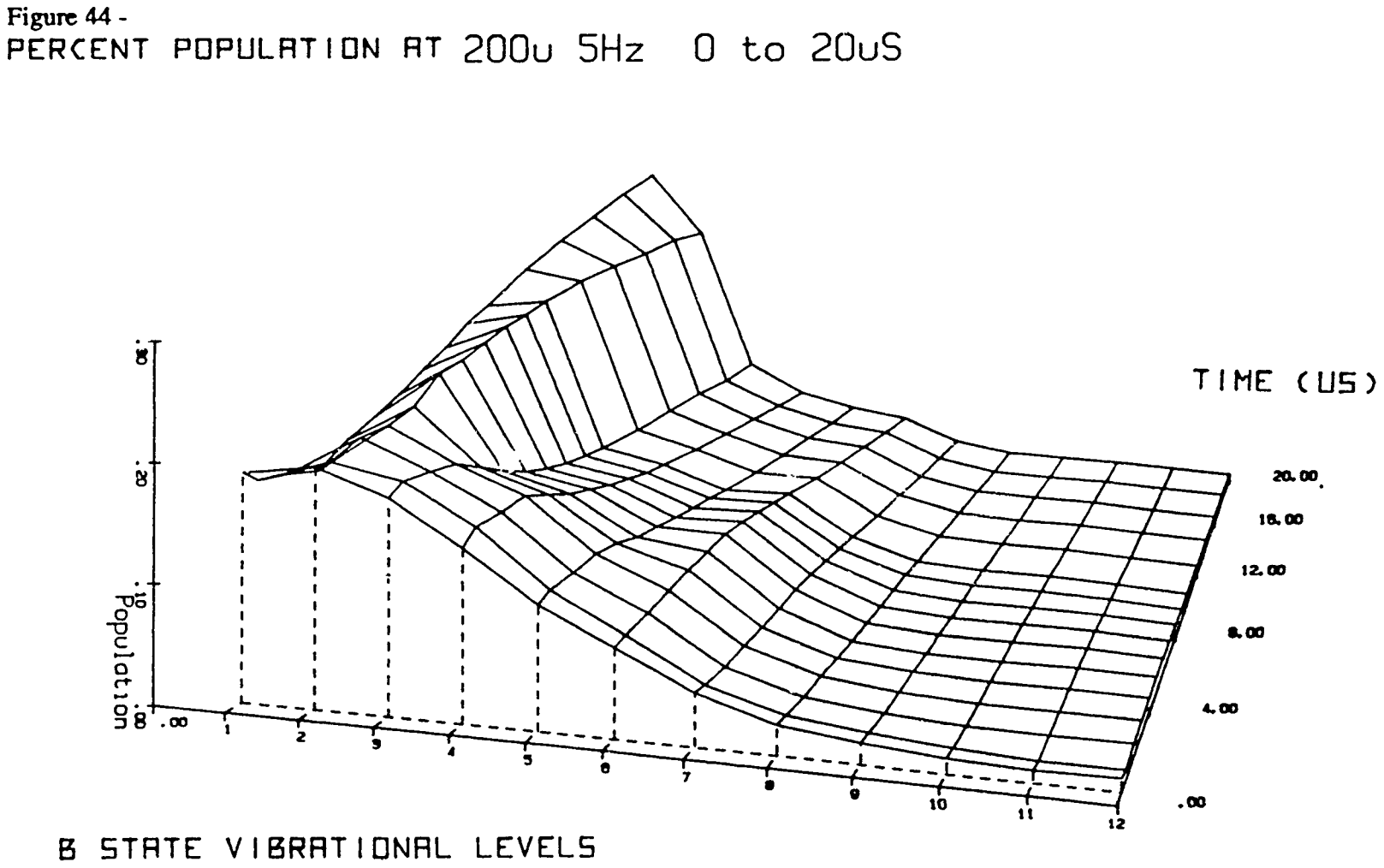
PERCENT POPULATION AT 200u 5Hz 0 to 20uS
TIME (US)
20.00
16.00
12.00
8.00
4.00
.00
Population
.30
.20
.10
.00
1
2
3
4
5
6
7
8
9
10
11
12
B STATE VIBRATIONAL LEVELS

Figure 45 -

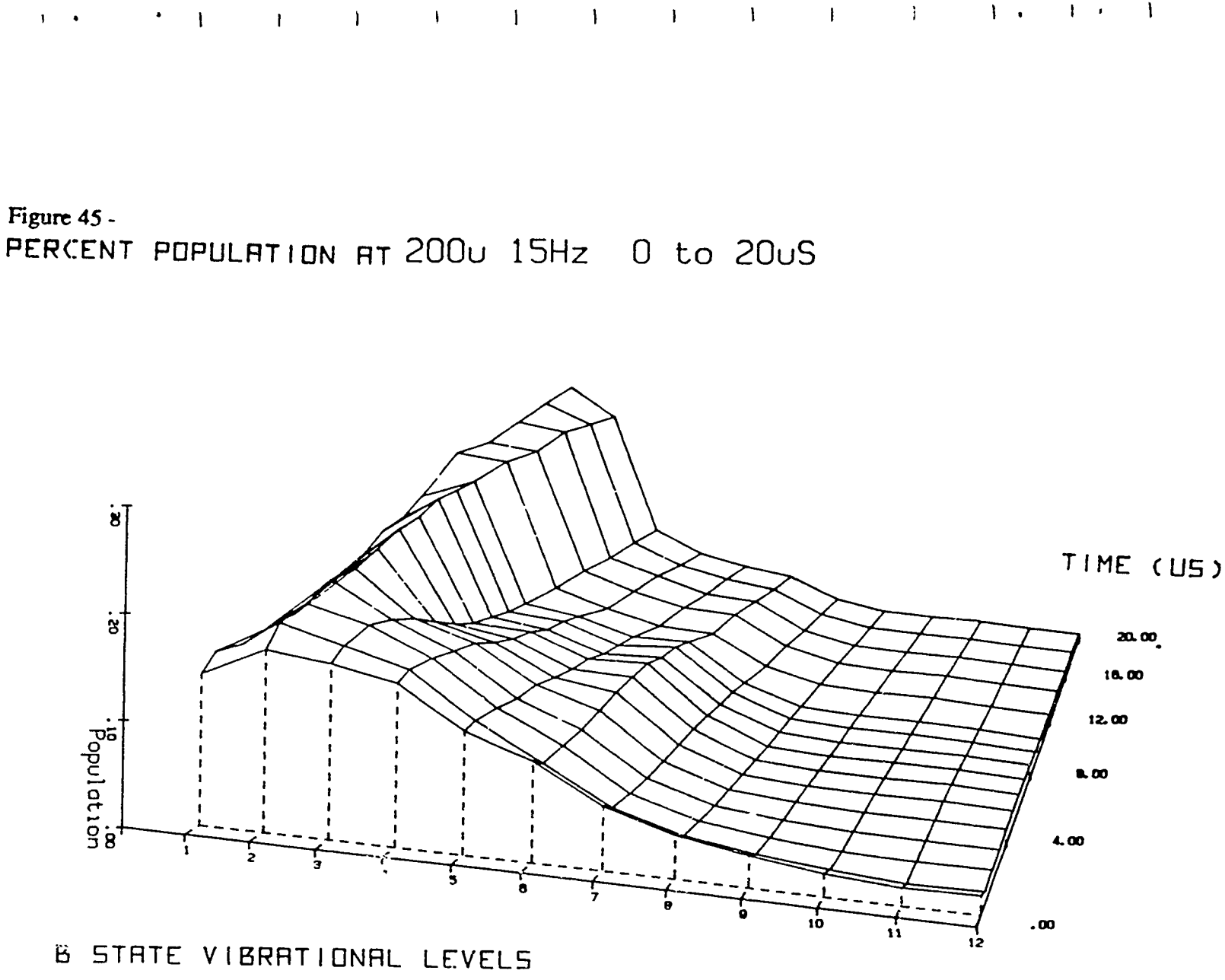
PERCENT POPULATION AT 200u 15Hz 0 to 20uS
TIME (US)
20.00
16.00
12.00
8.00
4.00
.00
Population
.30
.20
.10
.00
1
2
3
4
5
6
7
8
9
10
11
12
B STATE VIBRATIONAL LEVELS

Figure 46 -

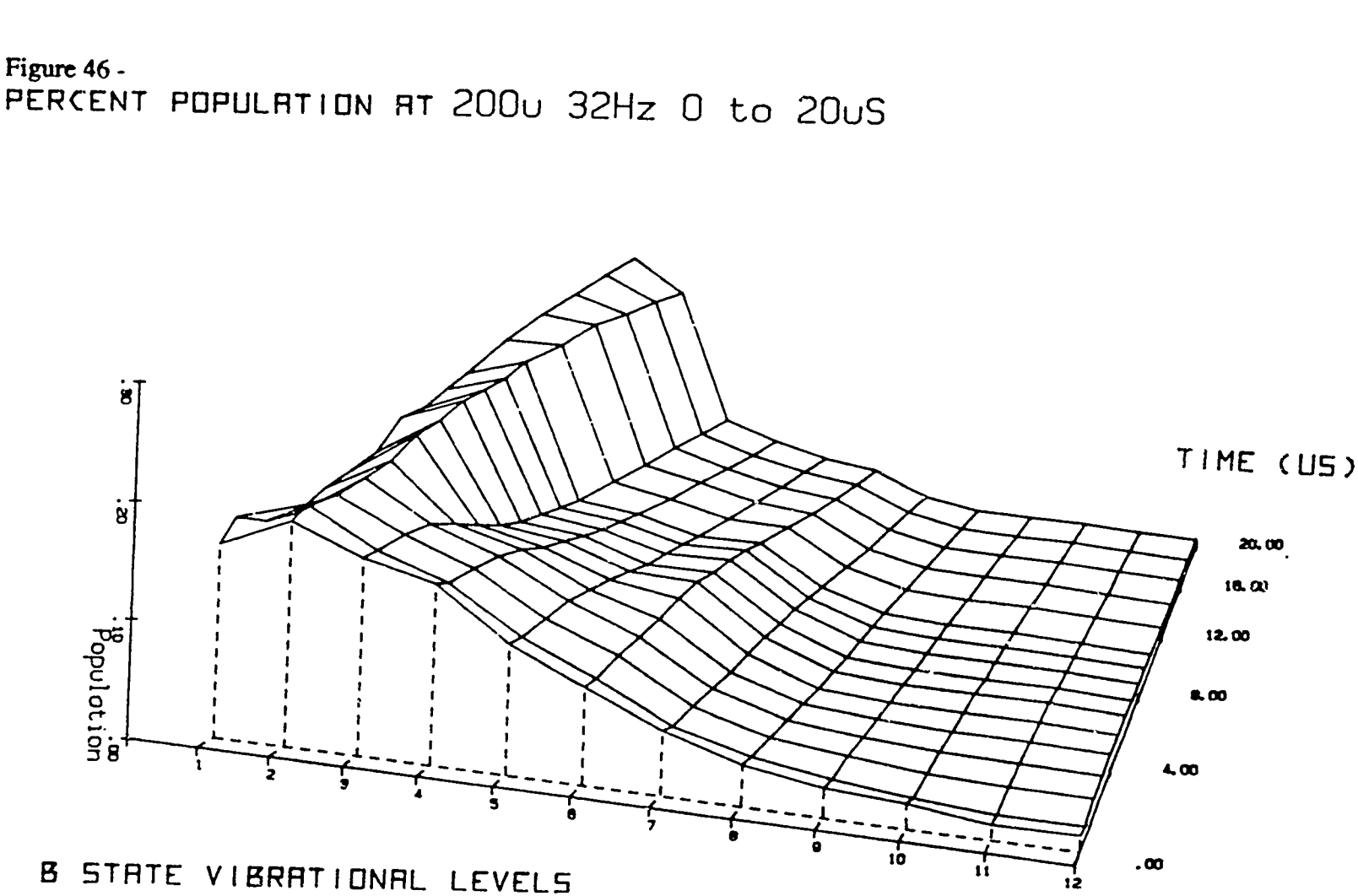
PERCENT POPULATION AT 200u 32Hz 0 to 20uS
TIME (US)
20.00
16.00
12.00
8.00
4.00
.00
Population
.8
.4
0
1
2
3
4
5
6
7
8
9
10
11
12
B STATE VIBRATIONAL LEVELS

Figure 47 -
PERCENT POPULATION AT 200u 50Hz 0 to 20uS

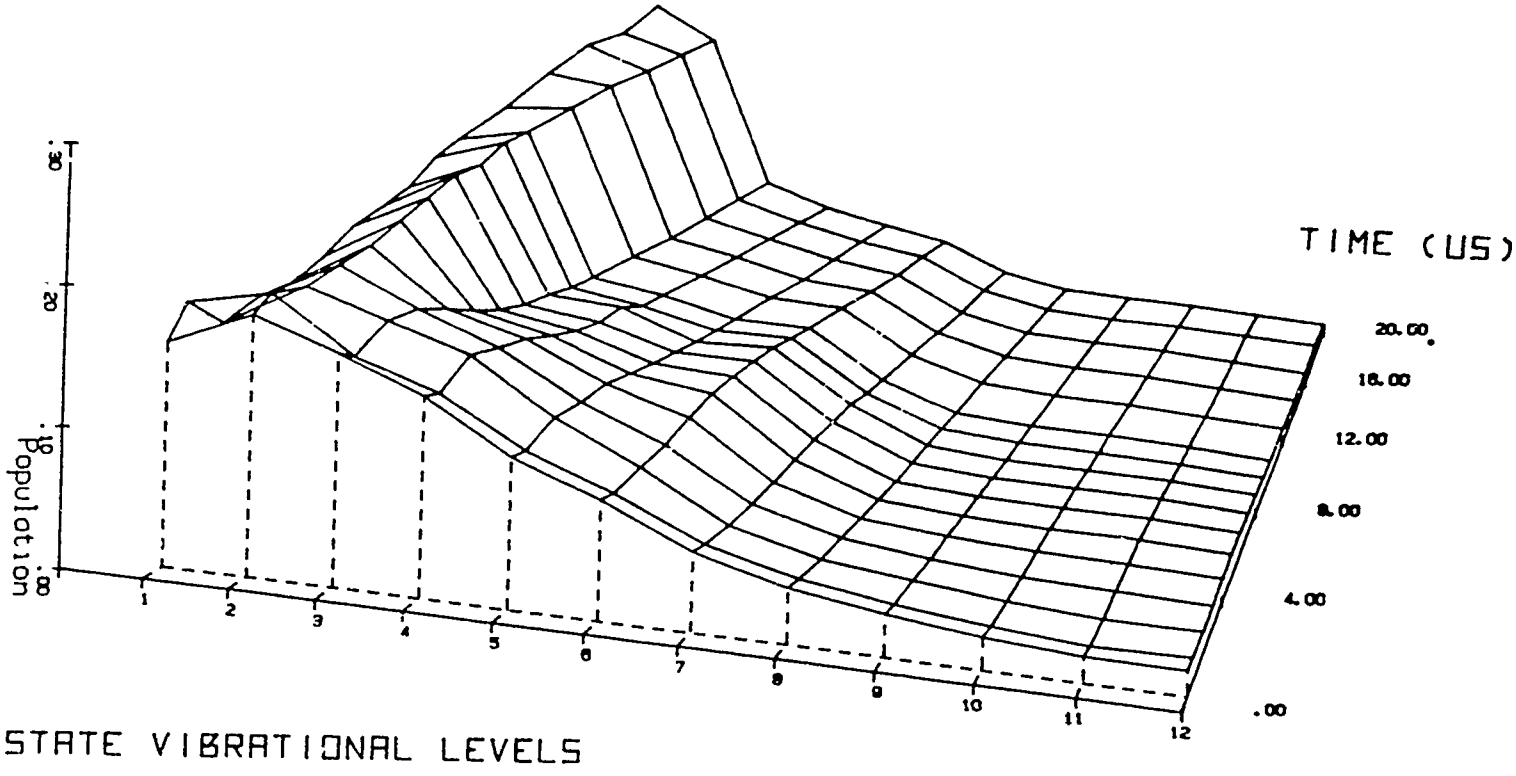

Figure 48 -

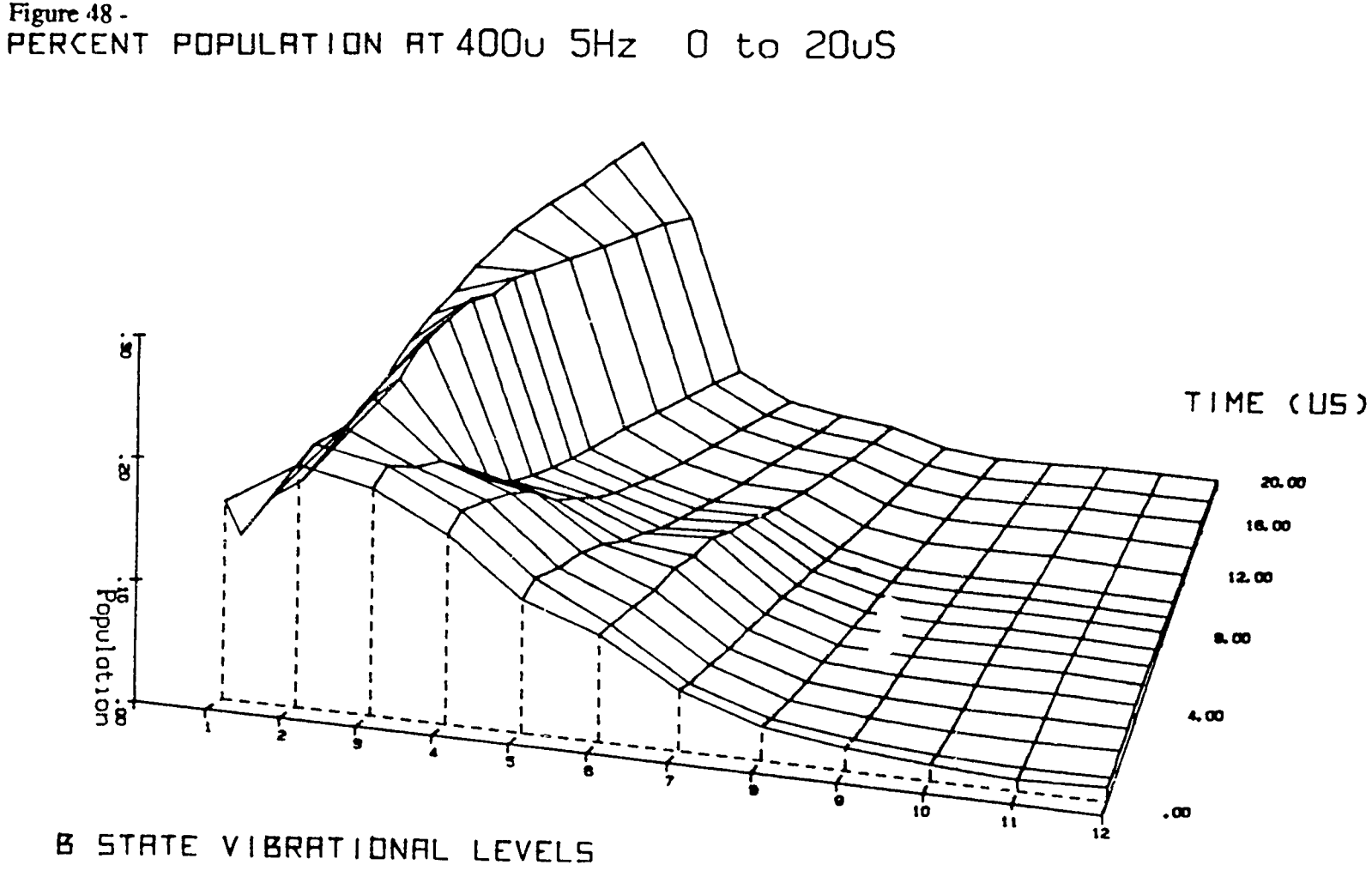
PERCENT POPULATION AT 400u 5Hz 0 to 20uS
TIME (US)
20.00
16.00
12.00
8.00
4.00
.00
Population
1
2
3
4
5
6
7
8
9
10
11
12
B STATE VIBRATIONAL LEVELS

Figure 49 -
PERCENT POPULATION AT 400u 15Hz 0 to 20uS

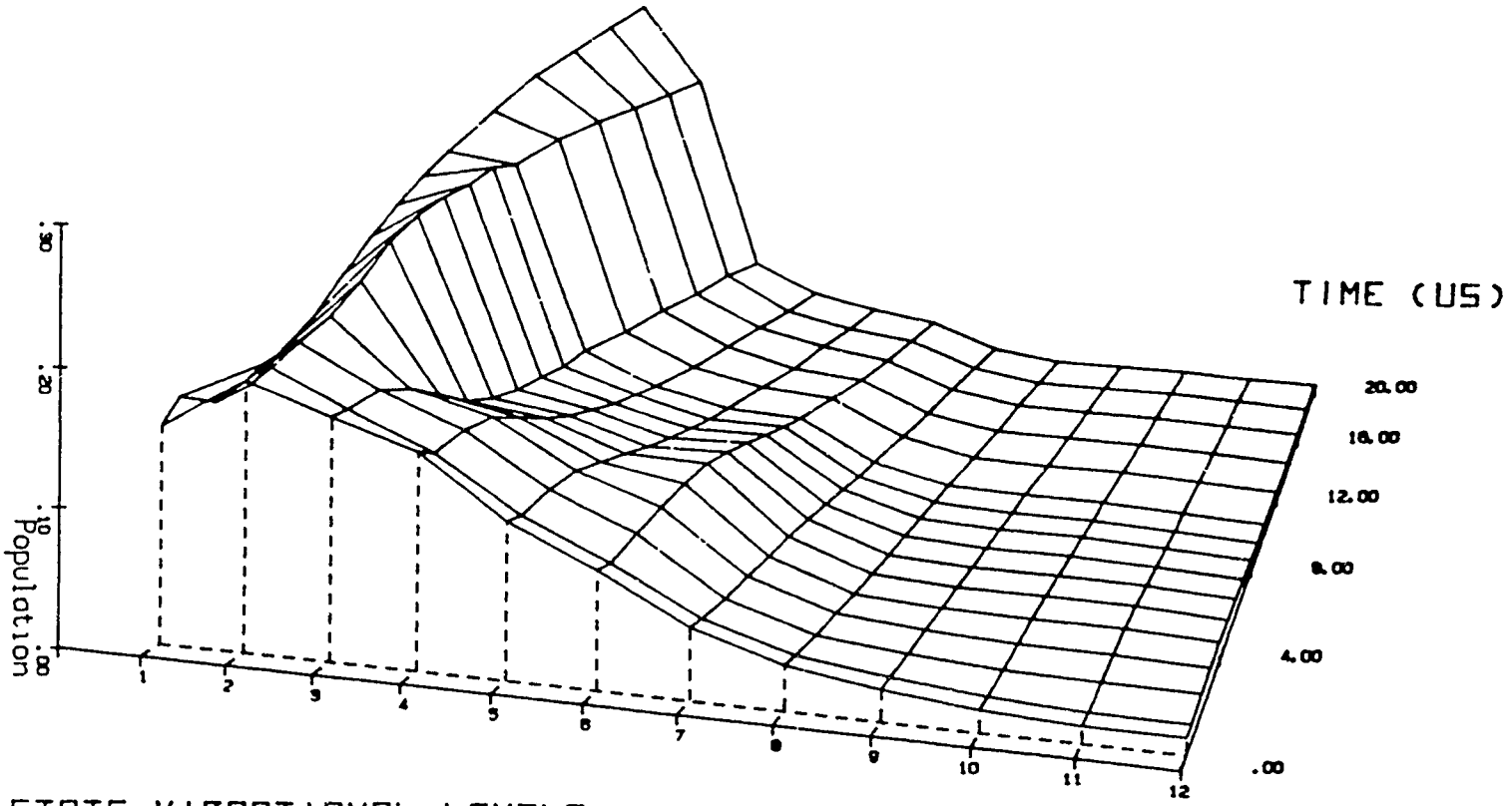

Figure 50 -

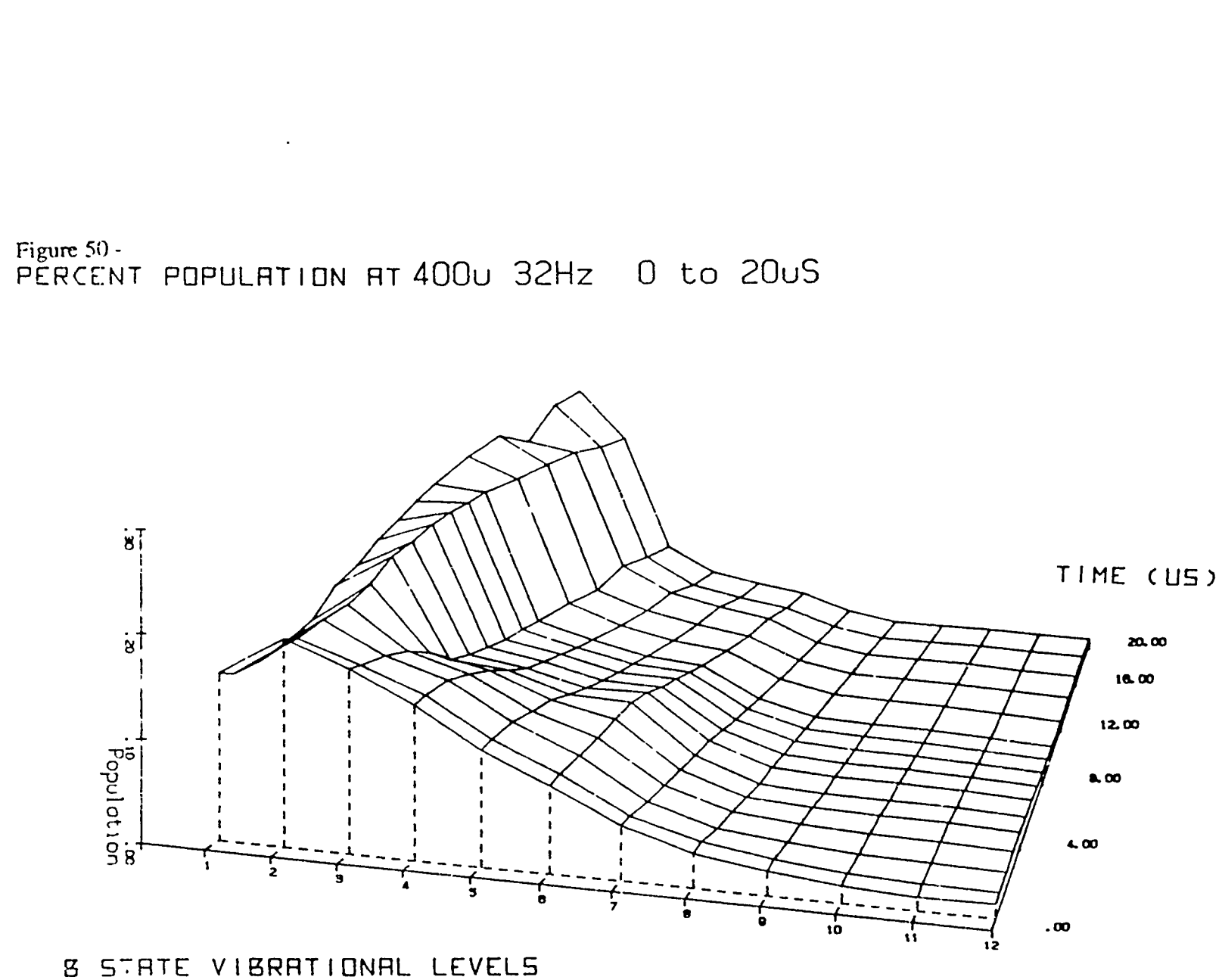
PERCENT POPULATION AT 400u 32Hz 0 to 20uS
TIME (US)
20.00
16.00
12.00
8.00
4.00
.00
Population
.8
.4
.0
1
2
3
4
5
6
7
8
9
10
11
12
8 STATE VIBRATIONAL LEVELS

Figure 51 -
PERCENT POPULATION AT 400u 50Hz 0 to 20uS

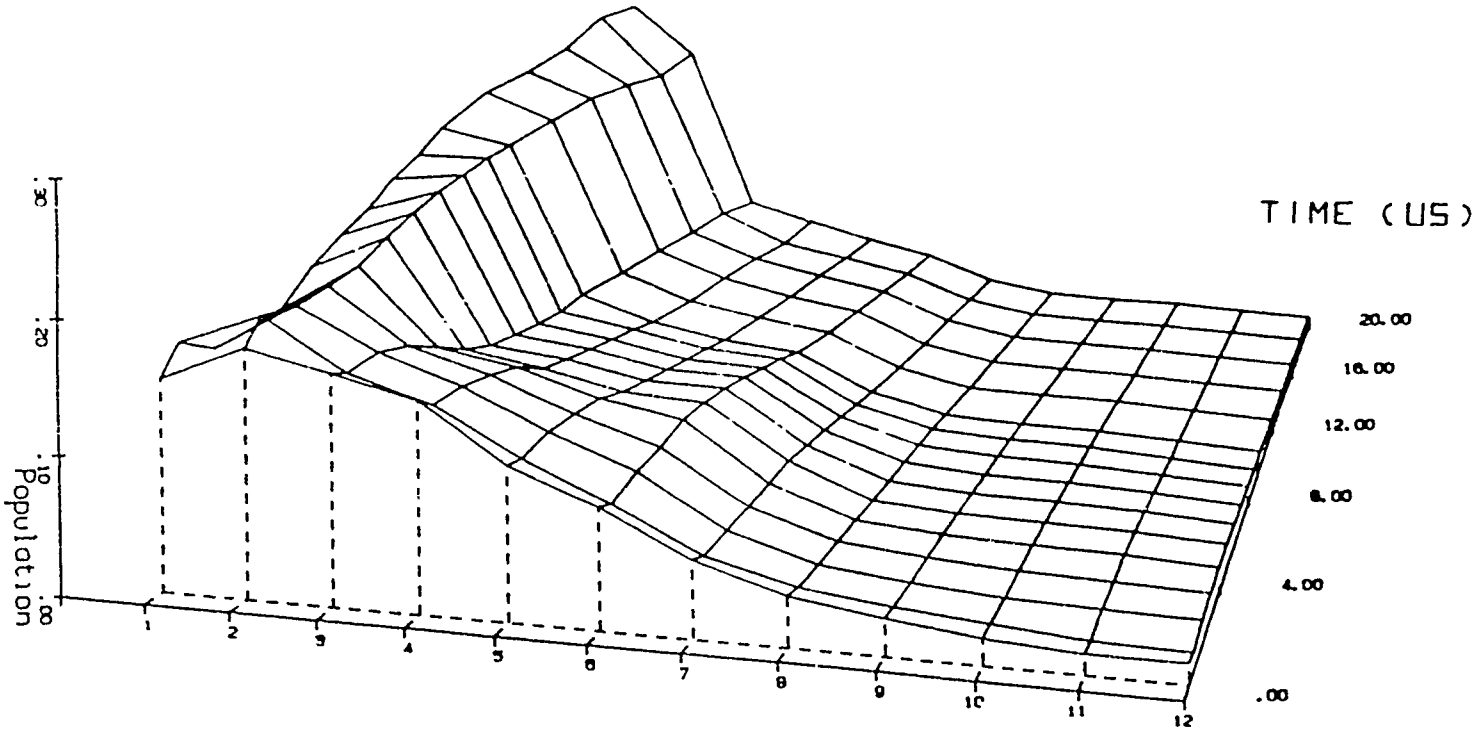

13 STATE VIBRATIONAL LEVELS

Figure 53 -

PERCENT POPULATION AT 50u 5Hz 0 to 200uS

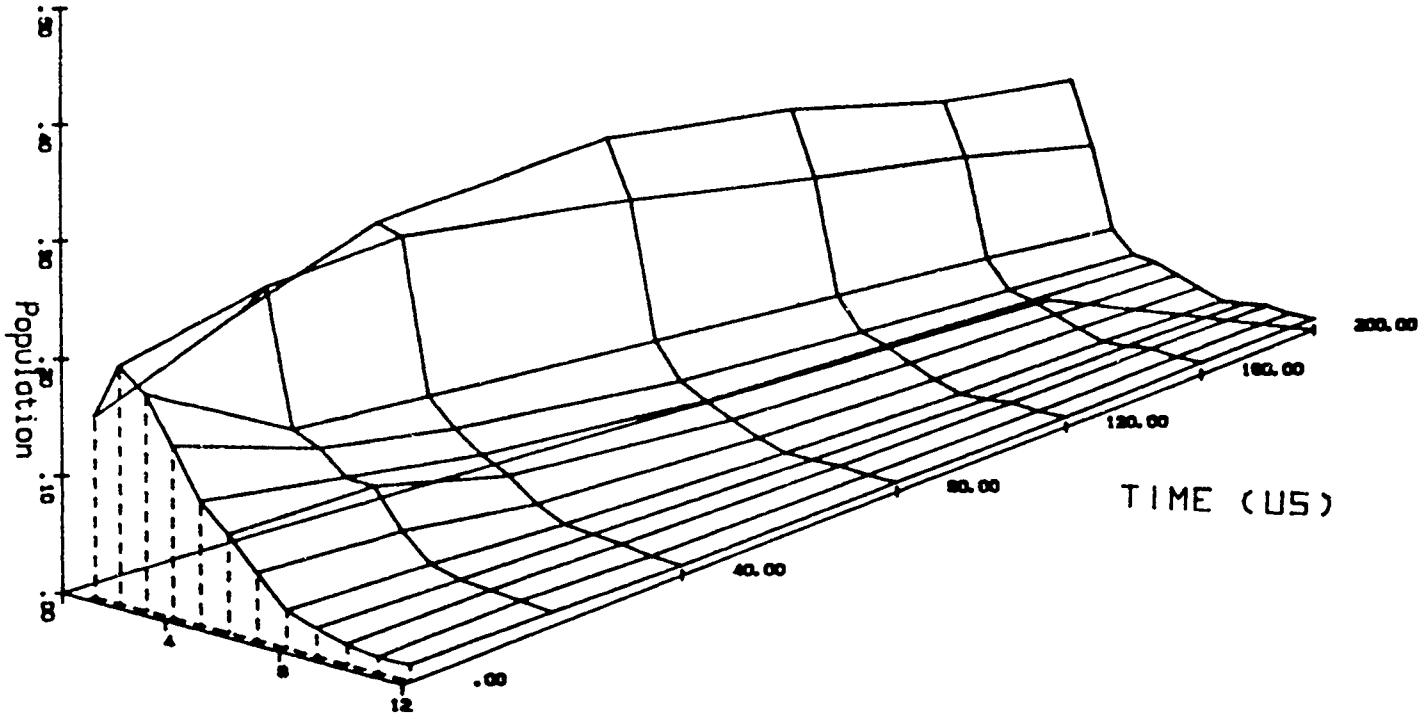

B STATE VIBRATIONAL LEVELS

Figure 54 -
PERCENT POPULATION AT 50u 15Hz 0 to 200uS

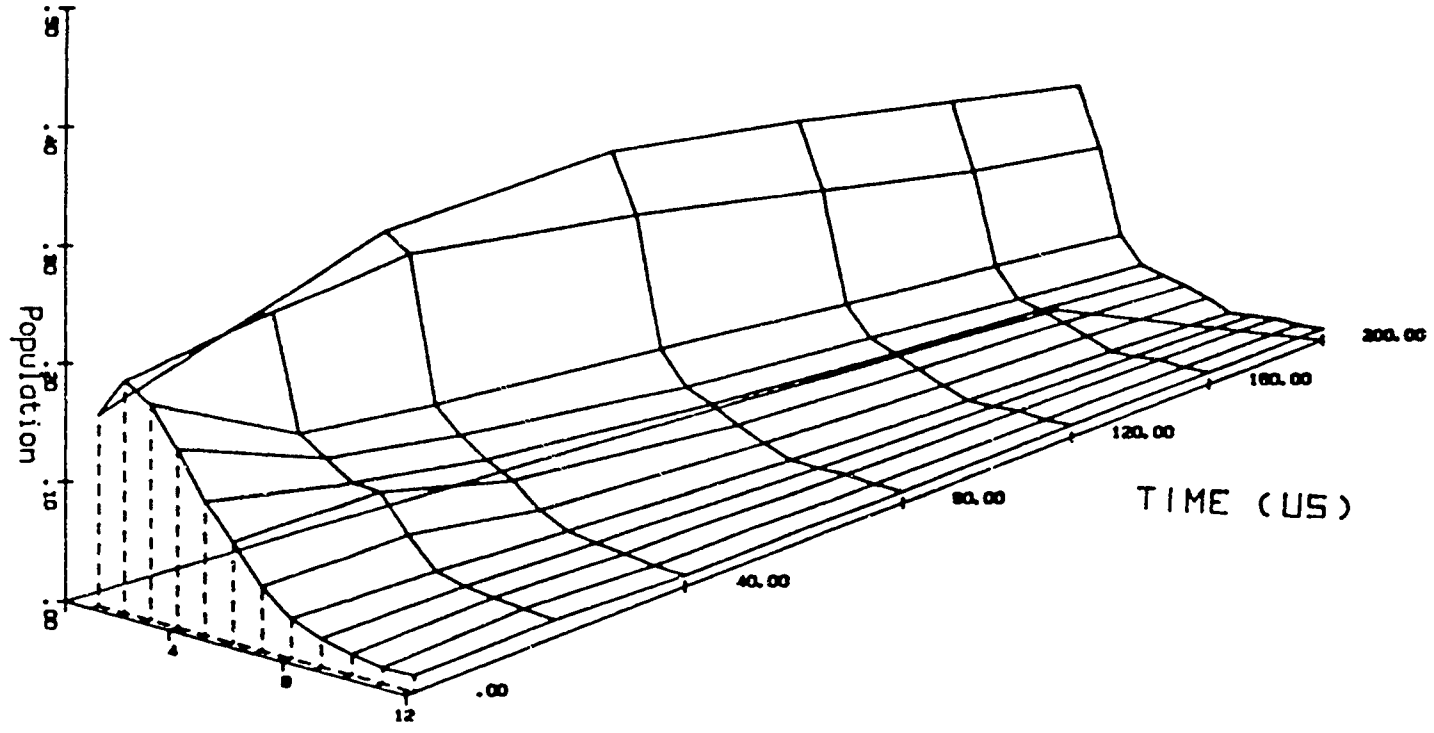

B STATE VIBRATIONAL LEVELS

Figure 55 -
PERCENT POPULATION AT 50u 32Hz 0 to 200uS

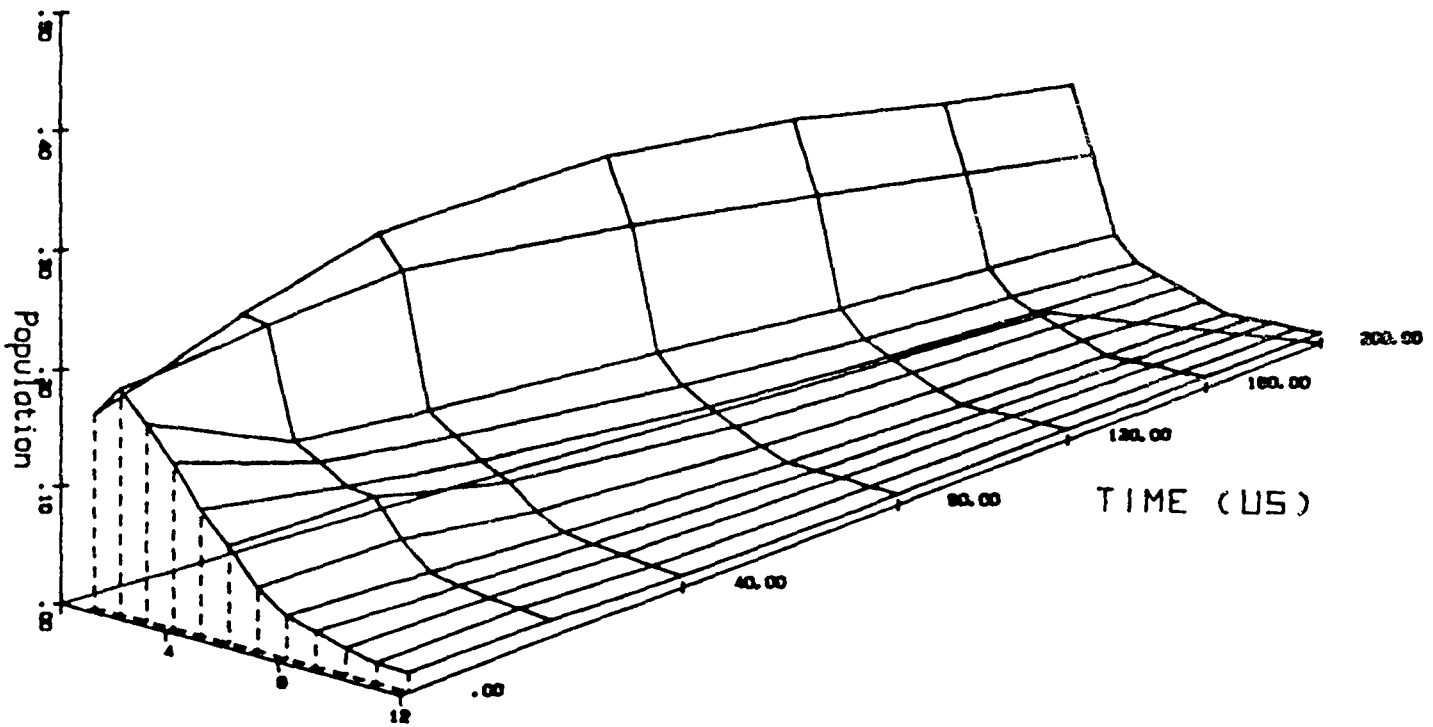

B STATE VIBRATIONAL LEVELS

Figure 56 -

PERCENT POPULATION AT 50u 50Hz 0 to 200uS

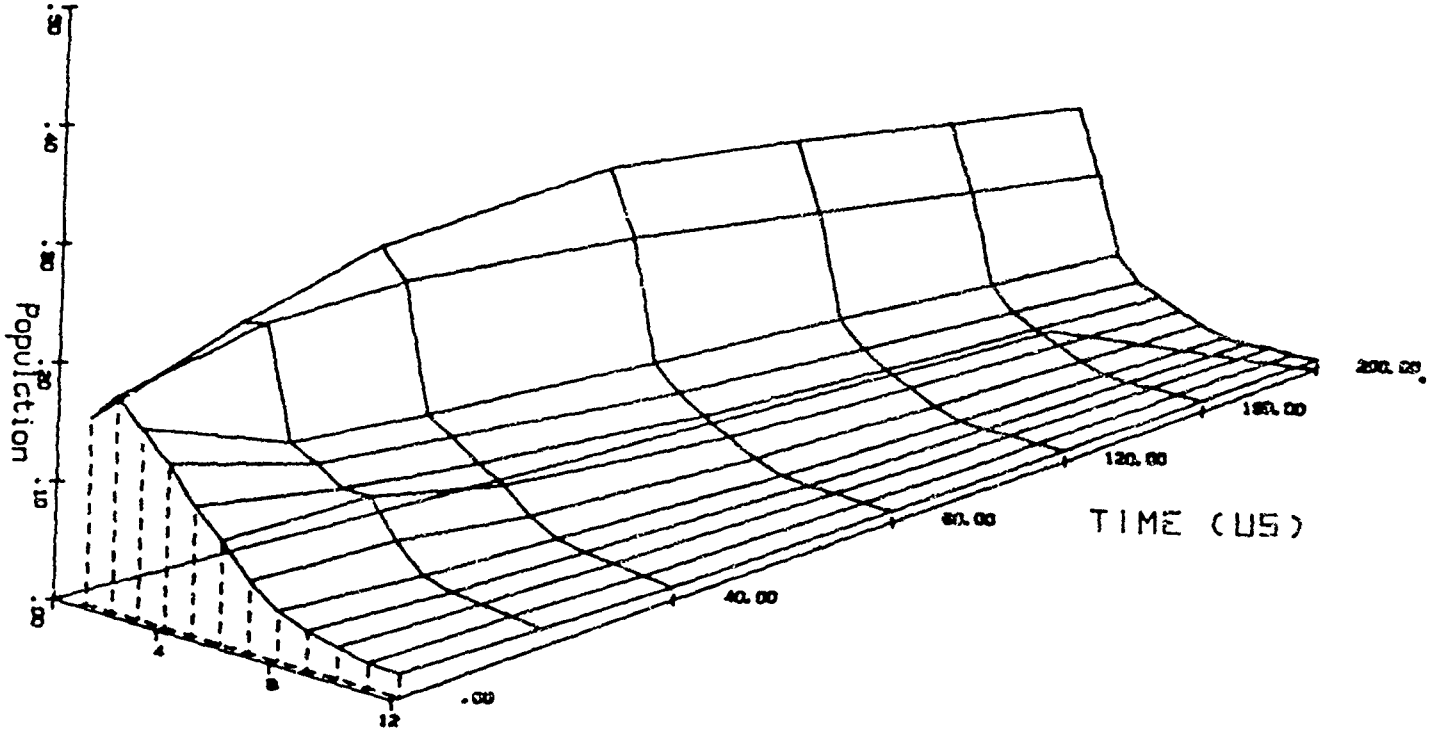

B STATE VIBRATIONAL LEVELS

Figure 57 -
PERCENT POPULATION AT 200u 5Hz 0 to 200uS

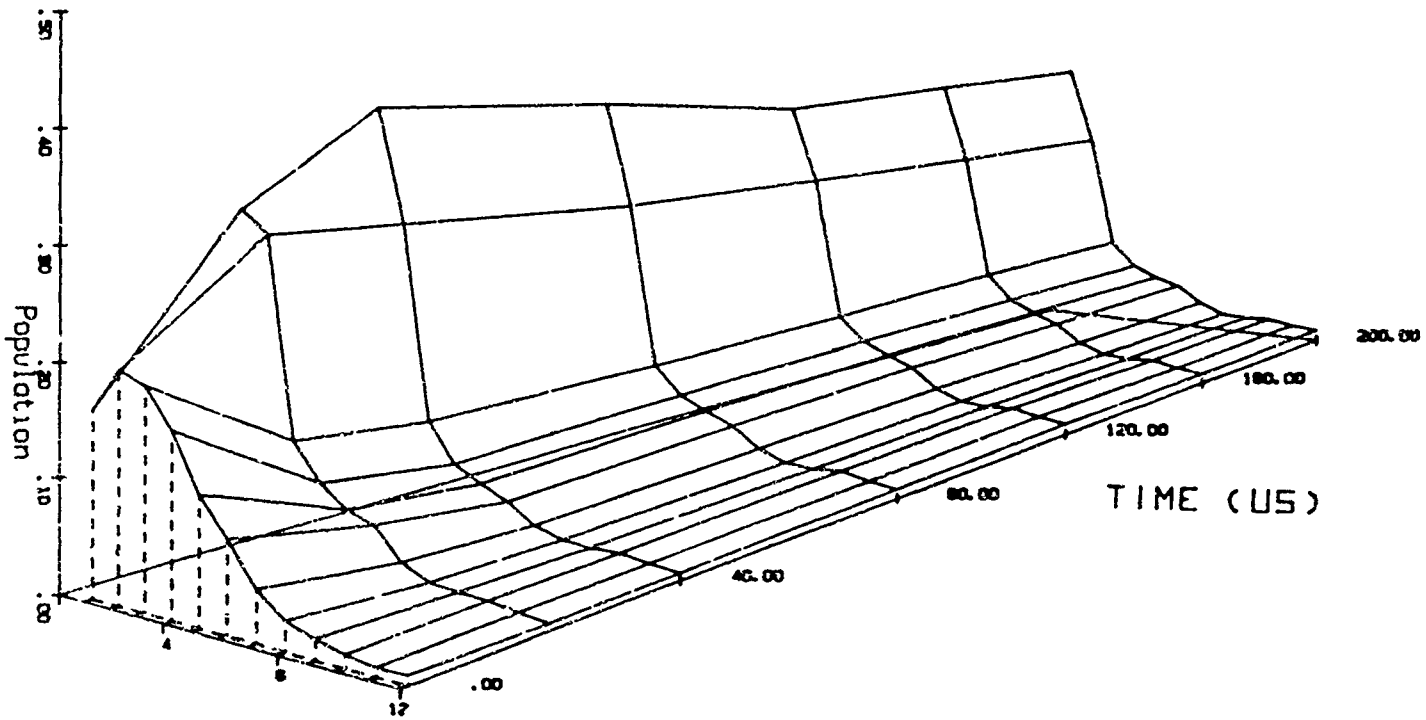

B STATE VIBRATIONAL LEVELS

Figure 58 -
PERCENT POPULATION AT 200u 15Hz 0 to 200uS

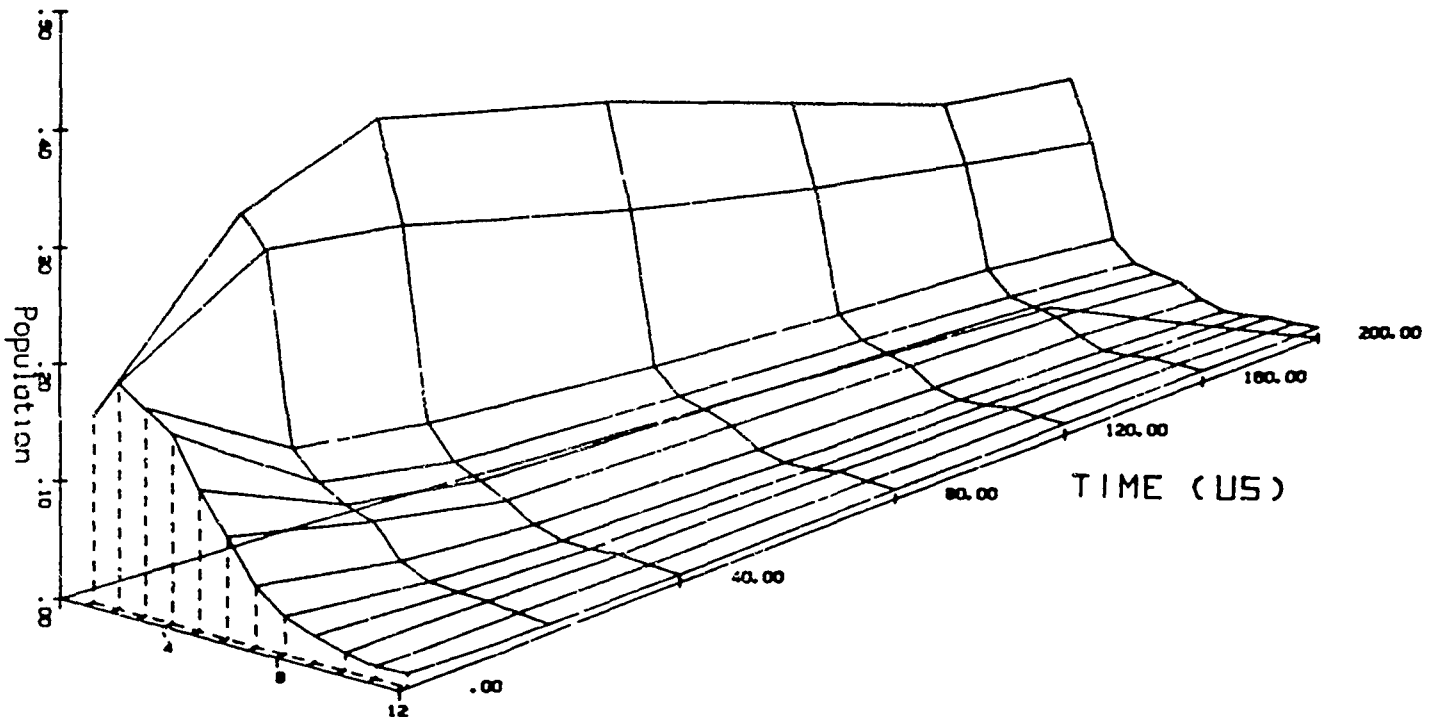

B STATE VIBRATIONAL LEVELS

Figure 59 -
PERCENT POPULATION AT 200u 32Hz 0 to 200uS

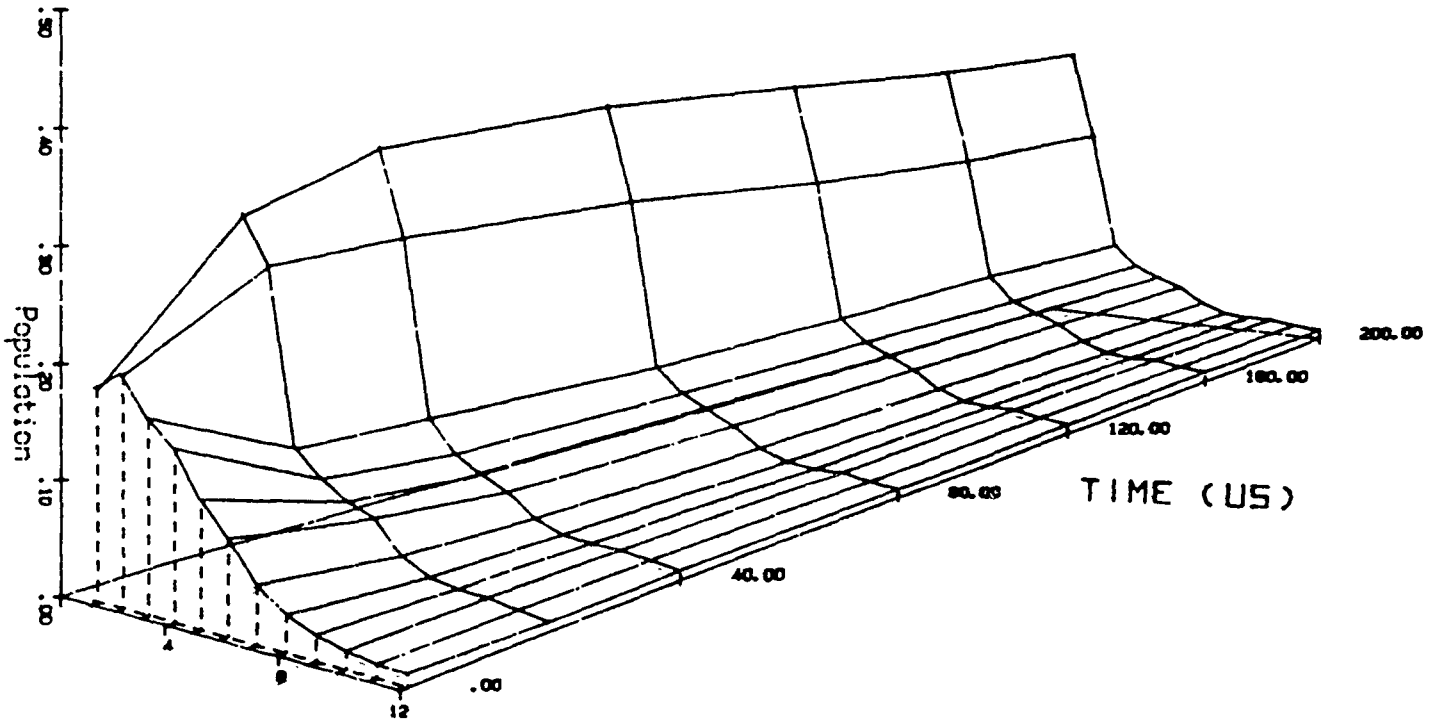

B STATE VIBRATIONAL LEVELS

Figure 60 -
PERCENT POPULATION AT 200u 50Hz 0 to 200uS

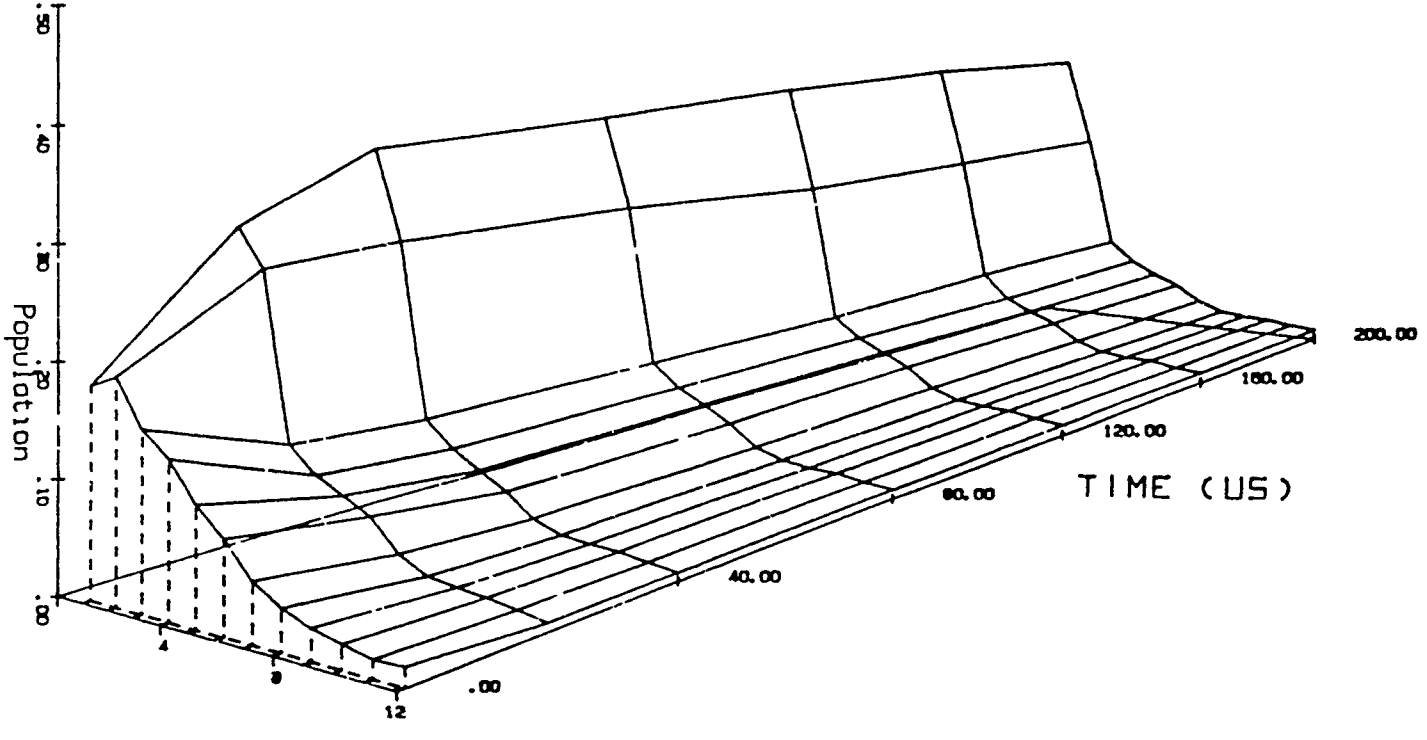

B STATE VIBRATIONAL LEVELS

Figure 61 -
PERCENT POPULATION AT 400u 5Hz 0 to 200uS

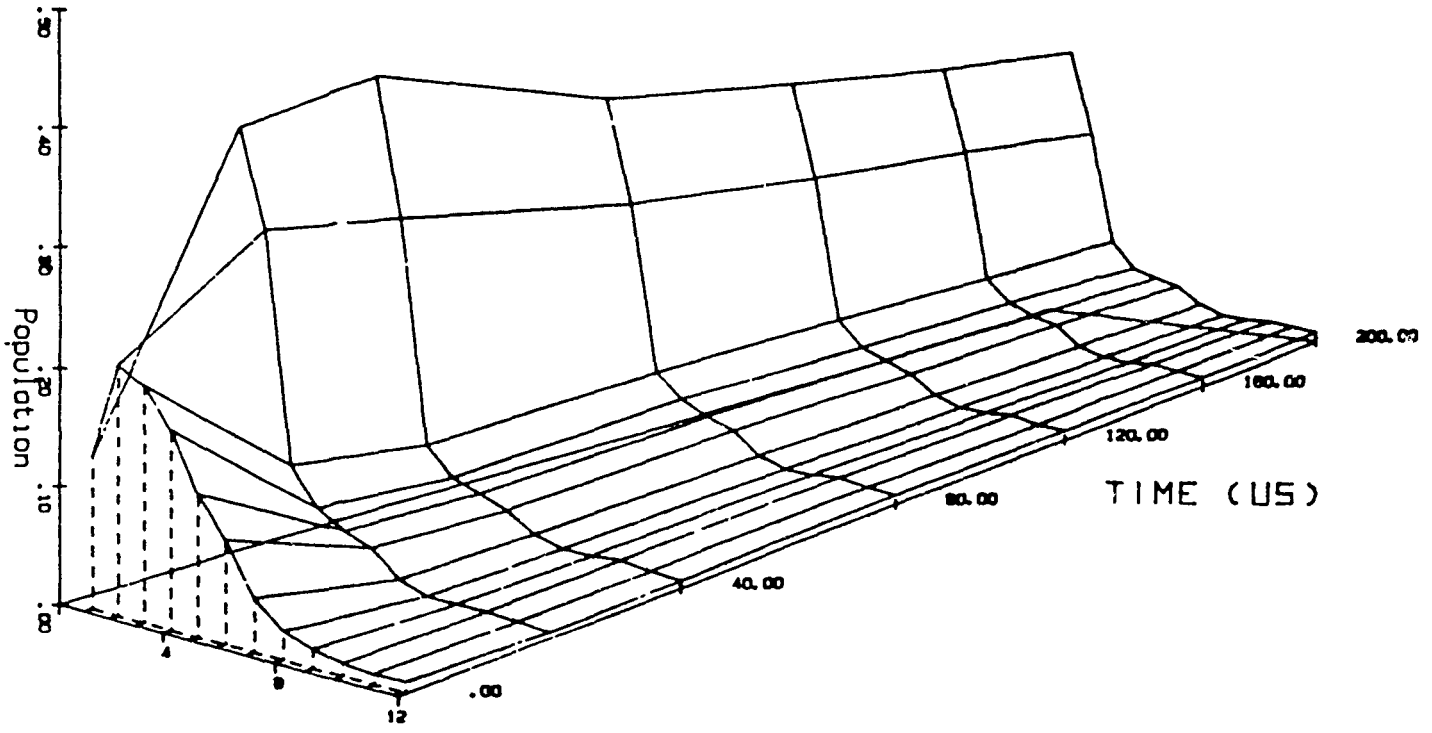

B STATE VIBRATIONAL LEVELS

Figure 62 -
PERCENT POPULATION AT 400u 15Hz 0 to 200uS

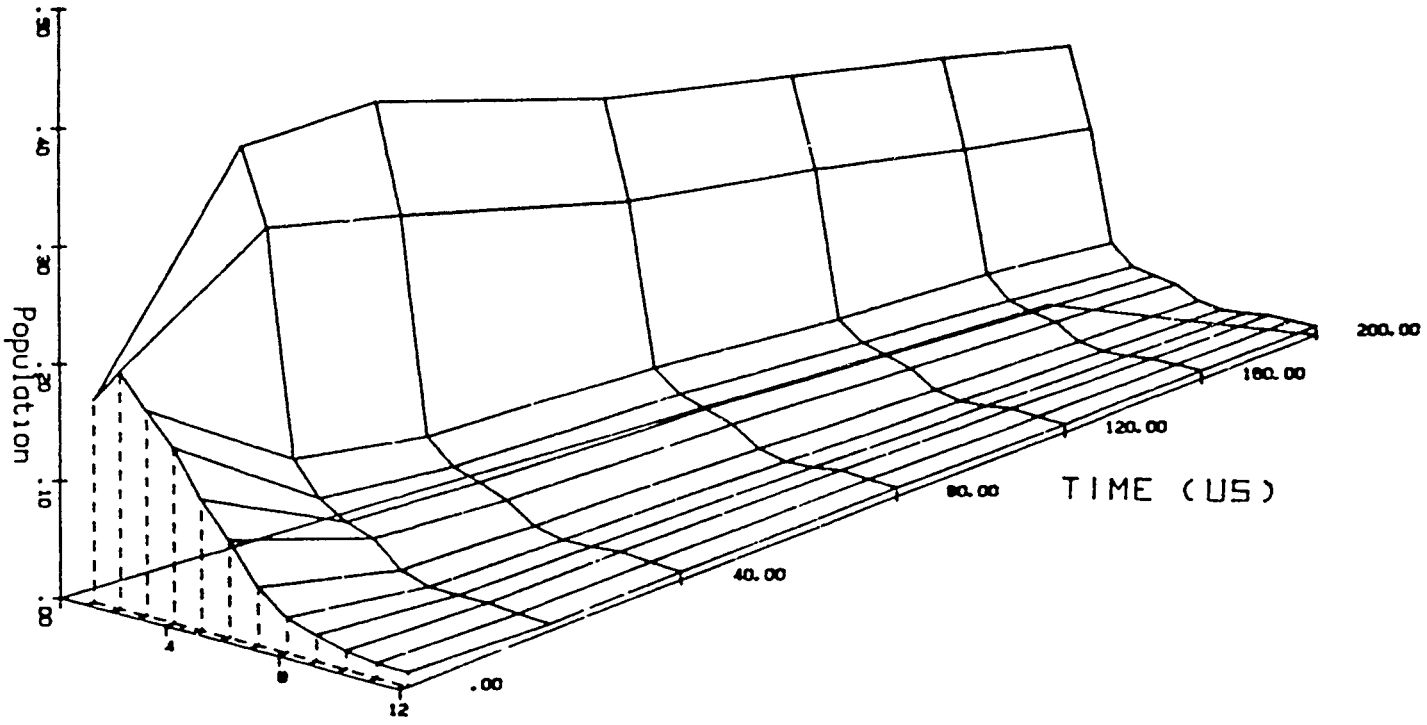

B STATE VIBRATIONAL LEVELS

Figure 63 -
PERCENT POPULATION AT 400u 32Hz 0 to 200uS

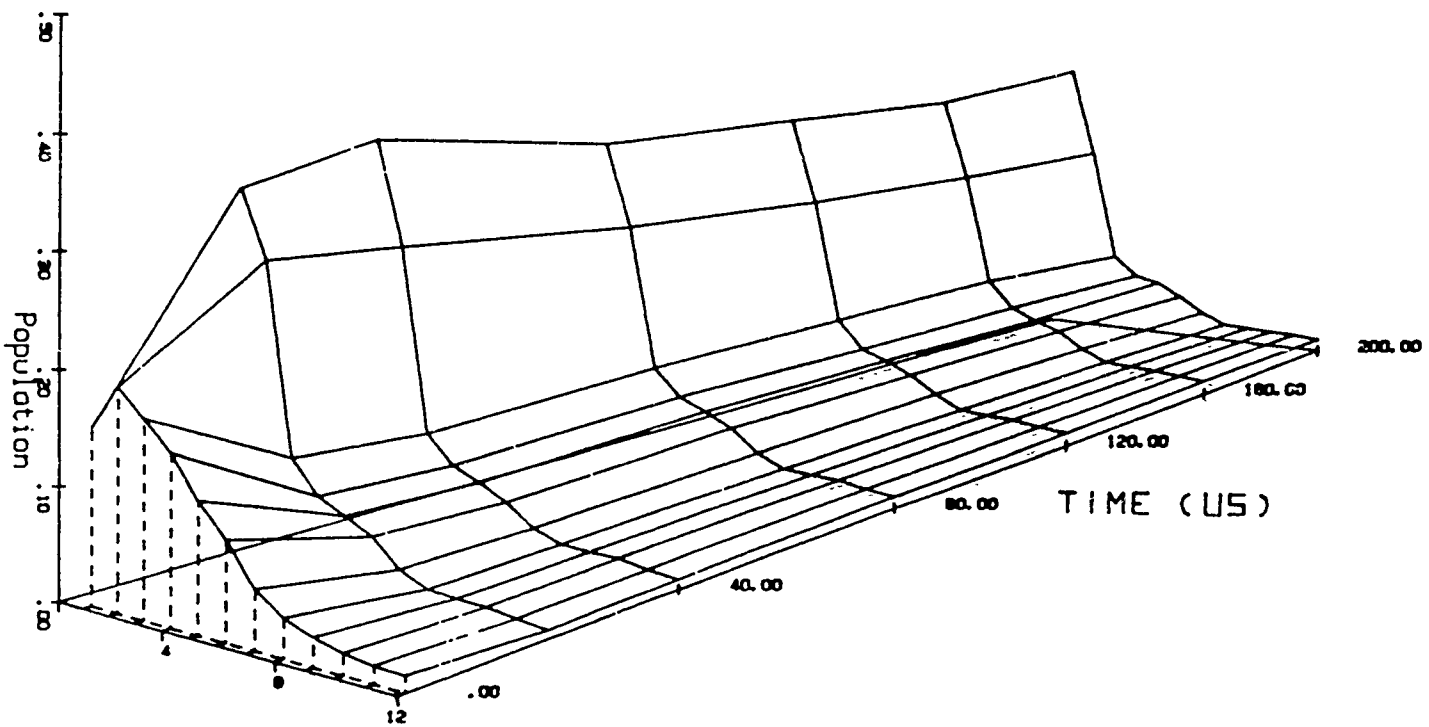

B STATE VIBRATIONAL LEVELS

Figure 64 -
PERCENT POPULATION AT 400u 50Hz 0 to 200uS

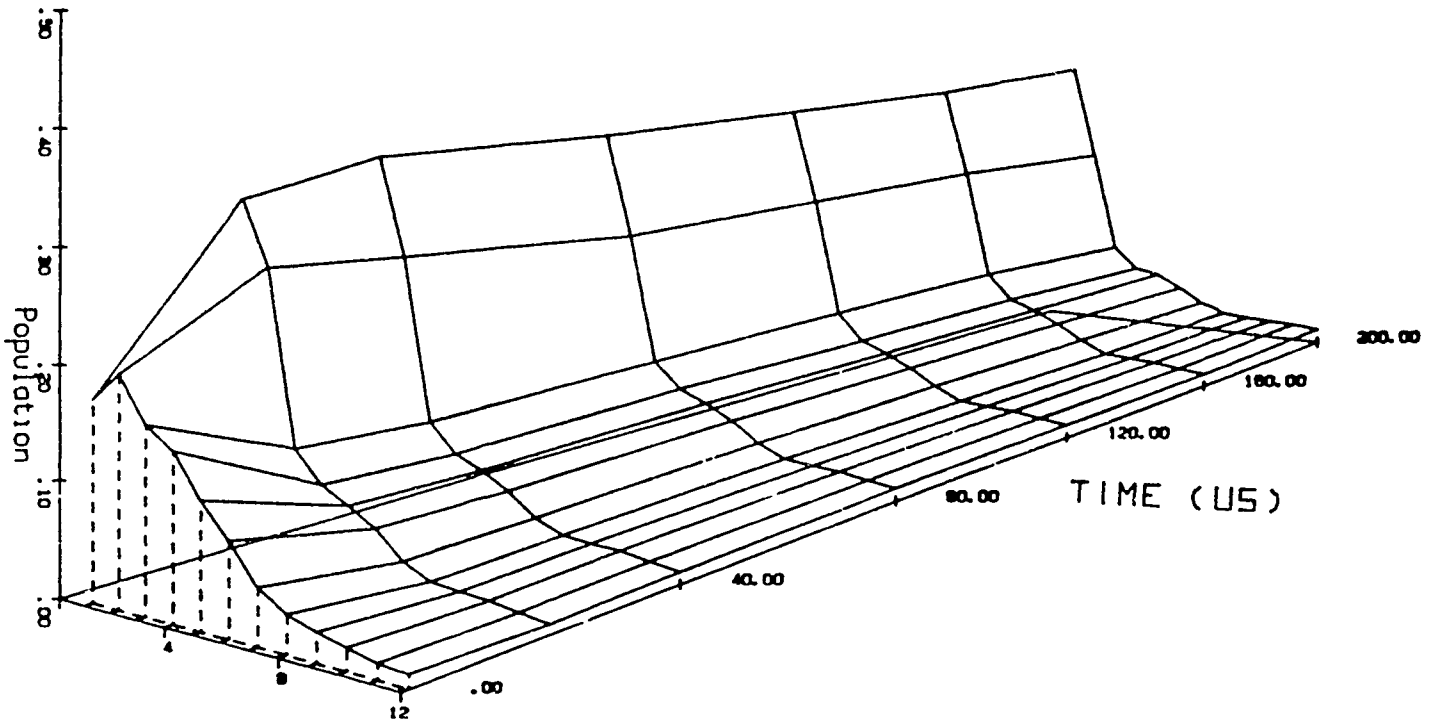

B STATE VIBRATIONAL LEVELS

CHAPTER 4 - RESULTS (V) - EFFECTS OF DISCHARGE FREQUENCY ON INITIAL DISTRIBUTIONS

One of the most striking discoveries of this study has been the effect of discharge frequency on the initial spectra which occur during the current pulse. Examples of this are shown in figures 68, 69 and 70 where 1PG spectra at 1, 5 and 50 Hz are compared. Again the sequences shown, from left to right are, δV = 4,3,2,1 respectively. As mentioned before each of these sequences feature bands due to emission from different groups of upper vibrational levels. Starting at the left, $\delta V = 4$ shows bands due to $v = 6$ thru 12, $\delta V = 3$ shows $V = 3$ thru 10, $\delta V = 2$ shows $V = 2$ thru 7 and $\delta V = 4$ shows $V = 1$ thru 3 (reference figure 14).

Figures 68, 69 and 70 show that as the time between each pulse decreases, the distributions of band intensities change dramatically. These changes are the effect of the gas being "pre-conditioned" by the previous pulse. As the time between pulses is varied, by changes in frequency, the degree to which the gas has been able to recover (or relax) from the previous pulse varies as well. Were the frequency low enough (<< 1Hz) the gas would relax completely. It would then be devoid of excited species, beyond a vibrational distribution in the ground state reflecting the gas temperture (~ 300 K). Spectra taken under these conditions would represent excitation from primarily the V=0 level of the ground state. So by "pre-conditioning" we mean that the system (the gas) has been previously excited and retains a certain amount of excitation at the start of the next pulse. Due to the variety of methods used in laboratory studies, the effects of pre-conditioning are not always evident in the results.

If we look at the above three spectra, the most significant differences occur in the δV=3 and 4 sequences. Specifically, these spectra show that increases in the percent populations of the higher vibrational levels are favored with increasing discharge

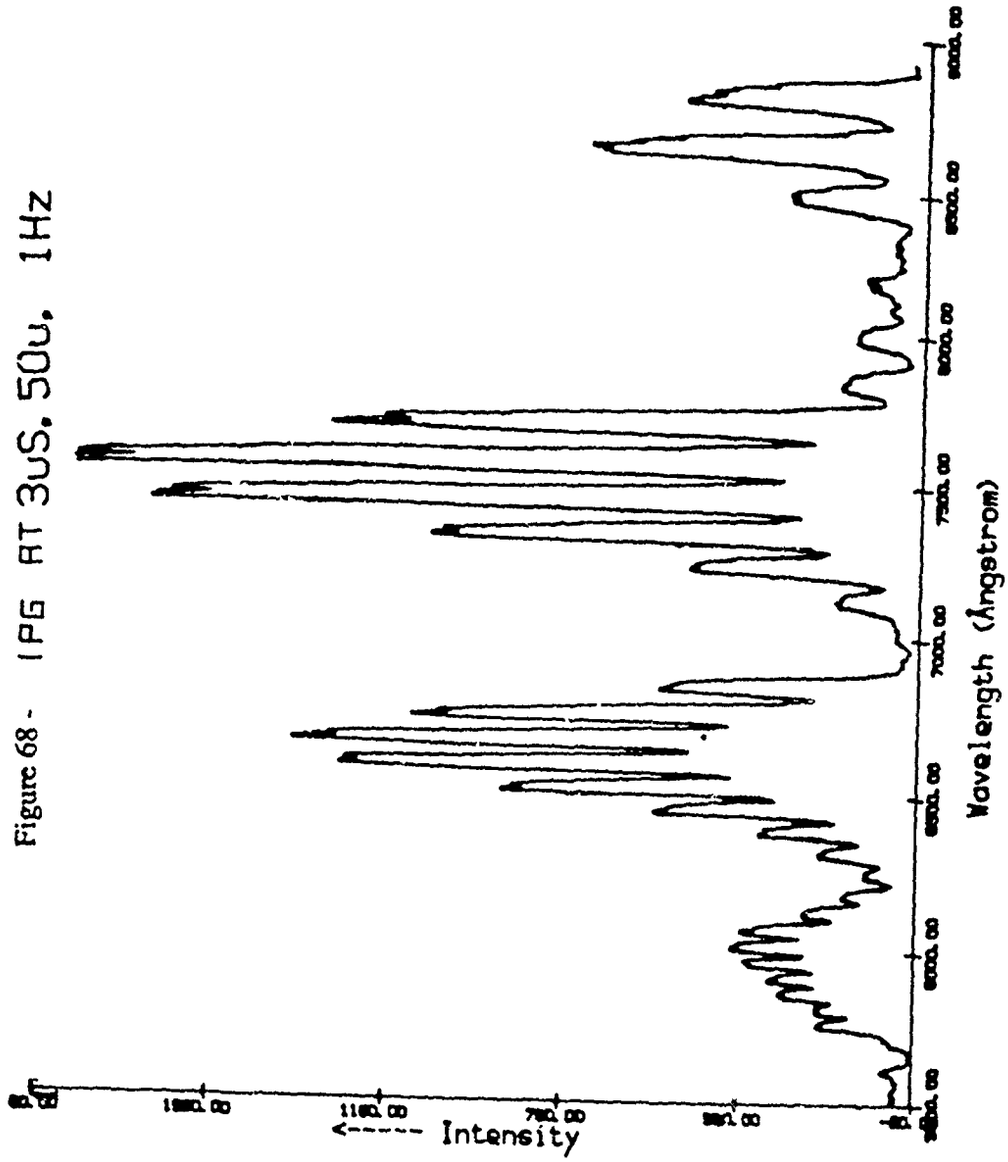

Figure 68 -

Figure 69 - IPG AT 3uS, 50u, 5Hz

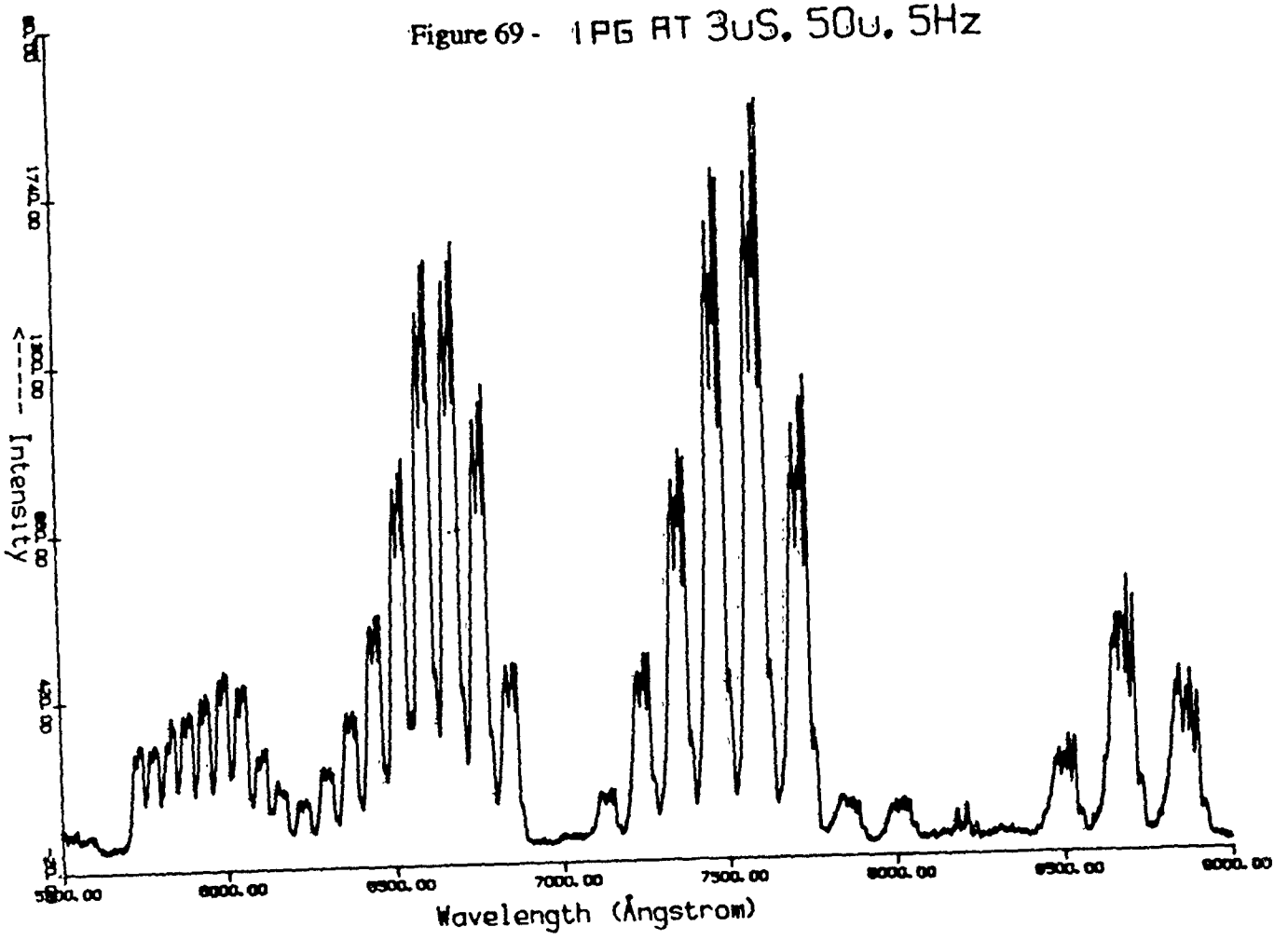

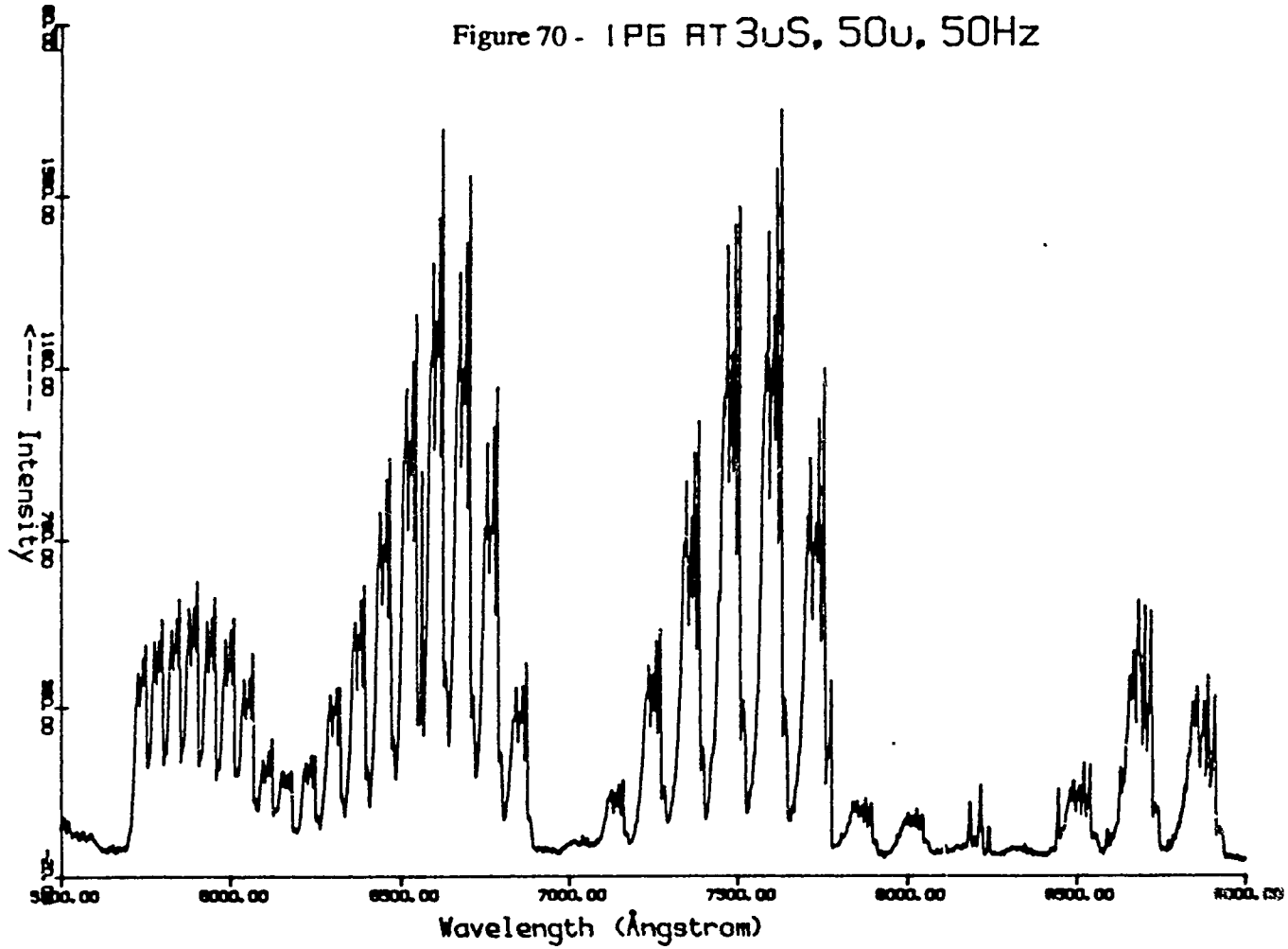
IPG AT 3uS, 50u, 50Hz
<----- Intensity
6000.00
6500.00
7000.00
7500.00
8000.00
8500.00
Wavelength (Ångstrom)

Figure 70 -

frequency. This is best shown in the $\delta V=4$ sequence. An example is shown in figure 71 which compares spectra at 5 and 50 Hz. These spectra have been normalized so that they reflect emission from the same total population (V= 1 through 12). This figure shows about a factor of two increase in the populations of levels V = 9 through 12. Compared to other populations in the overall distributions, the relative magnitude of these increases is small. Nonetheless, these changes reflect change in the overall B $^3\Pi_g$ state vibrational distribution and so can be related to an alteration in the source of excitation.

B $^3\Pi_g$ state vibrational distributions for 1 thru 50 Hz, at 3 μs and 50 μ, were taken from the population tables and are plotted in figure 72. This shows that as the frequency is increased the distribution tends to become less peaked. Also, the higher vibrational levels are increased with respect to the lower levels.

Previous work by Massabieaux et al.[28] indicated that ground state vibrational distributions with strongly over populated tails could be produced if the residence time in a DC discharge where long enough. They present results of calculations which show N_2 ground state vibrational distributions as a function of residence time. In general these plots are non-Boltzman and show the presence of an over populated tail extending up to V = 40 (see figure 12). The exception is the case of a 1.5 ms residence time. This appears to correspond to a vibrational temperature of about 5600 K. For residence times longer than this the distribution is predicted to become non-Boltzmann as mentioned above.

Other studies by Benesch et al. have analyzed Auroral spectra of the 1PG and 2PG. These studies have indicated that vibrational temperatures in excess of 2000 K were evident under certain conditions.[42, 43] The method of determining the apparent vibrational temperature used values of Franck-Condon factors which reflect the degree of overlap between the numerous vibrational levels of the ground state with those of the $B^3\Pi_g$ and C $^3\Pi_u$ states. We have used these factors coupled with ground state vibrational

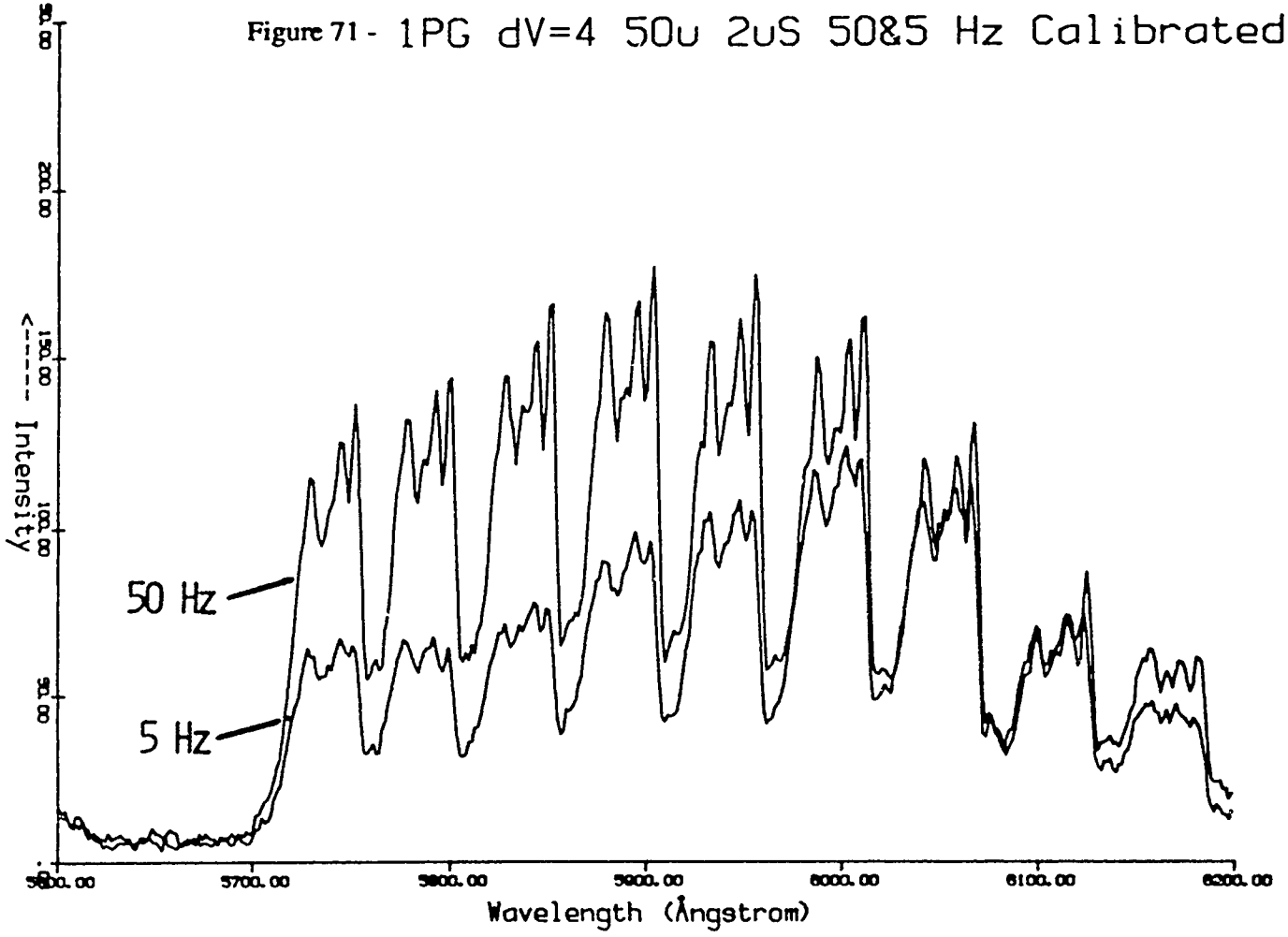
1PG dV=4 50u 2uS 50&5 Hz Calibrated
<------ Intensity
50 Hz
5 Hz
5700.00
5800.00
5900.00
6000.00
6100.00
6200.00
Wavelength (Ångstrom)

Figure 71 -

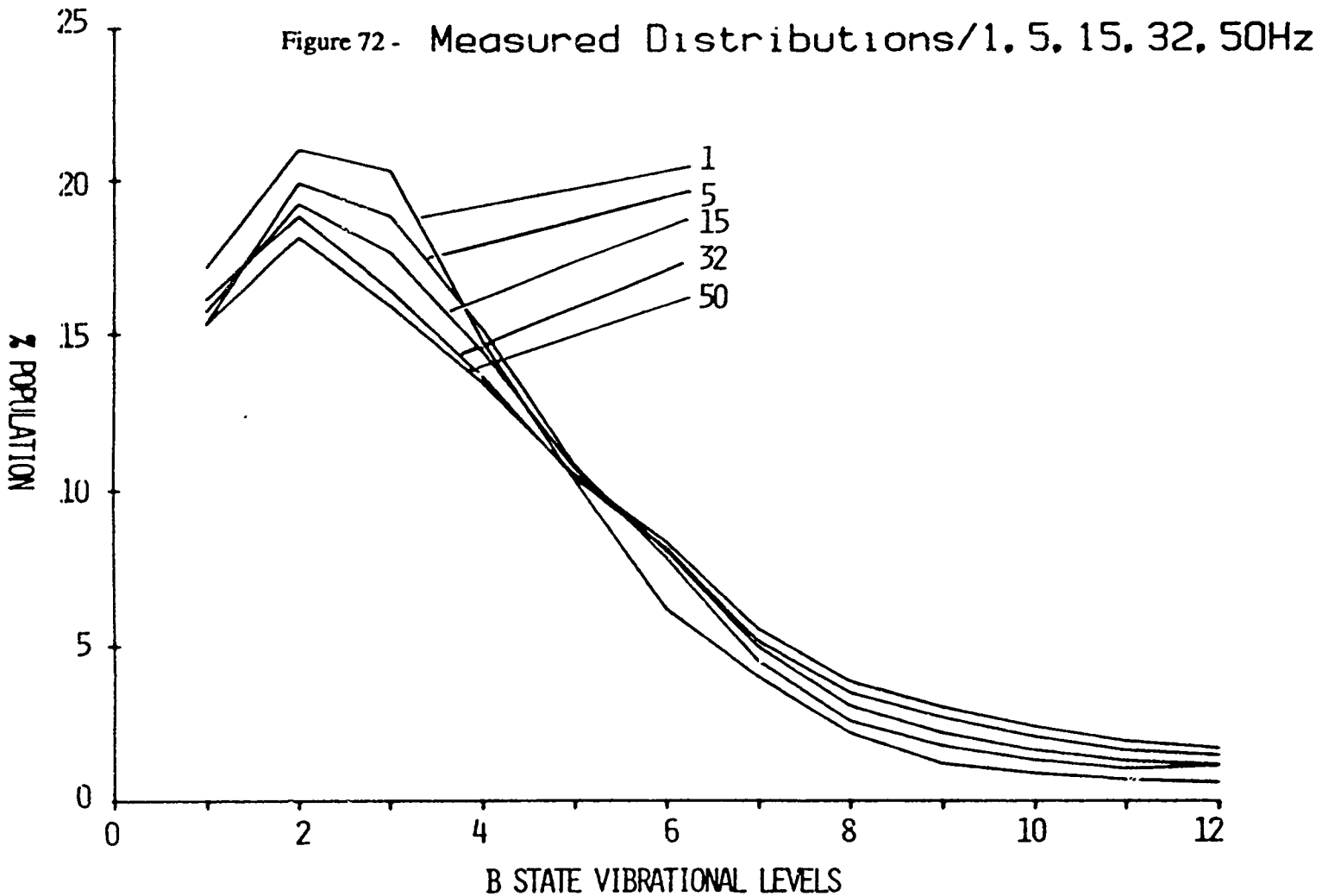
Figure 72 - Measured Distributions/1, 5, 15, 32, 50Hz
25
20
15
10
5
0
% POPULATION
1
5
15
32
50
0
2
4
6
8
10
12
B STATE VIBRATIONAL LEVELS

distributions, at various elevated temperatures, to estimate the excitation rates of the levels of the $B\,^3\Pi_g$ and $C\,^3\Pi_u$ states as a function of vibrational temperature. This has been the method of analysis used to determine the apparent vibrational temperatures of the initial distributions at the different frequencies and pressures of this study.

The fractional (or percent) excitaton rate, g(V'), for a given upper level, V', is given by,[43]

$$g(V') = \Sigma_{v''}\ N_{v''} * q_{v'v''}$$

where

V'' is the lower vibrational level in the $X\,^1\Sigma_g^+$ state

$N_{v''}$ is the percent population of the level V''

$q_{v'v''}$ is the Franck-Condon factor between levels V' and V''

The excitation rates for the vibrational levels of the $B\,^3\Pi_g$ state which result from this analysis are equated to the estimated initial vibrational distributions. This process of estimating rates has been done by a computer program which generates Boltzmann vibrational distributions in the ground state at elevated temperatures. These distributions are then coupled with the appropriate Franck-Condon factors. Finally the resulting contributions to each vibrational level in the $B\,^3\Pi_g$ state is summed and the results are compared to the experimental distributions. The apparent ground state vibrational temperature is found by incrementing the temperature and summing the absolute differences between the experimental and estimated distribution values. This is represented as

$$Z = \Sigma_{v'=1}^{12} |N_{exp}(V') - N_{theory}(V')|$$

The vibrational temperature was taken as the temperature for which Z was a minimum. For a given experimental distribution, the minimum Z values occur for the vibrational temperature which results in the best fit between estimated and measured B $^3\Pi_g$ state distributions. Of course, the lower the value of Z the better the fit and the more accurate the resulting vibrational temperature. This analysis was performed on the initial distributions for all sets of conditions. Distributions at the following times were used,

PRESSURE (μ)	TIMES(μs)
400	0.5,1,2
200	0.5,1,2,3
50	1,2,3,4.

The results are shown in figure 73 where the data has been fit to an equation with the form,

$$T_v = A + Bx(Hz)^{0.5} - Cx(Hz)^{-2}$$

with

	PRESSURE		
	50 μ	200 μ	400u
A =	1022.899	1061.909	841.7807
B =	255.9942	176.6419	192.0984
C =	977.8374	940.4904	735.8368 .

The apparent vibrational temperatures for the different conditions appear in table 31. The apparent vibrational temperature for 1 Hz (T_v ~ 300 K) was only measured at 50 μ This value is assumed to be the same at the other two pressures. The values of table 31 are

Figure 73 - Vibrational Temperature (K) vs Discharge Frequency (Hz)

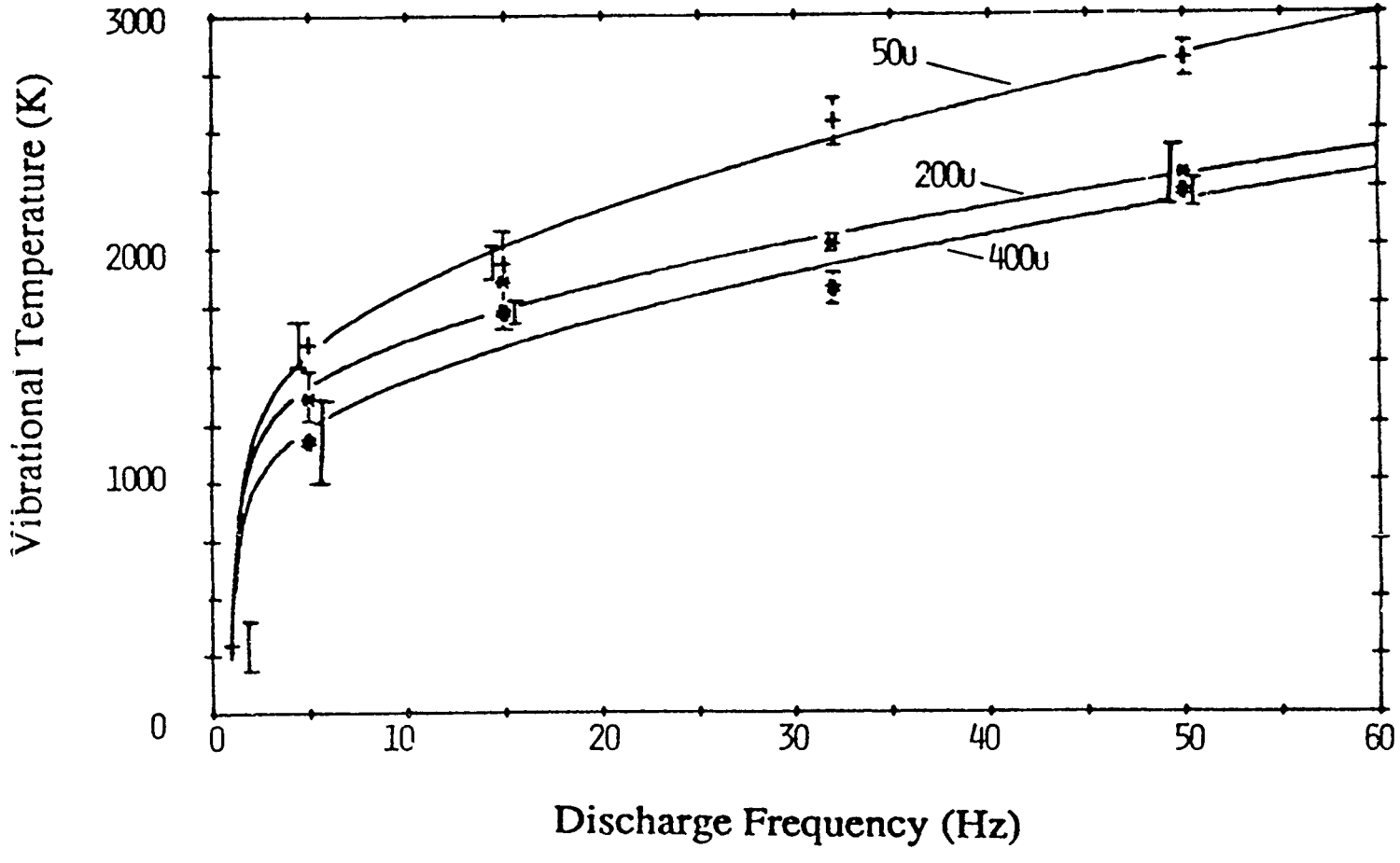

weighted averages which used the reciprocal of the Z parameter as a weight. Minimum Z values were on the order of 3 to 7% total difference between measurement and estimate. The error bars in figure 73 are the probable error (P.E.) associated with the average vibrational temperatures of table 31. The measured distributions can be found in tables 12 through 23.

A comparison between an estimated and experimental distribution appears in figure 74. One should notice that the best fit is between V = 3 through 10. Also the experimental distribution shows a larger fraction in the last few vibrational levels. Regardless, the overall estimated distribution appears to fit the experimental distribution quite well. These results show that the explanation for the observed changes in the spectra, based on an elevated vibrational temperature in the ground state, appears to hold for a large portion of these distributions.

At first glance these temperatures, of up to 2800 K, might seem enormous. They are in fact very large but reflect the fact that the system under study can be characterized as a non-equilibrium discharge. Here the energy distributions of the different degrees of freedom are not in equilibrium with one another. In a discharge, the electron energies need to be very high and, for the sake of discussion, can be considered to be Boltzmann with temperatures on the order of 10's of thousands of degrees Kelvin. At the same time the kinetic and rotational temperatures are expected to be on the order of hundreds of degrees (300 to 500 K). For the case of the vibrational distribution, temperatures on the order of thousands of degrees are evident.

The separation of the electron and the rotational-kinetic temperatures is largely due to the mass difference between the electron and the N_2 molecule as well as the pressure regime under study. For the case of vibration, vibrationally excited ground state molecules, whether produced by cascade from excited electronic states or from direct

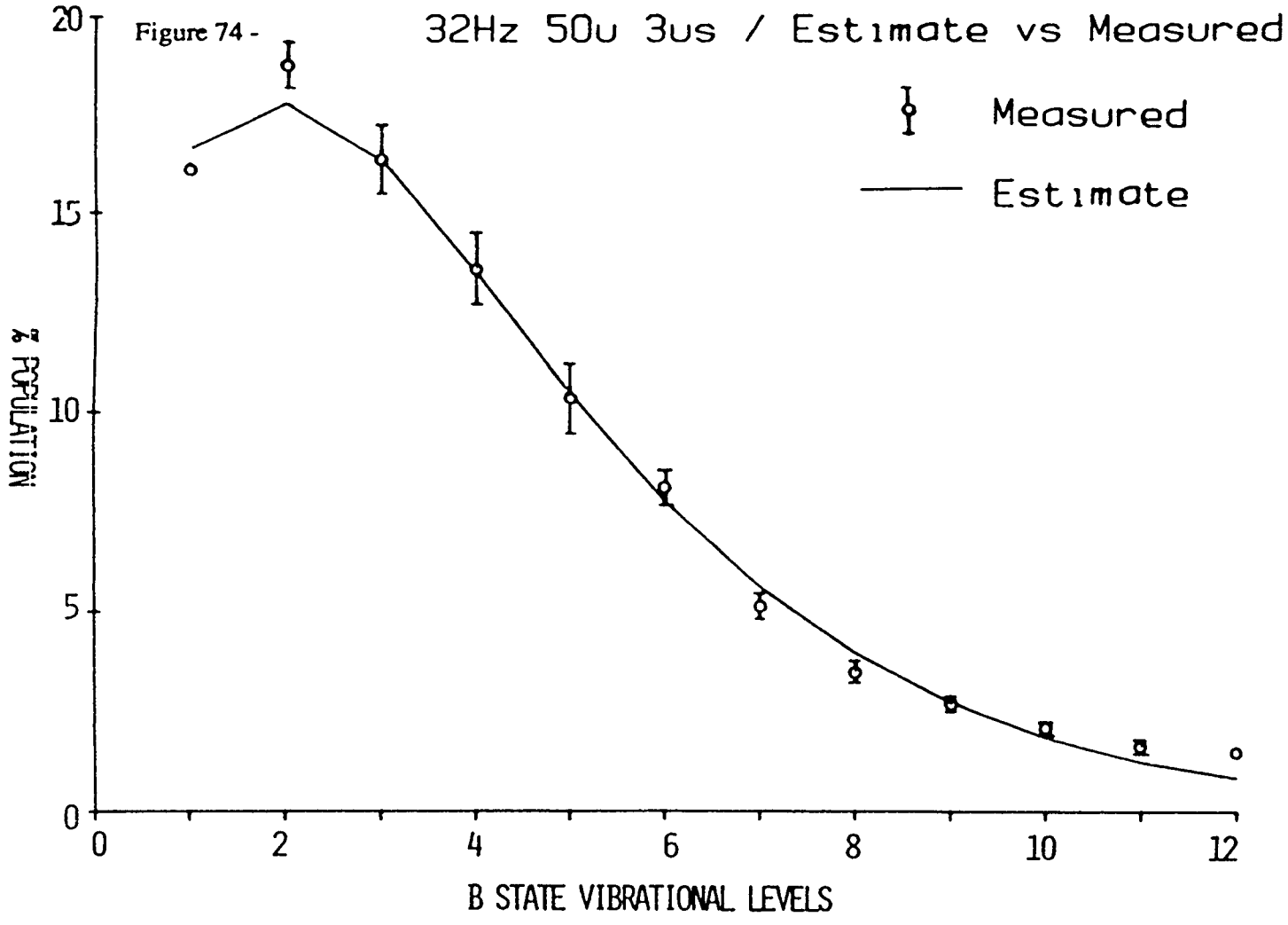
Figure 74 -
32Hz 50u 3us / Estimate vs Measured
Measured
Estimate
% POPULATION
B STATE VIBRATIONAL LEVELS
0
5
10
15
20
0
2
4
6
8
10
12

TABLE 31 - APPARENT VIBRATIONAL TEMPERATURE VS FREQUENCY AT 50, 200 AND 400μ

	Frequency (Hz)			
Pressure (μ)	5	15	32	50
50	1590 ±101	1930 ±74	2540 ±102	2810 ±67
200	1360 ±110	1850 ±205	2010 ±29	2310 ±121
400	1180 ±185	1720 ±48	1820 ±64	2230 ±59

upper entries - vibrational temperature (K)

lower entries - probable error

electron excitation, do not have an efficient mechanism by which to transfer vibrational energy into rotational or kinetic energy. This is due primarily to the large energy spacing between vibrational levels of the ground state compared to kT(g). For N_2, V = 1 is ~ 2300 cm^{-1} above V = 0 and T(g) is the gas temperature (kT(g) ~ 200cm^{-1} at 300 K).

Regardless of the source of excitation, collisions between vibrational excited molecules will tend to redistribute this vibrational energy. This redistribution will continue until the distribution becomes Boltzmann, time permitting. The resulting distribution will reflect some temperature and this temperature will reflect the average vibrational energy of the gas.

What we see in the present case is that for a constant pressure, the vibrational temperature of the ground state decays as the amount of time between pulses increases (figure 73). This increase in time can be related to an increase in the total number of collisions between pulses. Also, at constant frequency, as the pressure is increased the number of collisions between pulses increases as well. From figure 73 we see that the apparent vibrational temperature decreases with increasing pressure at constant frequency. Both issues are evidence showing a decrease in vibrational temperature with an increase in the number of collisions.

It is not clear from this data what the mechanism is for energy loss from the vibrational manifold. All that we can say is that the vibrational temperature drops with increased numbers of collisions.

These results have shown the importance of the process of "pre-conditioning" in the initial B $^3\Pi_g$ state distribution which results during direct electron excitation. Presumably, similar changes are occuring in the other excited states as well.

An interesting explanation which follows from these findings, involves the changes in the $\delta V=3$ sequence. Figure 75 compares the $\delta V=3$ sequence for a 1PG spectrum of an Aurora with that of a laboratory (DC) discharge.[7] Note the distribution of band intensities.

Figure 75 -

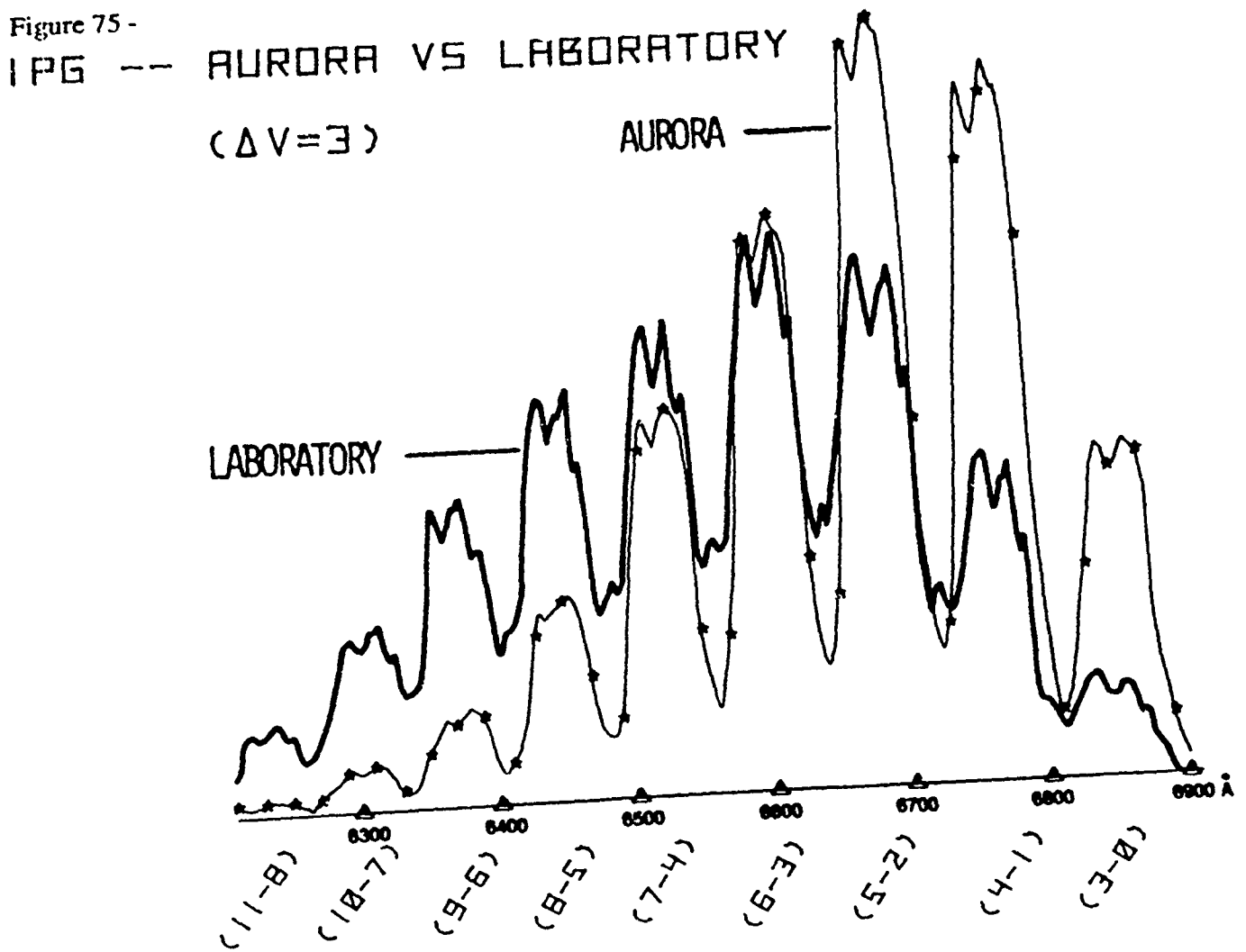
1PG -- AURORA VS LABORATORY
(ΔV=3)
AURORA
LABORATORY
6300
6400
6500
6600
6700
6800
6900 Å
(11-8)
(10-7)
(9-6)
(8-5)
(7-4)
(6-3)
(5-2)
(4-1)
(3-0)

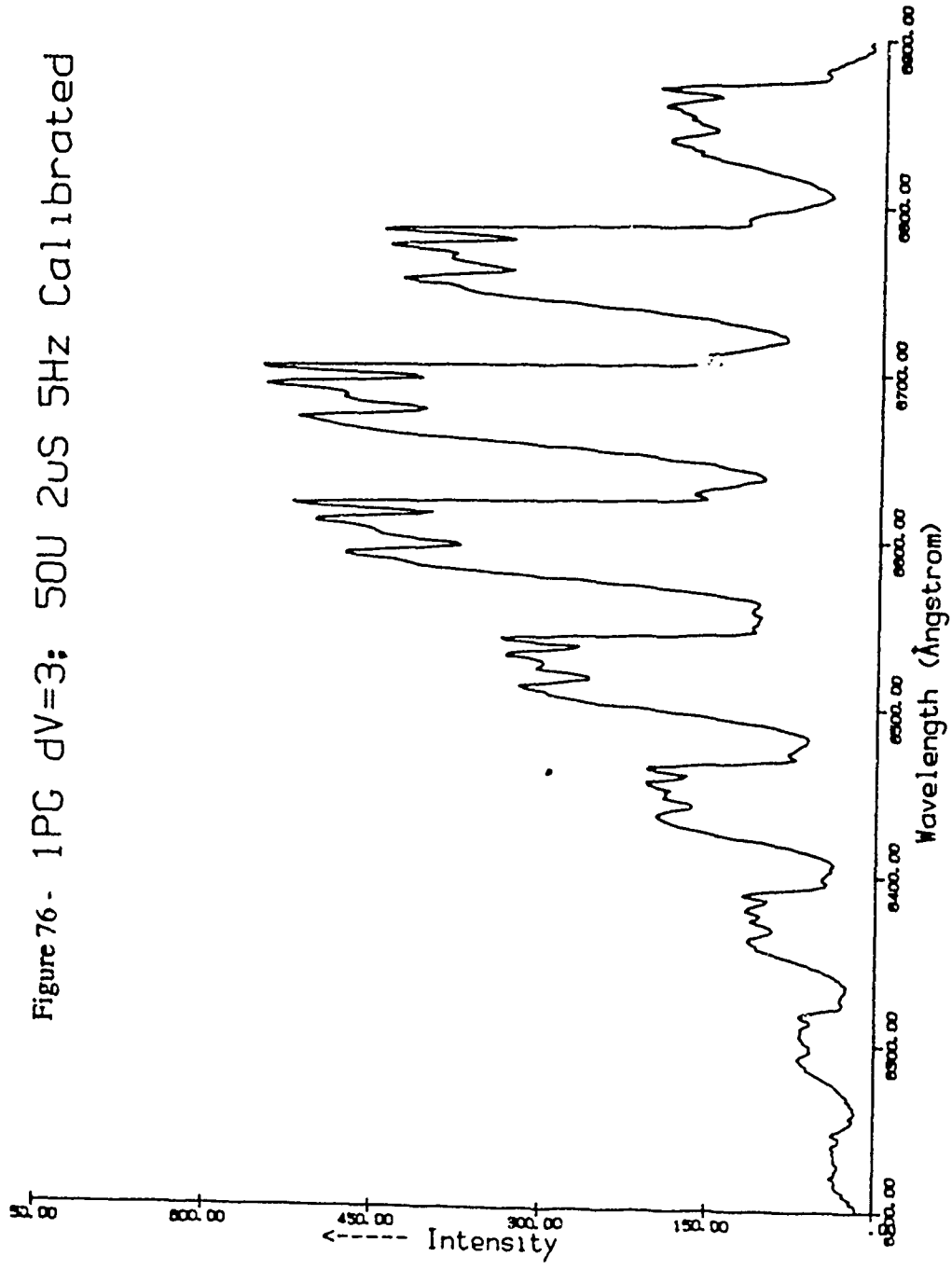

Figure 76 - 1PG dV=3; 50U 2uS 5Hz Calibrated

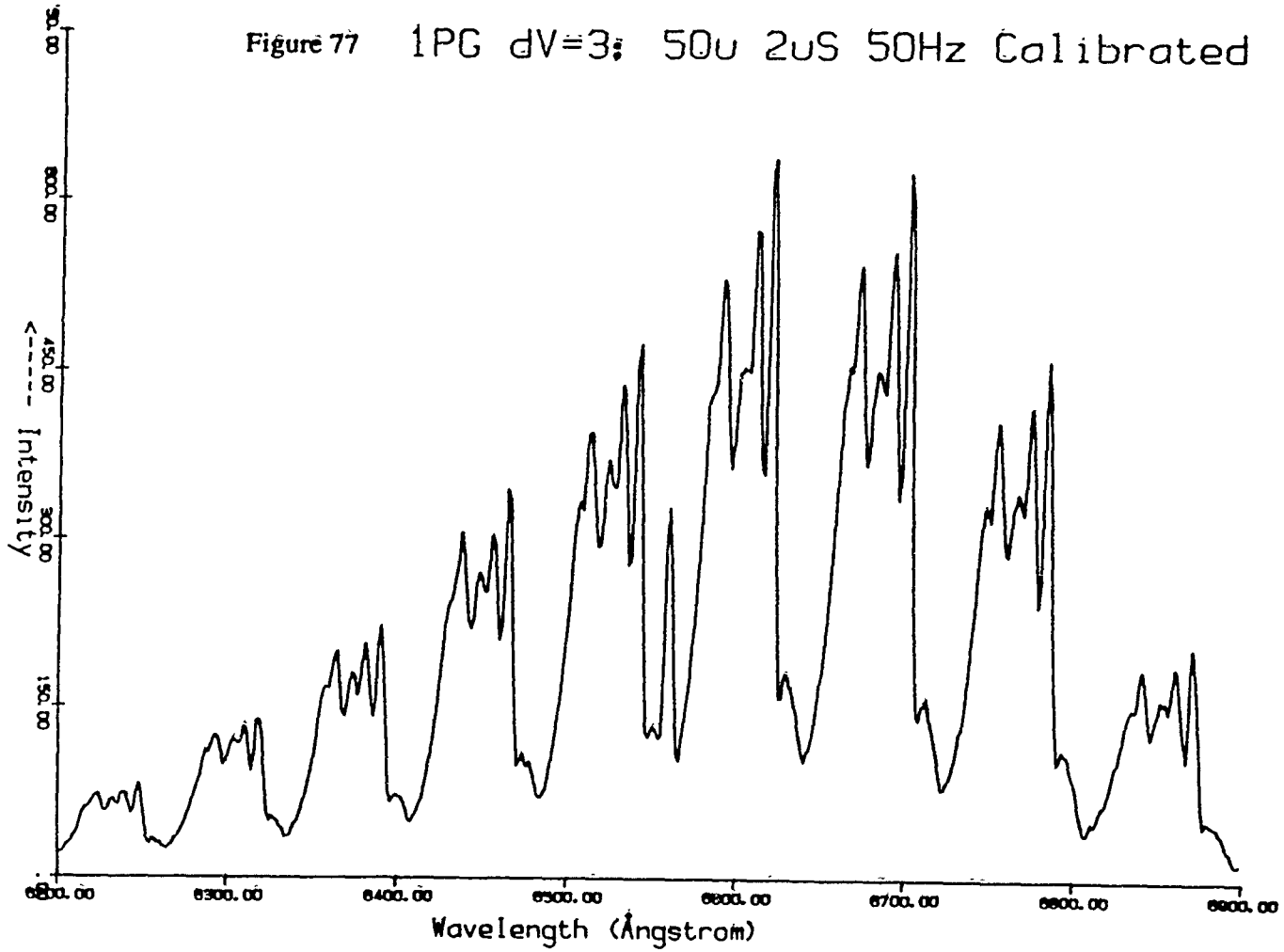
1PG dV=3; 50u 2uS 50Hz Calibrated
<----- Intensity
450.00
300.00
150.00
6300.00
6400.00
6500.00
6600.00
6700.00
6800.00
6900.00
Wavelength (Ångstrom)

Figure 77

For the Aurora, (5-2) and (4-1) are larger than (6-3). For the laboratory case (6-3) is larger than (5-2) which is larger than (4-1).

The results of this study do not show these extremes. They do, however, show distributions between these two spectra. Figures 76 and 77 show the effect of frequency (5 & 50 Hz) on the band intensities of $\delta V=3$. By starting with the Auroral spectrum of figure 75, proceeding through figures 76 and 77, then finally back to the laboratory spectrum of figure 75, we see a step-wise progression in the band intensities of the above three bands. This progression goes from a situtation of very low frequency (Aurora) to one of very high frequency (DC). If we consider the results of this section, the difference between the two spectra of figure 75 could be attributed to excitation from an elevated ground state vibrational distribution, for the case of the laboratory discharge.

Of course, the laboratory spectrum cannot be completely explained in terms of initial excitation alone since we must consider the effects of ICT, cascading and other processes. The effects of "pre-conditioning" will play an important role in the initial $B\ ^3\Pi_g$ state distribution which is continually being produced in a DC discharge. The subsequent redistribution of excitation via secondary excitation processes, will alter the equilibrium vibrational level populations to something similar to that shown in figure 65 rather than the initial distributions which are characteristic of this study (figure 74).

CHAPTER 5 - CONCLUSIONS

By the use of time resolved spectroscopy we have examined changes in the vibrational level populations of the $B\,^3\Pi_g$ state of molecular Nitrogen caused by the variation of pressure and pulsed-discharge frequency. The major process involving these changes as a function of pressure is Intersystem Collisional Transfer (ICT). Changes which occur with the variation of discharge frequency result from the effect of Plasma Pre-conditioning. Regarding the effect of pressure, the changes in the vibrational population distributions correlate strongly with the number of collisions which have occured rather than the amount of time which has elasped. The effect of discharge frequency, on the other hand, has been shown to produce changes in the initial $B\,^3\Pi_g$ vibrational distributions which occur. We have determined these changes to be primarily due to increases in the vibrational temperature of the ground electronic state.

Another important observation of this study is the different emission curves which result from the decay of the $C\,^3\Pi_u$ and $B\,^3\Pi_g$ states. The basic difference involves the position of the peak; about 1 μs for the $C\,^3\Pi_u$ state and about 3.5 μs for the $B\,^3\Pi$ state. The properties of these two states which were considered responsible for the difference in position, involve cascade, collisional coupling and the natural lifetimes. It is also clear from the long-time vibrational distributions and decay curves, that the population dynamics of the $B\,^3\Pi_g$ state is a much more complicated phenomenon. Consequently, a complete explanation of the two different sets of emission curves will involve cascade, collisional coupling as well as the lifetimes of these two states.

The long-time decay of the levels of the $B\,^3\Pi_g$ state have shown significant emission for times long after that expected, considering the natural lifetimes of these levels. Obviously, these levels are being fed by a secondary excitation process. The two processes which we proposed earlier, were energy pooling reactions involving the

metastable $A\ ^3\Sigma_u^+$ state and vibrationally excited ground state molecules. A possible explanation of the difference between these results and those of a previous study, using an electron beam, has been attributed to the energy pooling reaction involving vibrationally excited ground state molecules.

Our further observations regarding the long-time behavior of the $B\ ^3\Pi_g$ vibrational population distribution shows that the populations reach an identical distribution for all conditions under study. This observation may be an important clue as to the specific process that is occuring and the details of the mechanism.

The effects of the Intersystem Collisional Transfer process have been shown in the changes in the 3-D percent population plots as well as the decaying relative populations. Although this discussion was largely qualitative, trends expected due to the ICT process were clearly evident. The most notable observation being the number of collisions required to produce the peak in the percent population of V=6. Here the observed 2.5 to 3 collisions was interpreted to be the number of collisions required to equilibrate the populations of the V=6 level of the $B\ ^3\Pi_g$ state with the V=7 level of the $W\ ^3\Delta_u$ state.

The relative populations presented will be helpful in more elaborate models of the ICT process. This will require further measurments from this system, such as electron energy distributions or relative populations of overlapping electronic states. With the present data and the above additional measurements the comparison with calculated populations, based on the ICT process, will be possible.

Finally, we have shown that the effect of Plasma Pre-conditioning is able to produce changes in the initial vibrational distributions in the $B\ ^3\Pi_g$ state. These changes appear to be due to changes in the ground state vibrational temperature. The results show a decrease in the vibrational temperature with increasing number of collisions between each current pulse. From these results it was not clear what mechanism is responsible for the vibrational cooling of the gas. Presumably, collisions with the wall are important but

this remains an open question at this time.

From this study it is evident that Intersystem Collisional Transfer and Plasma Preconditioning are active and predominant processes in an electric discharge. An important question which remains, involves the explanation of the difference between N_2 spectra in the Aurora and in laboratory discharges. By the inclusion of these two processes with the other better known processes, such as emission and cascading, a more complete explanation of these differences will probably result. Such an explanation will be helpful in understanding the role of these two processes in energy transfer in laboratory discharges as well as atmospheric reactions involving molecular Nitrogen.

APPENDIX A - ESTIMATE OF THE EFFECT OF LIFETIME ON 1PG AND 2PG EMISSION PULSES

In order to estimate the effect of lifetime on the shape of the 1PG and 2PG emission curves, a number of assumptions and approximations must be made. First, it is assumed that these states emit according to first order decay. This implies that the measured intensity is directly proportional to the population of the upper level at all times. Discounting geometric factors and detector sensitivities this can be stated as

$$I(i,j) = N(i) \times A(i,j)$$

where

I(i,j) is the measured intensity of the (i,j) band

N(i) is the population of the upper level

A(i,j) is the transition probability between the levels i & j.

Second, owing to the short lifetimes of $C\,^3\Pi_u$ state, it is assumed that the emission curve of the 2PG is also directly proportional to the excitation pulse which produces the $C\,^3\Pi_u$ state. Thirdly, this pulse will be assumed to be the same excitation pulse as for the $B\,^3\Pi_g$ state. The excitation pulse will be approximated as the positive part of two sine waves that peak at different times (figure 31). This function has the form

$$g(t) = (A) \times \sin(\pi t/2) + \sin(\pi t/3.5) \qquad (1)$$

$$0 \leq t \leq 2$$

$$= \sin(\pi t/3.5) \qquad 2 \leq t \leq 3.5$$

$$= 0 \qquad t \geq 3.5$$

where A = 0.8 (an emperical constant)

Figure 31

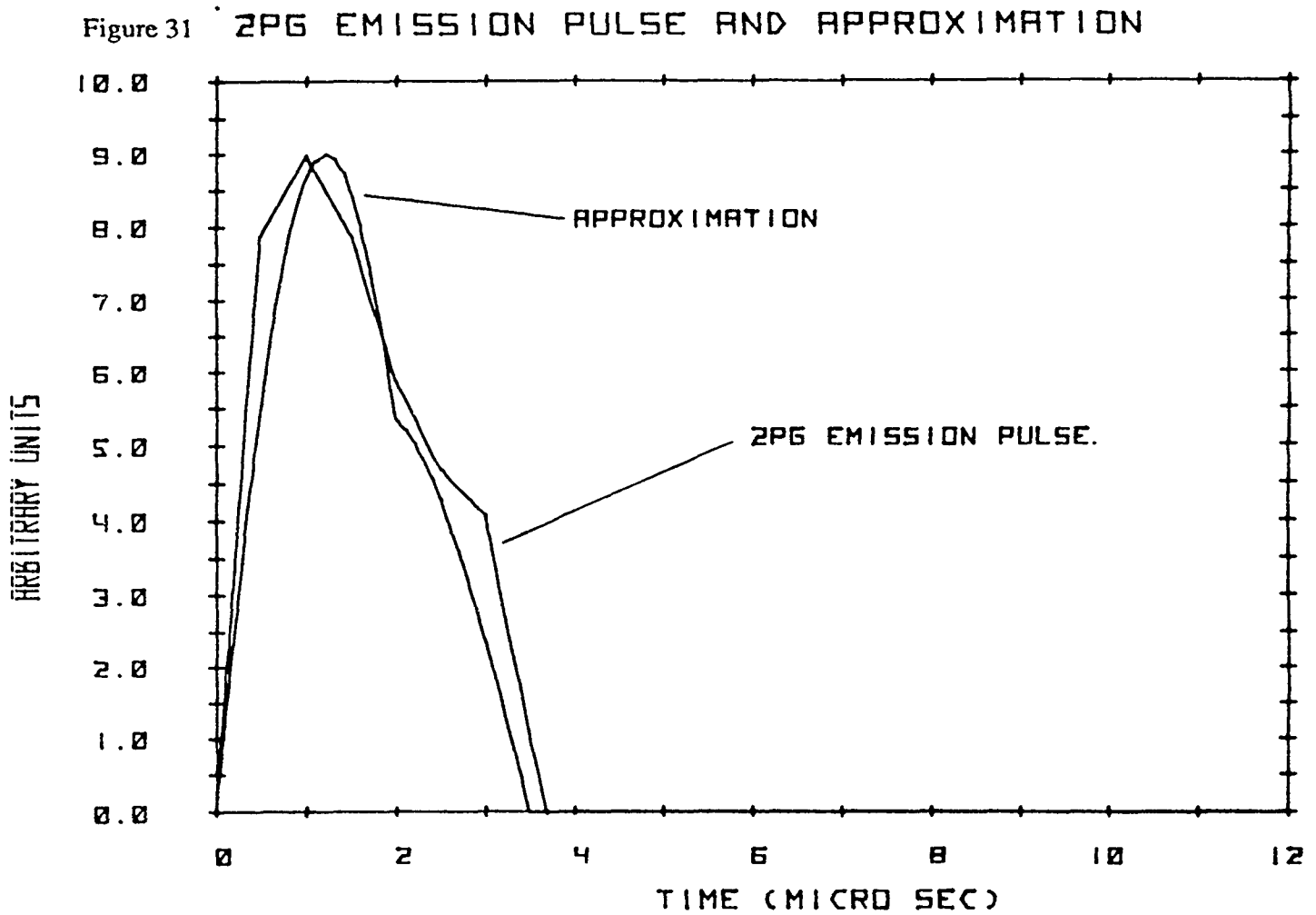
2PG EMISSION PULSE AND APPROXIMATION
10.0
9.0
8.0
7.0
6.0
5.0
4.0
3.0
2.0
1.0
0.0
ARBITRARY UNITS
APPROXIMATION
2PG EMISSION PULSE.
0
2
4
6
8
10
12
TIME (MICRO SEC)

The above function peaks at 1.2 μs rather than 1 μs (see figure 31). In this figure, values from the oscilliscope trace of a 2PG emission pulse (figure 27) were taken at 0.5 μs intervals. These values have been plotted in the same figure for comparison with the approximation. This approximation is made so that an analytic solution to the following differential equation can be derived.

The differential equation, which describes the time rate of change of a population with a given lifetime, is written as

$$\frac{dN(L,t)}{dt} = g(t) - N(L,t)/L \qquad (2)$$

where

g(t) is the excitation rate

N(L,t) is the population

and

L is the lifetime of the level

Substituting for g(t) we obtain

$$\frac{dN(L,t)}{dt} = (0.8) \times \sin(\pi t/2) + \sin(\pi t/3.5) - N(L,t)/L$$

$$0 \leq t \leq 2 \qquad (3)$$

$$\frac{dN(L,t)}{dt} = \sin(\pi t/3.5) - N(L,t)/L$$

$$2 \leq t \leq 3.5 \qquad (4)$$

and,

$$\frac{dN(L,t)}{dt} = -N(L,t)/L$$

$$t \geq 3.5 \qquad (5)$$

The solution to dN/dt is in three parts, one for each time region above.

$$N(L,t) = \frac{A\{(1/L) \times \sin(\pi t/2) - (\pi/2) \times \sin(\pi t/2)\}}{[(1/L)^2 + (\pi/2)^2]}$$

$$+ \frac{\{(1/L) \times \sin(\pi t/3.5) - (\pi/3.5) \times \sin(\pi t/3.5)\}}{[(1/L)^2 + (\pi/3.5)^2]}$$

$$+ \exp\frac{-t}{L} \times \frac{\{A(\pi/2)\}}{[(1/L)^2 + (\pi/2)^2]} + \frac{(\pi/3.5)}{[(1/L)^2 + (\pi/3.5)^2]}$$

$$0 \leq t \leq 2 \qquad (6)$$

$$N(L,t) = \frac{\{(1/L) \times \sin(\pi t/3.5) - (\pi/3.5) \times \cos(\pi t/3.5)\}}{[(1/L)^2 + (\pi/3.5)^2]}$$

$$+ \frac{\{A(\pi t/2) \times \exp -(t-2)/L\}}{[(1/L)^2 + (\pi/2)^2]}$$

$$+ \exp\frac{-t}{L} \times \frac{\{A(\pi/2)\}}{[(1/L)^2 + (\pi/2)^2]} + \frac{(\pi/3.5)}{[(1/L)^2 + (\pi/3.5)^2]}$$

$$2 \leq t \leq 3.5 \qquad (7)$$

and,

$$N(L,t) = \frac{\{A(\pi/2) \times \exp -(t-2)/L\}}{[(1/L)^2 + (\pi/2)^2]} + \frac{\{(\pi/3.5) \times \exp -(t-3.5)/L\}}{[(1/L)^2 + (\pi/3.5)^2]}$$

$$+ \exp -\frac{t}{L} \times \frac{\{A(\pi/2)\}}{[(1/L)^2 + (\pi/2)^2]} + \frac{(\pi/3.5)}{[(1/L)^2 + (\pi/3.5)^2]}$$

$$t \geq 3.5 \qquad (8)$$

This solution predicts the time varing population of an excited state produced by the excitation pulse (1), based only on the lifetime of the state. The population has been plotted for various lifetimes in figure 32. Here the results have all been scaled up by a factor of 2.77. Two of the four lifetimes chosen represent lifetimes of N_2 emission systems from the present discussion.

$$C\,^3\Pi_u\ (v=0) \Rightarrow 0.044\ \mu s$$
$$B\,^3\Pi_g\ (v=1) \Rightarrow 7.8\ \mu s \quad (9)$$

The value L = 1 x 10^6 μs (1 sec.) is the approximate lifetime of the $A\,^3\Sigma_u^+$ state. This is a metastable state which is the lower state of the 1PG. The spectrum associated with emission from the $A\,^3\Sigma_u^+$ corresponds to the forbidden transtion ($A\,^3\Sigma_u^+ \rightarrow X\,^1\Sigma_g^+$); this is known as the Vegard-Kaplan system. The lifetime of L=1 μs was used to see the effects of a lifetime intermediate between the $C\,^3\Pi_u$ and $B\,^3\Pi_g$ states.

The results, shown in figure 32. can be interpreted as follows. For the case of a very long lifetime (L = 1 x 10^6 μs) the population grows throughout the course of the

Figure 32 - ESTIMATE OF THE EFFECT OF LIFETIME

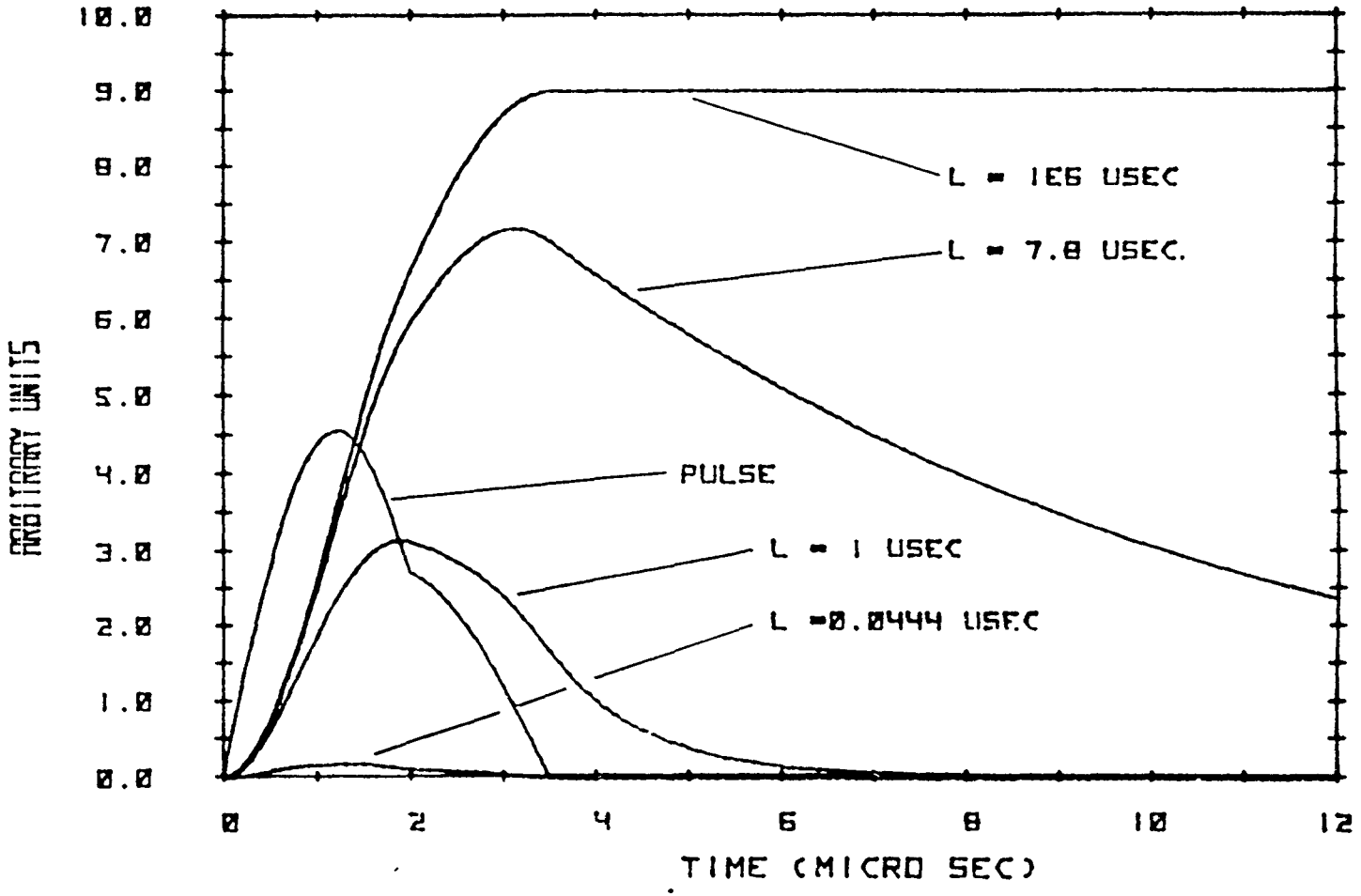

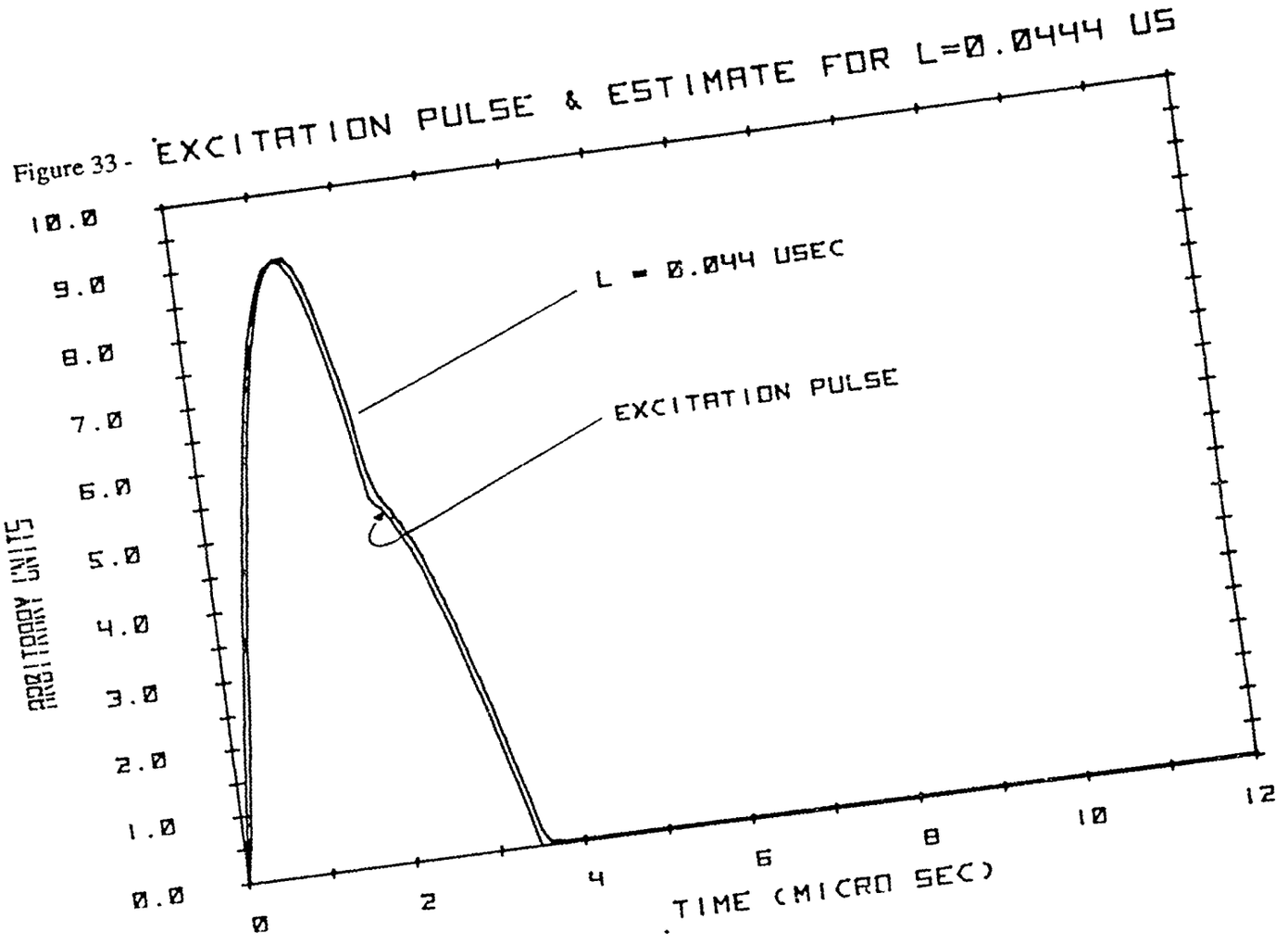
EXCITATION PULSE & ESTIMATE FOR L=0.0444 US
L = 0.044 USEC
EXCITATION PULSE
ARBITRARY UNITS
10.0
9.0
8.0
7.0
6.0
5.0
4.0
3.0
2.0
1.0
0.0
0
2
4
6
8
10
12
TIME (MICRO SEC)

Figure 33 -

excitation pulse. In this case the effect of loss by emission is negligible, and the population builds continuously to a peak value. This peak occurs at 3.5 μs; the end of the excitation pulse. The population remains at this peak value, virtually unchanged during the 12 μs period shown. This peak value reflects the total population produced by the excitation pulse. To test this result, the excitation pulse (1) was integrated between 0 and 3.5 μs. The result is the same value as N at 3.5 μs for L = 1 x 10^6 μs.

Conversely, for the case of a very short lifetime (L = 0.0444 μs), loss by emission is occurring almost as rapidly as excitation. Therefore, the population is never able to build to an appreciable amount (see figure 32). As a consequence, the shape of the population curve retains the shape of the excitation pulse (see figure 33).

For the intermediate cases of L = 1 μs and 7.8 μs, there are two important observations. First, as L increases, the peak value in the population increases. This is expected since the larger the value of L the smaller the loss due to emission at any time during the pulse. Second, as L increases, the position of the peak of the curve moves toward the end of the excitation pulse. Returning to equation (2) we know that at the peak,

$$dN(L,t')/dt = 0 = g(t') - N(L,t')/L$$

so

$$g(t') = N(L,t')/L$$

and finally

$$L = N(L,t')/g(t') \quad (10)$$

were t' is the time at the peak.

This says that the peak in the population occurs at the time when the ratio of the population to the excitation rate is equal to the lifetime. A fortuitious example is shown in figure 32 for L=1 μs. The peak in the curve occurs at the point where this curve crosses the excitation curve. At this point they both have the same value and so their

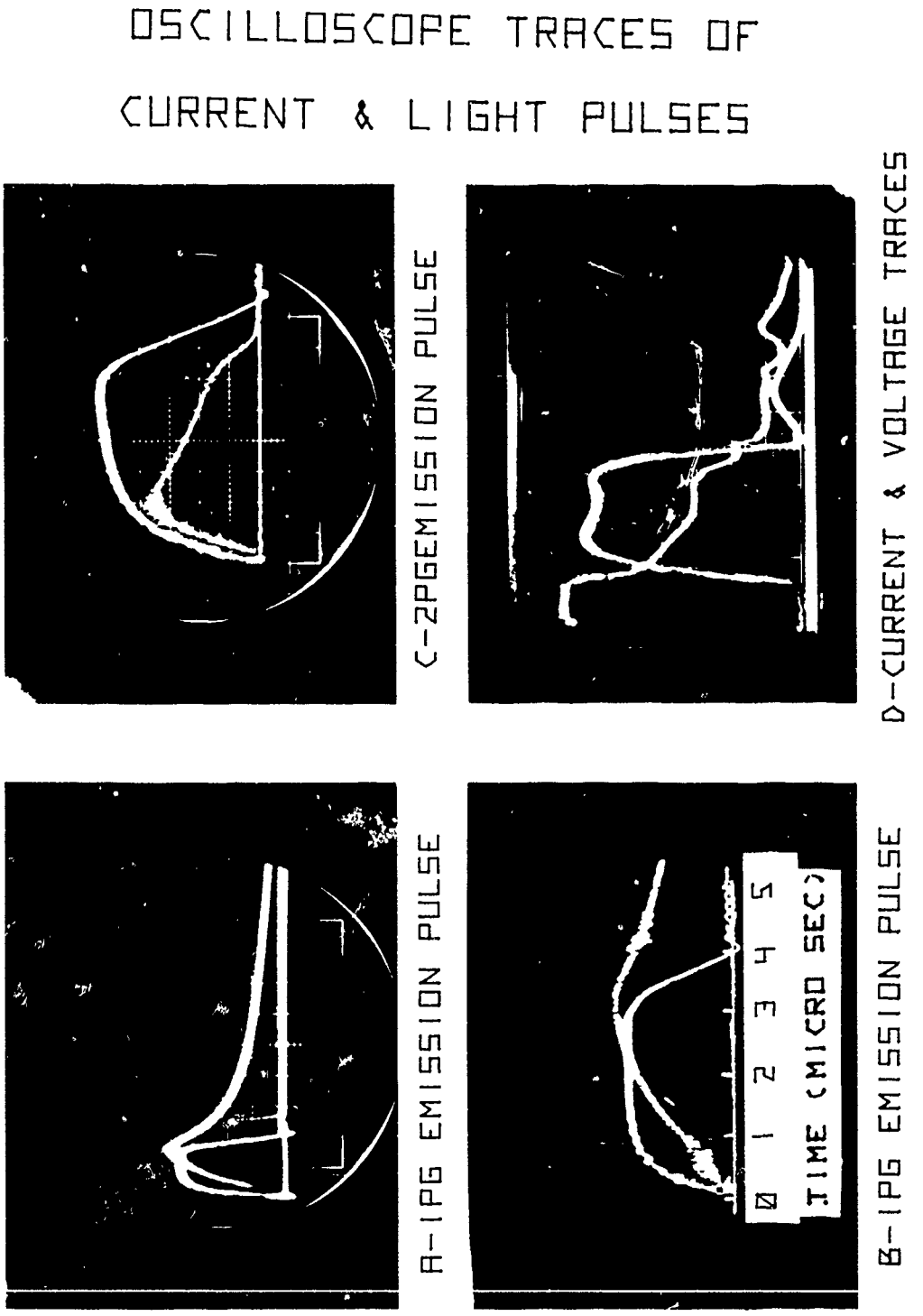
OSCILLOSCOPE TRACES OF
CURRENT & LIGHT PULSES
C-2PGEMISSION PULSE
D-CURRENT & VOLTAGE TRACES
A-1PG EMISSION PULSE
B-1PG EMISSION PULSE
0 1 2 3 4 5
TIME (MICRO SEC)

Figure 34 -

ratio equals unity as required for a lifetime of 1 μs. It is not obvious why equation (10) is generally satisfied at later times for larger lifetimes.

Comparison of figure 32 (L = 7.8 μs) with the emission pulse of figure 24 shows a strong similarity. A closer observation of the 1PG emission pulse is seen in the oscilliscope trace of figure 34b. This trace is of the (2-0) band, with the V = 2 level having a lifetime of 7us[19] The peak in this trace occurs at ~ 3.2 μ. The predicted value of the peak for this lifetime is at 3.1 μs. Given the imprecision in the location of t = 0 for this trace and the approximation used, these values are extremely close. A feature that is not apparent in the oscilliscope trace is the bump which occurs at 2 μs in the predicted curve for L = 7.8 μs (compare figures 32 & 34b). Presumably, this is a result of the approximation used.

These results show that the lifetimes of the different states need to be considered when analysing emission pulses of this type.

BIBLIOGRAPHY

1. (a) A. Fowler and J. Strutt, Proc. Roy. Soc. A 20,49 (1904).

   (b) S. Naude, Proc. Roy. Soc. A 136, 114 (1932).

2. A. Lofthus and P.H. Krupenie, J. Phys. Chem. Ref. Data 6, 133 (1977).

3. D.H. Katayama, J. Chem. Phys. 81, 3495 (1984).

4. W. Benesch and D. Fraedrich, J. Chem. Phys. 81, 5367 (1984).

5. A. Rotem and S. Rosenwaks, Optical Engineering 22, 564 (1983).

6. N. Sadeghi and D.W. Setser, J. Chem. Phys. 79, 2710 (1983).

7. W. Benesch, J. Chem. Phys. 78, 2978 (1983).

8. A. Rotem, I. Nadler and S. Rosenwaks, J. Chem. Phys. 76, 2109 (1982).

9. N. Sadeghi and D.W. Setser, Chem. Phys. Lett. 77, 304 (1981).

10. A. Rotem, I. Nadler and S. Rosenwaks, Chem. Phys. Lett. 83, 281 (1981).

11. W. Benesch, J. Geophys. Res. 86, 9065 (1981).

12. N. Sadeghi and D.W. Setser, Chem. Phys. Lett. 77, 304 (1981).

13. D.H. Katayama, T. Miller and V. Bondybey, J. Chem. Phys. 72, 5469 (1980).

14. T.A. Carlson, N. Duric, P. Erman and M. Larson, Physica Scripta 19,25 (1979).

15. N. Thompson and S.E. Williams, Pr·· Roy. Soc. A 147, 583 (1934).

16. M.F. Golde and B.A. Thrush, "Afterglows", Rep. Prog. Phys. 36, 1285 (1973).

17. D.C. Cartwright, S. Trajmar, A. Chutjian and W. Williams, Phys. Rev. A 16, 1041 (1977).

18. K.H. Becker, E.H. Fink, W. Groth, W. Jud and D. Kley, Disc. Faraday Soc. 53, 35 (1972).

19. D.E. Shemansky and A.L. Broadfoot, J. Quant. Spec. Rad. Transfer 11, 1385 (1971).

20. D.E. Shemansky and A.L. Broadfoot, J. Quant. Spec. Rad. Transfer 11, 1401 (1971).

21. D.E. Shemansky, J. Chem. Phys. 64, 565 (1976).

BIBLIOGRAPHY

22. S. Goldberg and J. Rothstein, "Hydrogen Thyratrons", Adv. in Electronics and Electron Physics 14, 207 (1961).

23. W. Benesch, D. Fraedrich and M. Ginter, Rev. Sci. Instr. 54, 776 (1983).

24. R. Alberty and F. Daniels, Physical Chemistry, p244, 5th ed. New York: John Wiley and Sons, 1974.

25. J.B. Hasted, Physics of Atomic Collisions. London: Butterworths, 1964.

26. J.M. Somerville, The Electric Arc. London: Methuen and Co. LTD, 1959.

27. G. Schulz, "A Review of Vibrational Excitation of Molecules by Electron Impact at Low Energy", Electron- Molecule Scattering, ed S. Brown. New York: John Wiley and Sons, 1979.

28. B. Massabieaux, A. Plain, A. Ricard, M. Capitelli and C. Grose, J. Phys. B: At. Mol. Phys. 16,1863 (1983).

29. J. Anketell and B. Brocklehurst, J. Phys B: At. Mol. Phys. 7, 1937 (1974).

30. D.C. Cartwright, S. Trajmar and W Williams, J. Geophys. Res, 76, 8368 (1971).

31. D.C. Cartwright, J. Geophys. Res. 83,517 (1978).

32. G. Hays and H. Oskam, J. Chem. Phys. 59, 1507 (1973).

33. M. Capitelli, C. Gorse and A. Ricard, J. Physique Lettres, 42, L-185 (1981).

34. M. Cacciatore, M. Capitelli, C. Gorse, B. Massabieaux and A. Ricard, Lettere Al Nuovo Cimento 34, 417 (1982).

35. D. Katayama, T. Miller and V. Bondybey, J. Chem. Phys. 72, 5469 (1980).

36. D. Katayama, T. Miller and V. Bondybey, J. Chem. Phys. 72, 1662 (1979).

37. V. Bondybey and T. Miller, J. Chem. Phys. 69,3597 (1978).

38. D. Kayatama and J. Welch, J. Chem. Phys. 79, 3627 (1983).

39. W. Benesch, J. Vanderslice, S. Tilford and P. Wilkinson, Astrophys. J 143, 236 (1966).

BIBLIOGRAPHY

40. K. Saum and W. Benesch, Phy. Rev. A 2, 1655 (1970).

41. R. Covey, K. Saum and W. Benesch, J. Opt. Soc. Am. 63, 592 (1973).

42. W. Benesch, J. Vanerslice and S. Tilford, J. Atmos. Terr. Phys. 28, 431 (1966).

43. W. Benesch, J. Vanderslice and S. Tilford, J. Atmos. Terr. Phys. 29, 251 (1967).

44. K. Saum and W. Benesch, Applied Optics 9, 195 (1970).

45. D. Katayama, Phys. Rev. Letters 54, 657 (1985).

APPENDIX B

POPULATION DEVELOPMENT OF AURORAL MOLECULAR NITROGEN SPECIES IN A PULSED ELECTRIC DISCHARGE

J. MORRILL, B. CARRAGHER, AND W. BENESCH

Institute for Physical Science and Technology

University of Maryland

College Park, Maryland 20742

ABSTRACT

A series of experiments has been performed with pulsed electric discharges in low-pressure nitrogen in order to elucidate excitation processes which underlie auroral photon emission. Flowing nitrogen in a large-volume glass container at 30 to 3000 mTorr is excited by 4 μsec pulses which, typically, are at 12000 volts and 900 amps. The radiation issuing from the discharge tube is analyzed by means of time-resolved spectroscopy with particular attention given to the nitrogen First Positive System, $B\ ^3\Pi_g \rightarrow A\ ^3\Sigma_u^+$. Dramatic changes have been noted in the relative band intensities of the 1PG spectra subject to the influence of the variation of the experimental conditions. In particular, the distribution of population among vibrational levels of the $B\ ^3\Pi_g$ state evolves in time both during and after the exciting electric pulse, with the trends strongly correlated with the numbers of collisions. Further, radiation from these excited vibrational levels continues at much higher emission rates than those commensurate with their radiative lifetimes. Both of these observations constitute evidence of the intersystem collisional transfer of excitation. The distinguishing feature of this array of experiments is the application of time-resolved spectroscopy which permits examination of the development of level populations on a collision-by-collision basis.

INTRODUCTION

We have conducted a series of experiments on the excitation and decay processes in molecular nitrogen with particular emphasis on the First Positive System (1PG) whose emission takes place generally from the green through the red and into the near infrared out to about 2000 nm wavelength. The principal motivation for the experiments is the achieving of a better understanding of parallel processes in the aurora. In particular, the program has sought to develop a model for the production of the dramatic color changes which occur in auroral forms as they descend to lower altitudes.(1)(2) Special attention has been given to the generation of the red lower border of type B auroras as the proposed effect of the increased collision frequency at the lower altitudes on the electronically excited nitogen molecules. More specifically, we have suggested that it is the intersystem collisional transfer (ICT) of excitation that brings about an alteration of the vibrational population distribution when the collision frequency reaches a critical level.

There have been a number of laboratory investigations which used laser-induced fluorescence (LIF) to study collisional transfer processes in molecular nitrogen. These have generally been based on the generation of N_2 $A\ ^3\Sigma_u^+$ in a pulsed discharge or flowing afterglow apparatus, followed by the excitation of selected $B\ ^3\Pi_g$ vibration-rotation levels by means of laser radiation. One of the earliest of these was that of Heidner et al. (3) where estimates were made of rate constants for ICT. Using similar techniques, Katayama et al.(4) and Katayama (5) undertook a series of LIF experiments on the nitrogen molecular ion, N_2^+. The work of Rotem, Nadler, and Rosenwaks (6) has shown that emission from a laser-excited level is accompanied by emission

from lower B $^3\Pi_g$ levels as well as emission from adjacent vibrational levels of overlapping electronic states. Both of these accompanying emissions are the result of collisional coupling of the vibrational levels of the low-lying triplet states of N_2 (ICT). In the LIF studies of Sedeghi and Setzer(7) and Rotem and Rosenwaks(8), the emis on is followed through a number of radiative lifetimes and the decay is analysed in terms of coupling with the B state. The results yield rate constants for collisional coupling from specific B state vibrational levels, though the detailed identification of the recipient levels of the transferred excitation has been somewhat uncertain. In the realm of electron beam excitation of nitrogen atmospheres, the experiments of Shemansky and Broadfoot(9), of Pendleton et al.(10), and of Green et al. (11) all bear rather closely on the problems addressed in the present work.

Field observations of the bright red of the auroral red border have been made by Boquist and Snyder(12) on an artificial aurora generated by atmospheric nuclear weapons testing. They were able to pinpoint the onset of the sharp color change as occurring within the 84-87 km altitude domain. Gattinger et al. on the other hand, observed no red emission below 91 km in natural auroras.(13) Older literature has the bright emission of type B red aurora ranging down to below 70 km.(14) In reviewing the extant literature in 1971, Hanna and Anger cautioned against an overemphasis on the want of instrumentally recorded spectral changes for type B aurora in the face of striking visual evidence to the contrary.(15)

In our laboratory, the emission spectrum of the nitrogen 1PG has proved highly variable in electric discharges. It has turned out that salient changes take place in the relative intensities of the various bands as func-

tions of pressure, time, and prior history of the discharge. Such changes go beyond even the alterations suggested by the model solely based on the intersystem collisional transfer of excitation. The challenge has been less in finding ways of altering the spectral distribution than in isolating the molecular processes that give rise to the underlying population rearrangements.

EXPERIMENTAL

A block diagram of the experimental set-up is given in Figure 1. The emission source is a large-volume high-current cylindrical discharge tube of Pyrex, 3 meters in length with a 16 cm inside diameter. This 60-liter volume is supplied with electrodes which are water-cooled, copper cylinders 12 cm in diameter and 3 cm long, mounted on copper shafts. Each electrode is projected into the Pyrex tube about 50 cm so that the distance between the electrodes is 2 meters. This results in a discharge volume of some 40 liters.

The excitation pulse supplied has peak currents which range from 400 to 1000 amps and a pulse length of 4 μsec. At 700 amps, the current density is approximately 3.5 amps/cm^2. Visual observations of the arc indicate that the current density is fairly uniform at the higher pressures of nitrogen (100 mTorr and up) but for pressures near 50 mT, the discharge shows enhanced pathways of larger relative intensity which correspond to channels of increased current density.

The primary component of the electronics generating the 4 μsec current pulse is a 5000 volt DC power supply which furnishes the electrical input to the pulse-generating system. It feeds an LC voltage doubler which charges four 1000-foot spools of coaxial cable, RG-8, to voltages of the order 10 to 15 kV. The voltage is maintained by a chain of high-voltage diodes which prevent cable discharge except as follows.

Once the cables are charged, a positive pulse is applied to the grid of a thyratron (EG&G HY-5). This voltage pulse fires the thyratron which connects

the charged cables to the anode of the discharge tube. The resulting current pulse through the discharge tube has a sharp rise time (~1 μsec). For present purposes, it is desirable also to have a sharp turn-off of the current pulse, but this cannot be accomplished through the agency of the voltage on the thyratron grid. Rather, the turn-off is brought about through the interaction of the end of the charge wave travelling down the coaxial cable with the impedence mismatch that it encounters at the discharge tube. A negative reflected wave develops at that moment (4 μsec after the igniting pulse) which serves to reverse bias the HY-5 anode and break off conduction through the thyratron.

Experimentation has shown that the conditions which must be met to generate the required reverse wave are that the impedence of the discharge must drop to but a few ohms and the pulse current levels must exceed 300 amperes. When such is the case, the current has sharp sides, the thyratron turns off at 4 μsec,and the entire process (including the cable charging phase) repeats dependably and reproducibly. Special precautions must be taken to assure these conditions, and the details, requirements, and hazards of the procedure have been dealt with elsewhere.(16)(17)

The supply of flowing nitrogen gas to the experiment consists of Ultra High Purity (99.999%) nitrogen introduced at the grounded (cathode) end of the discharge tube through a fitting in an aluminum end-plate. By varying the N_2 gas flow rate into the system and by throttling the exhaust, we are able to achieve a broad range of discharge pressures. The input is adjusted by means of a Brooks flow tube with a metered flow rate, while a combination of coarse and fine valves are used to throttle the exhaust to the mechanical vacuum pump. The control of both the intake and outflow rates allows us to maintain

good pressure control throughout the course of an experiment (~3%). The pressure in the system was measured with a Vacuum General capacitance manometer (1 Torr full scale).

A 2-meter spectrometer with off-axis parabolic mirrors and a 600 groove/mm grating receives the light from the discharge tube through a window at the cathode end. The optic axis of the system passes through a cut-out in the cathode itself and along the center-line of the Pyrex cylinder. The dispersed light is detected by a photomultiplier tube (PMT, Hamamatsu R-636), and the output of the PMT is preamplified and fed into an EG&G PAR 160 Boxcar Averager as well as a monitor oscilloscope. The reduced data from the Boxcar Averager is relayed, finally, to an IBM PC XT for ultimate treatment and storage. The spectrometer is equipped with a digital encoder connected to the grating drive shaft. It supplies a wavelength reading which is available to the computer at all times. Wavelength calibration was carried out with a mercury lamp, while an intensity calibration curve was generated from the spectrum of a black body oven.

This system is quite flexible; Figure 2 gives examples of types of display observed on the monitor and representative of several data-collection formats. The result of setting the spectrometer on the 2-0 band of the N_2 First Positive System while simultaneously tracking the discharge tube current and the boxcar averager aperture are shown in Figure 2A. The latter appears as the narrow vertical feature at 5 μsec (the horizontal scale here is 2 μsec/div). In this case, the aperture is approximately 200 μsec wide and delineates the time during which the boxcar averager is accepting signal form the photomultiplier tube.

Two modes of operation are possible here. We may fix the time selected for data registration (as shown here at 5 μsec) and scan the spectrometer wavelength drive, thus obtaining a spectrum characteristic of a certain point in time relative to the onset of the excitation pulse. An example of the data which this mode yields is given in Figure 3. With the gate of the boxcar averager set at 3 μsec, the spectrometer has been scanned from 550 to 900 nm. It is thus a "snapshot" of the spectrum at the 3 μsec mark. The discharge medium was 50 mTorr of flowing nitrogen, pulsed at a repetition rate of 5 Hz. The figure serves also to delineate the domain of interest of the present work, namely, the four sequences of the nitrogen 1PG, $\Delta V = 1, 2, 3,$ and 4.

Alternatively, we may fix the spectrometer on a particular spectroscopic feature of interest (here the N_2 2-0 band) and scan the boxcar averager aperture forward in time from the onset of the excitation pulse to the final epoch of experimental interest. This mode is illustrated by the long curve in Figure 2A. Here, the history of the 1PG 2-0 emission is tracked through several radiative lifetimes, comprising times both during and after the excitation pulse. The excitation pulse itself is represented by the oscilloscope trace of the discharge tube current. It is the curve which rises, flattens at the top, and ends at 4 μsec. Sharp current rise and fall times, as alluded to previously, were the objectives of considerable development effort in the early stages of the program.

Of particular interest in this photograph is the time relationship of the 1PG emission and the discharge current. The 1PG emission shows a monotonic increase throughout the current pulse. The same trend is shown on an expanded time scale in Figure 2B, the photograph of a similar experiment, where again

the current is the flat-topped feature, while the 1PG band is the extended trace which falls slowly after the current is cut off.

This behavior is to be contrasted with that of the emission feature in Figure 2C. Here the emission is that of the 0-2 band of the N_2 Second Positive System $C\ ^3\Pi_u \rightarrow B\ ^3\Pi_g$. The light pulse, in this case, peaks in the first microsecond of the current pulse and declines continually thereafter. Its decay becomes even more precipitous when the current pulse itself begins to fall.

The trend of the 2PG emission feature is, in fact, more in concert with that of the voltage pulse, as may be observed in Figure 2D. On that rectangular oscilloscope screen image, the voltage trace appears as a short horizontal line at the 11,000 volt level (the vertical scale here is 3000 volts/div and extends from -9000 volts at the bottom of the screen to +15,000 volts at the top). The voltage falls sharply as the current rises, rests for a microsecond at zero, and then reverses to negative values as the current pulse collapses. At least qualitatively, the 2PG emission tracks the tube voltage downward, whereas the 1PG emission continues to rise while the current is flowing in spite of the fact that the electric field has vanished.

RESULTS: EVOLUTION OF 1PG SPECTRA

One of the most interesting aspects of the time-resolved spectrum of molecular nitrogen in a pulsed electric discharge is the evolution of the relative intensities of the various bands following the expiration of the excitation pulse. This phenomenon will be illustrated by selecting the $\Delta V = 2$ sequence near 750 nm (see Figure 3) and taking snapshots of the spectrum (as explained in the section above) at various times and under various conditions of excitation.

Such a series of snapshots is presented in Figure 4, where the $\Delta V = 2$ sequence has been excited by the usual 4 μsec pulse in 400 mTorr of flowing nitrogen. The repetition rate is 5 Hz. This set of shots carries the sequence of bands through the excitation pulse and out into the afterglow for a total time elapse of 9 μsec. Clearly discernible change in the relative intensities begins at 4 μsec (just at the end of the excitation pulse) and proceeds rapidly up to the 8 μsec mark. Beyond 8 μsec the speed of evolution slows considerably, and a detailed analysis of the complete body of data indicates that a long-term stabilization sets in at about 12 μsec. It will be recognized that all intensities are falling here accordance with the general depletion of population resulting from the observed emission which continues after the primary excitation mechanism has been cut off. In these graphs, however, the general declining trend of intensity has been overridden by normalization of the maximum band in order to permit ready comparison from one time to another.

What is to be gleaned from the data set taken at 400 mTorr on the $\Delta V = 2$

sequence is that a major redistribution of population takes place during the 8 μsec immediately following the excitation pulse. Since the gas kinetic collision frequency under these conditions is 2.7/μsec, the number of collisions which will have occurred between excitation and stabilization is

$$2.7/\mu\text{sec} \times 8\ \mu\text{sec} = 22 \text{ collisions}$$

For spectra generated at a pressure of 40 mTorr, a much longer period of time is required for the onset of the stabilization of the relative vibrational populations. This point is illustrated in Figures 5 and 6, displaying the $\Delta V = 2$ and $\Delta V = 3$ sequences, respectively, taken at 35 Hz and 40 mTorr. Again, casual inspection cannot reveal a precise epoch for the stabilization, but it may be observed that an estimate of ~ 100 μsec deduced from a somewhat more rigorous procedure is within reasonable bounds. Applying the same arithmetic as above, then, we obtain for the present stabilization requirement a value of some 26 collisions. In consideration the body of data as a whole, it is concluded that about 25 gas kinetic collisions are required to bring about population equilibration regardless of the amount of time consumed in the process. At present, we feel that the source of this increase may be attributed at least partially to intersystem collisional transfer from the $A\ ^3\Sigma_u^+$ state. The reason for this conclusion will be discussed more fully later, but it primarily involves the fact that the peak in the initial vibrational distribution in the A state corresponds approximately to V = 1 of the $B\ ^3\Pi_g$.

As indicated above, we have been dealing with normalized spectra in Figures 4, 5, and 6, graphed so that the peak values come at the same height. To demonstrate the true rise and fall of emitted intensity, we present Figure

7 showing the four IPG sequences at 1 and 2 μsec intervals from 0.5 to 20 μsec elapsed time. This is an example of the type of spectra to be dealt with in the next section. The pressure is 150 mTorr and the repetition rate is 15 Hz. Such a compound spectrum is the product of the application of about half a million pulses.

RESULTS: POPULATION PLOTS

Following the observation and analysis of the evolution of the relative band intensity patterns, we proceeded to the determination of relative individual $B\ ^3\Pi_g$ vibrational level populations based on the recorded spectral data. The procedure is initiated with the intensity calibration of each spectrum by means of the computer-stored black-body data mentioned in the Experimental section.

The vibrational levels treated were the $B\ ^3\Pi_g$ V = 1 through 12. Conditions in the discharge tube comprised the following

Pressures: 50,200,400 mTorr

Repetition rates: 5,15,32,50 Hz

Peak current: 600 amps

Through use of the first mode of operation above, spectra were recorded and characterized according to the time delay between the onset of the excitation pulse and the instant of their snapshot. Sets of spectra with time delays of 0.5 to 20 μsec were taken for each combination of pressure and repetition rate listed above.

Each set of spectra was taken through the 0.5 to 20 μsec time delay sequence at a constant photomultiplier tube (PMT) voltage so as to preserve the changes in relative intensity which develop with the passage of time. An example has been given in Figure 7 (above). In order to optimize the signal at the peak of the light emission pulse, we were required to vary the PMT voltage

for each set of discharge conditions. In general, the peak of the 1PG emission pulse occurs at approximately 3 μsec. Through adjustment of the PMT voltage, the spectra were arbitrarily altered to conform to the same peak value, which utilizes the full dynamic range of the detection and amplification system.

All spectra used in the population determinations were calibrated with the intensity curve discussed above. The populations were evaluated from the calibrated spectra using a computer program that integrates band intensities over a constant wavenumber region around the band origin of each vibrational band considered. A total of 26 bands were analyzed from each spectrum, with the resulting populations of each level reflecting the average of at least two bands, except for the cases of V = 1 and 12. Corrections for band overlapping were made in consideration of the relative positions of band origins and the relative intensities of close-lying bands according to the transition probabilities given by Shemansky and Broadfoot.(18) An example of the spectra used in the determination of populations is that of Figure 3.

An adjustment to the raw population distributions was carried out by means of scaling spectra obtained under each set of discharge conditions at the 3 μsec mark. This set of scaling spectra was taken with the same PMT voltage throughout. One of the results of the above procedure is the determination that the overall intensity of these scaling spectra increases with the pressure. This indicates that the total number of excited molecules in the discharge tube is increasing as the density increases. The fractional excitation, however, decreases with density, which fact is determined from the ratio of the scaling factor to the gas density for each of the three pressures in-

volved. The values are listed in Table 1. What these values show is that the peak density of excited molecules in the discharge does not increase as fast as the gas density when the peak discharge current is held constant.

Table 1 FRACTIONAL EXCITATION AS FUNCTION OF PRESSURE

Pressure(mTorr)	Factor/density	Normalized
50	0.21	1
200	0.11	0.52
400	0.07	0.33

A portion of the populations obtained from the adjusted band intensities appear in Tables 2 through 4 and in Figure 8. These tables and figures constitute the results from experiments at three pressures: 50, 200, and 400 mTorr, and a discharge frequency of 5 Hz. A broader set of these data, obtained at frequencies up to 50 Hz, may be found in ref. 19.

As mentioned, steps were taken to put all results on a common scale and, in particular, the relative vibrational populations (upper entries of Tables 2 through 4). Relative populations mean, then, that there is a multiplicative factor which would convert the upper entries from relative populations to absolute densities of B $^3\Pi_g$ state molecules in their respective vibrational levels. The errors associated with the populations in Tables 2 through 4 are considered generally to be of the order of 5 to 15%.

DISCUSSION

A point of comparison may be useful in clarifying the interpretation of the plots of percent population. By percent population we mean the percentage of the remaining population at a particular time. Figure 9 shows the effect of the non-uniformity of the lifetimes of the various levels on a decaying vibrational distribution. The first line, at t = 1 μsec, is the initial distribution at 15 Hz rep rate and 150 mTorr pressure. This figure shows that as time goes by and the initial distribution decays, we should expect the percentage share of lower vibrational levels to increase because of their longer lifetimes. In point of fact, we do see a trend in the distributions in which the band intensities of the lower levels (V = 1 and 2) increase with time. This type of behavior was shown in the series of spectra for $\Delta V = 2$ in the previous section. Such a characteristic rise in the lower levels can be seen in all of the experimental vibrational population plots as well. As shown in the experimental spectrum plots, however, there is a significant enhancement of that trend with increased pressure. For higher pressures, a larger increase in the percent population of the lower levels has come about by the 20 μsec mark.

Longer time plots show that for all conditions the distributions of percent populations are almost identical for times between 100 and 200 μsec. This common distribution will be referred to as the "long-term quasi-stationary distribution" and two examples are shown in Figure 10. The distributions at 120 μsec for these two figures appear in Table 5. Looking back to the 0 to 20 μsec plots, we see that the greater the pressure, the greater the progress of the distribution toward this long-term quasi-stationary distribution which has been achieved by 20 μsec.

In the 0 to 20 μsec plots, a number of other features are notable and appear in varying degrees throughout. First, there is a pronounced rise in the plots associated with the level V = 6. Notice that its position in time varies with pressure. Table 6 gives the measured times at which the peak occurs in the percent population for V = 6 for all sets of conditions. On the whole, the distribution does not change drastically during the 4 μsec of the current pulse, so in order to determine the significant time to the peak in V = 6, 4 μsec is subtracted from the elapsed time. These reduced times are the middle entries in Table 6. Averaging these times for plots of identical pressure yields the following values:

400 mTorr > 1.0 μsec

200 mTorr > 2.25 μsec

50 mTorr > 7.8 μsec

The product of these times and the collision frequencies for the corresponding pressures determines the number of gas kinetic collisions which have occurred at the time of the observed peak. The values are:

400 mTorr → 2.7 collisions

200 mTorr → 3.0 collisions

50 mTorr → 2.6 collisions

It appears, then, that for all conditions of these experiments, 2.5 to 3.0 collisions are required to produce the peak in this level of the $B\ ^3\Pi_g$ state vibrational distribution. The timing of this peak reflects the number of collisions necessary to equlibrate the populations of the V = 6 level of the

$B\ ^3\Pi_g$ state with the V = 7 level of the $W\ ^3\Delta_u$ state via the ICT process. It should be noted that, in general, the overall distributions are otherwise similar at the times when the peak in V = 6 occurs. Consequently, we may feel confident that the position of the peak has not been affected by drastic changes in the percent populations of the lower levels.

The role of collisional coupling between the $B\ ^3\Pi_g$ and $W\ ^3\Delta_u$ states has been considered previously in explanation of the red lower border of Type-B auroras (1),(2). Of particular interest here are the implications of the 85 km turn-on altitude which was noted by Benesch as having been quite sharply defined in artificial auroras. As pointed out in ref. 2, the auroral 85 km corresponds to a kinetic collision frequency of approximately 2 collisions per radiative lifetime of the levels V = 6, 7, and 8 of the W state. In the aurora, this appears to be the critical count required to divert excitation from the W → B system to the B → A system.(1) With our present applications of time-resolved spectroscopy to the same problem, the progress of the collisional coupling of the levels of these states, for example B(6) and W(7), can be directly observed and, as indicated in the analysis above, some 2.5 to 3 collisions are required to couple these levels. This is in good agreement with Benesch's estimate.

The fact that the percentage population rises for the $B\ ^3\Pi_g$ V = 6 level indicates that the relative populations of the B(6) and the W(7) are initially out of equilibrium. In order to estimate basis populations for these two levels, we must make some assumptions as to the quantities of the two states directly produced by the discharge. Computer studies which we have carried out have indicated that the production rate ratio of W to B in the early

stages of the discharge pulse is about 0.75. Since it may be assumed that the excitation occurs from the V = 0 level of the ground state, X $^1\Sigma_g^+$, then the distribution into the two upper levels is governed largely by the Franck-Condon factors (FCF) between X(0) and those levels. The resulting relative populations will be given by

$$\begin{aligned} N[W(7)] &= FCF[W(7)] * Ratio(W:B) \\ &= (0.105) * (0.75) \\ &= 0.081 \\ N[B(6)] &= FCF[B(6)] * Ratio(B:B) \\ &= (0.0659) * (1.0) \\ &= 0.066 \end{aligned}$$

Thus, we calculate that there is an unbalance of about 20% in the two initial populations in favor of the B(6) over the W(7). Furthermore, there is a tendency for the unbalance between these two levels to persist since the B(6) depopulates ten times more rapidly than the W(7) through spontaneous emission.(20) For the duration of the unbalance, W(6) supplies secondary excitation to B(7) through ICT.

Another feature in Figure 8, which becomes more prominent with increased pressure, is the depression or trough at V = 3. The values for percentage population do not go through a well-defined minimum, so it is difficult to determine precisely the number of collisions necessary for achieving an equilibrium, presumably with V = 3 of the W $^3\Delta_u$ state. However, an analysis similar to the previous one may be undertaken. Proceeding as before,

$$N[W(3)] = FCF[W(3)] * Ratio(W:B)$$
$$= (0.0438) * (0.75)$$
$$= 0.032$$
$$N[B(3)] = FCF[B(3)] * Ratio(B:B)$$
$$= (0.191) * (1.00)$$
$$= 0.19$$

In this case, the population of the B(3) level is calculated to be much larger than that of the W(3) level so that a bleed-off of excitation into the W(3) is to be expected.

The trough at B(3) has been noted also by Benesch and Fraedrich(21). Their data is shown in Figure 11 and depicts the relative populations of the $B\ ^3\Pi_g$ and the $B'\ ^3\Sigma_u^-$ levels in a DC discharge, each state to its own scale. It was postulated in ref. 21 that every B' level is equilibrated by ICT with an adjacent B level. However, the reverse statement is true only down to B(4) where the B' levels end with B'(0). B(3), then, while losing excitation to $W\ ^3\Delta_u$, has no appreciable influx from $B'\ ^3\Sigma_u^-$ and manifests a depressed population in both experiments.

At B(3) and B(4), the evidence of ICT coupling with B' comes about as a result of the sudden default of B' below B'(0). Conversely, an enhancement of excitation in B state levels adjacent to the peak in the B' initial excitation rate distribution may be observed in the relative population plots. Figure 12 gives a plot of the distribution of direct electron excitation rates for levels of the $B'\ ^3\Sigma_u^-$. Each of these levels(V) is adjacent to a level(V+4) of the

$B\ ^3\Pi_g$, so that the excitation peak at B'(7) is manifested as a population peak at B(11). It appears at some 2 μsec or 2.5 collisions after the termination of the discharge as shown in Figure 13.

CONCLUSION

The results discussed above demonstrate the role of collisions in the redistribution of vibrational population in the B $^3\Pi_g$ state of N_2. This redistribution is seen both in changes in relative band intensities and in the corresponding changes in the 3-D plots of population percentages. With respect to the 3-D plots, the important observations are (1) that the rates with which these changes take place increase directly with pressure, and (2) that marked changes occur at B $^3\Pi_g$ vibrational levels which lie adjacent to levels of overlapping states where peaks arise in the initial population distributions.

Referring to the Franck-Condon factors between the ground state and the overlapping triplet states, we may anticipate vibrational population peaks in these states at the following levels: A $^3\Sigma_u^+$, v=8; W $^3\Delta_u$, v=7; and B' $^3\Sigma_u^-$, v=7. The peaks lie adjacent to B $^3\Pi_g$ vibrational levels v=1, 6, and 11, respectively. As was shown in the previous section, these are the B $^3\Pi_g$ levels in the 3-D plots which show distinct changes as a function of pressure. Thus, from such observations, we may conclude that the ephemeral peaks in the 3-D plots reflect the ICT process connecting the B $^3\Pi_g$ and the other low-lying triplet states (W, A, and B'). This is not to say that the low-lying singlets do not also participate in the ICT process with the triplet manifold, but that the present observations correlate most obviously with ICT amongst the triplets. An important point to recognize regarding the 3-D population plots is the efficacy of this mode of presentation in the detection of detailed features of the B $^3\Pi_g$ excitation distributions.

The absolute population data (upper entries) for all levels in Tables 2 through 4 show significant trend deviations when compared with the decay curves to be expected from spontaneous radiative transition probabilities. Consideration of the present data indicates that for the intermediate and lower vibrational levels, their apparent lifetime decreases with pressure during the first few microseconds after the end of the excitation pulse (Figure 14A). For the higher levels, the situation appears more complicated, in that at 50 millitorr the emission peaks at 4 μsec rather than 3 μsec (Figure 14B). This latter behavior is not to be expected where direct electron excitation from the ground state constitutes the sole populating mechanism. Again, what such an analysis does <u>not</u> readily reveal is the wealth of structure that is evident in the 3-D percentage population plots of Figures 8 and 10.

The following discussion traces the processes which we consider to be operative during and immediately after the 4 μsec excitation pulse. First, the triplet states in question are generated at relative rates determined by the electron energy distribution and the electron excitation cross sections associated with the low-lying triplets. Second, the initial vibrational population distributions within these states are determined largely by the Franck-Condon overlap between each state and the ground state, $X\ ^1\Sigma_g^+$. The Franck-Condon factors vary with vibrational quantum number within a given excited state and the electron excitation cross sections vary among the electronic states.

The levels thus populated emit continually according to their transition probabilities and, in keeping with the trends of Figure 10, begin an evolution down the vibrational level ladder. Such emission constitutes an irreversible

loss of excitation from all coupled sets of levels. Furthermore, as might be expected, the direct electron excitation generates an ensemble of excited molecular states wherein the populations of adjacent vibrational levels are initially out of equilibrium vis-a-vis the ICT process. An example of an initial set of distributions is shown in Figure 15.

For the case of $B' \rightarrow B$, $W \rightarrow B$, $B \rightarrow W$, and $A \rightarrow B$ emission, the radiative decay process constitutes a source of excitation for a group of cascade lower levels. In addition, the collisions which occur during and after the excitation pulse will tend to shift any remaining population toward proportions which reflect an ICT equilibrium. This shifting of populations has been demonstrated in the 3-D population plots and in the changing relative band intensities.

In applying these results to an enhanced understanding of auroral processes, we have always been cognizant of the circumstance that much auroral activity takes place in an environment characterized by considerably lower collision frequencies than those of laboratory discharges. On the other hand, with time-resolved spectroscopy capable of time resolution extending to the sub-microsecond level, we have been able to examine the spectral evolution of auroral features on a collision-by-collision basis down to and including spectra which occur effectively prior to the first collision after excitation.

Through the course of these investigations, we have come to regard auroral emission as an inherently dynamic phenomenon in the sense that even under steady excitation conditions, there is generated a manifold of molecular emitters of increasing age and, thus, of evolving population distribution. As has

been illustrated in Figure 9, this evolution takes place in the absence of collisions, but it is much accelerated by molecular interaction. The continually aging populations of emitters become increasingly subject to the collisional effects elaborated on above depending, of course, on the altitude of the auroral form. At 100 km there will be only a small influence on the part of collisions since they occur at 400 μsec intervals, whereas at 80 km, where there is but 10 μsec between collisions, the presence of neighboring molecules strongly affects the population distribution and, accordingly, the emitted spectrum.

Acknowledgments

This research was supported by the Atmospheric Sciences Section, National Science Foundation and by the Optical Physics Division, Air Force Geophysics Laboratory. The computer time for this project was supported in part through the facilities of the Computer Science Center of the University of Maryland.

REFERENCES

1. W. Benesch, J. Geophys. Res. 86, 9065 (1981).
2. W. Benesch, J. Chem. Phys. 78, 2978 (1983).
3. R.F. Heidner, III, D.G. Sutton, and S.N. Suchard, Chem. Phys. Lett. 37, 243-248, 1976.
4. D.H. Katayama, T. Miller and V. Bondybey, J. Chem. Phys. 72, 5469 (1980).
5. D.H. Katayama, J. Chem. Phys. 81, 3495 (1984).
6. A. Rotem, I. Nadler, and S. Rosenwaks, J. Chem. Phys. Lett. 77, 304 (1981).
7. N. Sedeghi and D.W. Setser, Chem. Phys. Lett. 77, 304 (1981).
8. A. Rotem and S. Rosenwaks, Optical Engineering 22, 564 (1983).
9. D.E. Shemansky and A.L. Broadfoot, J. Quant. Spec. Rad. Transfer 11, 1401 (1971).
10. W.R. Pendleton, Jr., P.J. Espy, A.J. Steed, R.R. O'Neil, EOS Transactions, American Geophysical Union, 64, 272, (1983).
11. B.D. Green, W.J. Marinelli, L.G. Piper, W.A.M. Blumberg and S.J. Wolnik, to be published.
12. W.P. Boquist and J.W. Snyder, Conjugate auroral measurements from the 1962 U.S. high altitude nuclear test series, in Aurora and Airglow, Proceedings of the NATO Advanced Study Institute, edited by Billy M. McCormac, pp. 325-339, Reinhold Publishing Corp., New York, 1967.
13. R.L. Gattinger, F.R. Harris and A. Vallance Jones, Planet, Space Sci., 33, 33, 207-221, (1985).
14. C. Störmer, The Polar Aurora, Clarendon, Oxford, 1955.
15. P.B. Hanna and C.D. Anger, Auroral colour variations, Planet. Spac Sci., 19, 399-411, (1971).

16. S. Goldberg and J. Rothstein, "Hydrogen Thyratrons", Advances in Electronics and Electron Physics, XIV, 207 (1961).

17. W. Benesch, D. Fraedrich and M. Ginter, Rev. Sci. Instr. 54, 776 (1983).

18. D.E. Shemansky and A.L. Broadfoot, J. Quant. Spec. Rad. Transfer 11, 1385 (1971).

19. J. Morrill, Dissertation University of Maryland, 1986.

20. R. Covey, K.A. Saum and W. Benesch, JOSA, 63, 592-596, (1973).

21. W. Benesch and D. Fraedrich, J. Chem. Phys. 81, 5367 (1984).

Figure Captions

Figure 1 - Experimental block diagram showing the pulsed supply for the discharge tube and the optics and electronics used for time-resolved spectroscopy. Note that the boxcar averager is triggered by the discharge tube current pulse through a current transformer near ground. Light exits the discharge tube through a window at the right end and is directed into the spectrometer by a mirror and a lens.

Figure 2 - Oscilloscope traces of the time-development of the electrical and optical signals from the discharge.

A - Current and light emission for the 2-0 band of the nitrogen 1PG on a time scale of 2 μsec per division. The current pulse is nearly rectangular, starting at 0 and ending at 4 μsec. The 1PG emission rises throughout the current pulse, peaks at approximately 4 μsec and then decays with a long tail. Also shown is the 200 ns boxcar gate which appears at 5 μsec.

B - Expanded view of the current pulse and the 1PG (2-0) band light emission. The light signal is seen to begin dropping at the same instant as the current which is a characteristic common to all of the 1PG bands examined.

C - Expanded view of the current pulse and the 2PG (2-0) band light emission. Note the differences between C and B. In particular, the 2PG begins to fall just after the onset of the discharge pulse.

D - Current and voltage in juxtaposition. The voltage trace starts at the

12,000 volt level and drops rapidly at the onset of the current pulse. Note how closely the 2PG light emission (C) follows the voltage as contrasted with the 1PG emission (B).

Figure 3 - The First Positive Group emission spectrum between 5500 and 9000 Å. Four distinct sequences of vibrational bands are labeled. Time-resolved spectra of this type were used to measure the vibrational population distributions during and after the current pulse. This spectrum was taken at 3 μsec into the discharge pulse with an N_2 gas pressure of 50 mTorr and a discharge pulse repetition rate of 5 Hz.

Figure 4 - Time-resolved spectra of the 1PG, $\Delta V = 2$ sequence from 1 to 9 μsec. The pressure was 400 mTorr of N_2 and the discharge repetition rate 5 Hz. The figure shows the dramatic shift of population to the lower vibrational levels during the period just following the end of the current pulse.

Figure 5 - Time-resolved spectra of the 1PG, $\Delta V = 2$ sequence from 1 to 200 μsec at a lower pressure. The gas pressure for this figure was 40 mTorr and the discharge frequency 35 Hz. Here the length of time required to transfer population to the lower levels is seen to be considerably greater than for the higher pressure case of Figure 4.

Figure 6 - Time-resolved spectra of the $\Delta V = 3$ sequence from 1 to 200 μsec at low pressure (40 mTorr). The figure shows a definite outcropping of the (6-3) and (7-4) bands during the interval between 6 and 60 μs.

Figure 7 - Three dimensional display of 1PG spectra showing the same four

sequences of Figure 3. The spectra were calibrated (in rayleighs) in order to maintain the significance of relative intensity. Note the ripple effect in the V = 4 sequence and the increase in the relative intensity of the (2-0) band between the first and last spectrum.

Figure 8; A, B, C - 3-D plots of population percentages among the vibrational levels of the B $^3\Pi_g$ state taken from IPG spectra measured at each of the indicated times. All plots are from spectra obtained at a discharge pulse frequency of 5 Hz. The pressures are (A) 50 mTorr, (B) 200 mTorr, and (C) 400 mTorr. Note the trough which develops at V = 3 and that the rate at which it develops increases with pressure. Also note the bump in V = 6 which moves to earlier times at higher pressures. The Z axis is percent population. The underlying data appears in Tables 2 through 4. Distortions in the early distributions are due to atomic lines initially present in the spectra.

Figure 9 - A theoretical model demonstrating the effect of lifetime alone on the development of the relative populations of the B state levels. This is a 3-D plot of the estimated change in percent population of the decaying B $^3\Pi_g$ vibrational distribution. Here the only effect considered is spontaneous emission according to the radiative lifetimes which vary among the levels. The initial distribution is from the spectrum at 3 μsec with a pressure of 150 mTorr and a discharge pulse frequency of 15 Hz.

Figure 10; A, B - Long term 3-D plots of population percentages among the vibrational levels of the B $^3\Pi_g$ state (1 to 200 μsec). Pressures are (A) 50 mTorr and (B) 400 mTorr. The plots show that the long term quasi-stationary distribution is reached more rapidly at the higher pressure.

Figure 11 - Population distributions for B $^3\Pi_g$ and B' $^3\Sigma_u^-$ in a DC discharge (from ref. 21). Each distribution is on its own scale. Attention has been drawn to the striking proportionately between the two sets of relative populations down to the B' $^3\Sigma_u^-$ V = 0 level.

Figure 12 - Estimated initial population distribution in the B' $^3\Sigma_u^-$ state. Note that the distribution peaks at V = 7 which lies adjacent to V = 10 in the B $^3\Pi_g$ state. The largest effects due to ICT from B' $^3\Sigma_u^-$ should, accordingly, occur in the levels around V = 10, in agreement with the data of the previous figure.

Figure 13 - 3-D plot of percent population for the B' $^3\Sigma_u^-$ levels 8 through 12. The figure shows a distinct rise in levels 10 through 12 which is considered to be due to collisional coupling with the B' $^3\Sigma_u^-$ state (ICT).

Figure 14; A, B - Comparison of the time development of level populations with calculated trends based on the lifetimes of the levels. The system pressure was 50 mTorr of N_2 and the discharge frequency 5 Hz.

(A) is for B $^3\Pi_g$(V=3) and shows the decay to be more rapid than that to be expected from radiative losses alone. Here ICT should be from B(V=3) into W(V=3).

(B) is for B $^3\Pi_g$(V=11) and shows the emission to be peaking after the end of the current pulse. In this case, ICT is to be expected into B(V=11) from B'(V=8), as well as from high levels of the W $^3\Delta_u$.

Figure 15 - Estimated initial vibrational level population distributions of the A, B, W, and B′ states calculated for an electron temperature of 35,000 ^{o}K. The tic marks above the distributions label the positions of the vibrational levels. This is to demonstrate that the anomalies which have been observed in the 3-D population plots all have their origins in corresponding population peaks in neighboring states which are coupled to the B $^{3}\Pi_{g}$ through ICT.

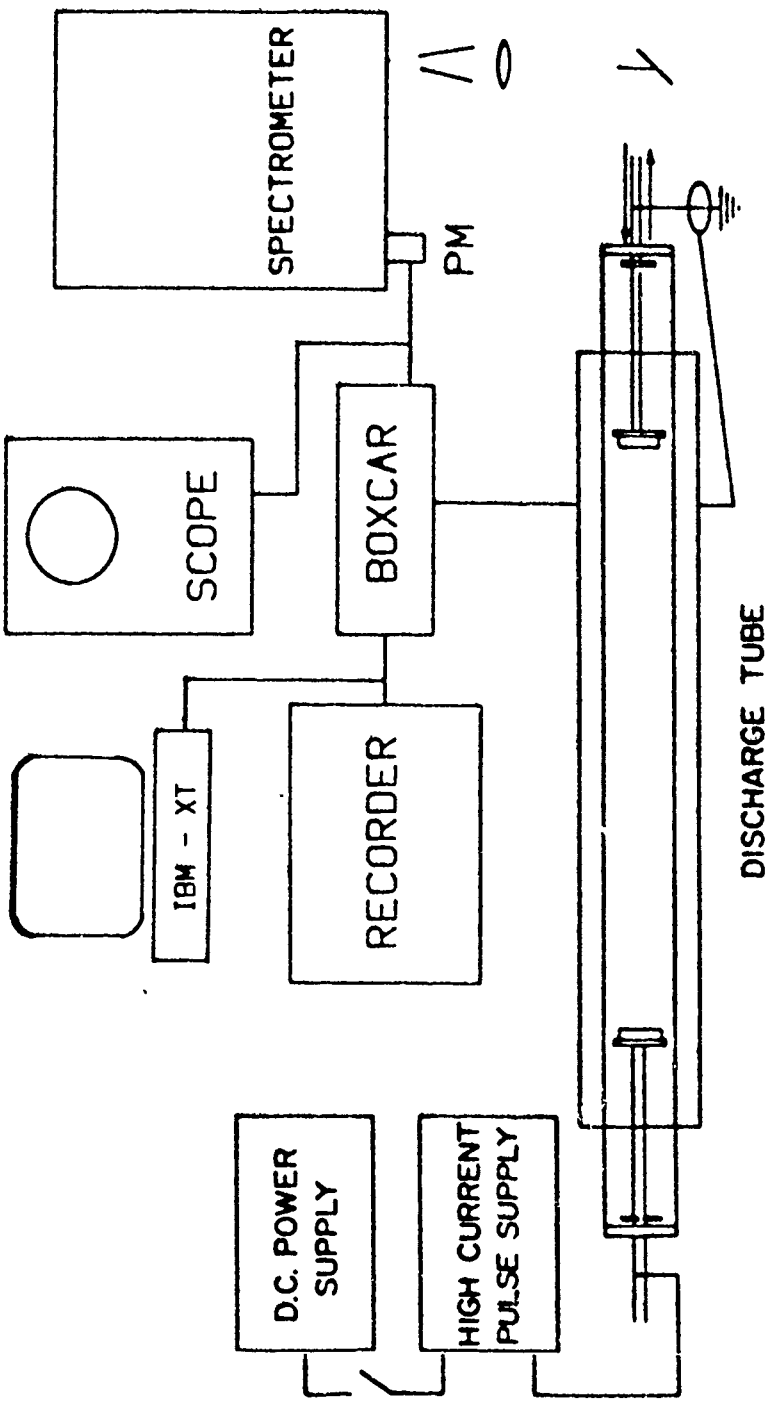
SPECTROMETER
PM
SCOPE
BOXCAR
IBM - XT
RECORDER
D.C. POWER SUPPLY
HIGH CURRENT PULSE SUPPLY
DISCHARGE TUBE

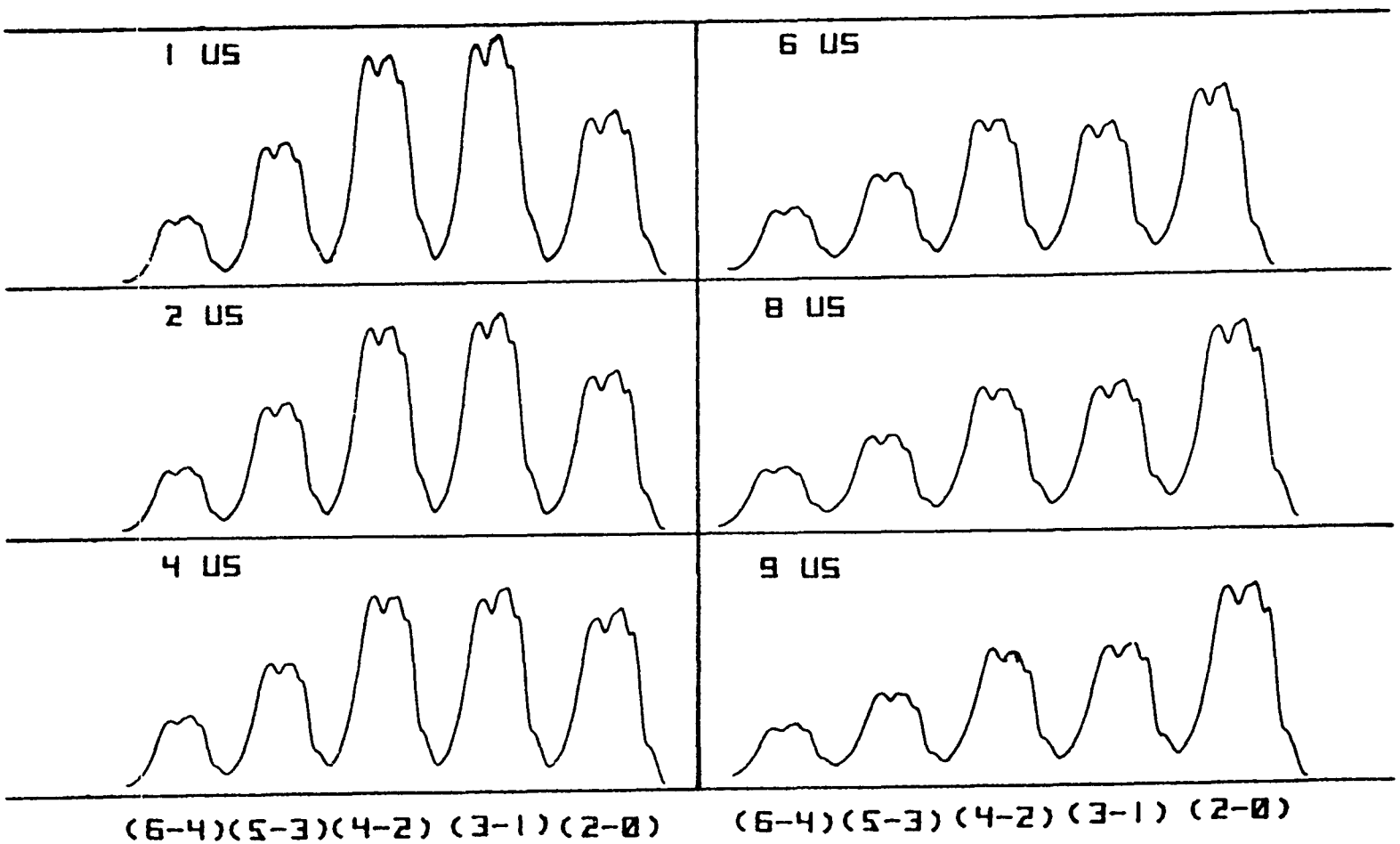
1 US
6 US
2 US
8 US
4 US
9 US
(6-4)(5-3)(4-2) (3-1)(2-0)
(6-4)(5-3)(4-2)(3-1) (2-0)

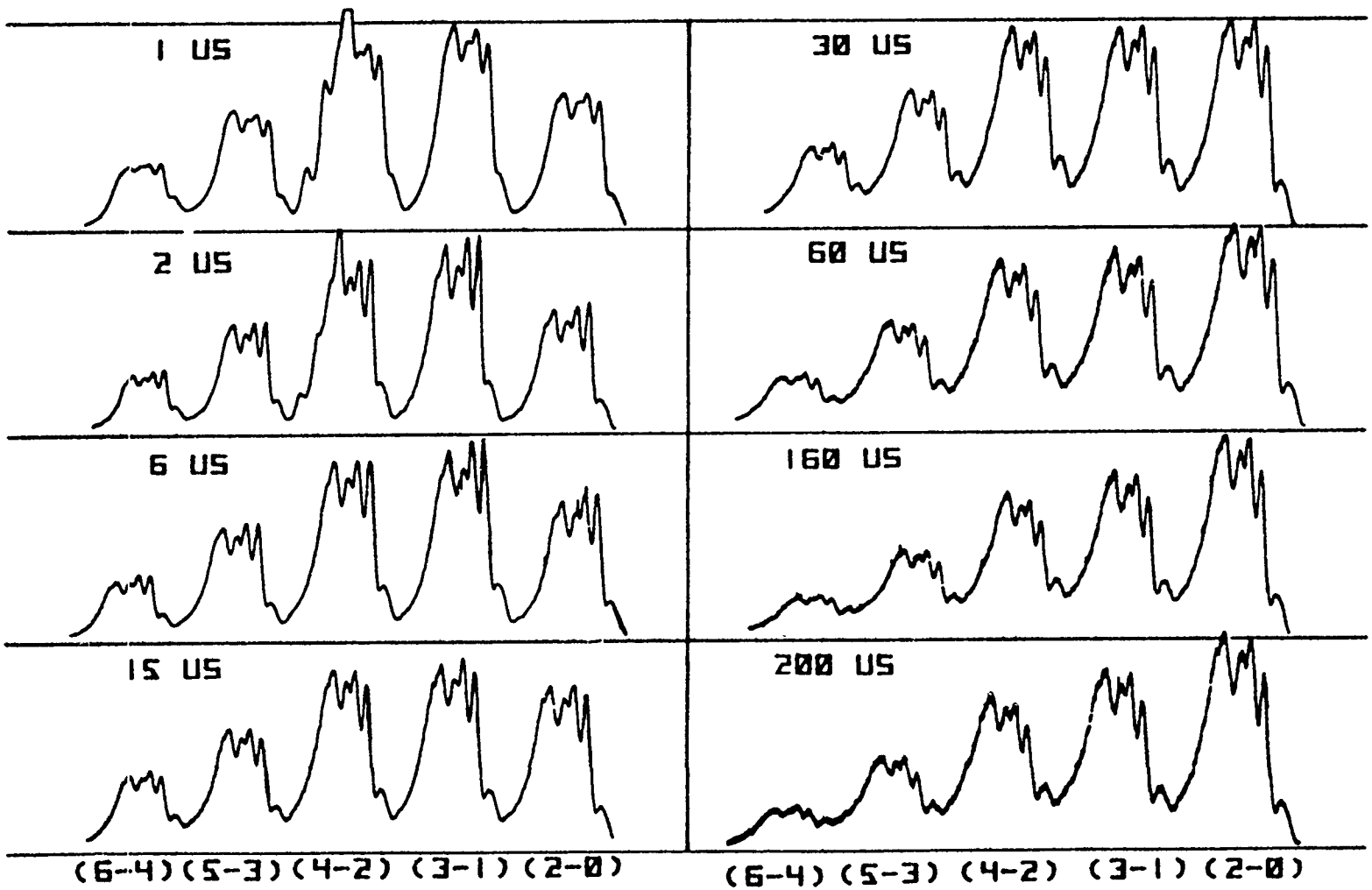
1 US
30 US
2 US
60 US
6 US
160 US
15 US
200 US
(6-4) (5-3) (4-2) (3-1) (2-0)
(6-4) (5-3) (4-2) (3-1) (2-0)

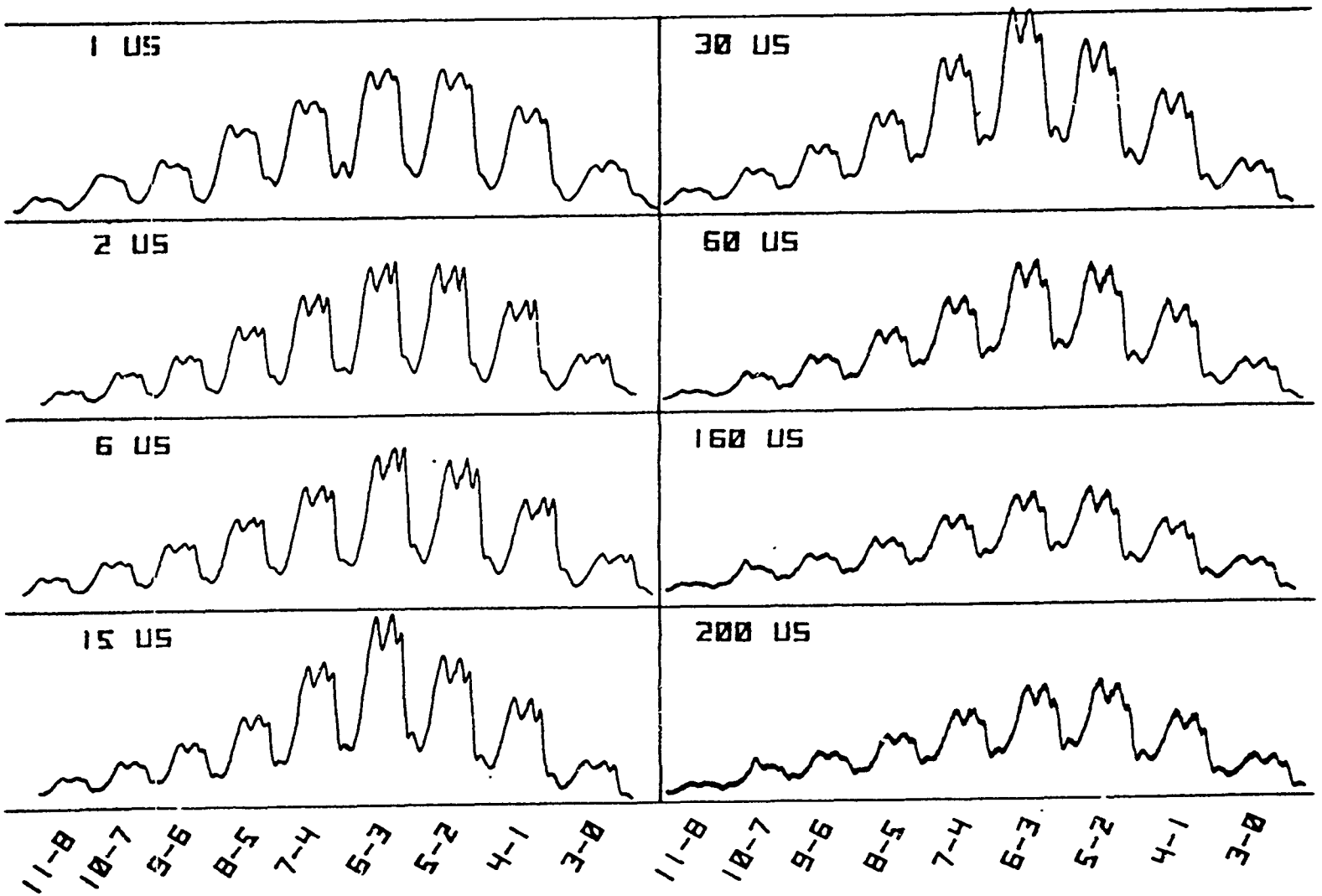
1 US
30 US
2 US
60 US
6 US
160 US
15 US
200 US
11-8
10-7
9-6
8-5
7-4
6-3
5-2
4-1
3-0

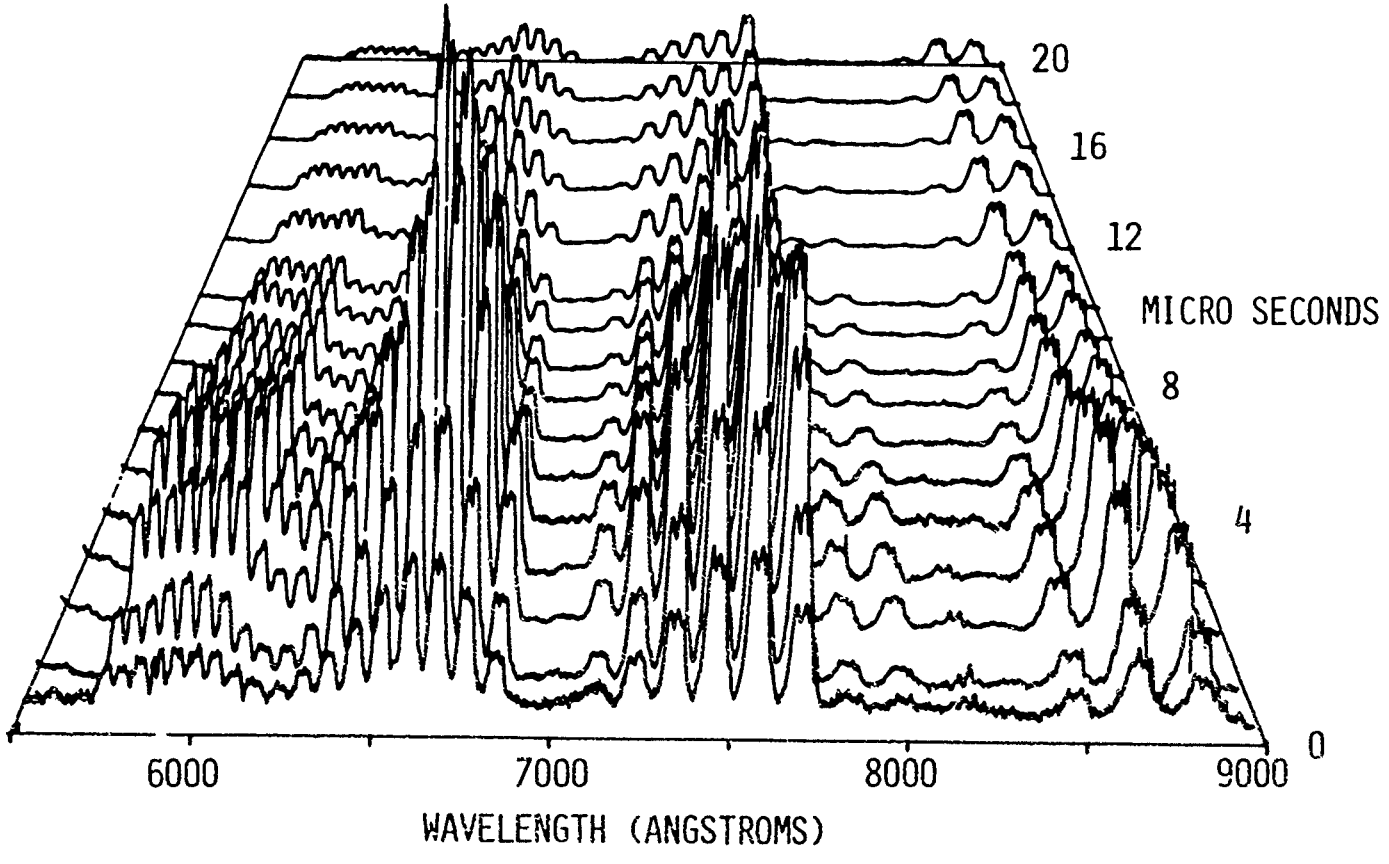
20
16
12
MICRO SECONDS
8
4
0
6000
7000
8000
9000
WAVELENGTH (ANGSTROMS)

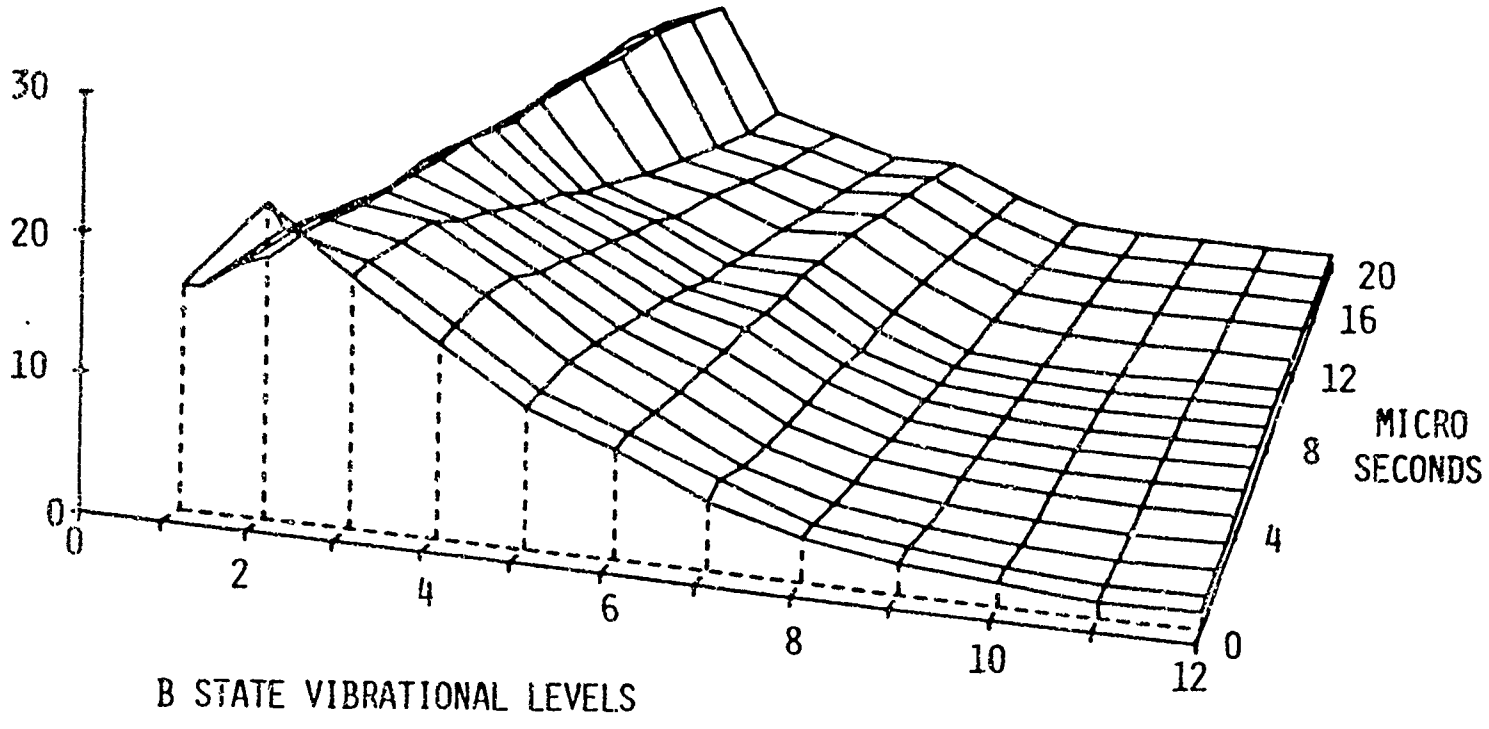
30
20
10
0
0
2
4
6
8
10
12
B STATE VIBRATIONAL LEVELS
0
4
8
12
16
20
MICRO
SECONDS

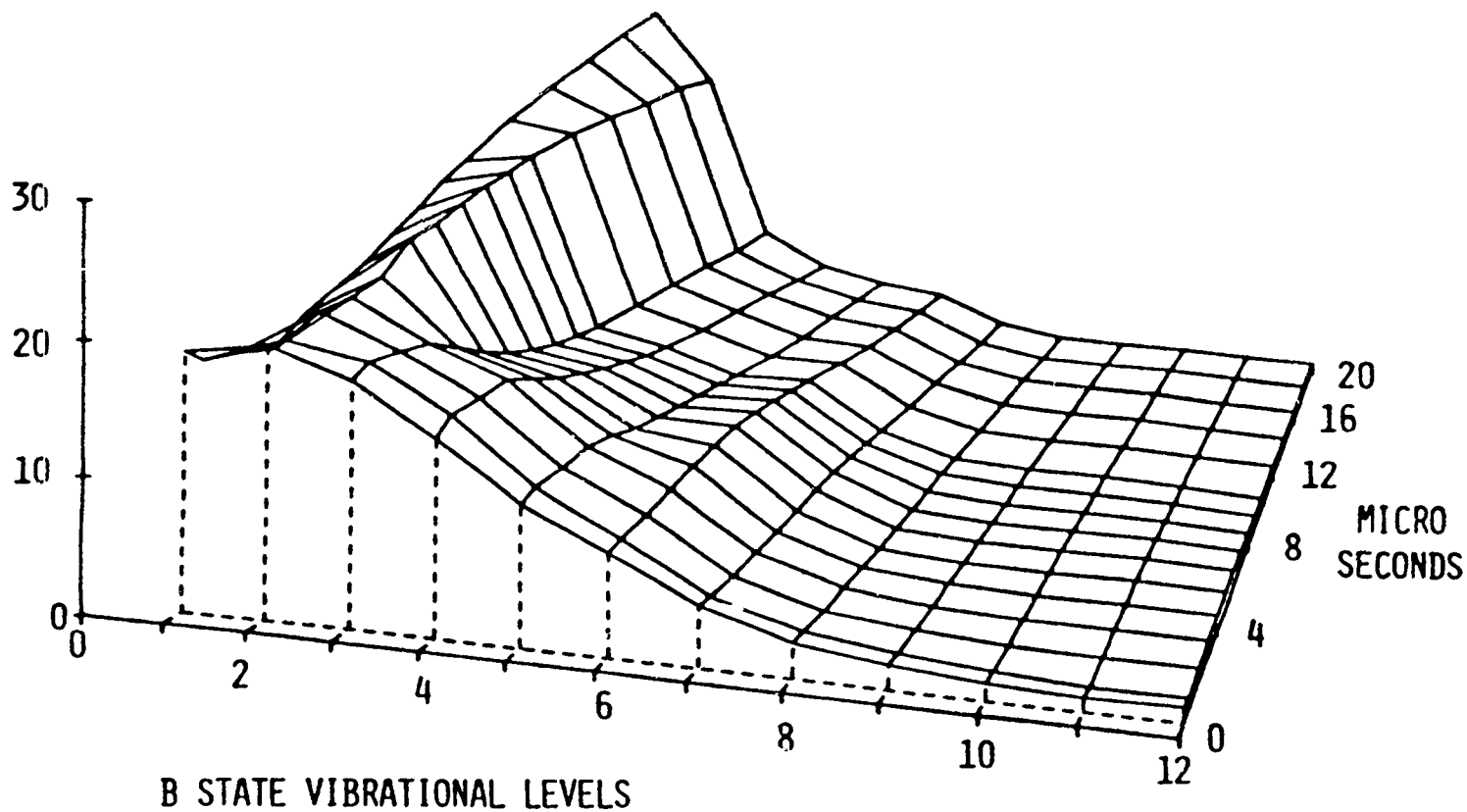
30
20
10
0
0
2
4
6
8
10
12
B STATE VIBRATIONAL LEVELS
0
4
8
12
16
20
MICRO
SECONDS

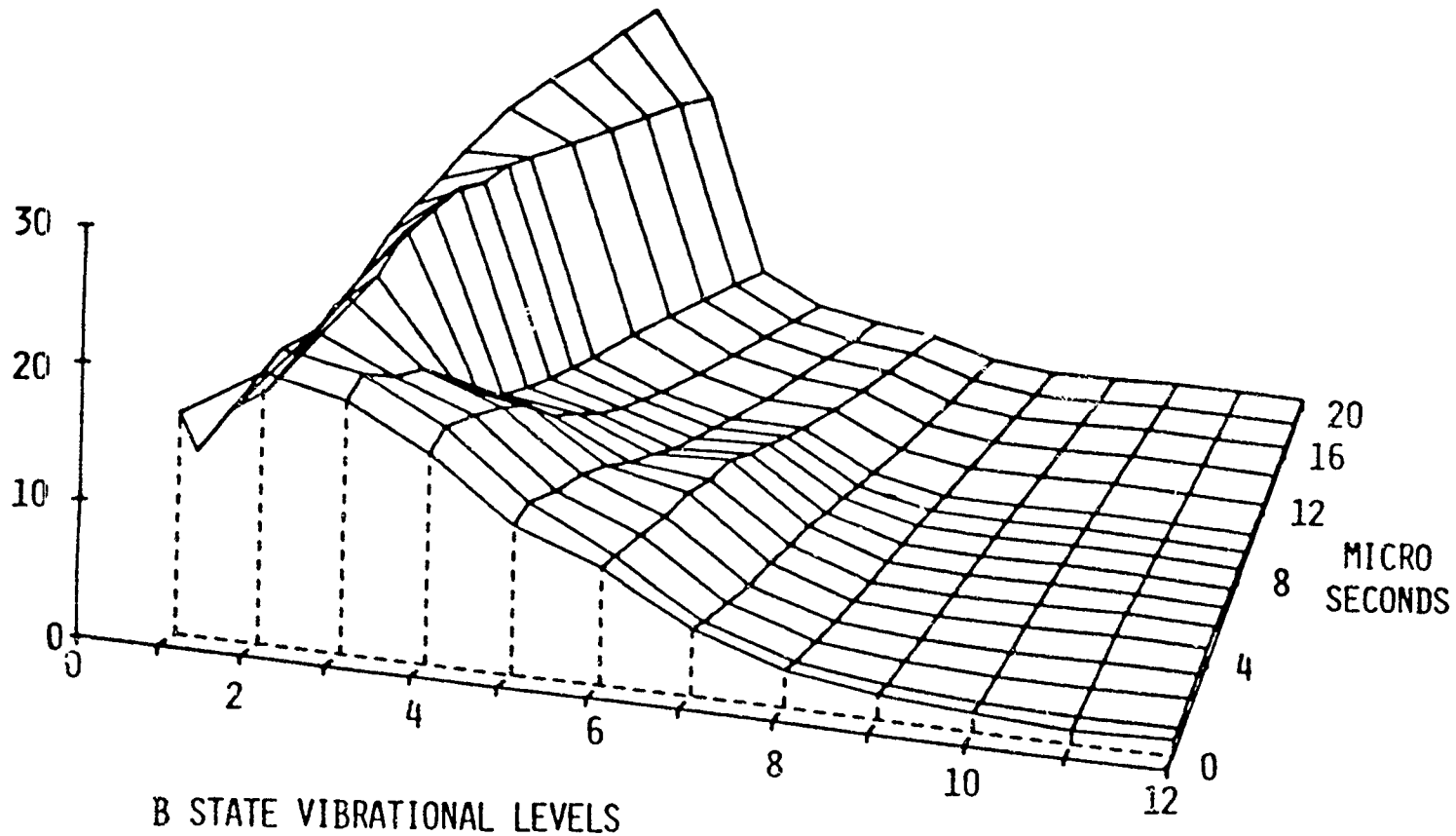
30
20
10
0
0
2
4
6
8
10
12
B STATE VIBRATIONAL LEVELS
0
4
8
12
16
20
MICRO
SECONDS

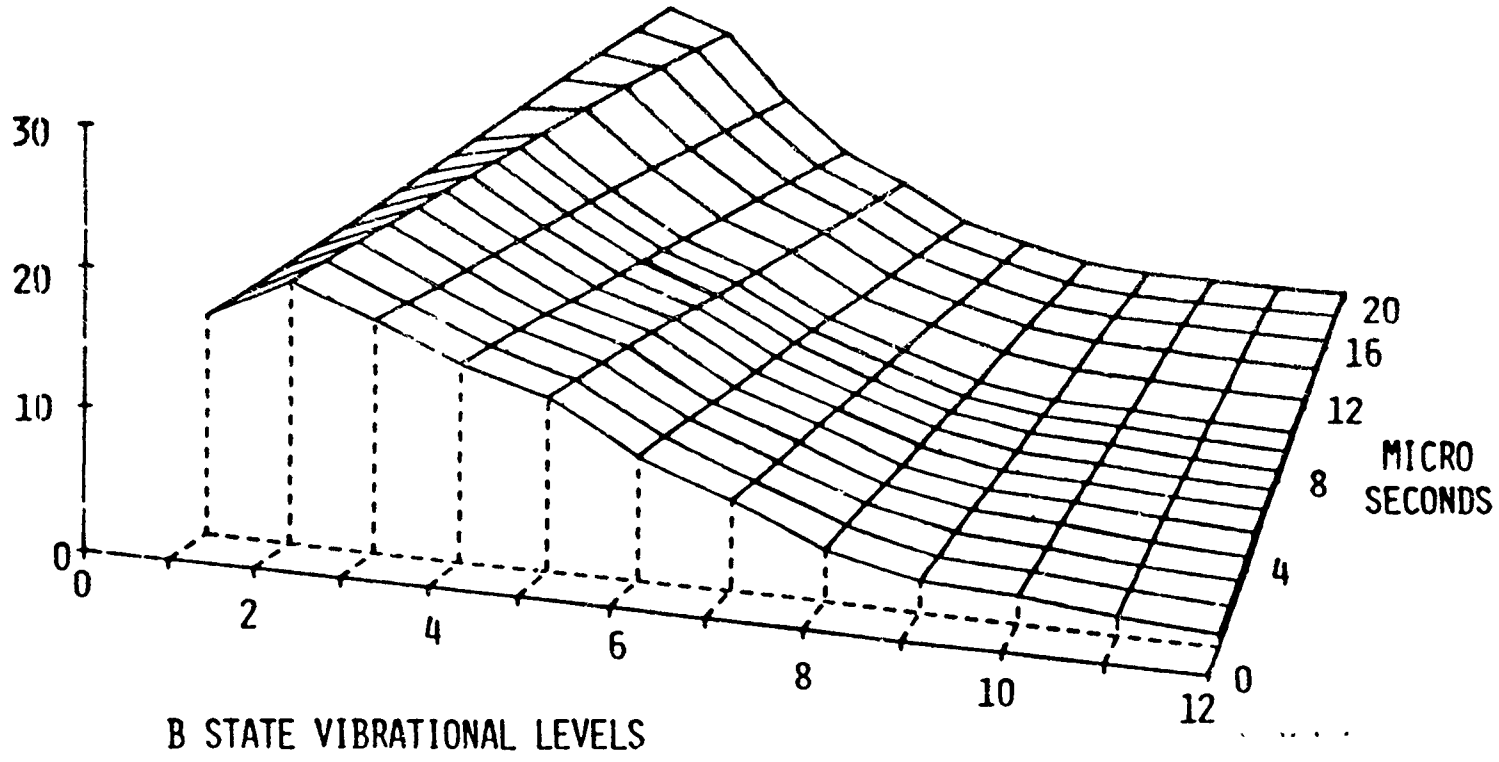
30
20
10
0
0
2
4
6
8
10
12
B STATE VIBRATIONAL LEVELS
0
4
8
12
16
20
MICRO
SECONDS

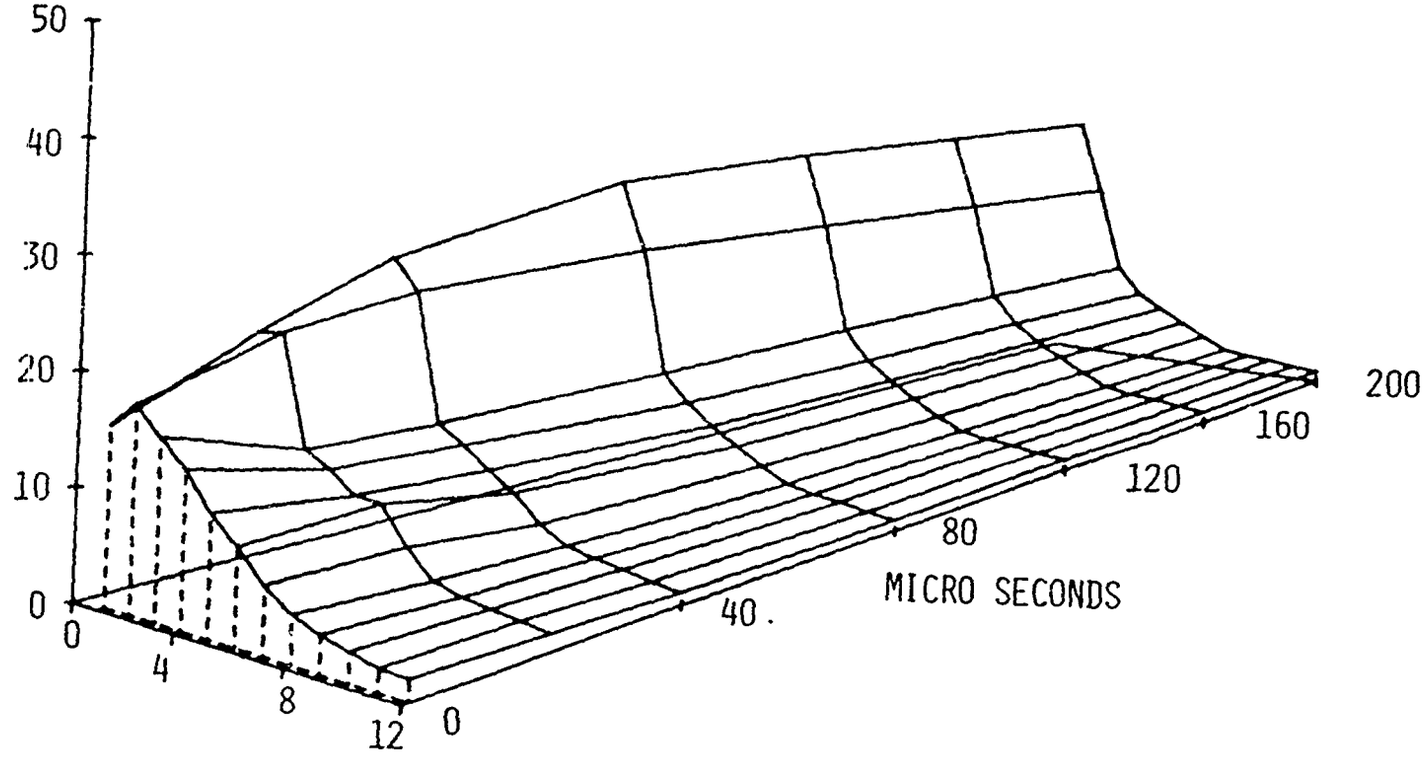
50
40
30
20
10
0
0
4
8
12
0
40.
80
120
160
200
MICRO SECONDS
B STATE VIBRATIONAL LEVELS

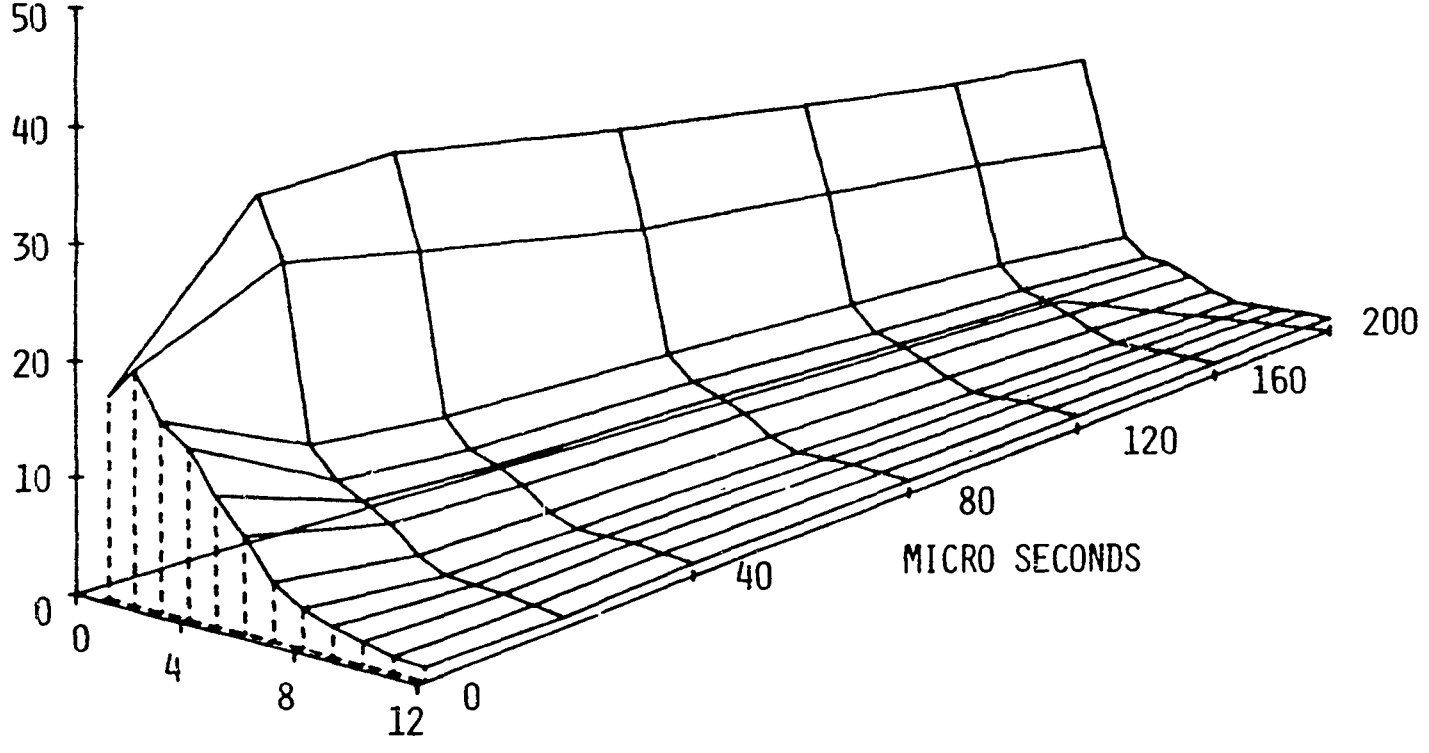
50
40
30
20
10
0
0
4
8
12
0
40
80
120
160
200
MICRO SECONDS
B STATE VIBRATIONAL LEVELS

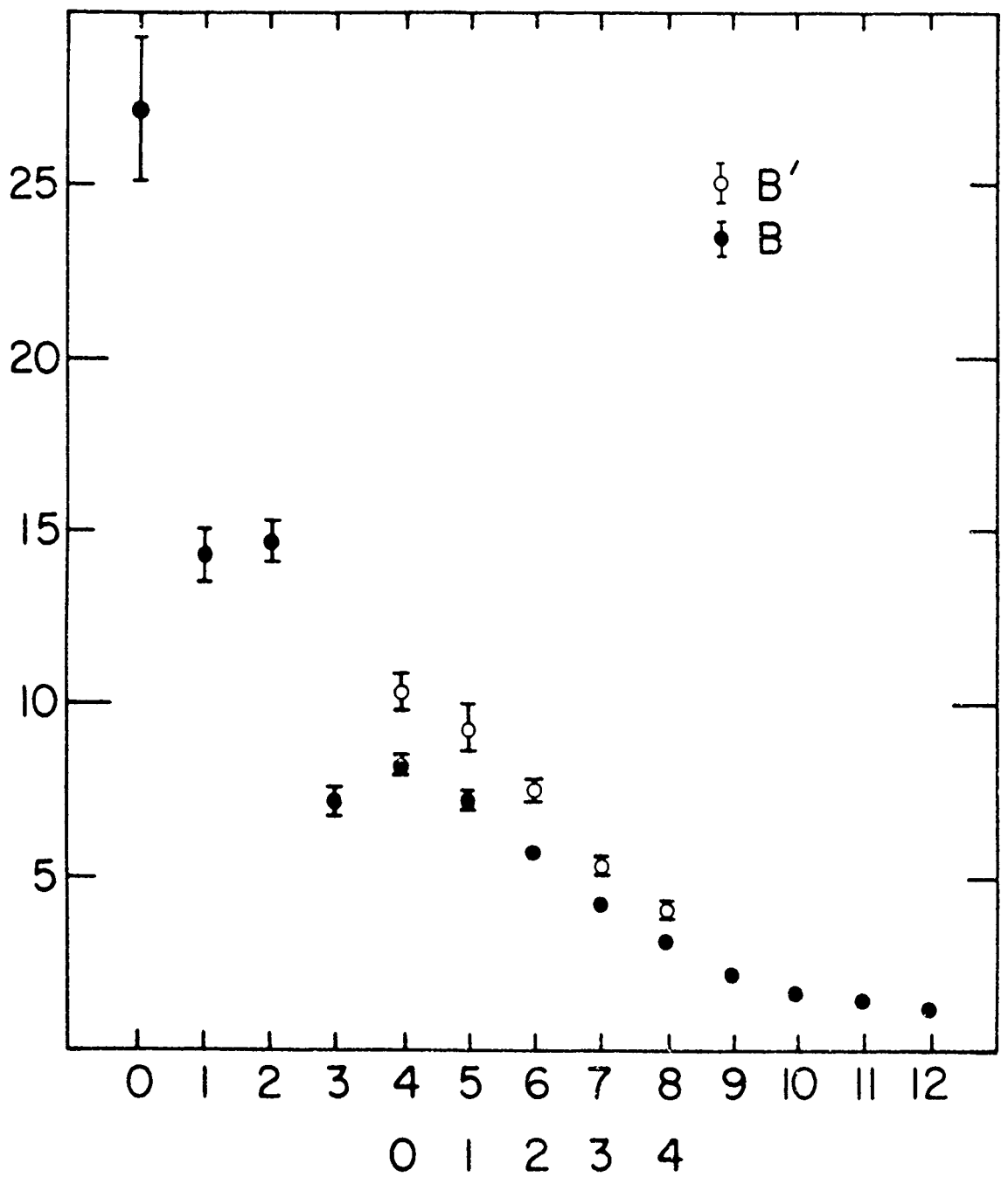
25
20
15
10
5
B′
B
0 1 2 3 4 5 6 7 8 9 10 11 12
v B $^3\Pi_g$
0 1 2 3 4
v′ B′ $^3\Sigma_u^-$

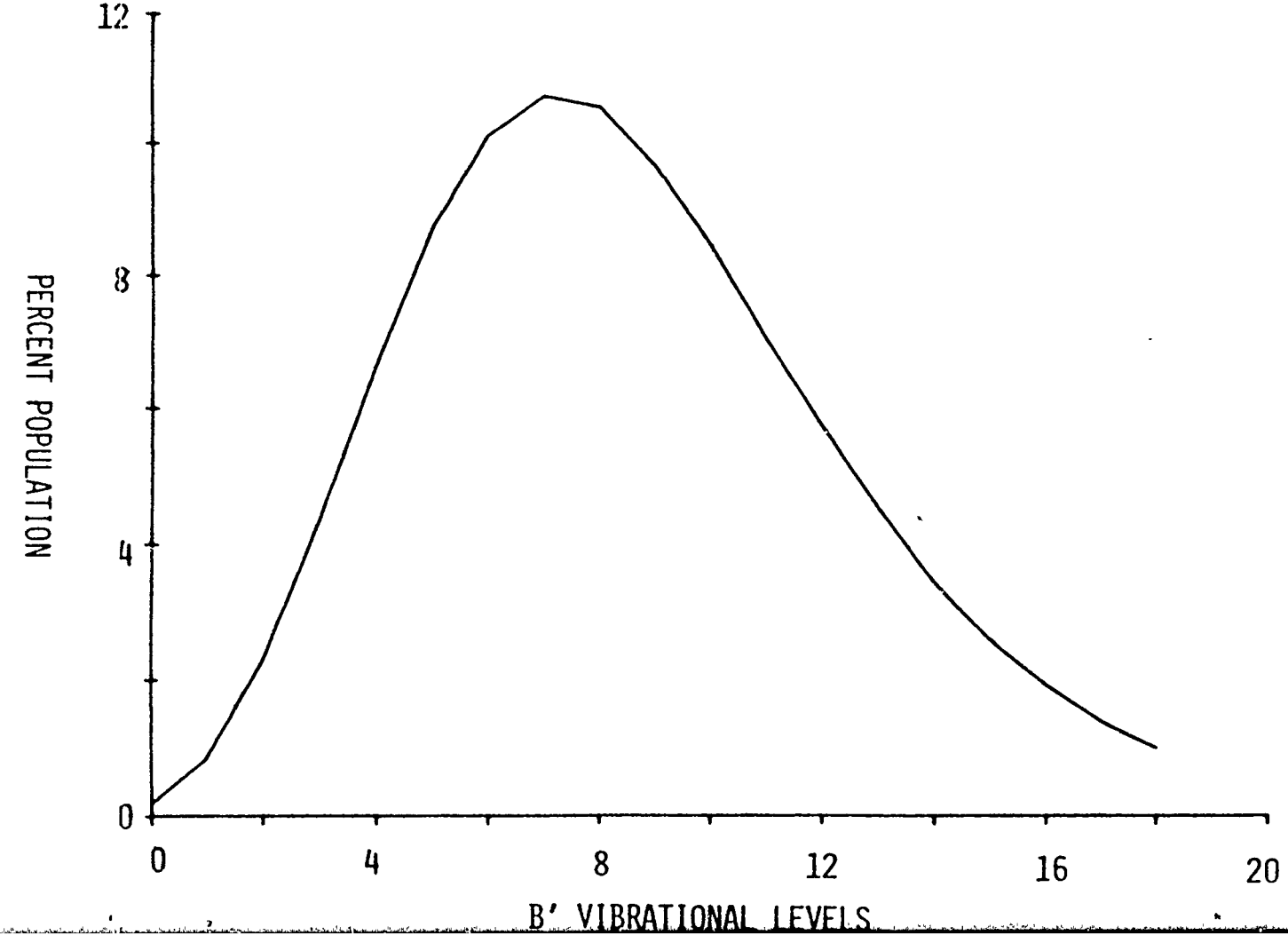
12
8
4
0
PERCENT POPULATION
0
4
8
12
16
20
B′ VIBRATIONAL LEVELS

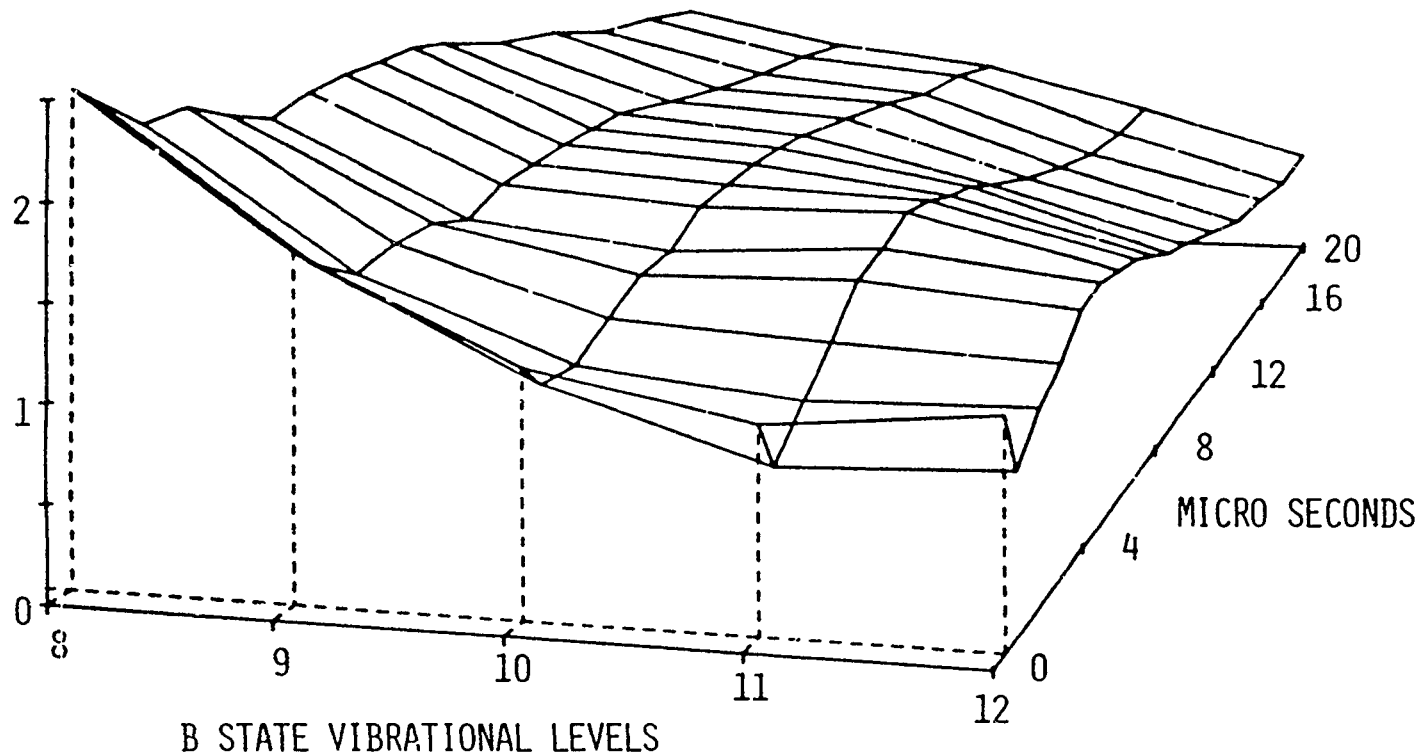
2
1
0
8
9
10
11
12
B STATE VIBRATIONAL LEVELS
0
4
8
12
16
20
MICRO SECONDS

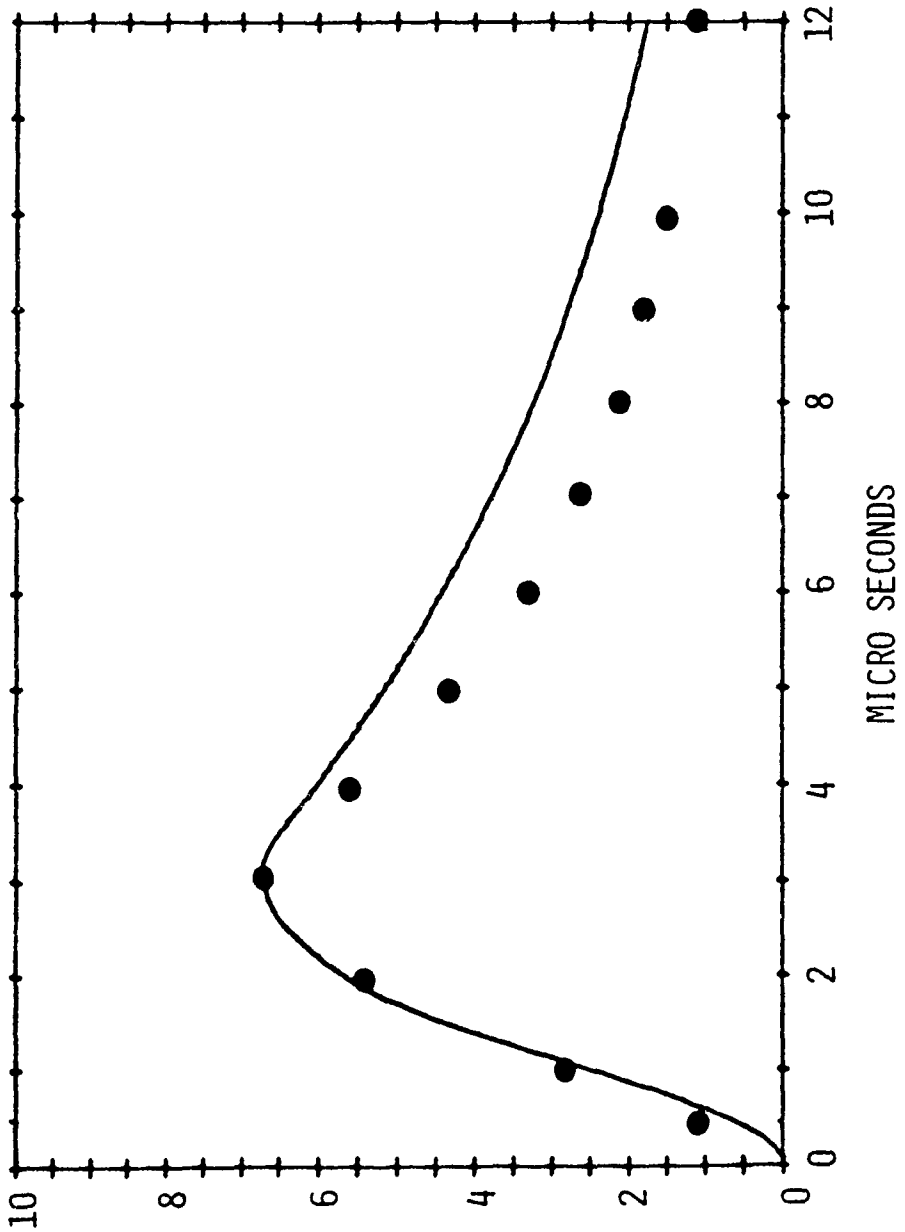
10
8
6
4
2
0
0
2
4
6
8
10
12
MICRO SECONDS

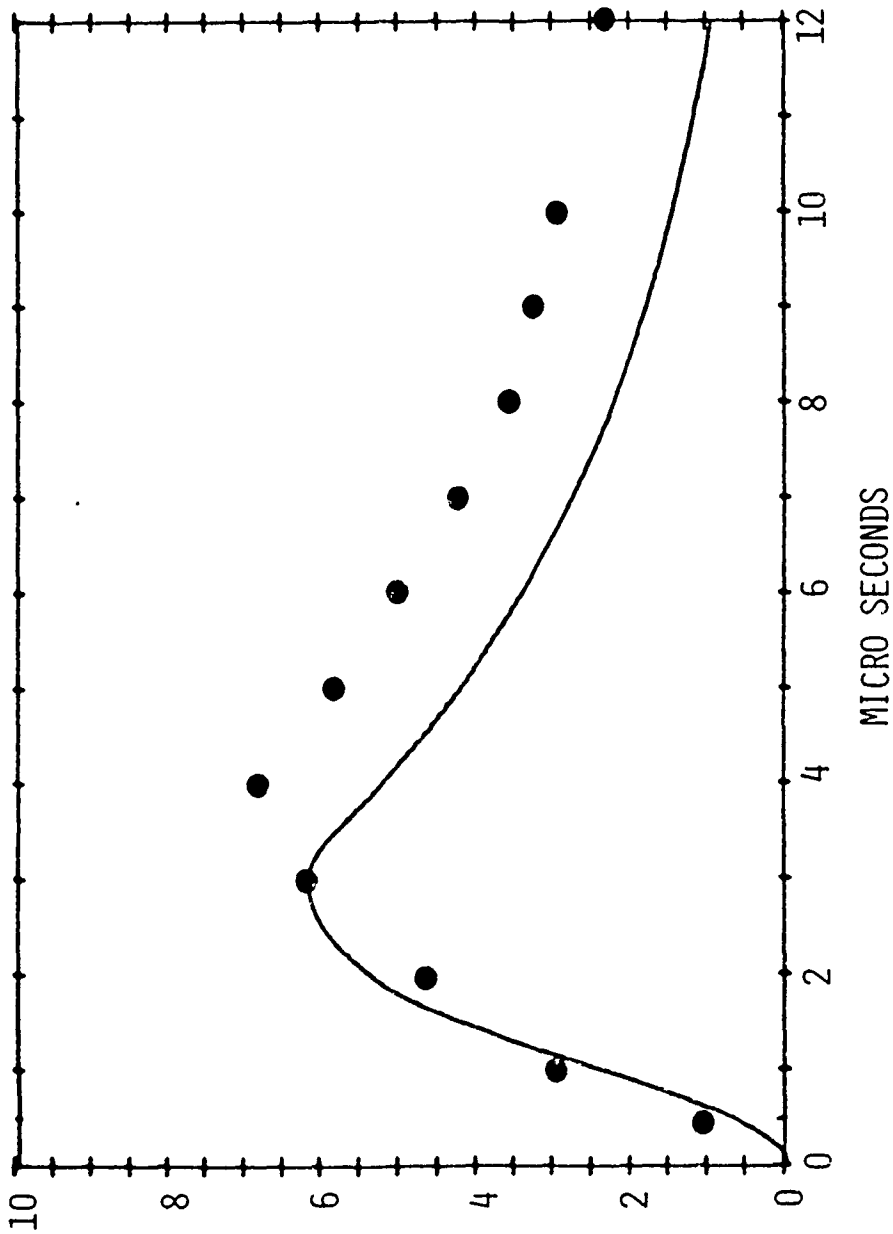
0
2
4
6
8
10
12
MICRO SECONDS
10
8
6
4
2
0

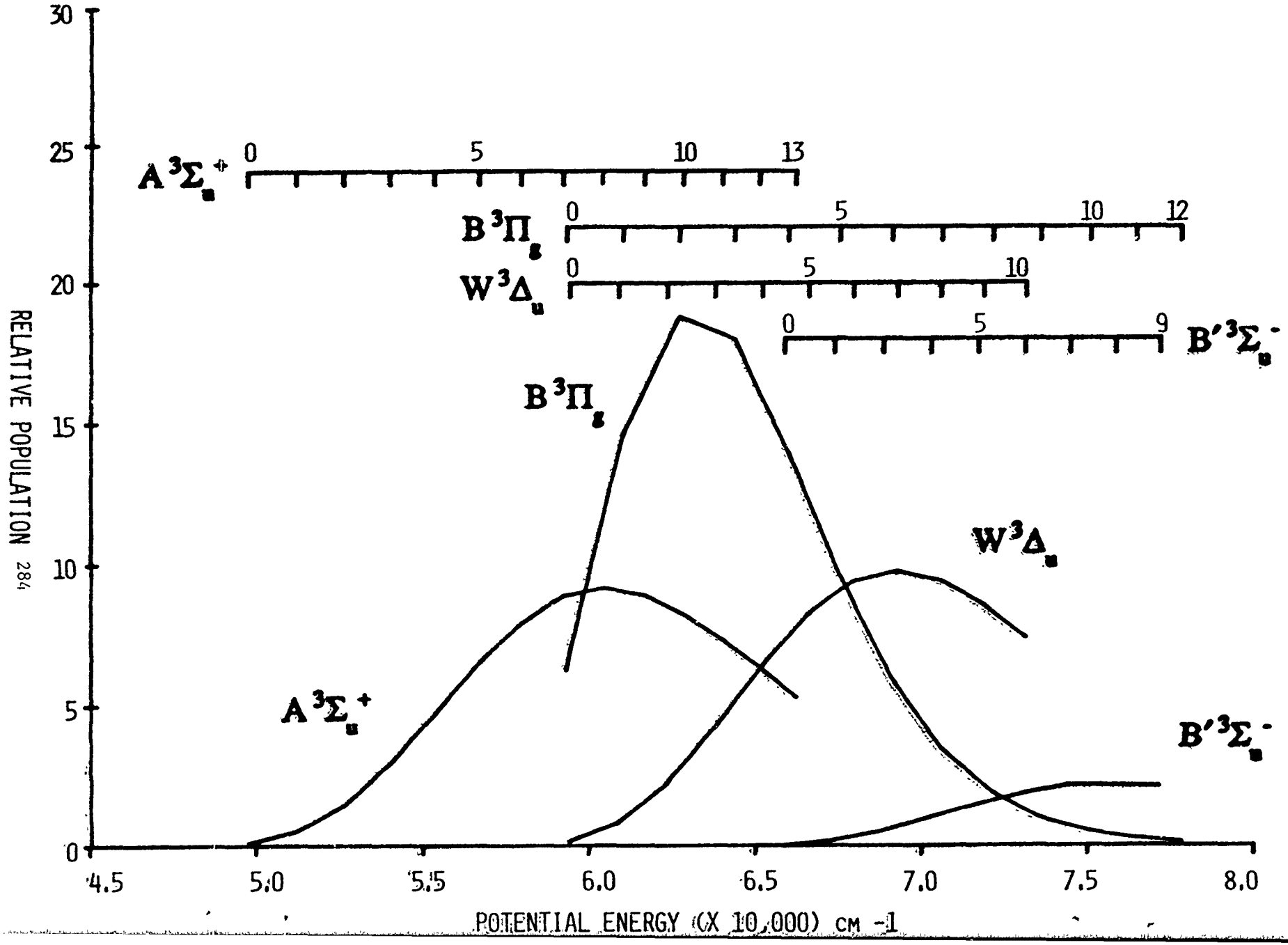
30
25
20
15
10
5
0
RELATIVE POPULATION
284
$A^3\Sigma_u^+$
0
5
10
13
$B^3\Pi_g$
0
5
10
12
$W^3\Delta_u$
0
5
10
$B'^3\Sigma_u^-$
0
5
9
$B^3\Pi_g$
$W^3\Delta_u$
$A^3\Sigma_u^+$
$B'^3\Sigma_u^-$
4.5
5.0
5.5
6.0
6.5
7.0
7.5
8.0
POTENTIAL ENERGY (X 10,000) CM -1

Table Captions

Tables 2 through 4 - Relative and percent populations of B $^3\Pi_g$ vibrational levels 1 through 12 during the first 20 μsec of the pulsed discharge. The system pressure is (2) 50 mTorr, (3) 200 mTorr, and (4) 400 mTorr of N_2. The upper entries are relative populations and so reflect the rise and fall of each B $^3\Pi_g$ level during and after the current pulse. Relative populations in all three tables are on the same scale. The lower entries are the percent population of the 12 levels shown at each indicated time. These data underlie the plots of Figure 8; A, B, and C.

Table 5 - Percent population at 120 μsec, showing the long-term quasi-stationary distribution. The system discharge was 50 Hz and the system pressures were 50 mTorr and 400 mTorr as indicated. These data underlie the plots of Figure 10; A and B.

Table 6 - Lapse of time and number of collisions to the peak in the percent population of V = 6. In all cases the number of collisions is between 2.5 and 3 after the end of the current pulse (4 μsec).

Populations of 13 11g levels
50u & 5Hz from 0 to 20us in N2
time (us) v' ---------->

		1	2	3	4	5	6	7	8	9	10	11	12
.500		.120E+01	.168E+01	.132E+01	.102E+01	725.	561	347.	218.	145.	113.	79.1	69.1
	.	16.1	22.4	17.7	13.6	9.70	7.51	4.65	2.92	1.94	1.51	1.06	.928
1.00	.	.287E+01	375E+01	.339E+01	.265E+01	.188E+01	147E+01	998.	557	407.	287.	223.	173.
	.	15.4	20.1	18.2	14.2	10.1	7.88	5.35	2.98	7 18	1.54	1 19	.925
2.00	.	.563E+01	.712E+01	.661E+01	.541E+01	.388E+01	.279E+01	.165E+01	962.	657.	459.	343.	327.
	.	15.7	19.9	18.4	15.1	10.8	7.77	4.61	2.74	1.83	1.28	.957	.912
3.00	.	.673E+01	.825E+01	.828E+01	.664E+01	.478E+01	.344E+01	.199E+01	.114E+01	785.	580.	462.	423.
	.	15.3	19.9	18.8	15.1	10.9	7.82	4.53	2.60	1.78	1 32	1.05	.962
4.00	.	.622E+01	.767E+01	.693E+01	.554E+01	.414E+01	.313E+01	.179E+01	.109E+01	766.	610.	514.	451.
	.	16.0	19.7	17.8	14.3	10.7	8.07	4.60	2.79	1.97	1.57	1.32	1.16
5.00	.	.495E+01	.613E+01	.534E+01	.431E+01	.320E+01	.251E+01	.143E+01	812.	602.	467.	441.	393.
	.	16.2	20.0	17.5	14.1	10.5	8.19	4.69	2.66	1.97	1.53	1.44	1.29
6.00	.	.390E+01	.492E+01	.404E+01	.327E+01	.248E+01	.207E+01	.119E+01	632.	478.	397.	375.	341.
	.	16.2	20.4	16.8	13.6	10.3	8.58	4.94	2.62	1.98	1.65	1.56	1.42
7.00	.	.334E+01	.418E+01	.321E+01	.266E+01	.198E+01	.169E+01	986.	531.	391.	320.	317.	286.
	.	16.8	21.0	16.1	13.4	9.96	8.52	4.96	2.67	1 97	1.61	1.59	1 44
8.00	.	.296E+01	.353E+01	.264E+01	.215E+01	.157E+01	.143E+01	799.	426.	331.	273.	265.	238.
	.	17.8	21.3	15.9	12.9	9.43	8.60	4.81	2.57	1.99	1.65	1.60	1.43
9.00	.	.266E+01	.307E+01	.220E+01	.180E+01	.141E+01	.134E+01	751.	388.	293.	246.	242.	216.
	.	18.1	20.9	14.9	12.8	9.56	9.15	5.12	2.64	2.00	1.67	1.65	1.47
10.0	.	.220E+01	.277E+01	.185E+01	.154E+01	.119E+01	.116E+01	682.	332.	252.	216.	218.	185.
		18.0	21.9	14.6	12.1	9.36	9.16	5.37	2.62	1.99	1.70	1.72	1.46
12.0	.	.186E+01	.227E+01	.139E+01	.123E+01	947.	960.	559.	275	204.	174.	172.	136
	.	18.3	22.3	13.7	12.1	9.30	9.43	5.49	2.70	2.00	1.71	1.69	1.34
14.0	.	.172E+01	.197E+01	.115E+01	997.	788.	787.	473.	238.	182.	157.	149.	117.
	.	19.7	22.6	13.2	11.4	8.94	9.03	5.42	2.73	2.09	1.80	1.71	1.34
16.0	.	.145E+01	.170E+01	907.	790.	638.	648.	391.	196	145.	128.	117.	90 0
		20.1	23.6	12.6	11.0	8.86	9.00	5.43	2 72	2.01	1.77	1 63	1 25
18.0	.	.133E+01	.146E+01	762.	679.	541.	546.	325.	171	125.	109	98 8	79 3
		21.3	23.7	12.2	10.9	8.68	8 77	5.21	2 75	2 01	1 76	1 59	1 15
20.0		.126E+01	.137E+01	731.	616.	499	485.	300	150	[illegible]	108	90 6	66 4
	.	21.6	23.6	12.6	10.6	8.60	8 35	5 16	2 75	2 11	1 85	1 56	[illegible]

Populations of B3Ilq Levels
200u & 5Hz from 0 to 20us in NZ
time (us) v' ---------->

		1	2	3	4	5	6	7	8	9	10	11	12
.500	.	.592E+04	692E+04	627E+04	.500E+04	.360E+04	.250E+04	.156E+04	868.	602.	425.	348.	311.
	.	17.2	20.1	18.2	14.5	10.5	7.51	4.54	2.52	1.75	1.24	1.01	.904
1.00	.	.139E+05	.172E+05	.164E+05	.135E+05	.936E+04	.665E+04	.370E+04	.209E+04	.141E+04	944.	644.	609.
	.	16.1	19.9	19.0	15.6	10.9	7.71	4.29	2.42	1.64	1.09	.747	.706
2.00	.	.269E+05	.361E+05	.322E+05	.269E+05	.187E+05	.139E+05	.698E+04	.385E+04	.258E+04	.186E+04	.164E+04	.147E+04
	.	15.5	20.9	18.6	15.6	10.8	8.50	4.03	2.23	1.49	1.07	.945	.848
3.00	.	.298E+05	.422E+05	.366E+05	.317E+05	.221E+05	.169E+05	.855E+04	.453E+04	.313E+04	.243E+04	.228E+04	.193E+04
	.	14.7	20.8	18.1	15.7	11.1	8.36	4.22	2.23	1.55	1.20	1.13	.952
4.00	.	.257E+05	.342E+05	.265E+05	.232E+05	.169E+05	.138E+05	.674E+04	.336E+04	.249E+04	.211E+04	.215E+04	.174E+04
	.	16.2	21.5	16.7	14.6	10.6	8.70	4.24	2.11	1.57	1.33	1.35	1.10
5.00	.	.206E+05	.284E+05	.182E+05	.161E+05	.118E+05	.108E+05	.530E+04	.242E+04	.179E+04	.163E+04	.170E+04	.136E+04
	.	17.2	23.6	15.2	13.4	9.84	9.01	4.41	2.02	1.49	1.35	1.41	1.13
6.00	.	.170E+05	.223E+05	.130E+05	.118E+05	.889E+04	.862E+04	.429E+04	.195E+04	.149E+04	.141E+04	.142E+04	.104E+04
	.	18.2	24.0	13.9	12.6	9.54	9.26	4.60	2.09	1.60	1.51	1.52	1.11
7.00		.153E+05	.195E+05	102E+05	.930E+04	.716E+04	.719E+04	.358E+04	.167E+04	.127E+04	.121E+04	.117E+04	833.
	.	19.5	24.9	13.1	11.9	9.13	9.17	4.56	2.13	1.62	1.55	1.49	1.06
8.00		.138E+05	.171E+05	.828E+04	.755E+04	.585E+04	.591E+04	.300E+04	.143E+04	.110E+04	.105E+04	957.	659.
	.	20.7	25.6	12.4	11.3	8.77	8.86	4.50	2.14	1.66	1.58	1.43	.988
9.00	.	.131E+05	.153E+05	.706E+04	.631E+04	.498E+04	.497E+04	.253E+04	.126E+04	982.	933.	821.	529.
	.	22.2	26.0	12.0	10.7	8.48	8.46	4.31	2.15	1.67	1.59	1.40	.900
10.0	.	.112E+05	.129E+05	.564E+04	.499E+04	.390E+04	.391E+04	.198E+04	.102E+04	817.	763.	656.	415.
	.	23.3	26.7	11.7	10.4	8.10	8.13	4.12	2.11	1.69	1.59	1.32	.862
12.0	.	.105E+05	.113E+05	.475E+04	.400E+04	.313E+04	.304E+04	.155E+04	817.	663.	631.	489.	308.
	.	25.5	27.4	11.5	9.71	7.60	7.39	3.75	1.98	1.61	1.53	1.19	.747
14.0	.	.940E+04	.955E+04	.396E+04	.318E+04	.246E+04	.232E+04	.119E+04	659.	532.	507.	371.	220
	.	27.4	27.8	11.5	9.26	7.16	6.75	3.45	1.92	1.55	1.48	1.08	.641
16.0	.	.826E+04	.802E+04	.351E+04	.253E+04	.199E+04	.176E+04	918.	513.	434.	398.	286.	169
	.	28.9	28.0	11.6	8.84	6.95	6.21	3.21	1.79	1.52	1.39	.994	590
18.0		.739E+04	.686E+04	.271E+04	.202E+04	.160E+04	.140E+04	716.	424.	362.	335	238.	129
		30.5	28.4	11.2	8.35	6.61	5.79	2.96	1.75	1.49	1.39	987	533
20.0		7066E+04	.621E+04	.250E+01	.177E+04	141E+04	.119E+04	617.	371.	320	290	221	113
	.	32.0	28.1	11.3	8.03	6.40	5.40	2.79	1.68	1.45	1.31	1.00	534

Populations of B3Πg Levels
400u & 5RR. from 0 to 20us in N2
time (us) v' - - - - >

time (us)		1	2	3	4	5	6	7	8	9	10	11	12
500		[illegible]	[illegible]	.795E+04	.656E+04	.457E+04	.358E+04	.203E+04	.113E+04	744.	[illegible]	376.	386.
	.	16.3	19.7	18.3	15.1	10.5	8.23	4.66	2.59	1.71	1.20	.863	.888
1.00		.108E+05	.175E+05	.164E+05	.138E+05	.967E+04	.696E+04	.363E+04	.194E+04	.125E+04	835.	662.	616
		12.9	20.8	19.5	16.4	11.5	8.28	4.31	2.31	1.49	.993	.787	.733
2.00	.	.303E+05	.430E+05	.373E+05	.326E+05	.223E+05	.170E+05	.844E+04	.418E+04	.283E+04	.213E+04	.194E+04	.179E+04
	.	14.9	21.1	18.3	16.0	10.9	8.34	4.14	2.05	1.39	1.05	.954	.878
3.00	.	.386E+05	.583E+05	.453E+05	.394E+05	.278E+05	.212E+05	.995E+04	.471E+04	.330E+04	.267E+04	.267E+04	.214E+04
		15.1	22.8	17.7	15.4	10.8	8.27	3.89	1.84	1.29	1.04	1.04	.836
4.00	.	.335E+05	.473E+05	.321E+05	.291E+05	.207E+05	.177E+05	.803E+04	.372E+04	.278E+04	.252E+04	.259E+04	.194E+04
	.	16.6	23.4	15.9	14.4	10.2	8.74	3.98	1.84	1.38	1.25	1.28	.959
5.00		.270E+05	.371E+05	.193E+05	.174E+05	.130E+05	.118E+05	.546E+04	.243E+04	.197E+04	.187E+04	.185E+04	.128E+04
	.	19.2	26.4	13.7	12.4	9.23	8.42	3.89	1.73	1.40	1.33	1.32	.911
6.00	.	.218E+05	.284E+05	.129E+05	.118E+05	.897E+04	.900E+04	.412E+04	.185E+04	.146E+04	.145E+04	.131E+04	846.
	.	21.0	27.3	12.4	11.4	8.62	8.72	3.96	1.77	1.40	1.40	1.26	.812
7.00		.213E+05	.253E+05	.105E+05	.906E+04	.697E+04	710E+04	.324E+04	.153E+04	.122E+04	.120E+04	.100E+04	634.
	.	23.9	28.4	11.8	10.2	7.82	7.97	3.64	1.72	1.37	1.35	1.12	.712
8.00	.	.202E+05	.221E+05	.895E+04	.741E+04	.583E+04	.591E+04	.279E+04	.140E+04	.114E+04	.111E+04	914.	563
	.	25.8	28.2	11.4	9.47	7.45	7.55	3.57	1.79	1.45	1.42	1.17	.719
9.00	.	.186E+05	.198E+05	.766E+04	.616E+04	.485E+04	.475E+04	.221E+04	.115E+04	936.	939.	697.	418
	.	27.4	29.0	11.2	9.04	7.12	6.98	3.24	1.69	1.37	1.31	1.02	.613
10.0		.174E+05	.173E+05	.660E+04	.509E+04	.401E+04	.386E+04	.192E+04	951.	806.	765.	590.	331.
	.	29.3	29.0	11.1	8.55	6.74	6.48	3.06	1.60	1.35	1.29	.991	.557
12.0	.	.147E+05	.134E+05	.510E+04	.364E+04	.284E+04	.764E+04	.123E+04	681.	592.	555.	411.	213.
	.	32.0	29.1	11.1	7.91	6.17	5.74	2.68	1.48	1.29	1.21	.893	.464
14.0	.	.125E+05	.108E+05	.404E+04	.280E+04	.220E+04	.193E+04	945.	526	458.	434.	331.	156.
		33.7	29.1	10.8	7.52	5.92	5.19	2.54	1.41	1.23	1.17	.890	.420
16.0	.	.108E+05	.903E+04	.327E+04	.223E+04	.173E+04	.147E+04	733.	424	380.	371.	281.	169.
	.	35.0	29.2	10.6	7.23	5.59	4.75	2.37	1.37	1.23	1.20	.909	.546
18.0		.942E+04	.751E+04	.264E+04	.176E+04	.135E+04	.114E+04	585.	324	290.	278.	207.	115.
	.	36.7	29.3	10.3	6.87	5.28	4.47	2.28	1 27	1.13	1 09	.800	449
20.0		.870E+04	.658E+04	.225E+04	.149E+04	.118E+04	954	484	287	247	246.	198.	97.0
	.	38.3	29.0	9.91	6.56	5.20	4.20	[illegible]	[illegible]	1 09	1.08	.872	427

PERCENT POPULATION AT 120 μs

50Hz

Vibrational Level	50μ	400μ
1	31.9 —	33.6 —
2	23.7 ±1.1	23.3 ±1.2
3	11.7 ±0.9	10.6 ±1.9
4	8.7 ±0.7	7.7 ±0.7
5	6.8 ±1.0	6.6 ±1.5
6	5.1 ±0.4	5.3 ±0.5
7	3.6 ±0.3	3.6 ±0.6
8	2.4 ±0.2	2.3 ±0.2
9	1.9 ±0.1	2.1 ±0.06
10	1.8 ±0.01	2.0 ±0.01
11	1.3 ±0.06	1.7 ±0.2
12	0.9 —	1.1 —

TIMES TO PEAK IN V=6 (PERCENT POPULATION)

Frequency(Hz)	Pressure(μ) and Collision Frequency(#/μs) 50μ 0.33#/μs	200μ 1.3#/μs	400μ 2.7#/μs
5	12 8 (9.42)	6 2 (9.26)	4/6 0/2 (8.7/8.7)
15	12 8 (9.34)	7 3 (9.72)	5 1 (9.44)
32	9/14 5/10 (9.2/9.2)	6 2 (9.36)	5 1 (9.41)
50	12 8 (9.48)	6 2 (9.45)	5 1 (9.41)
Average Time (μs)	7.8	2.25	1.0
S.D.	0.89	0.29	0.35
Average Number of Collisions	2.6	3.0	2.7
S.D.	0.30	0.38	0.95